

ABSTRACT

BATENY, FATEMEH. Fluid Absorption and Release of Nonwovens and their Response to Compression. (Under the direction of Dr. Eunyoung Shim and Dr. Behnam Pourdeyhimi).

Fluid handling is a key property in one of the major nonwoven applications in absorbent product such as wipes, hygiene products, and baby diapers. These products are subjected to various levels of compression in real-use. The aim of this study was to investigate the liquid absorption and release properties of nonwovens to establish the absorption structure-property relationship at various compression levels. A comprehensive methodology, considering various flow directions, was employed to establish the relationship by decoupling the effect of structural parameters and material properties in two phases of this study respectively. In the first phase, the mechanism of absorption by pore structure was investigated through considering various fiber cross-sectional size and shape, as well as heterogeneous layered structures having a pore size reduction and expansion. In the second phase, the mechanism of absorption by fiber and consequent swelling was evaluated in view of fluid diffusion into the rayon fibers in samples having different percentages of PET fiber (non-absorbent) and rayon fiber (absorbent). The analysis of absorption and release properties through the entire dissertation was based on the pore characteristics of the nonwovens by measuring the average pore sizes, pore size distribution, and solidity. The investigation revealed that the absorption and release properties of nonwovens are governed by their pore characteristics. In homogeneous non-layered nonwoven fabrics, maximum absorption is mainly governed by the available pore volume. Absorbency rate is determined according to pore size and the maximum rate of absorption is achieved at a specific range of pore sizes. This indicates that an in-depth understanding of the absorption and release properties brings about valuable information for the absorbent product engineering.

© Copyright 2015 by Fatemeh Bateny

All Rights Reserved

Fluid Absorption and Release of Nonwovens and their Response to Compression

by
Fatemeh Bateny

A dissertation submitted to the Graduate Faculty of
North Carolina State University
in partial fulfillment of the
requirements for the degree of
Doctor of Philosophy

Fiber and Polymer Science

Raleigh, North Carolina

2015

APPROVED BY:

Dr. Eunkyong Shim
Committee Co-Chair

Dr. Behnam Pourdeyhimi
Committee Co-Chair

Dr. Benoit Maze

Dr. Orlando Rojas

DEDICATION

This dissertation is dedicated to my mother for her never-ending love, support, and ultimate guidance. Also, I want to express my gratitude to my sweetheart husband, Dr. Soheil Sajjadi, my philosopher brother Mehdi, and my lovely sister Farzaneh for their encouragement and support in this hard path.

BIOGRAPHY

Fatemeh Bateny comes from Tehran, Iran. She received her Bachelor of Textile Technology Engineering in 2004 in Yazd University, Iran. She pursued her education in Amirkabir, Tehran polytechnic university, Iran, where she received her Master of Science degree in Textile Technology Engineering in 2007. She worked as a textile engineer in different departments including foreign order staff, technical sales, and product engineer in two different companies in Tehran, Iran for 4 years. She entered North Carolina State University in spring 2012 for pursuing a Ph.D. in Fiber and Polymer science. She worked as a graduate research assistant at the Nonwoven Institute during her Ph.D. study.

ACKNOWLEDGMENTS

First and foremost, I want to express my deepest gratitude to Dr. Eunkyong Shim for the invaluable lessons in life and science during the past three years. She gave me a confidence, which I had never experienced before. I couldn't ask for a better mentor and advisor. I would also like to extend a special thank you to Dr. Behnam Pourdeyhimi for his continuous support and guidance, in my research and in life. I will move forward with the knowledge he bestowed upon me. Thank you to Dr. Benoit Maze for all his invaluable guidance on this project. His profound suggestions helped me a lot for preparation of this research. Also thanks to my industrial advisors for their helpful recommendation and the Nonwovens Institute and its member for their financial support.

I would like to thank all of the people who helped me with my research, especially the nonwoven Institute staffs, Bruce Anderson for his patient and continues support on building the experimental testing system, Compression GATS, Amy Minton, John Fry, Sherwood Wallace, Jimei Wang, and Sharon Wright.

I would like to thank all of my friends and colleagues at the Institute, who consistently encouraged and supported me.

TABLE OF CONTENTS

LIST OF TABLES	VIII
LIST OF FIGURES	IX
1 INTRODUCTION	1
1.1 RESEARCH OBJECTIVES AND APPROACHES	2
1.2 ORGANIZATION OF DISSERTATION	4
REFERENCES	6
2 LITERATURE REVIEW	7
2.1 FLUID ABSORPTION BASICS OF NONWOVEN FABRICS	7
2.1.1 Liquid absorption in the porous structure	8
2.2 NONWOVEN ABSORPTION	44
2.2.1 Parameters affecting nonwoven absorption behavior	48
2.2.2 Absorbency behavior of nonwovens	56
2.2.3 Compression of nonwovens and its impact on absorption	79
REFERENCES	88
3 EFFECT OF BINDER FIBERS AND STRUCTURAL PARAMETERS ON COMPRESSION AND RECOVERY BEHAVIOR OF THROUGH-AIR BONDED NONWOVEN FABRICS	102
3.1 INTRODUCTION	102
3.2 MATERIAL AND EXPERIMENTAL	106
3.2.1 Description of samples	106
3.2.2 Basic web properties	107
3.2.3 Compression test procedure	108
3.3 RESULTS AND DISCUSSION	113
3.3.1 The effect of fiber cross-sectional size on compressional behavior	113
3.3.2 The effect of fiber cross-sectional shape on compressional behavior	120
3.4 CONCLUSION	128
REFERENCES	129
4 INVESTIGATION OF EFFECT OF STRUCTURAL PARAMETERS ON ABSORPTION AND RELEASE PROPERTIES OF NONWOVENS- PART I: FIBER SIZE STUDY	132
4.1 INTRODUCTION	132
4.2 MATERIAL AND EXPERIMENTAL	135

4.2.1	Description of samples.....	135
4.2.2	Basic web properties	136
4.2.3	Pore size measurement - porometry technique	136
4.2.4	Pore size measurement of compressed samples- porosimetry technique	136
4.2.5	Through-plane absorbency testing under compression.....	137
4.2.6	In-plane wicking measurement	139
4.2.7	Vertical wicking measurement	140
4.2.8	Evaluation of liquid holding capacity under compression.....	141
4.2.9	Theoretical determination of maximum absorption capacity of nonwovens....	143
4.3	RESULTS AND DISCUSSION	144
4.3.1	Thickness and solid volume fraction	144
4.3.2	Pore diameter	144
4.3.3	Absorption properties.....	146
4.3.4	Release properties	168
4.4	CONCLUSION.....	172
	REFERENCES	173
5	INVESTIGATION OF EFFECT OF STRUCTURAL PARAMETERS ON ABSORPTION AND RELEASE PROPERTIES OF NONWOVENS UNDER COMPRESSION- PART II: FIBER CROSS-SECTIONAL SHAPE STUDY.....	180
5.1	INTRODUCTION	180
5.2	MATERIAL AND EXPERIMENTAL.....	182
5.2.1	Description of the samples.....	182
5.2.2	Basic web properties	183
5.2.3	Pore size measurements- porometry technique.....	184
5.2.4	Pore size measurement of compressed samples- porosimetry technique	184
5.2.5	Experimental technique for absorption and release properties	184
5.3	RESULTS AND DISCUSSION	185
5.3.1	Thickness and solid volume fraction	185
5.3.2	Pore diameter	185
5.3.3	Absorption properties.....	192
5.3.4	Release properties	206
5.4	CONCLUSION.....	211
	REFERENCES	213
6	INVESTIGATION OF EFFECT OF STRUCTURAL PARAMETERS ON ABSORPTION PROPERTIES OF NONWOVENS UNDER COMPRESSION- PART III: HETEROGENEOUS LAYERED STRUCTURE STUDY	216
6.1	INTRODUCTION	216
6.2	MATERIAL AND EXPERIMENTAL.....	217
6.2.1	Description of the samples.....	217
6.2.2	Basics web properties	219

6.2.3	Compression testing procedure.....	219
6.2.4	Experimental technique for absorption testing under compression.....	220
6.2.5	Theoretical determination of maximum absorption capacity of nonwovens....	222
6.3	RESULTS AND DISCUSSION	223
6.3.1	Thickness and solid volume fraction	223
6.3.2	Compression properties	224
6.3.3	Absorption properties.....	229
6.4	CONCLUSION.....	241
	REFERENCES	242
7	INVESTIGATION OF EFFECT OF FIBER ABSORBENCY ON ABSORPTION AND RELEASE PROPERTIES OF NONWOVENS UNDER COMPRESSION.....	245
7.1	INTRODUCTION	245
7.2	MATERIAL AND EXPERIMENTAL.....	249
7.2.1	Description of the samples.....	249
7.2.2	Basic web properties	250
7.2.3	Pore size measurement.....	250
7.2.4	Compression properties measurement	250
7.2.5	Swelling characteristics	251
7.2.6	Experimental technique for absorption and release properties	251
7.3	RESULTS AND DISCUSSION	252
7.3.1	Basic web characteristics	252
7.3.2	Pore diameter	253
7.3.3	Compression properties	254
7.3.4	Swelling properties	259
7.3.5	Absorption.....	260
7.3.6	Release properties	275
7.4	CONCLUSION.....	282
	REFERENCES	284
8	CONCLUSIONS AND RECOMMENDATIONS	288
8.1	CONCLUSIONS.....	288
8.2	RECOMMENDATIONS.....	290

LIST OF TABLES

Table 2.1: surface energies of different fibers (Gupta with Hyun Suk Whang 2000; Gupta and Whang 1999).....	17
Table 3.1: details of various Through-air bonded fabric	107
Table 3.2: details of various Through-air bonded fabric	107
Table 4.1: sample details.....	135
Table 4.2: structural characteristics of nonwoven samples	144
Table 4.3: liquid penetration rate and distance in vertical test-various fiber sizes	167
Table 5.1: sample details.....	182
Table 5.2: basic web characteristics.....	185
Table 5.3: the pore size distribution of nonwovens containing round, pentalobal, and 4DG fiber cross-sections at no compression and under 20%, 30%, and 40% compression.....	191
Table 5.4: the liquid front rate and distance for various fiber cross-sectional shape- vertical wicking test	206
Table 6.1: sample details.....	218
Table 6.2: structural characteristics of separate layers	223
Table 7.1: samples characteristics.....	249
Table 7.2: web structural characteristics.....	253

LIST OF FIGURES

Figure 2.1: liquid drop resting on the solid surface	10
Figure 2.2: a small droplet in equilibrium over a horizontal surface:(a) and (b) partial wetting, while wetting being stronger in (b), (C) complete wetting ($\theta=0$) (de Gennes 1985).....	12
Figure 2.3: schematic of capillary filled with the liquid (wicking) (Pan and Zhong 2006) ...	20
Figure 2.4: schematic of (Right) positive capillary pressure for a wetting liquid (Left) negative capillary pressure for a non-wetting liquid.....	22
Figure 2.5: liquid infiltration through an inclined capillary tube (M. Landeryou, Eames, and Cottenden 2005).....	27
Figure 2.6: numerical results of rise of water in glass capillaries of different radii versus time (Hamraoui and Nylander 2002)	29
Figure 2.7: imbibition and drainage of triangular tube- curvature vs saturation for a triangular tube (Mason and Morrow 1991)	31
Figure 2.8: schematic diagram of expansion-contraction and contraction-expansion capillaries (Young 2004).....	33
Figure 2.9: changes in fiber dimensions due to swelling (Morton, Hearle, 2008)	40
Figure 2.10: different kinds of pores: (a) closed pore (b) through pore (c) blind pore.....	50
Figure 2.11: tortuosity.....	51
Figure 2.12: vertical wicking test.....	57
Figure 2.13: downward vertical wicking test (Konopka 2001)	59
Figure 2.14: GATS (the plastic tube which connect the reservoir to the porous plate not shown)(Konopka 2001)	61
Figure 2.15: typical GATS curve.....	62
Figure 2.16: (a) principal of capillary flow porometry (b) pore diameter measured by flow porometry (A. Jena and Gupta 2003).....	65
Figure 2.17: (Left) basic arrangement for liquid Porosimetry (right) prototype output for a liquid extrusion experiment (Bernard Miller and Tyomkin 1994)	66
Figure 2.18: (left) plot of total absorption capacity against packing density (right) plot of the rate of absorption against packing density for different fiber diameter (Das, Pradhan, and Pourdeyhimi 2012).....	78
Figure 2.19: effect of compression on the geometric pore size distribution of the fibrous structure (S. Jaganathan et al. 2009).	84
Figure 3.1: schematic of the compression procedure on Instron	109
Figure 3.2: typical compression test results, compression and recovery curve	110
Figure 3.3: distance between two contact points in a fiber mass.....	112
Figure 3.4: compressive pressure versus compression percentages for various fiber sizes and binder percentages	114
Figure 3.5: the compressive resistance in order to reach to various compression percentages for samples containing various fiber sizes and binder percentages	116
Figure 3.6: compressive pressure versus solidity cube in order to determine the resistance to compression based on van Wyks model	117

Figure 3.7: calculated slope α in order to determine the resistance to compression based on van Wyks model	118
Figure 3.8: energy loss measurements in varying fiber diameter and binder percentages ...	119
Figure 3.9: recoverability measurements in varying fiber diameter and binder percentages	120
Figure 3.10: compression pressure vs. compression percent, different fiber cross-section at various binder percentages.....	122
Figure 3.11: compressive resistance for different fiber cross-sections at various compression levels	124
Figure 3.12: compressive pressure vs. cube solidity in different fiber cross-sections.....	125
Figure 3.13: calculated slope α based on van Wyk equation.....	126
Figure 3.14: percentage of energy loss in samples of various fiber cross-section and binder percentages.....	127
Figure 3.15: recoverability measurements in varying fiber cross-section and binder percentage	127
Figure 4.1: modified NWI GATS (compression GATS).....	138
Figure 4.2: typical GATS curve.....	139
Figure 4.3: schematic of the Teflon plate for the in-plane wicking testing system	140
Figure 4.4: desorbency testing set up under compression based on GATS.....	141
Figure 4.5: desorbency testing system under compression based on Basket test	142
Figure 4.6: experimental result for pore diameter for 90%PET-10%Co-PET.....	145
Figure 4.7: the experimental result for pore diameter for 80%PET-20%Co-PET.....	146
Figure 4.8: the GATS results for different fiber diameter- 90% PET-10% Co-PET- at various compression levels	148
Figure 4.9: the GATS results for different fiber diameter- 80% PET-20% Co-PET- at various compression levels	149
Figure 4.10: the maximum absorption results for different fiber diameters measured via different methods- (a) 90% PET-10% Co-PET (b) 80% PET-20% Co-PET	150
Figure 4.11: the GATS maximum absorption results for different fiber diameter under different compression level- (a) 1.5 denier (b) 3 denier (c) 6 denier (d) 9 denier	152
Figure 4.12: maximum absorbency (Theory, GATS) versus solidity (a) 10% binder (b) 20% binder- solid line shows the theoretical results and dots show the experimental result	154
Figure 4.13: through-plane absorbency rate at various fiber sizes and binder percentages .	156
Figure 4.14: through-plane absorbency rate for various fiber sizes and binder percentages according to their mean flow pore sizes- line shows the theoretical results built on left vertical axis, and dots show the experimental result built on right vertical axis	158
Figure 4.15: absorbency rate for (a) 1.5 Denier (b) 3 Denier (c) 6 Denier and (d) 9Denier structures @ 0,10,20,30, and 40 % compression levels.....	160
Figure 4.16: median pore size measured by compression Porosimetry technique for samples of 6 denier fibers at varied compression level	162
Figure 4.17: through-plane absorbency rate for 6-denier fiber sizes (20% binder percentages) according to their median flow pore sizes- line shows the theoretical results built on left vertical axis, and dots show the experimental result built on right vertical axis	163

Figure 4.18: in-plane absorbency rate of samples- Fiber size effect	164
Figure 4.19: in-plane absorbency rate of samples vs. mean flow pore size- Fiber size effect	165
Figure 4.20: vertical wicking test results for various fiber sizes for the samples containing 20% binder fibers.....	167
Figure 4.21: the vertical wicking experiments after 42 hours	167
Figure 4.22: liquid holding capacity of the samples with different fiber sizes at no-compression (Left) 90% PET-10% Co-PET (Right) 80%PET-20% Co-PET	169
Figure 4.23: liquid holding capacity of the samples with different fiber sizes-compression effect (Left) 90% PET, 10% Co-PET (Right) 80% PET, 20% Co-PET.....	170
Figure 4.24: liquid retention capacity of samples of various fiber sizes, containing 10% binder fibers at varying solidity levels.....	171
Figure 4.25: liquid retention capacity of samples of various fiber sizes, containing 20% binder fibers at varying solidity levels.....	171
Figure 5.1: schematic of various fiber cross-sectional shape (a) round (b) pentalobal (c) 4DG	183
Figure 5.2: the porometer results for various fiber cross-sectional shape (a) 10% binder (b) 20% binder	187
Figure 5.3: the median pore diameter measured by porosimetry technique at varied compression levels	189
Figure 5.4: the GATS results for different fiber cross-sectional shape- 90% PET-10% Co-PET- at various compression levels.....	193
Figure 5.5: the GATS results for different fiber cross-sectional shape- 80% PET-20% Co-PET- at various compression levels.....	194
Figure 5.6: the GATS maximum absorption for various fiber cross-sectional shape and binder percentages at varied compression levels	196
Figure 5.7: the GATS maximum absorption results vs. solidity for different fiber cross-sectional shape of nonwoven samples containing 90% PET-10% Co-PET	197
Figure 5.8: the GATS maximum absorption results vs. solidity for different fiber cross-sectional shape of nonwoven samples containing 80% PET-20% Co-PET	197
Figure 5.9: the GATS absorbency rate in through-plane direction for various fiber cross-sectional shape and binder percentages	199
Figure 5.10: the GATS absorbency rate in through-plane direction at varied compression levels for various fiber cross-sectional shapes of the nonwoven samples containing 90% PET-10% Co-PET.....	200
Figure 5.11: the GATS absorbency rate in through-plane direction at varied compression levels for various fiber cross-sectional shapes of the nonwoven samples containing 80% PET-20% Co-PET.....	201
Figure 5.12: absorbency rate vs. median pore size for different fiber cross-sectional shapes for nonwoven samples containing 80% PET-20% Co-PET	202
Figure 5.13: schematic view of through-plane absorbency of nonwoven samples containing non-circular fiber cross-sectional shape.....	203

Figure 5.14: the GATS in-plane absorbency rate for various fiber cross-sectional shape and binder percentages	204
Figure 5.15: vertical wicking result, liquid front distance vs. time for various fiber cross-sectional shapes of nonwoven samples containing 90% PET-10% Co-PET fiber	205
Figure 5.16: liquid holding capacity of samples with different fiber cross-section and binder percentages.....	207
Figure 6.1: the schematic of the compression procedure on Instron	220
Figure 6.2: the modified NWI GATS (Compression GATS)	221
Figure 6.3: typical GATS curve.....	222
Figure 6.4: typical curves of compression pressure vs. compression percentages during loading and unloading (a) 3den, 3den/6den, 6den (b) 3den, 3den/9den, 9den (c) 3den, 3den/15den, 15den	225
Figure 6.5: compressive resistance at 40% compression and slope alpha according to van Wyk equation for (a) 3den, 3den/6den, 6den (b) 3den, 3den/9den, 9den (c) 3den, 3den/15den, 15 den.....	226
Figure 6.6: thickness recoverability for homogenous and heterogeneous layered nonwoven samples (a) 3den, 3den/den, 6den (b) 3den, 3den/9den, 9den (c) 3den, 3den/15den, 15den	228
Figure 6.7: typical GATS curve for homogeneous layered structures (a) 3den (b) 6den (c) 9den (d) 15 den	230
Figure 6.8: typical GATS curve for the nonwoven structures having a pore size expansion (a) 3den/6den (b) 3den/9den (c) 3den/15den	232
Figure 6.9: typical GATS curve for the nonwoven structures having a pore size reduction (a) 6den/3den (b) 9den/3den (c) 15den/3den	233
Figure 6.10: absorbency vs. solidity for homogenous layered nonwovens (control samples)	235
Figure 6.11: absorbency vs. solidity for heterogeneous layered structures having pore size reduction	236
Figure 6.12: absorbency vs. solidity for heterogeneous layered structures having pore size expansion	237
Figure 6.13: absorbency rate at different compression levels for homogeneous layered structures (control samples).....	238
Figure 6.14: absorbency rate at different compression levels for heterogeneous layered structure having pore size expansion (the results for the control samples of 3 denier fibers is given)	239
Figure 6.15: absorbency rate for structures having pore size reduction at different compression levels (a) 6den/3den, 6den (b) 9den/3den, 3den (c) 15den/3den, 3den	240
Figure 7.1: mean flow pore diameter of the samples with different rayon percentages	254
Figure 7.2: compression pressure vs. compression percent, different rayon fiber percentages (legend show the rayon fiber percentages)	255
Figure 7.3: compressive resistance at 40% compression- different rayon fiber percentages	256
Figure 7.4: compressive Pressure vs. cube solidity in samples containing different rayon fiber percentages.....	257

Figure 7.5: calculated slope α based on van Wyk equation.....	258
Figure 7.6: recoverability measurements in varying rayon fiber percentages	259
Figure 7.7: cross-sectional images of trilobal rayon fibers (left) dry (right) wet- instantaneously.....	260
Figure 7.8: typical GATS absorbency curve for samples containing various fractions of rayon fiber at different levels of compression	262
Figure 7.9: the GATS maximum absorption results under different compression levels for samples containing various rayon fiber percentages	264
Figure 7.10: maximum absorbency (theory, GATS) versus solidity for the samples containing various rayon percentages- solid lines shows the theoretical results and dots show the experimental result.....	266
Figure 7.11: absorbency with 0.1% triton solution (non-swelling liquid) and n-octane (swelling liquid).....	267
Figure 7.12: through plane absorbency rate of samples containing different rayon fiber percentages.....	269
Figure 7.13: through-plane absorbency rate versus pore size for the samples containing various percentages of rayon fibers	271
Figure 7.14: absorbency rate of samples containing various percentages of rayon fibers at different compression levels	272
Figure 7.15: in plane absorbency rate of samples containing different rayon fiber percentages	273
Figure 7.16: in-plane absorbency rate versus pore size for the samples containing various percentages of rayon fibers	274
Figure 7.17: comparison between the amount of liquid retention of the samples on the GATS and after removing from the GATS	276
Figure 7.18: liquid holding capacity of samples with different rayon fiber percentages at no compression after removing from the GATS.....	277
Figure 7.19: liquid holding capacity of samples with different rayon percentages under various compression percentages.....	278
Figure 7.20: liquid retention capacity versus solidity for the samples containing various rayon fiber percentages	280
Figure 7.21: liquid retention capacity versus solidity for the samples containing various rayon percentages- solid line shows the theoretical maximum absorption capacity results and cross symbols show the experimental result	281

1 INTRODUCTION

Nonwoven fabrics are a specific type of porous structure composed of fibers that bonded together by mechanical, thermal or chemical means. Nonwovens are used in a broad range of applications including wipes, medical applications such as gowns, masks, etc., hygiene products, filters, geotextiles, composites, and other durable and disposable products. One of the key applications of nonwovens is in absorbent materials which consist of a wide range of products including baby wipes and diapers, personal hygiene, tampons, adult incontinent pads, paper towels, tissues and sponges, and industrial wipes. Fluid handling is a key functionality of these products. The nonwoven fabrics need to be engineered to meet the requirement of liquid absorption depending on their particular application. In order to develop innovative product based on a scientific approach, understanding of the relation between fabric structure and liquid absorption is required (Mao and Russell 2003). This indicates the necessity of the in-depth scientific study of absorbency phenomena in nonwoven fabrics (Chatterjee and Gupta 2002a).

Major contributors to absorption and release behavior of nonwovens are geometrical aspects of the structure and the material properties, along with finish. With a given liquid, the porous structure plays an important role on the absorption properties of nonwovens. The pore size of the nonwoven structure is affected by fiber geometry including both of the size and shape of fiber, nonwoven structure which can be solidity or packing density and fiber orientations, and finally by the external factors such as compression. The fluid absorption of nonwoven materials is complex because of their complicated pore structure as well as the deformation of pore structure either due to the compression applied during the application or dimensional changes resulted from liquid absorption. Although the study of liquid absorption in porous media is a relatively mature topic, the effect of nonwoven structural parameter and materials on the pore structure and fluid absorption behavior is still indefinable.

Moreover, little attention has been paid to the interaction of fluid absorption and the porous structural changes due to compression.

Absorbency is defined as a phenomenon that deals with the absorption of liquids by porous media of nonwoven fabrics. Liquid absorption is a spontaneous flow of liquid into a porous structure, which is driven by capillary forces. The absorption mechanism has been studied as a flow through a configuration of capillary tubes using standard capillary flow equation since a century ago. Many classical theories have been frequently applied on liquid flow in porous structures through a simple capillary flow model to study their liquid absorption behavior, but with limited success. The highly complex design and intricate pore geometry of nonwoven fabrics is a major limitation of application of the classical theories on them. Although, the limitations of these models for analysis of more complicated porous structure have motivated researchers to take into account different geometrical factors (Cai et al. 2014; Young 2004; Shou, Ye, Fan, and Fu 2014; Shou, Ye, Fan, Fu, et al. 2014; Mao 2009a; Staples and Shaffer 2002; Figliuzzi and Buie 2013). The studies have shown that the physical and mechanical properties of fibers, as well as the structural and compressional characteristics of fabrics play an important role in the ability of the textile fiber assemblies to wick and hold fluid. A deep scientific understanding of the role these factors play in absorbency will significantly influence on innovative designing and more functionally effective products of future(Chatterjee and Gupta 2002a).

1.1 RESEARCH OBJECTIVES AND APPROACHES

Nowadays, the share of nonwovens market in absorbent products increases day by day, and as a consequence the industry leaders pay more attention to the absorbent properties of the products in more realistic situations. If the connection between the compression and the liquid distribution can be

made then the liquid flow can be modeled as a function of the compression pressure and from there the absorbent product can be made such that the absorbency behavior is engineered to meet a specific purpose. The first requirement for this is to measure the absorbency behavior of nonwovens fabric under compression. There are some experimental and numerical works in the field of fibrous porous materials such as nonwoven fabrics where they concerned with fluid absorption with no attention to the fluid release. Moreover, they lack any sort of control over the experimental conditions.

On the other hand, the release properties of nonwovens play a very important role in the functionality of many absorbent product including wipe, and hygiene products. To the knowledge of the writer, there is no study in this field.

Accordingly, objectives of this study are 1) to understand fluid absorption and release behavior of nonwovens and the effect of compression on these behaviors, 2) to develop techniques and protocols to evaluate the fluid absorption and release behavior under varied compression profiles, and 3) to evaluate the effects of fiber geometry and fiber absorbency on fabric pore structures and fluid absorption and release behavior on compression.

To meet the objectives of this research, this study will focus on absorbency and release behavior of nonwovens at different compression levels. For this purpose, developing the methodology and techniques is the first goal that should be met. In order to decouple the effect of structural parameters and fiber properties on the absorption properties of nonwovens, this study is divided in two phases. The effect of structural parameters and fiber absorbency properties are being evaluated in two phases of the project respectively. Two of the main factors, which define the fiber geometry include fiber size and fiber cross-section. Our initial goal is to realize the effect of fiber geometry on the pore structure and absorption behaviors of nonwovens under compression through understanding their

absorption, as well as their compression behavior. Then the effect of heterogeneity is evaluated in layered structures with non-uniform pore size along the flow direction.

Therefore experiments for the study of individual variables, which most govern the porous structure, are designed with all other well controlled. Through air bonding and binders were used in order to control solidity and keep it constant among our samples. On the other hand in order to control the compressibility of the structures, 2 different percentages of binder were used. The resiliency of the fabric is one of the factors plays an important role on determination of porous structure. Material properties also influences on the absorbency behavior, therefore in the second phase, the samples containing different percentages of absorbent fibers were produced and the effect of fiber absorbency is discussed.

1.2 ORGANIZATION OF DISSERTATION

Chapter 2 of this dissertation is a review of literature. It discusses the fundamental of fluid absorption including mechanisms of absorption both by the pore and by the fibers. Moreover the absorbency behavior is discussed in terms of nonwovens and the influencing parameters of nonwovens. It is continued by the characterization techniques of pore structure of nonwovens and their absorbency behavior. Finally it talks over the compressional behavior of nonwovens and its importance on the absorption behavior of nonwovens.

Chapter 3 of this dissertation argues how various fiber cross-sectional sizes and shapes, and binder fiber percentages influence on the resistance to compression and recovery behavior of nonwovens. Furthermore, the results are analyzed according to van Wyk compression theory as well.

Chapter 4 of this dissertation discusses the first part of the effect of structural parameters on absorption and release properties of nonwovens under compression, considering the effect of fiber

cross-sectional size. The absorption properties were measured at different flow directions. With the knowledge that the fiber size controls the pore size of the nonwovens at a given solidity, the absorption and release results were analyzed based on the solidity (porosity) and pore size of the samples at various compression levels.

Chapter 5 of this dissertation continues the study on the effect of structural parameters on absorption and release properties under compression by considering the effect of fiber cross-sectional shapes. Different geometries of pores are generated with various fiber cross-sectional shapes including round, pentagonal, and 4DG fibers. How these different pore geometry influences on absorbency behaviors of nonwovens is disputed in this chapter. The pore characteristics were measured for various fiber shapes at different compression levels.

Chapter 6 of this dissertation is the last part of the structural parameters effect study. In this chapter, the effect of heterogeneity of the nonwovens along the flow direction is discussed. For this purpose the layered structures were made considering both the pore size reduction and expansion. Furthermore, the compression and recovery properties of these samples are argued.

Chapter 7 of this dissertation is an investigation of the fiber absorbency effect. The absorbency behavior is compared for the samples containing various percentages of PET fibers (non-absorbent fiber) and rayon fiber (absorbent fibers). The rayon fiber swelling and its influence on the pore characteristics and consequently on absorption behavior is talked over.

REFERENCES

- Cai, Jianchao, Edmund Perfect, Chu-Lin Cheng, and Xiangyun Hu. 2014. "Generalized Modeling of Spontaneous Imbibition Based on Hagen–Poiseuille Flow in Tortuous Capillaries with Variably Shaped Apertures." *Langmuir* 30 (18): 5142–51. doi:10.1021/la5007204.
- Chatterjee, P. K., and B. S. Gupta. 2002. *Absorbent Technology*. Amsterdam; Oxford: Elsevier Science. <http://www.sciencedirect.com/science/book/9780444500007>.
- Figliuzzi, B., and C. R. Buie. 2013. "Rise in Optimized Capillary Channels." *Journal of Fluid Mechanics* 731 (September): 142–61. doi:10.1017/jfm.2013.373.
- Mao, N. 2009. "Unsteady-State Liquid Transport in Engineered Nonwoven Fabrics Having Patterned Structure." *Textile Research Journal* 79 (15): 1358–63. doi:10.1177/0040517509342312.
- Mao, N., and S. J. Russell. 2003. "Anisotropic Liquid Absorption in Homogeneous Two-Dimensional Nonwoven Structures." *Journal of Applied Physics* 94 (6): 4135. doi:10.1063/1.1598627.
- Shou, Dahua, Lin Ye, Jintu Fan, and Kunkun Fu. 2014. "Optimal Design of Porous Structures for the Fastest Liquid Absorption." *Langmuir* 30 (1): 149–55. doi:10.1021/la4034063.
- Shou, Dahua, Lin Ye, Jintu Fan, Kunkun Fu, Maofei Mei, Hongjian Wang, and Qing Chen. 2014. "Geometry-Induced Asymmetric Capillary Flow." *Langmuir* 30 (19): 5448–54. doi:10.1021/la500479e.
- Staples, Thomas L, and Donna G Shaffer. 2002. "Wicking Flow in Irregular Capillaries." *Colloids and Surfaces A: Physicochemical and Engineering Aspects* 204 (1-3): 239–50. doi:10.1016/S0927-7757(01)01138-4.
- Young, Wen-Bin. 2004. "Analysis of Capillary Flows in Non-Uniform Cross-Sectional Capillaries." *Colloids and Surfaces A: Physicochemical and Engineering Aspects* 234 (1-3): 123–28. doi:10.1016/j.colsurfa.2003.12.007.

2 LITERATURE REVIEW

2.1 FLUID ABSORPTION BASICS OF NONWOVEN FABRICS

Nonwovens are the assemblies of short staple fibers or infinitely long continuous filaments, which are bonded together through mechanical, thermal or chemical process. For sake of brevity a detail account is not given here, readers could refer to (Batra and Pourdeyhimi 2012) for technologies and methods used to produce nonwoven fabric. The nonwovens can be highly dense and strong and on the other hand they can be porous and compressible (Pourdeyhimi, Maze, and Tafreshi 2006). Since nonwovens are capable of forming a stable structure even at very high porosity, they are being used in many functional end-uses.

Nonwoven have been used in lots of different applications including air filters, wipes, insulations, barrier fabrics, surgical masks, cosmetic products, and hygiene products such as diapers. One of the main applications of the nonwoven is in absorbent products. In case of absorbent product the ability to absorb the liquid very fast and also holding large quantity of the liquid are very important.

Absorption phenomenon in absorbent product is a multiphase flow where the air is replaced by the invading liquid. When an absorbent product is in contact with the fluid, the fluid can be wicked by pore inside the structure or it can be absorbed by the fiber itself. In the following sections, the literatures are reviewed to cover the theoretical background of absorption phenomenon, also two different phenomena of absorption by pore and absorption by fiber.

2.1.1 Liquid absorption in the porous structure

Absorption phenomena are the spontaneous physical imbibition of a liquid in contact with a solid.

The absorption can occur by either of two different modes. In the first mode, the pores include those in the macroscopic length scale either related to a continuous porous media or a porous media in the form of closely adjacent particles. These pores are filled with the gas or vapor at ambient pressure and liquid enter the pores by bulk convection. This phenomenon is referred to as capillary absorption or wicking. In the other mode, the porous media involve the molecular dimension voids where the liquid enters by diffusion process. This process happens when the macroscopically continuous solid has a molecular structure of a cross-linked network and the molecules have sufficient affinity to cause the liquid to diffuse inward them and expand the network gradually. This generally is referred to diffusion and is accompanied by swelling phenomena(Chatterjee and Gupta 2002a). In the next section, first I will discuss the absorptions by pores and then I will explain the phenomena of absorption by fibers or diffusion.

2.1.1.1 Mechanism of absorption by pore

A porous material consists of different states of matter and the non-solid phase called as pores or void (Bear 1988). Since some of the pores are interconnected, they form an open path to others and they called open pores, while the other pores are surrounded by solid phase in the way that non-solid state cannot escape and they called closed pores. Moreover, there are dead end pores, which are open to one side of porous media, but they end inside the structure. Depending on the invasion direction, the liquid may enter these pores however cannot flow through the porous structure.

Two main processes in describing the liquid uptake and transport into the materials include wetting and wicking. Wetting is the displacement of a fiber-air interface with a fiber-liquid interface. Wicking

phenomena is spontaneous transport of liquid into the porous structure by capillary force. The liquid is able to wick into a fabric and being transported by the porous structure only if it at least partially wets the fibers (Kissa 1996; Patnaik et al. 2006; Pan and Zhong 2006). In order to wicking be practically significant, the interfacial areas in the system should be large in comparison with the bulk volume. It means that the ratio of solid-liquid interfacial areas is large compared to the liquid bulk volume (Chatterjee and Gupta 2002b). The two phenomena of wetting and wicking will be discussed in the following section.

2.1.1.1.1 Wetting

Wetting is a very important and complicated phenomenon, which influences many manufacturing processes, as well as the functionality of end use materials. Wetting phenomena is even further complicated in case on fibrous materials. The wetting of a solid surface is resulted from its contact with a specified liquid under specific conditions (Patnaik et al. 2006).

Considering the molecules of a liquid, the molecules in the bulk of liquid have an equal attractive force in all directions. However, molecules in the surface of the liquid experience an imbalance of force, with the net force directed towards the interior or the bulk liquid. This causes that the molecules in this dynamic surface layer always has a tendency to move towards the interior.

Consequently there is a free energy at the surface of the liquid. This energy is called "surface free energy" of the liquid and it tends to keep the liquid surface area in a minimum and so it prevents from the advancement of the liquid over the solid surface. In the interaction of the liquid with a solid surface, if the solid surface has a sufficient surface energy, which overcomes the free surface energy of the liquid, the liquid can wet the solid completely. Surface free energy is also termed as surface tension and is quantifies as force per unit length with unit of mN/m or dynes/cm (Patnaik et al. 2006). The surface tension of a liquid is a force parallel and in the surface of the liquid. The surface tension

and the specific surface free energy are dimensionally and mathematically identical, however the specific surface energy is more general and it can be used for solids as well as liquid surfaces and interface. The driving force in any closed systems comes from the tendency for minimizing the free energy of the system, F . To spontaneously change the system configuration in a capillarity system, it is required that the dF of the whole system be negative and not just for the phase interfaces (Chatterjee and Gupta 2002b).

Considering the liquid resting on a solid surface, there are various contact interactions as it is shown in the figure 2.1 between solid, liquid and vapor.

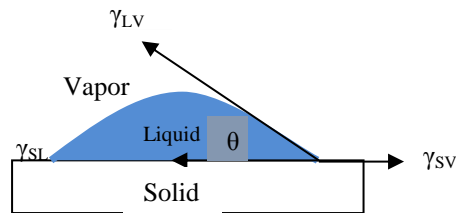


Figure 2.1: liquid drop resting on the solid surface

The forces involved in this situation are given by the Young-Dupre equation as it is shown in the equation (2.1).

$$\gamma_{SV} - \gamma_{SL} = \gamma_{LV} \cos \theta \quad (2.1)$$

γ is the interfacial tension that exists between the contacting surfaces and S, L and V stand for solid, liquid, and vapor and θ is the equilibrium contact angle. This equation is widely used in explaining wetting and wicking, although the equation is valid only for a drop resting at equilibrium on a smooth, homogeneous, impermeable, and nondeformable surface. The young equation appears as a force balance derivation, and consequently it leaves the quantities of the terms γ_{SV} , and γ_{SL} undefined

operationally and almost impossible to measure. It is the motivation behind some study to define the young equation with a thermodynamic meaning (Adam 1964; Adamson and Ling 1964). According to Young-Dupre equation, the contact angle provides the relation between the adhesion of the liquid to the solid, and its cohesion to itself (Adam 1964).

The wetting phenomena in non-ideal surfaces such as nonwoven surfaces are complicated because of surface roughness and other factors. The contact angle, θ , as it is shown in the figure1 is the angle between the tangent to the liquid-vapor interface and the solid-liquid interface and consequently it depends on three interfacial tensions γ_{SV} , γ_{SL} , and γ_{LV} . When the interfacial energy of the solid in contact with vapor (γ_{SV}) is higher than the interfacial energy between the solid and the liquid (γ_{SL}), the solid- air interface is replaced by the solid-liquid interface. In this situation, θ must be between 0° and 90° . If γ_{SV} is smaller than γ_{SL} , the contact angle will be between 90° and 180° . In the other word, if the adhesion of the liquid to the solid is less than the self-cohesion of the liquid to itself, a contact angle takes place between the liquid and solid. Larger the contact angle, lower is the adhesion between the solid and liquid. Otherwise, if the adhesion is equal to or greater than the cohesion, the contact angle is zero and the liquid spread over the surface of the solid and is said to wet the solid. Therefore two different equilibrium regimes may be found including partial wetting with a finite contact angle θ , or complete wetting ($\theta=0$) as it is shown in figure 2.2 (de Gennes 1985).

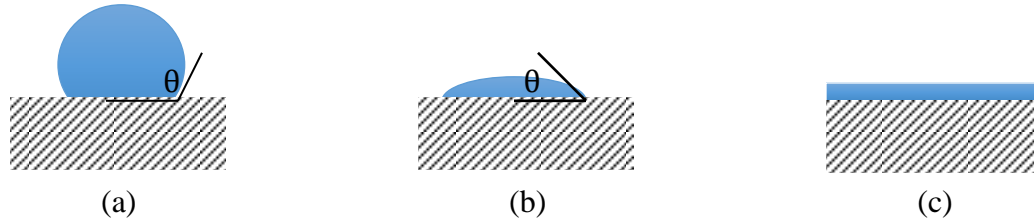


Figure 2.2: a small droplet in equilibrium over a horizontal surface:(a) and (b) partial wetting, while wetting being stronger in (b), (C) complete wetting ($\theta=0$) (de Gennes 1985)

In the other way, for a given system of liquid, solid, and air contact, it may be shown that (Richards 1931).

$$\gamma_{LV} + \gamma_{SV} - \gamma_{SL} = W = \gamma_{LV}(1 + \cos \theta) \quad (2.2)$$

Where γ_{LV} , γ_{SV} , and γ_{SL} are the surface densities of free energy for the air-liquid, air-solid and liquid-solid respectively, θ is the contact angle between liquid-solid interface, and W is the work necessary to separate unit area of liquid from solid. If $W < 2\gamma_{LV}$, θ may vary anywhere between 0° and 180° . If, However, $W \geq 2\gamma_{LV}$ then θ is zero and the liquid will spread over the solid surface. It means that the liquid wet the solid (Richards 1931).

Zisman introduced an empirical criterion for the wetting of solid substrate. The critical surface tension for each solid substrate (γ_c) determines the wetting situation of a solid with a given liquid.

There is partial wetting when the liquid surface tension $\gamma > \gamma_c$ and total wetting when $\gamma < \gamma_c$ (Zisman 1964).

Spreading is the flow of liquid at least two molecular layers thick over a solid. In spreading the solid-liquid and liquid-vapor interfaces increase, while the solid-vapor interface decreases. In non-equilibrium situation, we have the spreading coefficient, which is defined based on the interfacial energies as below:

$$S = \gamma_{SO} - \gamma_{SL} - \gamma \quad (2.3)$$

Where γ_{SO} is a solid/vapor interfacial energy associated with a dry solid surface, while γ_{SV} is the solid/ vapor interfacial energy in a moist surface. For spreading to be spontaneous, the spreading coefficient has to be positive (Patnaik et al. 2006; de Gennes 1985).

The Physical contact angle is the physically measurable angle between the liquid-air interface and the solid-liquid interface in a static liquid-solid-vapor system. In this definition, it does not matter whether or not the system is in stable thermodynamic equilibrium. The equilibrium contact angle, however, is defined in terms of the interfacial free energies at three-phase line boundary by Young's equation. The physical contact angle and equilibrium contact angle are not necessarily equal. With special manipulation, the physical contact angle might show a higher or a lower value. The highest achievable static value of physical contact angle is called the advancing contact angle and the lowest static value is called the receding contact angle (Minor et al. 1959).

A serious practical problem associated with the concept of contact angle is the fact of existence of hysteresis between advancing and receding contact angles. The advancing contact angle is measured when the fluid intruding the capillary and displacing another fluid. The displaced fluid is usually understood to be the vacuum; in contrast the receding one is measured through the same fluid while it is being displaced. Therefore the contact angle measurement is very difficult (Dullien 1991). Gupta and Whang showed while the receding value is governed mostly by the chemical make-up of materials, the advancing is influenced by other factors such as the physical and morphological structures, properties such as molecular orientation, crystallinity, and surface texture or roughness (Gupta and Whang 1999). According to Adamson, the three types of causes of contact angle hysteresis are contamination of either liquid or solid, surface roughness, and surface immobility on a macromolecular scale. The immobility, for example, happens where the liquid contains a surfactant (Adam 1964).

Either the liquid or solid movement by some external factors results in the changes in static arrangement of an equilibrium liquid-solid contact angle. This phenomenon is very critical especially in the situation where the dynamic wetting behavior of system is important for instance in coating process. Researchers showed that the dynamic contact angles are strong functions of the apparent viscosity of the liquid at the particular wetting speed whether the liquid is Newtonian or non-Newtonian.

Surface wetting characteristics of fibers include the cosine of contact angle, the work of adhesion, and the surface energy. All of these characteristics are related as we observed in the previous discussion, but they describe various behaviors. Surface energy is the inherent ability of a material to interact with other materials and the contact angle is the result of such interactions. Employing two different liquids, one polar and one non-polar liquid in order to determine the surface energy of the materials, it is possible to determine the polar contribution and dispersive contribution of surface energy of the solid. In the fluid absorption properties, the contact angle plays a very important role and the cosine of contact angle represents the wettability of a materials and also it is used in predicting the capillary forces and imbibition rate of a fluid as we discuss them later (Gupta with Hyun Suk Whang 2000). The contact angle can be obtained via different methods (a) from a direct photograph (b) from the reflection (or deflection) of rays by the liquid prism (c) by knowing the interfacial energies, especially for small contact angles (d) from the rise of liquid column in a fine capillary. We will discuss the latter techniques in the section 2.1.1.1.2 (de Gennes 1985).

There are different methods available for measuring the contact angle in fibers. The static contact angle can be measured by direct observation of the physical contact angle on the fiber through optical microscopy. But the value obtained from this method is not satisfactory for fibers due to the irregularity and heterogeneous in characteristics along the fiber length. The other method, for

determination of dynamic contact angle is through wilhelmy principle. The Wilhelmy dynamic procedure is considered to be the most effective and useful way of assessing this property (Gupta with Hyun Suk Whang 2000). In this method, the vertical component of advancing and receding attractive forces across an interface between a liquid surface and a partially immersed solid is calculated.

According to the Wilhelmy formula, the pull, F , exerted on a solid rod inserted into a mass of liquid is expressed as

$$F = p\gamma \cos \theta \quad (2.4)$$

Where p is the perimeter of the solid rod along the three-phase boundary line, γ is the liquid surface tension, and θ is the contact angle of the system. The validity of this equation is questioned in some authorities (Minor et al. 1959).

However it is difficult to conduct this method on staple fibers because they are short, fine, or crimped (Gupta with Hyun Suk Whang 2000). Moreover a challenging part for conducting this method is the calculation of perimeter of the fiber at the three-phase contact line. This is a problem mainly in the situation that the liquid does not wet the fiber completely.

Whang and Gupta studied the wetting forces for cotton, rayon Galaxy, and regular rayon through wilhelmy testing method. They used the sinkers in order to assure that fibers are straight, rigid, and vertically oriented during immersion (Gupta with Hyun Suk Whang 2000). Therefore the force measured by the microbalance is

$$F = mg + F_w - F_{bs} - F_{bf} \pm F_v \quad (2.5)$$

$$F_w = P\gamma_{LV} \cos \theta \quad (2.6)$$

Where mg is the combined weight of the sample and sinker; F_w the actual wetting force, F_{bs} the buoyancy force of the sinker, F_{bf} the buoyancy force of the sample, and F_v is the viscous frictional force of the liquid on the fiber sample. The viscous frictional force has the negative sign for

advancing and positive sign for the receding mode. Usually the weight of the sample and sinker is tared out at the beginning of the test. Also the viscose frictional force and buoyancy force of the fiber are negligible compared to wetting force. The Sinkers buoyancy force can be calculated from the dimension of the sinker and the density of the liquid. They also measured the perimeter of the fibers through image analysis of SEM micrographs of fiber cross-sections. The result showed the wetting forces vary among different fibers with Galaxy rayon fiber having the largest, regular rayon the lowest, and cotton an intermediate value. On the other hand, the fluctuations vary in reverse order. They are maximum for regular rayon and minimum for Galaxy. The fluctuations in the wetting force represent the random or systematic surface irregularities (Bendure 1973). It was also observed that Galaxy fiber with trilobal cross-section having the lowest and rayon fibers the largest contact angle. The cosine of contact angle reflects the relative abilities of these fibers to attract and imbibe fluid by capillary action. This was in agreement with their separate study showing the webs made of Galaxy and cotton had much higher rates of water absorption than a web of regular rayon with the same structures. The lowest hysteresis between the receding and advancing contact angle was observed in case of Galaxy fibers. The Galaxy fibers is spun from a standard viscose solution employing standard spinning conditions, the only exception is that the spinneret holes are trilobal rather circular, and compared to regular rayon has higher purity, smoother, and more homogenous surface (Wilkes and Bartholomew 1995). This is why less hysteresis and fluctuation is observed in Galaxy fibers. They also discussed the difference in cross-sectional morphology of Galaxy fibers having the longitudinal ridges along the surface of the trilobal fiber as another factor results in a lower hysteresis. The ridges imbibe the fluid ahead of the fluid-fiber interface, and it makes the situations of the advancing and receding mode more comparable. They also measured the polar and dispersive surface energy of different fiber by immersing a fiber separately in two different liquids with known polar and

dispersive contributions to the surface tension. In case of hydrophilic materials such as cellulosic fibers, polar contribution accounts for larger portions of the total energies.

Table 2.1: surface energies of different fibers (Gupta with Hyun Suk Whang 2000; Gupta and Whang 1999)

Fiber	Advancing contact angles in Water	Surface energy, mN/m		
		Polar	Dispersion	Total
Cotton	34.0	41.6	19.3	60.9
Galaxy (Rayon with trilobal cross-section)	21.5	51.7	16.4	68.1
Regular Rayon	55.5	24.4	21.7	46.1
Cellulose acetate	54.8	17.4	35.04	52.4
Polyester	79.2	4.1	37.74	41.88
Polypropylene	98.5	1.8	21.2	22.99

In another research (Gupta and Whang 1999), Gupta and Whang studied the surface wetting behaviors of polyester, polypropylene, and cellulose acetate fibers in several different sizes and cross-sectional shapes. They observed that among these fibers, the cellulose acetate has the lowest and polypropylene the highest value of the contact angles. These differences are largely due to the differences that existed in the chemical structures of the fibers. Cellulose acetate fibers, among the three, have the highest value of the wettability index because of the molecular structure of the fiber. The cellulose acetate fiber is only partially acetylated by replacing some of the hydroxyl groups by comparatively inert acetyl ($\text{CH}_3\text{COO-}$) and still had hydroxyl groups. Moreover the better wettability property of polyester fibers over polypropylene is because of the presence of more polar ester groups. Polypropylene is strictly a hydrocarbon material and lacked such groups. The values of total surface energy, as well as polar and dispersive contribution of the surface energy for these fibers is given in table 2.1. The surface energy is highest in cellulose acetate fiber, polyester fibers, and polypropylene fibers respectively. Also it is seen that the polar fraction of polypropylene fibers, and polyester fibers are not sizable with the dispersive fraction. They also showed that the assumption of a zero receding

contact angle for a low surface tension fluid which wet out a fiber is not always valid. For instance use of hexadecane as the fluid on cellulose acetate did not support this assumption and led to the underestimation of the perimeter values.

2.1.1.1.2 Wicking

Spontaneous flow of a liquid in a porous structure is called wicking, which is driven by capillary pressure, and partially wetting is a prerequisite for wicking. It was seen in the previous section that the initial wetting process, in which a liquid spread over a dry porous medium, is involved with the adhesive forces due to their influence on the contact angle. But after the medium is wetted the adhesive force does not influence on producing a motion of the liquid. They just hold the adsorbed thin layer in contact with the solid surface and the liquid outside the adsorbed layer is free to move under the action of unbalanced forces (Richards 1931).

According to the fiber-liquid interactions, the wicking processes can be divided into four categories: capillary penetration only; simultaneous capillary penetration and diffusion of the liquid into the interior of the fibers; capillary penetration and adsorption of a surfactant on fibers; and simultaneous capillary penetration, diffusion of the liquid into the interior of the fibers, and adsorption of surfactant on fibers. Wicking can be taken place from an infinite liquid reservoir and wicking from a finite or limited reservoir (Pan, Gibson, and Textile Institute (Manchester) 2006).

The term capillarity initially used to describe the action of liquids in fine tubes. However it is nowadays used in connection with a wide variety of phenomena including the flow of liquids through porous media. It was indicated that the capillary conduction of liquids through porous media is similar to the flow of liquids through pipes or fine tubes to the extent that the flow may be described in terms of the pressure gradient in the liquid and gravity (Richards 1931). Therefore, capillary pressure is a basic parameter in the study of the liquid transport into a porous medium. A capillary

phenomenon is resulted from the forces acting in the boundary surfaces of liquid, and the origins of these forces are in the cohesive and adhesive attractions, which are applied between molecules. One of the most prevalent cases of capillary action takes place when one surface of the liquid is in contact with air. In the case of contact between the liquid and solid such as liquid flow in porous media, the free energies of these surfaces also play an important role.

Capillary pressure relates the pressures in the two fluid phases. In a single capillary tube, the capillary pressure is defined as the pressure increment between the concave side and the convex side of a meniscus (Dullien 1991). Pressure in the capillary flow of a porous medium is determined by the tension and the curvature of the air-water interface. The difference in the pressure across the concave, P_1 , and the pressure in the convex side, P_2 , of the curvature of a liquid-vapor interface is caused by the liquid surface tension, γ , and is given in the Young-Laplace equation as below:

$$P_1 - P_2 = \gamma \left(\frac{1}{r_1} + \frac{1}{r_2} \right) \quad (2.7)$$

In which r_1 , and r_2 are the principal radii of curvature of the surface.

Liquid surface free energy decreases due to the curvature of meniscus in the narrow boundaries of the pores (Since shrinking decreases the surface energy), the tendency of do so must be balanced by a pressure difference across the liquid-air interface ΔP such that the work against this pressure difference is just equal to the work done in forming the additional amount of surface in the curvature of meniscus (Adamson 1997).

Applying this definition into the liquid movement into a pore structure, the capillary pressure means the differential pressure across the liquid-air interface due to the meniscus curvature in the narrow confines of the pores (Chatterjee and Gupta 2002b). For a capillary with a circular cross section where the two principal radii of the curvature (r_1 and r_2) are equal, the Laplace equation (given in equation 6) is commonly used to express the magnitude of the capillary pressure. This equation is

applied to simple capillary tubes. Moreover in this equation the radius of curvature is converted to capillary pore radius through the geometrical relationship between these two as shown in figure 2.3

$$p = \frac{2\gamma \cos \theta}{r_c} \quad (2.8)$$

r_c : The capillary (pore) radius

γ : The surface tension of the advancing liquid

θ : The contact angle at the liquid-solid-air interface

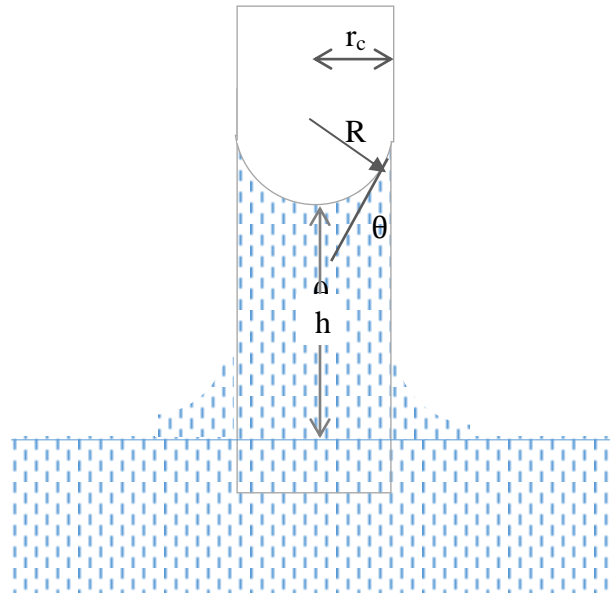


Figure 2.3: schematic of capillary filled with the liquid (wicking) (Pan and Zhong 2006)

As it was mentioned in the previous discussion, contact angle is a material property. Consequently according to Laplace equation, the magnitude of the capillary pressure is related to the material properties through contact angle and also to the structure through capillary radius that is the pore radius in the nonwoven structure. Equation 2.6 indicates that lower the pore radius, higher the magnitude of the capillary pressure is. Thus, considering the capillary pressure as a driving force for

wicking phenomena, it means that for a given liquid and a specific nonwoven material, the wicking phenomena occurs more spontaneously in the structure with smaller pore diameter.

Minor III, et al. studied the behavior of different liquids on parallel array of the two fibers for a thorough understanding of the wicking process. They observed that the liquid did not wick in a system of higher contact angle until the fibers were spaced enough close to each other. From a thermodynamic point of view, wicking occurs when the changes in the free energy of the system, dF , relative to the changes in the distance traveled by the liquid front, ds , in the direction away from the liquid reservoir is negative. The free energy changes can be described through the equation 2.9

$$\frac{dF}{ds} = \frac{d}{ds} (\text{Area } LV) \cdot \gamma_{LV} + \frac{d}{ds} (\text{Area } SL) \cdot k_2 \quad (2.9)$$

Where γ_{LV} is the interfacial free energy of liquid-air interface and k_2 is the difference between the interfacial free energy of solid-liquid interface, γ_{SL} , and solid-air interface, γ_{SV} . In the system, where the contact angle is less than 90° , k_2 is negative and only in these system dF/ds can be negative and the wicking can occur. In a close spacing between the two parallel fibers, the $d(\text{Area } LV)/ds$ decrease while $d(\text{Area } SL)/ds$ remain constant. In this situation, wicking takes place (Minor et al. 1959).

The capillary pressure equation is also defined and derived by the internal wetting force (F_{wi}) in the capillary area (πr_i^2)

$$p = \frac{F_{wi}}{\pi r_i^2} = \frac{2\pi r_i \gamma \cos \theta}{\pi r_i^2} = \frac{2\gamma \cos \theta}{r_i} \quad (2.10)$$

Capillary forces can be measured with a microbalance through vertically connecting a capillary to the microbalance (Hsieh 1995).

When the capillary rise is stopped, the capillary pressure must be equal to the hydrostatic drop in the column of liquid in the capillary due to the gravity.

$$\Delta P = \Delta \rho g h = (\rho - \rho_v) g h \approx \rho g h \quad (2.11)$$

Where ρ and ρ_v are the densities of the liquid and the vapor. The maximum height reached by the liquid is expressed as Jurin's equation and it is given as below:

$$h_{eq} = \frac{2\gamma \cos \theta}{r\rho g} \quad (2.12)$$

In this system, in case of having a contact angle lower than 90° or positive $\cos \theta$, the capillary pressure is higher than zero and spontaneous intrusion of fluid into the pore structure occurs. On the other hand for contact angle higher than 90° or negative $\cos \theta$, the capillary pressure is negative and fluid cannot intrude spontaneously (Figure 2.4). Visualizing the porous medium as an assemblage of capillaries, the combined pressure in all capillaries will give rise to the capillary pressure.

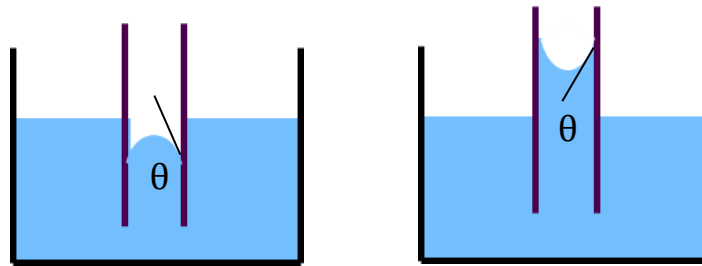


Figure 2.4: schematic of (Right) positive capillary pressure for a wetting liquid (Left) negative capillary pressure for a non-wetting liquid

2.1.1.1.3 Liquid penetration through Porous materials

The Capillary flow might happen in two different modes in the porous mediums. The “wetting” process is the process in which the wetting phase displaces the non-wetting phase. This process is also called “spontaneous imbibition”. If the capillary pressure is defined as the difference between the pressure of non-wetting phase and wetting phase, the capillary pressure must be decreased in a wetting process. It means the pressure on the non-wetting phase is gradually decreased. In this case, the wetting fluid will penetrate into the capillary (displacing the non-wetting phase) until the locally widest pore cross-section, with the greatest pore radius is reached. At this point, the capillary pressure is a local minimum and the capillary pressure is less than the minimum capillary pressure in the

narrower portion of pore with the smaller pore radius. Therefore the intrusion of the wetting phase happens in a non-equilibrium manner in the narrower portion of pores. The non-equilibrium penetration of the wetting phase continues until the meniscus reach the next wider pore cross-section. At this point in order to continue penetration, it is required to reduce the pressure applied on the non-wetting phase further. On the other hand, "Drainage" is the process in which the non-wetting phase displaces the wetting phase. This process also called as "desaturation" or "de-wetting". The throat pore is defined as the local minimum pore radius. In drainage process, the non-wetting fluid will penetrate into the capillary (displacing the wetting phase) until the pore throat is reached. At that point the capillary pressure must be increased further to overcome the equilibrium value at the pore throat. Since the capillary pressure at the pore throat exceed the equilibrium value in the expanding portion of pores with larger pore radius. When the capillary pressure is enough to displace the non-wetting phase in pore throat, the displacement of the wetting phase happens in the expanding portion of the pores in a non-equilibrium penetration manner. This non-equilibrium penetration continues until the meniscus reached the next narrower pore throat. At this point, it is required to increase the pressure applied on the non-wetting phase further in order to penetration of non-wetting phase continues (Dullien 1979). The non-wetting phase in these definitions is non-wetting only relative to the certain other fluids, which had greater wettability with the solid surface preferentially.

One of the limitations of the capillary pressure concept is the existence of the phenomenon of hysteresis. In other word, the capillary pressure curves are different for drainage and imbibition process. The instability of interface configuration is one reason for the hysteresis (Scheidegger 1974). In the liquid absorption on nonwovens, basically it is assumed that the air at atmospheric pressure is the non-wetting fluid and the nonwoven as an assemblage of the pores is connected with a preferentially wetting fluid that is also in atmospheric pressure. In this situation, a meniscus will be

formed in the connecting area of porous medium with the wetting fluid. There will be a pressure drop in the wetting fluid between the concave side of the meniscus and the convex side where the air is at atmospheric pressure. The meniscus will advance spontaneously to the convex side. This process is called “free spontaneous” or “uncontrolled” imbibition.

There are some limitations in the application of Laplace equation into nonwoven structures in order to determine the capillary pressure. Some of the aspects which make a nonwoven structure a complex structure and cause some limitation to the application of Laplace equation to the nonwoven structures include different sizes of pores, interconnectivity of pores in three-dimensional network, and tortuous path of liquid inside the porous media.

The wicking dynamics or the kinetics of wicking is very important in absorption behavior of fibrous materials. In the following, we are going to discuss it.

The Hagen-Poiseuille law for laminar flow through pipes can be employed for an idealized tube structure. This law states that the volumetric flow rate is proportional to the pressure drop gradient along the tube.

$$q = \left(\frac{r_c^2}{8\eta} \right) \frac{\Delta p}{L} \quad (2.13)$$

Where Δp in the net driving pressure or pressure drop across L , r_c the capillary radius, L the wetted length of tube, η the fluid viscosity, and q the volume flux. As the Hagen-Poiseuille law is applied to capillary rise, L would be the height of rise and Δp would be $p - \rho g L$ for upward flow where p is the capillary pressure given by Laplace equation, ρ is the liquid specific gravity, and g is gravitational acceleration.

There are different ways that the fluid flow in the porous media can be viewed. The porous media can be considered, as an assemblage of conduit and therefore it is required to estimate the equivalent

channel diameter of the conduit. Moreover, the porous media can be looked at as an assemblage of submerged objects and the drag resistance will be studied.

In one approach, the liquid flow into a porous material is described by Lucas-Washburn equation (Chen et al. 2009). Lucas-Washburn equation (equation 2.14) is the equation that deals with the wicking or the rate of liquid penetration into the capillaries when they are under capillary pressure and flow happens from a saturated reservoir. This equation is resulted from applying the Hagen-Poiseuille law to the capillary diffusion and determines the variation of liquid height as a function of time in a one direction. Therefore, rate of liquid penetration into a horizontal capillary and under the capillary pressure is defined as:

$$\frac{dl}{dt} = \frac{r \gamma}{\eta 4l} \cos \theta \quad (2.14)$$

In case of vertical wicking where the flow is resisted by gravity, the rate of liquid penetration is defined as

$$\frac{dl}{dt} = \frac{r^2}{8\eta l} \left(\frac{2\gamma \cos \theta}{r} - \rho g l \right) \quad (2.15)$$

Where l is Height of liquid at time t , r the capillary (pore) radius, γ the surface tension of liquid, η the viscosity of the liquid and θ is the contact angle between liquid and fiber.

It shows that the rate of liquid penetration, when it is only under its own capillary pressure is directly proportional to the pore radius, to the cosine of contact angle (wettability index), to the ratio of the surface tension to the viscosity of the liquid and on the other hand inversely proportional to the capillary rise or the length already filled by the liquid (Washburn 1921). It is noteworthy to mention that the flow is resisted also by a viscose shear stress exerted by the capillary wall.

By integrating the equation 2.14, Washburn suggested the correlation between the penetration distance by a liquid and time as in equation 2.16. This law ignores the gravitational effect and holds

when a liquid flow under capillary pressure alone into a horizontal capillary or one with a small internal surface (Washburn 1921).

$$h = \left(\frac{\gamma r \cos \theta}{2\eta} t \right)^{0.5} \quad (2.16)$$

This law shows the importance of the interaction of liquid with the surface by the term $(\gamma \cos \theta / 2\eta)$, which is called the coefficient of penetrance or the penetrability of the liquid, as well as the capillary structure by the term capillary radius or r . In order to apply the Washburn equation into the penetration of liquids into a porous structure, it is assumed that the porous medium behaves as an assemblage of very small cylindrical capillaries (Washburn 1921). According to this equation, the depth of penetration into a uniform porous structure increases as the square root of time.

This equation shows that the same as capillary pressure, the rate of liquid intrusion for a given liquid is also affected by the material properties through the cosine of contact angle and the structure of the material through pore radius. However in the later one, the rate is in direct relationship with the pore radius, but the capillary pressure is in inverse relationship with the pore radius. In the other word, the lower the pore radius, the higher the capillary pressure and the lower the rate of liquid penetration are. The Laplace equation and Lucas-Washburn equation show the importance of the pore size in the absorption behavior. Higher capillary pressure in smaller pore size result in the greater liquid advancement in a smaller pore, however it should be mentioned that the mass of liquid that can be hold by a small pore size might be lower than a large pore.

Washburn's model of flow in the situation of liquid infiltration into an inclined capillary tube with liquid being introduced at one end was given as below

$$u = -K_s [\nabla P + \rho g \sin \alpha \hat{x}] \quad (2.17)$$

Where P is the pressure, ρ is the density of the flowing liquid, g is gravitational acceleration, α is the inclination of the tube, K_s is the saturated permeability and \hat{x} is a unit vector.

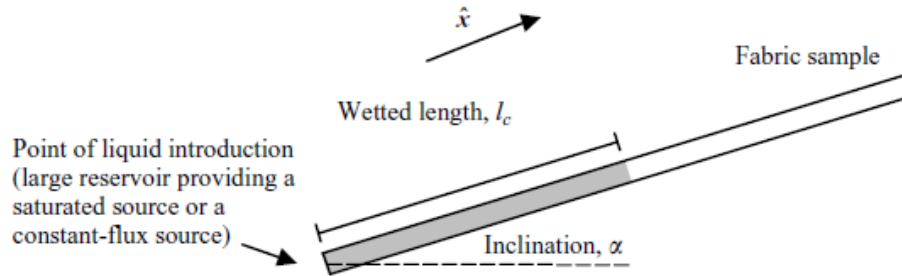


Figure 2.5: liquid infiltration through an inclined capillary tube (M. Landeryou, Eames, and Cottenden 2005)

By integrating the above mentioned equation over a distance l_c , and imposing the boundary conditions, for an upward inclined capillary tube, the below equation is obtained

$$l_c \frac{dl_c}{dt} = K_s P^* - l_c K_s \rho g \sin \alpha \quad (2.18)$$

Where P^* is the pressure at l_c .

For horizontal capillary tube with $\alpha=0$, the flow only is driven by capillary forces at the meniscus and the equation becomes

$$l_c = (2K_s P^* t)^{1/2} \quad (2.19)$$

Therefore the length of wetted region grows diffusively.

And finally for the case of inclined downwards with $\alpha < 0$, the only forces that act on the flow are the gravitational acceleration and a retarding viscous drag force, and it is independent of the capillary pressure. The equation in this situation is as follow:

$$l_c = -K_s \rho g t \sin \alpha \quad (2.20)$$

In this situation, the length increases linearly with time (M. Landeryou, Eames, and Cottenden 2005).

There are, however, several criticisms on Washburn equation when we employ it for the case of fibrous porous media such as nonwovens. In Lucas-Washburn equation, porous media is modeled

and assumed as a bundle of capillary tubes, but in real porous media, the pores are interconnected and it is the reason behind the intrinsic permeability to fluid flow. The main limitations of the Lucas-Washburn equation for applying the equation to the nonwoven systems include not considering the gravity effect, difficult measurement of the pore radius and considering a constant contact angle. Moreover one of the assumptions in the Washburn equation is the complete saturation under wetting front for all time. However under gravitational effects, Corey has been shown that the mean radii of the interface curvature continually change as the wetted length increases. The changes in radii and capillary pressure resulted in variation in saturation profile across the sample (Corey 1994). Finally it should be noticed that based on Washburn equation, we will have:

$$\frac{dl}{dt} \rightarrow \infty, \text{ as } t \rightarrow 0 \text{ (or } l \rightarrow 0)$$

Therefore this approach is somewhat questionable in cases that one would wish to extrapolate the capillary rise data obtained from Washburn equation to time=zero, For example in high instability of the initial structure of the medium with liquid penetration, such as in characterizing the wettability of solid particles. However experimental dl/dt may be readily extrapolated to $l \rightarrow 0$ (Szekely, Neumann, and Chuang 1971). Szekely, et al. took inertial and gravity forces into account to resolve this inadequacy, however the resulting equation is a nonlinear, second order, ordinary differential equation that cannot be solved analytically (Masoodi, Pillai, and Varanasi 2007). Masoodi, et al. employed a new energy balance method, as well as capillary method based on bundle of capillary tube assumption in order to determine the suction pressure for pulling up the liquid through a polymer wick. In the energy balance method, He considered the amount of energy required to raise the liquid in the wick is equal to the sum of the viscose energy dissipated by the fluid, the energy needed to accelerate the fluid from zero to the wicking speed, and required energy against gravity effect. Neglecting the inertial energy and gravity, the surface energy released due to the wetting is equated to

the viscous loss due to the liquid motion. He showed that energy balance method in conjunction with gravity provides the most satisfying prediction. Compared to capillary method which is based on the assumption of hypothetical capillary tube, energy balance method includes some additional microstructural parameters such as porosity, effective bead radius, and the mean pore size compared to the capillary model (Masoodi, Pillai, and Varanasi 2007).

Hamraoui studied the modeling of the complex structure of porous media as an assembly of vertical capillaries. In his approach, he considered gravity, inertia, and viscosity of the liquid acting as opposing forces for the liquid rise in the capillary and as sources of energy dissipation and on the other hand, surface tension as a contributory force for the capillary rise. As it is shown in figure 2.6, an oscillatory regime is observed in the height versus time around the equilibrium height. However this oscillation disappears when the capillary radius is lower than the critical value since above the critical value the effect of inertia is significant. He proposed the relation for calculating the critical capillary radius.

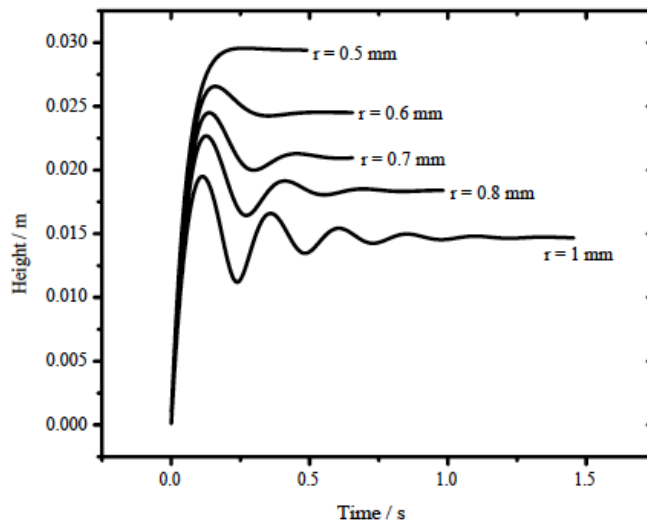


Figure 2.6: numerical results of rise of water in glass capillaries of different radii versus time (Hamraoui and Nylander 2002)

They showed that in case of capillary rise of a nonviscous liquid moving inside a porous media, the dominant forces are because of the gravity and the surface tension except at short times. The main difficulties discussed in this paper lied in separately estimation of the effective mean radius of the capillaries and the contact angle between the liquid and the pore. The dynamic nature of the contact angle between the liquid meniscus and porous media is what makes the contact angle a complex issue. They considered the dynamic character of the contact angle via introducing a retardation coefficient, which accounts for viscous dissipation, as well as frictional dissipation. Neglecting the effect of inertia and liquid viscosity in non-viscous liquid, this paper predicts a linear relationship between the height of liquid rise and time, which is in contrast with the original Lucas-Washburn equation (Hamraoui and Nylander 2002).

In order to better understanding of the capillary behavior of more complex systems, Mason et al. studied the capillary behavior of a perfectly wetting liquid in irregular triangular tubes. It is obvious that a composite of flat or convex surface can model the pore structure of highly complex pore structures better than the commonly assumed cylindrical tubes since the meniscus curvature is the parameter that directly is related to capillary pressure through $P_c = \sigma C$, where P_c is the capillary pressure, σ the interfacial tension, and C the meniscus curvature. Moreover, the angular corners in the triangle pores can retain liquid and a wide range of pore shapes can be obtained in this way. During drainage, a triangular tube may show a threshold drainage curvature, at which the level of wetting phase saturation is lowered to a definite level at constant curvature, although, once the central portion of the tube has emptied along the entire tube length, decrease in the saturation level is followed with increasing curvature. This later part is related to further removal of liquid from the corners or by evaporation. For triangular pores with an aspect ratio of base to height beyond about 5, they showed the latter regime in the dominant drainage mechanism. As it can be seen in figure 2.7, the curvature C_i

at which the arc meniscus forms an unstable cylindrical interface in the imbibition phase is lower than the threshold curvature C_d at which the central region drained in drainage phase; this means that the tube fills at a lower curvature than that at which it empties, and therefore it exhibits curvature hysteresis. At C_i the liquid in the tube redistribute spontaneously to fill part of the tube. This spontaneous redistribution of the liquid is accompanied by the rise of curvature from C_i to C_d . Finally, they defined a natural normalizing shape factor is shown to be A/P^2 (where A is the triangle area and P its perimeter). Tubes with the same shape factor show the same capillary behavior. Even though they are geometrically different (Mason and Morrow 1991).

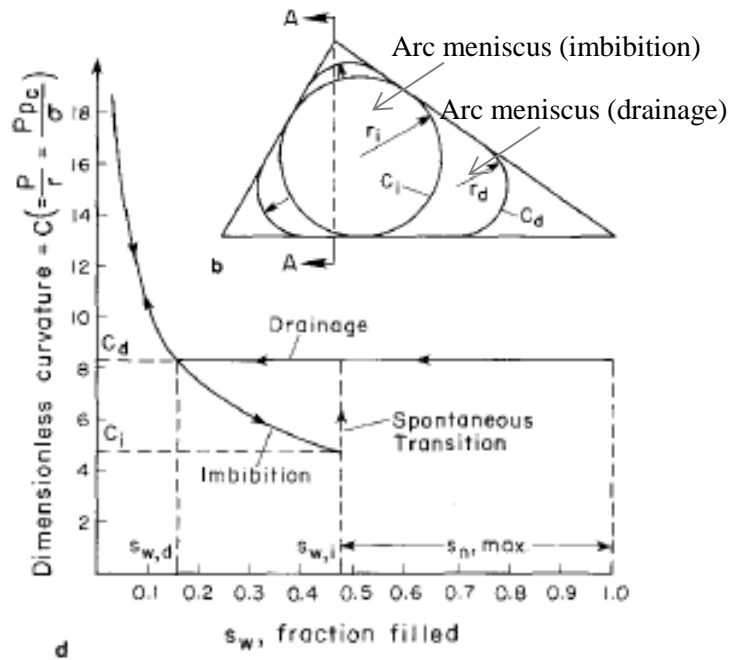


Figure 2.7: imbibition and drainage of triangular tube- curvature vs saturation for a triangular tube (Mason and Morrow 1991)

Young analyzed the capillary flow in non-uniform cross-sectional capillaries along the capillary length based on Lucas-Washburn equation. He found that the wetting times depend on some

parameters of the capillary geometry in case of capillary advancement along horizontal pipes without the effect of gravity. In this situation the capillary pressure depends on the position of the interface due to the non-uniform cross-section of the capillary. Speed of the interface meniscus also determines the velocity based on mass equilibrium relation. Therefore considering the effect of non-uniform cross-section of the capillary, the Lucas-Washburn equation can be written as

$$\eta \frac{dh}{dt} = p_c - \rho g h \sin \phi \quad (2.21)$$

Where h is the position of interface, p_c the capillary pressure, ρ the density, g the gravity, ϕ the inclination angle of the capillary, and

$$\eta = \mu A(h) \int_0^h \frac{dx}{kA(x)} \quad (2.22)$$

Where μ the viscosity, $A(h)$ the cross-section area at the interface, k the permeability, and $A(x)$ the cross-sectional area of the capillary in flow direction x .

In the above equation both the capillary pressure p_c and permeability k depends on the capillary diameter D , which is a function of the position x for a non-uniform capillary. He used a contraction-expansion and expansion-contraction capillaries in his study as it is shown in figure 2.8.

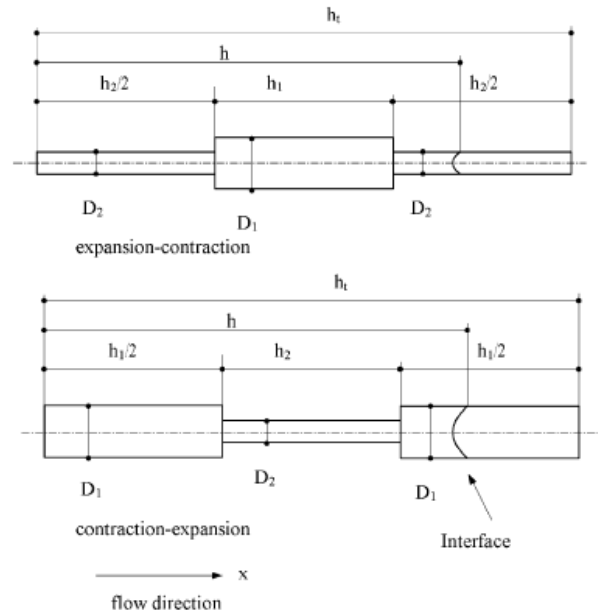


Figure 2.8: schematic diagram of expansion-contraction and contraction-expansion capillaries (Young 2004).

He found that both the non-uniform capillaries reach the end-point significantly later than the straight capillaries, however the required times to reach to the end-point is similar for the two different arrangements of the pores with the same total length. The same result was shown for the flow in a capillary with two contraction-expansion. Inside the length of each capillary, however the wetting speed is faster in a smaller diameter region and vice versa. On the contrary, it was found that smaller capillary diameter would in general increase the wetting time for either straight or non-uniform capillaries. Moreover, for a non-uniform capillary the wetting time is longest if the total length of each cross-section is the same disregarding of the number of section it has been divided. If the effect of gravity is considered, in case of contraction-expansion capillary, at the later stage where the capillary diameter is larger, and so the capillary pressure is lower, the large gravity force and small capillary pressure resulted in extremely low wetting speed. Considering the effect of gravity it was

shown that the wetting times are different for various arrangement of capillaries with dissimilar diameters (Young 2004).

Prior to Young, Hemmat, et al. also studied the motion of viscose drops and air bubbles through a vertical capillary with periodic contraction-expansion with consideration of Buoyancy-driven motion. They characterized the instantaneous drop shapes at various axial position through the length of capillary with periodic constriction using digital image analysis and found that the periodic changes in the capillary wall have a considerable retarding effect on the mobility of drops in comparison with the experimental result from a straight cylindrical capillary (Hemmat and Borhan 1996).

Larson studied the effect of the sample size on capillary pressure in porous media. He noted the importance of accessibility of the pores from the surface of the sample, which influence on the capillary pressure curve and hysteresis. In the procedure to measure the pore size distribution based on imbibition and drainage curve, the point is that the access to pores with large throats are controlled by smaller throats and therefore the larger pores are invaded at high capillary pressure, and then incorrectly they will be assigned to the smaller pores with high capillary pressure. This results that more of the pores will appear to be entered through the small throats than actually are. They found that for the consolidated sample of thickness greater than 70 pore-throat dimensions, the sample thickness effect is small. This number for the unconsolidated materials reduces to about to 30 pore-throat diameter (Larson and Morrow 1981).

In another approach Darcy's law is being employed in order to describe the fluid flow through porous media (Beuther, Veith, and Zwick 2010; Zhong, Ding, and Tang 2002). Henri-Philibert Darcy empirically found that the volumetric flow rate through a porous media is directly proportional to the cross-sectional area A , pressure drop across the porous media ΔP and inversely proportional to thickness T of the porous media. Therefore Darcy's law was proposed as below:

$$Q = -KA \frac{\Delta P}{T} \quad (2.23)$$

where K is permeability of the media (1856 Darcy) . Darcy's law also can be stated in terms of superficial velocity U, which is volumetric flow rate per cross-sectional area (Q/A), intrinsic or specific permeability, and fluid viscosity μ as

$$U = -\frac{k}{\mu} \frac{\Delta P}{T} \quad (2.24)$$

In the later form, intrinsic permeability is independent of fluid properties and is only a function of porous media's geometry, and it has a unit of L^2 .

Darcy's Law is only applicable in the Stokes flow regime. It means the Reynolds number of fibrous media must be less than 1. Moreover Darcy's law is not applicable to the situation when mean free path length of fluid molecules becomes comparable to the fiber diameter. The reader is referred to Jaganathan Sudhakar PhD dissertation at North Carolina State University for further information (Sudhakar 2008). In comparison with Washburn equation, the advantages of using Darcy's law to predict wicking rate is that it can be extended into modeling two- or three-dimensional wicking flows however Washburn equation is limited to unidirectional wicking flow (Masoodi and Pillai 2010).

As it was mentioned earlier, in the Washburn's model, it is assumed that the flow behind the front is fully saturated. However in real situation and specially in the case of vertical wicking, it is questionable to assume this is applicable, and the partially saturated region behind the liquid front influences on both the capillary pressure, as well as permeability. Thus Richards proposed that the filtration velocity is proportional to the gradient of pressure and dependent on the moisture content or saturation, and in his model with an analogy with Darcy's law, he considered both the permeability and capillary pressure as function of saturation or local moisture content as below:

$$u = -K(\theta)(\nabla P(\theta) + \rho g \sin \alpha \hat{x}) \quad (2.25)$$

Where K is the permeability, P is the pressure, ρ is the density of the flowing liquid, g the gravitational acceleration, α the inclination of capillary tube, and \hat{x} is a flow unit vector (M. Landeryou, Eames, and Cottenden 2005). The variation of capillary pressures with moisture shows a hysteresis as the infiltration and draining take place due to increase and decrease in capillary pressure. This is the main difficulty in applying the Richard's equation.

Ghali developed experimental techniques for measurement of both capillary pressure and permeability over a broad range of saturations. The purpose was to employ this information in Darcy's law in order to determine the liquid flow through fabrics. Capillary pressure was obtained via capillary head in a vertical wicking rise experiment. He found that initial state of saturation plays a role in determining capillary pressure. It means that there is a hysteresis in capillary pressure head versus saturation, and the hysteresis is larger for cotton fibers than polypropylene fibers (Ghali, Jones, and Tracy 1994).

2.1.1.2 Mechanism of absorption by fiber

Textile fibers used in absorbent materials can be divided in two main categories depending on their propensity to absorb or repel water known as hydrophilic and hydrophobic fibers respectively.

Generally, all the naturally occurring fibers have groups in their molecule to absorb water. Although various fibers interact differently with liquids depending on the chemical nature of the liquid, and on the chemical and physical structure of the fiber.

Liquids may interact with the fibers in two different modes, absorption and adsorption. The term "sorption" refers to both adsorption and absorption (Venkatesan 2013). The adsorption and absorption should not be confused by each other. The adsorption process is the preferentially bounding of

molecules from bulk fluid to a solid surface and it can occur at any solid-fluid interface. On the other hand, absorption is a process where a component penetrates or dissolved into the bulk of solid.

The adsorption phenomenon occurs due to the attractive forces between the solid surface and liquid molecules. These forces include van der Waals' forces (dispersion and repulsion), electrostatic forces, and chemical bonding (Venkatesan 2013). Adsorption is a very critical phenomenon for the capillary movement of liquid in the pores. For the capillary movement of liquid to happen, it is required that a continuous liquid phase to be present. Since the adsorption phenomenon forms a continuous film on the fiber and this film has some mobility that allows the molecules to be transported to small pores, it provides the fiber with the liquid continuity of the pores even at saturation approaching zero (Ghali, Jones, and Tracy 1994).

The absorption phenomenon only happens in the absorbent fibers with hydrophilicity in nature. The absorbent fibers used in absorbent products include the cotton cellulose, wood pulp in form of fluff and then tissue, rayon, and superabsorbents (Schuchardt and Berg 1991; Chatterjee and Gupta 2002b). The emergence of superabsorbents at the late 1960's made a great impact in this field. A superabsorbent absorbs a considerable amount of fluid and retains a substantial quantity of liquid in its internal network because of its unique structure. It is able to hold significantly more liquid than a conventional absorbent fiber such as cotton, rayon or wood pulp. On the other hand, hydrophobic fibers in nature may not have a direct relationship to absorbency, but they have the potential to improve the functionality of the porous structure to imbibe and hold fluids. In term of fiber properties, two influencing factors on absorbency behavior include various wetting properties of fibers and swelling phenomenon. In the following section, these subjects will be discussed respectively.

The most commonly used fibers in absorbent articles include different types of cellulosic-based fibers (e.g. wood-pulp, cotton, or rayon fibers), and synthetic fibers (e.g. polymeric fibers such as polyester,

polypropylene, or polyethylene fibers) (Chappell, Hammons, and Keeler 1994). The chemical constitution, and the fine structure of individual fiber types determines their wetting properties. The cellulose polymer accounts for the molecular structure of the cellulosic fibers such as cotton, rayon, and wood pulp. The cellulose molecules consist of a series glucose rings joined together. The cellulose polymer is highly reactive due to the existence of three free hydroxyl groups (-OH) on each basic repeating unit of cellulose. These hydroxyl groups are the principal sorption sites for water molecule. Reader could refer to the following reference for further information (Morton, Hearle, and Textile Institute (Manchester 2008). Water molecule can be chemically absorbed on the hydroxyl group via hydrogen bonding, or the additional water is held through secondary polar interactions, which is less firmly. Having more hydrophilic group, as well as less crystalline regions resulted in higher extent of liquid absorption by the fibers. In the crystalline region due to the closely packed structure of fiber molecules, the water molecules cannot penetrate into this region easily. However, if the basic molecule gets hydrated, the crystalline region will open up allowing water molecules to penetrate in (Chatterjee and Gupta 2002b).

The synthetic fibers are all linear polymers in which in addition to the basic repeat unit, there may be some other group inserted within chains, at chain ends, or as chain branches in order to modify their properties. The most commonly used synthetic fibers basically contains very few or no groups that attract water and this is the reason for their low moisture absorption. For example, the Polyester (PET) molecules contain two kinds of group. The aliphatic sequence, $-\text{CO.O.CH}_2.\text{CH}_2.\text{O.CO}-$ and benzene ring, none of which attracts water strongly (Morton, Hearle, and Textile Institute (Manchester 2008).

The liquid absorption behavior is complicated in case of absorbent fibers because of the interaction of liquid and the materials, and consequently the partial dissolution and swelling of the absorbing

materials. The liquid absorption phenomena in the web containing hygroscopic fibers is considerably associated with hysteresis, heat effect, the influence of moisture on physical properties, limited swelling of fibers and consequent pore dimensional changes, and elastic recovery effect. The influence of these phenomena in the non-hygroscopic fibers is very small or zero. Swelling happens because the fiber molecules are pushed apart by the absorbed water molecule, however this occurs in a limited extent because the water molecule can only penetrate into the non-crystalline region or between fibrils and they fail to penetrate into crystalline region (Morton, Hearle, and Textile Institute (Manchester 2008). Among the associated phenomena, the swelling significantly influences the constructional parameters of fibrous materials (Ibbett and Hsieh 2001) and consequently their absorbency behavior.

Therefore, in the absorbent fiber systems such as cellulosic fibers, liquid transport is governed by both capillary action in the pore spaces and diffusion of the liquid through the absorbent fiber. This two mechanism however are not separated from each other since the diffusion of the liquid into the absorbent fibers generally changes the pore size (dimension of the interfiber pore space) and influences the rate of absorption. Changes in the volume of fibers during swelling might be less than the volume of absorbed water, which means the water molecules, is fitted to the space available within the structure. Although in an extreme case, swelling can cause the gel blocking in which the wicking channels becomes completely closed. It is noteworthy to mention that swelling may show its effect in either an overall expansion of the structure or in the partial filling of the pore spaces between the fibers. Moreover, the swelling takes place either transversely and/or axially, and it may be expressed in terms of increase in diameter, area, length or volume (figure 2.9) (Morton, Hearle, and Textile Institute (Manchester 2008).

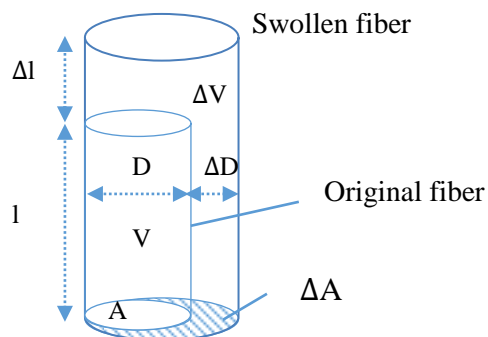


Figure 2.9: changes in fiber dimensions due to swelling (Morton, Hearle, 2008)

Morehead studied the cross-sectional swelling of different textile fibers through photo-micrographs. The outlines of the dry viscose rayon fiber and swollen viscose rayon fiber shown in Morehead study makes clear that measurement of diameter swelling is not a precise way of expressing the transverse swelling in a fiber with an irregular cross-section due to the variation of diameter in different positions. The area swelling must be used for the irregular fibers (Morehead 1947). Preston and Nimkar collected the different swelling data of various fibers reported by various authors. The data showed the considerable variation in data reported by different authors, which is due to the real differences between different specimens of a given type of fibers, as well as experimental difficulties. It was also shown that the fibers that absorb most water swell to the greatest extent. Moreover the absorbent fibers show a large transverse swelling with a small axial swelling (Morton, Hearle, and Textile Institute (Manchester 2008). Stamm also verified that this in the case of wood pulp cellulosic no swelling occurs in the axial direction of the fiber by cellulosic fibers (Locke 1965).

Swelling of the different materials including both fibrous materials and others such as woods has been measured via different approaches including visual approach, employing digital calipers, using linear variable displacement transducers (Yong-Sung et al. 2000), centrifuge method (Schiefer and Kropf 1946), and Wilhelmy method (Jungil Son and Gardnert Douglas J. 2004).

Schiefer, et al. measured the swelling of the fiber gravimetrically. In this method, the swelled fiber samples was placed in a screen basket and centrifuged for one minute at a centrifugal acceleration of 750000-cm/ sec^2 . The centrifuged sample was weighed immediately in a sealed weighing bottle and was then dried to constant weight at 105 to 110°C. Swelling was measured as the amount of water retained by the centrifuged sample, expressed as a percent of the dry weight. Variation in the swelling of a variety of the cellulosic samples is ascribed to the variation in density and in the character and manner of packing of the cellulosic structural unit. Greater the density of the cellulosic fiber resulted in smaller swelling percentages (Schiefer and Kropf 1946).

Schuchardt et, al. (Schuchardt and Berg 1991) examined the wicking flow of water in composite networks of wood pulp cellulose and carboxymethyl cellulose (CMC) fibers. They used dynamic electrotensiometry to measure the wetting and swelling characteristics of the individual cellulose and CMC fibers according to Wilhelmy principle. They quantified the net pore restriction due to fiber swelling through the permeability factor. The permeability factor was defined as the ratio of the wicking-equivalent radius in the swollen state to that in the unswollen state. According to Lucas-Washburn equation, the slope of the plot of wicking distance versus square root of time can be used to determine the wicking equivalent radius if the liquid properties (surface tension and viscosity) and the advancing contact angle of the liquid on the fibers are known. Therefore the permeability factor can be determined by measuring the Lucas-Washburn constant, k , for a given fiber network with the swelling liquid and with a nonswelling reference liquid (n-octane) and taking the ratio of the wicking equivalent radius in the swollen state to that in the unswollen reference state. They found that cellulose fibers swell almost simultaneously to a small degree, while CMC fibers swell over a period of several minutes and to twice their original diameter. They showed that the Lucas-Washburn capillary model described the imbibition of a nonswelling liquid (n-octane) in all of the fiber

networks. They proposed a modified capillary model for the water imbibition into cellulose –CMC fiber networks. They considered the observed swelling rates of single CMC fibers, and therefore the effective capillary radius is a function of time and position of the wetted portion of the structure. The Lucas-Washburn is re-derived as below for this situation

$$\frac{dh}{dt} = \frac{r_h^2}{8\mu} \left[\frac{\Delta p}{h} \right] = \frac{r_h^2}{8\mu} \left[\frac{2\sigma \cos \theta}{r_0 h} \right] \quad (2.26)$$

Where $\Delta p/h$ is the effective pressure gradient, r_h that is a function of time is the effective hydrodynamic radius behind the advancing liquid front and r_0 is the capillary radius observed by the meniscus. Assuming that r_h is a linear function of time as equation 24, it means effective hydrodynamic radius behind the advancing liquid front is decreased with time with the constant rate of restriction a .

$$r_h = r_0 - at \quad (2.27)$$

Therefore the modified capillary model was introduced as below:

$$h(t) = \left[\frac{r_0 \sigma \cos \theta}{2\mu} \right]^{1/2} \left(t - \frac{a}{r_0} t^2 + \frac{a^2}{3r_0^2} t^3 \right)^{1/2} \quad (2.28)$$

They observed the Lucas-Washburn model provides a good description for the wicking of individual fibers such as cellulosic fibers when swelling is not extensive and takes place quickly. They modified the Lucas-Washburn equation for the absorbent systems where the swelling is extensive and changing with the time, for example in the case of superabsorbent fibers. Compared the swelling of the cellulosic fibers with the CMC fibers, they observed that the perimeter of the cellulose fibers increased approximately 10%, with volumetric swelling of 20% and it happened effectively and instantly (usually within 5 seconds of contact with water). While the CMC fiber perimeter increased approximately 120% with 400% volumetric swelling, and 80% of the increase were observed at a constant rate over times ranging from 30 to 60 second, and the rest of the increase took place in two

to five minutes. It was observed that the permeability factor of fibrous structure containing the superabsorbent fiber increased at low superabsorbent content. This was attributed to the formation of open channels in the structure when the wet-formed strips were dried (Schuchardt and Berg 1991). Continuing the Schuchardt study, Wiryana and Berg studied the wicking behavior of wet-formed paper strip with composition of cellulose fibers and various proportion of carboxymethyl cellulose superabsorbent powders. They found that the degree of pore blocking is significantly greater in these structures than the similar composites made with superabsorbent fibers. Since the swelling happens simultaneously in case of cellulosic fibers, samples containing only the cellulosic fibers maintains the linear relationship between the wicking distance and square root of time. However compared with the wicking of non-swelling liquid (n-octane), the rate of absorption is lower. But with addition of superabsorbent, the swelling is a function of time and therefore the straight-line of Lucas-Washburn is not maintained anymore. Despite that the permeability factor increased at low content of superabsorbent fibers, this trend was not observed at the structure with low content of superabsorbent powders. It may be explained by the shape of the open spaces created when these structures are dried. The structure containing absorbent fiber forms long channels, however the structure containing absorbent powder forms isolated cells. Formation of long channels improves the wicking and flow in the former structures. It shows the importance of the shapes of the open spaces created when the composite structure is dried. They also verified the zero-degree contact angle of n-octane against the fibers by the fact that the liquid yielded mirror-image force traces in the advancing and receding modes(Wiryana and Berg 1991).

Benltoufa, et al. developed a model according to Washburn capillary law and the geometrical conformation of fibers and yarns in a jersey knitted fabric. He aimed at the determination of yarn and fiber swelling by consideration of macro-pore and micro-pore size after swelling using a capillary rise

method. They showed the estimated fiber and yarn diameters after swelling calculated based on the capillary rise method are in good agreement with those obtained from the microscopic method (Benltoufa, Fayala, and Nasrallah 2012).

Moghaddam et al. proposed a method in order to determine the dynamic wetting and swelling properties of wood according to multicycle Wilhelmy plate method. This method is based on influence of sample perimeter on measured force in wilhelmy technique, as well as changes in the perimeter of the sample by the swelling. Therefore the model has been suggested based on linear combination of the measured force and final change in the sample perimeter (Sedighi Moghaddam et al. 2013).

2.2 NONWOVEN ABSORPTION

Nonwoven fabrics are widely used in various absorbent products. They are used for example as disposable towels, facial tissues, toilet tissues, or absorbent core in products like disposable diapers, incontinence systems, and sanitary napkins (Weisman and Goldman 1989). The fluid absorption and release behaviors of nonwoven play a very substantial role in the functional properties of these products (Nederveen 1994; Hardy 2009).

Transport of liquid into an absorbing material is called the absorbency phenomena. In order to study the liquid absorption of nonwovens, first it is important to understand the interaction of fluids with the surface. The presence of affinity between the molecules of the absorbent and the absorbed is a key requirement for the liquid transfer to happen (Chatterjee and Gupta 2002b). The second important phenomenon is the liquid motion in the porous structure. The fundamental phenomena, which determine the absorbency behavior of materials, are include wetting, wicking and fiber absorption. Different aspects of wetting and wicking phenomena were discussed in the previous sections. Wetting properties of fiber surfaces is determined by the fiber-surface properties and the liquid's properties,

although capillary-driven of liquid transport into any porous structure is governed by the liquid's properties, liquid-medium surface interaction, and the geometric characteristics of medium's porous structure (Kissa 1996). Therefore to design and evaluate the new fibrous structures, it is critical to separate the surface wetting and pore geometry contribution to the absorbency behavior of porous materials because of complexity of the wetting and wicking phenomena. Hsieh proposed an approach to individually identify the wetting and wicking components based on liquid mass transfer data using a microbalance (Hsieh 1995). The key factors that determine the absorption behaviors of nonwoven fabrics for a given liquid might be divided into three sub-categories including nonwoven structural parameters, nonwoven materials, and external forces (Rebenfeld and Miller 1995). Regarding the nonwoven materials, it is noteworthy to mention that absorbent articles have employed various types of absorbent pads composed of both hydrophilic and hydrophobic fibers. In this section, we will discuss the parameters that are essential for study of nonwoven liquid absorption.

Fluid flow into porous materials can be divided into two types of single-phase flow and multiple phase flow. In the case of single-phase flow, we assumed that the porous media is completely saturated with a single-phase fluid such as fluid flows in filter media. On the other hand, in the multiple phase flow, there are more than one phase which simultaneously flow through the porous media for example in the capillary rise of fluid in nonwoven absorbent products during liquid absorption and release, where both the air and liquid simultaneously flow through the porous media (Sudhakar 2008). Two-phase flow in porous media is studied via numerical simulations and experiments, and it has been studied in various field such as underground oil and gas field (Ciegis et al. 2006), water absorption in concretes (Lockington and Parlange, 2003), and rocks (Li, 2008).

The main requirements for the absorbent product include reaching the maximum capacity of the absorbent product before it fails, a sufficient rate of fluid uptake by the absorbent product especially in the consequent liquid surges, and the ability to hold the liquid and resist against the liquid desorption or release back. These requirements cause the main limitation of the absorbent products (Latimer, Matthews, and Shershin 2002). Therefore discussions about the absorption behavior of nonwoven materials mainly focus on the maximum absorption capacity, rate of liquid absorption, and liquid holding capacity. The importance of these parameters is shown with an example in absorbent products. In the case of diapers application, for example, micturition can occur at rates as high as 15 to 20 milliliters per second and at velocities as high as 280 centimeters per second. For the conventional diaper with the absorbent structure containing a mixture of absorbent gelling particles and cellulosic fluffed pulp, the initial uptake rate is about 8 milliliters per second and afterwards in next liquid surges is deteriorated (Latimer, Matthews, and Shershin 2002). The differences between the liquid delivery and liquid uptake result in the pooling of liquid on the surface of the fabric and consequently leakage. Therefore, many works have attempted to overcome the main limitations, as well as the associated problems. Attempts involve product design modification such as providing the physical barriers in order to reduce the leakage and optimization of the amount or configuration of the absorbent materials including hydrophilic and hydrophobic fibers, and also hydrogels (Latimer, Matthews, and Shershin 2002; Weisman and Goldman 1989). Particular absorbent products have been designed to control the distribution of absorbed liquids.

Maximum absorption capacity of the nonwoven materials is theoretically calculated by sum of the interstitial space between the fibers or micro-scaled pore volume of the structure, and the amount of liquid diffused into the fiber itself or the nano-scaled pore volume because the absorption phenomena in nonwovens are governed by the capillary action in the interstitial space between the fibers. In the

situation when the diffusion happens, swelling alters the pore structure and this effect should be taken into account. However for the partially swellable fibers, this effect may be neglected assuming that a fiber swelling happens by exchanging the pore volume with the diffused liquid volume into the fiber. Absorbency rate, on the other hand, is governed by the capillary action and might be theoretically calculated by the Washburn equation (Gupta and Hong 1994). Even though the nonwoven fabrics have complex pore structure, their absorbency behavior is frequently treated using a simple capillary tube flow model. The magnitude of the capillary pressure is commonly given by the Laplace equation in an idealized capillary tube. In application of the Washburn equation to the nonwovens, the limiting factor is determination of the pore radius. The porous structure of nonwovens is consisted of a pore size distribution and not only a single pore radius. Moreover, the capillaries follow a tortuous axial path in contrast to the model assumption that considers perfectly straight and parallel capillaries. The shape of the capillaries in a nonwoven web is also noncircular and they owe a non-uniform cross-sectional shape in their length.

Besides the requirements regarding the absorbency behaviors, the other requirements of the absorbent products contain the stability of the web, and good hand. A solution for the stability of web offers the utilization of a heterogeneous blending of shorter and longer fibers. In this way, the longer fibers help to stabilize the position of shorter length fibers; moreover the product provides enough strength and good hand. However the other solution may be the impregnation of the web with bonding agent, but this solution result in a stiff web with reduced absorbency (Ruffo 1970).

In order to have an in-depth study of the absorption properties of nonwovens, it is a driving factor to relate the nonwovens properties such as fiber characteristic or manufacturing process to the pore characteristics.

2.2.1 Parameters affecting nonwoven absorption behavior

2.2.1.1 Nonwoven structural parameter

Nonwoven materials can be characterized in various ways including bulk density, fiber size, fiber orientation, fiber cross-section, and pore-related parameters such as pore volume, pore size, pore size distribution, tortuosity, uniformity of pore volume, and permeability. These parameters are influenced by each other, however determination of the former parameters in the mentioned list is easy but the pore-related parameters are difficult to quantify. Nonwoven fabrics can be categorized into homogenous isotropic nonwoven fabrics, homogenous anisotropic nonwoven fabrics and heterogeneous patterned nonwoven fabric with a dual-scale porosity structures (Mao 2009b).

Researches in order to understand the relationship between the constructional parameters and absorption behavior of absorbent articles extends back several decades (Larose 1942). It is well-known that different pore characteristics affects capillary liquid transport in porous materials (Hsieh 1995; Li and Joo 2012; Seong Hun Kim et al. 2003; Chen et al. 2009; Dubrovski and Brezocnik 2012; Dubrovski and Brezocnik 2014; A. K. Jena and Gupta 1999; De Schoenmaker et al. 2011; Lu Zhu et al. 2008). Moreover, the modeling approaches have been broadly developed in order to simulate the capillary flow in the porous structure (Young 2004; Shou, Ye, Fan, and Fu 2014; Cai et al. 2014; Masoodi, Pillai, and Varanasi 2007; Masoodi and Pillai 2010; Masoodi, Tan, and Pillai 2012; Masoodi, Tan, and Pillai 2012; HyvÄluoma et al. 2006) and specifically in the nonwovens (Mao 2009b; Ashari, Bucher, and Vahedi Tafreshi 2010; Ashari et al. 2010; Mao and Russell 2003; Sudhakar 2008; M. Landeryou, Eames, and Cottenden 2005). These models include the simple one directional pore space of fibrous materials to the very complex three-dimensional models. Here we discuss the pore characteristics that are essential for the thesis.

2.2.1.1.1 Porosity

Porosity is defined as the fraction of void spaces in the nominal bulk volume of a material. Solid volume fraction, solidity, is complement of pore volume fraction defined as 1-porosity. The absorption performance of a nonwoven fabric is influenced by its porosity. However the average porosity informs us very little about the nonwoven structure. Entirely different nonwoven structures can have the same porosity values (Rebenfeld and Miller 1995). Pore volume has the higher volume fraction and lower weight fraction compared to the fiber volume. Solidity and porosity can be determined as follow

$$\text{Solidity} = \frac{(w/A \times t)}{\rho} \quad (2.29)$$

$$\text{Porosity} = 1 - \text{solidity} \quad (2.30)$$

Where w is the sample mass (g), A sample area (cm^2), t sample thickness (cm), and ρ is the fiber mass density (g/cm^3).

In practice, the fibrous system is not quasi-homogenous. It means they are not such that the relative proportion of the fiber and air is constant throughout the system due to limit of processing techniques, consequently the local fiber-air concentration will vary from point to point in the system, even though the total fiber and air volume fractions remain constant (Pan, Gibson, and Textile Institute (Manchester 2006).

2.2.1.1.2 Pore size

Pore dimension which is a very important factor determining the nonwoven structure can be described in many terms such as their volume, surface areas, average diameters, and minimum

diameters. There are three different kinds of pores present in a material including closed pore, through pore, and blind pore. Through pores are of primary interest for many nonwoven application since they are open to the outside and it permits fluid flow. The blind pores terminate inside the materials and do not allow fluid flow and closed pores are not accessible (A. Jena and Gupta 2003).

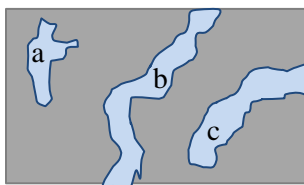


Figure 2.10: different kinds of pores: (a) closed pore (b) through pore (c) blind pore

In the study of the absorption properties of nonwovens, pore volume determines capacity for liquid uptakes. However the average value of the quantities such as average and minimum diameter also provide some useful information about the structure, because of the invariably heterogeneous porous structure of nonwovens, it is important to take into account the pore size distribution. Pore size distribution of nonwoven materials might be unimodal, bi- and tri-modals depending on their structural parameters. However in all cases, they are relatively broad and covers a range of values in several order of magnitude (Rebenfeld and Miller 1995). Defining pore size distribution for a given materials is one way to characterize and compare different porous materials. Different techniques have been developed to obtain a pore size distribution for a given porous material such as porosimetry. The characterization techniques are discussed in a separate section.

2.2.1.1.3 Tortuosity

Tortuosity is defined as the ratio of the length of a true flow path for a fluid and the straight-line distance between inflow and outflow. It is a kinematic quantity since the flow itself may alter the path (Patnaik et al. 2006).



Figure 2.11: tortuosity

$$\xi = \frac{l_t}{l} \text{ (Tortuosity)} \quad (2.31)$$

2.2.1.1.4 Permeability

Nonwoven materials are capable of forming a stable structure even at very low solid volume fractions. It makes the production of nonwovens with high permeability possible. Having a high permeability is an essential requirement for the porous media used in many applications such as absorbent products and filtration. Therefore determining the permeability of nonwoven materials is very important to many industries (S. Jaganathan, Vahedi Tafreshi, and Pourdeyhimi 2008a).

Permeability is a natural choice to discuss the flow resistance of a porous medium. Darcy's law is the empirical formula, which relates the flow velocity to the medium's permeability for a given fluid system with a particular pressure drop, fluid viscosity and media thickness. Permeability of the fibrous porous media is governed by the material's microstructural parameters including fiber size, solid volume fraction, and the fiber arrangement (Jackson and James 1986). It was shown that permeability is independent of the driving pressure, fluid viscosity, and fiber surface wettability (Adams and Rebenfeld 1987). Therefore for a particular fiber arrangement, the permeability relation in a non-dimensional term is as below:

$$\frac{k}{a^2} = f(\Phi) \quad (2.32)$$

Where k is the permeability, a fiber diameter, and Φ solid volume fraction (Jackson and James 1986). However it should be mentioned that the fiber orientation also markedly affects permeability. For example in case of a unidirectional structure, the maximum and minimum permeability are obtained

in the same direction and in the perpendicular direction as that the fibers are oriented respectively (Mao and Russell 2000b; Mao and Russell 2000a). Therefore in the case of anisotropic medium, the permeability is usually considered as a tensor and many attempts have been made to study the directional permeability of nonwovens. Moreover the relationship between fabric permeability and fabric structural parameters has been modeled for both homogenous nonwoven fabrics and patterned nonwoven fabrics (Mao 2009a).

The two main parameters that all the analytical models have in common are fiber radius and either solid volume fraction or porosity of the media. These models assumed a homogenous medium with different microstructures of aligned structure with the axis of the cylindrical fibers orienting either perpendicular or parallel to the flow direction, layered structure with the axes of cylindrical fibers lying randomly in the plane perpendicular to fluid flow, and random structures with the fiber axes arranging randomly in any spatial direction. The inhomogeneity and presence of non-uniformities in nonwovens leads to the inaccuracy of model's prediction. Different approaches were taken by authors in order to predict the permeability of these microstructures. They are based on two different assumptions that fluid flow happens first through conduit or pores, and second around the fibers. Readers could refer to (Dullien 1991) for the detailed information on these two modeling approaches. Jaganathan, et al. proposed a realistic approach for modeling the permeability of hydroentagled nonwoven materials based on digital volumetric imaging techniques and also compared the predictions of some previous analytical models with that of real media. It was observed that the dimensionless permeability decreases by increasing SVF. They found that the layered anisotropic models could best predict the permeability of hydroentagled material (S. Jaganathan, Vahedi Tafreshi, and Pourdeyhimi 2008a).

Siphon test is one method in order to determine the planar permeability of fiber webs. In this method, the web transfers liquid from a beaker at a higher elevation to another one at a lower elevation. The amount of liquid transferred between the beakers and use of Darcy's law, the permeability of the web near fully saturated state is obtained.

2.2.1.1.5 Fiber orientation

Fiber orientation is another important characteristics, which influence on the liquid flow through porous media (Rengasamy et al. 2011; Ashari et al. 2010; Konopka 2001a). Orientation of fibers in a fibrous structure can be classified into three categories including unidirectional structures, layered structures, and random structures. In unidirectional structures, the axes of the cylindrical fibers are oriented either perpendicular or parallel to the flow direction. However in layered and random structures, respectively, axes of cylindrical fibers lies randomly in the plane perpendicular to fluid flow or randomly in any spatial direction. The fiber orientation in nonwoven fabrics is basically governed by the way in which the fiber web is originally laid down or in other word nonwoven processing technique (J. W. S. Hearle and P. J. Stevenson 1963).

There are direct and indirect experimental techniques for measuring fiber orientation. Image analysis techniques has been extensively employed in order to determine the planar fiber orientation distribution (Pourdeyhimi, Ramanathan, and Dent 1996a; Pourdeyhimi, Ramanathan, and Dent 1996b; B. Pourdeyhimi, R. Dent, and H. Davis 1997).

Konopka developed a new testing instrument in order to investigate the effect of fabric anisotropy on in-plane liquid distribution of nonwoven fabrics. It was shown that the in-plane liquid movement follows the orientation distribution of the material (Konopka 2001a).

2.2.1.2 Material composition

Fibers as the structural element of the nonwoven fabrics have a major influence on the absorbency characteristics. The fiber properties which exert an influence on the absorbency behavior include polymer type, linear density or fiber denier, fiber cross-sectional shape, crimp, fiber finish, and fine structure (Chatterjee and Gupta 2002b). According to the literature review on earlier sections, the factors that determine the liquid absorption of absorbent products include the surface tension, and capillary action. The surface tension is the determination factor of the wetting process and it determines how easily the material is wetted. On the other hand, Capillary action depends to some extent on the surface tension but it is also affected by the size of the capillary. In the nonwoven fabrics, the size of the capillary depends on the size of fibers, type of fibers, fiber orientations and fabric structure (Larose 1942).

The component parts of absorbent structures include various types of wettable, hydrophilic materials, as well as nonwetable thermoplastics polymers. Examples of intrinsically wettable materials being used in absorbent products include organic fibers such as cellulosic fibers, and synthetic fibers composed of cellulose or cellulose derivatives such as rayon fibers. Moreover, the other examples of material being used in absorbent products consist of inorganic fibers such as glass fibers, as well as synthetic fibers composed of inherently wettable thermoplastic polymers such as particular polyester or polyamide fibers and also nonwetable thermoplastic polymers such as polypropylene fibers (Latimer, Matthews, and Shershin 2002). The hydrophobic materials may be hydrophilized by employing different treatments or finishes including plasma treatment (Gouveia, Antunes, and Gomes 2011).

Fibrous structures composed of polymers derived from renewable resources such as cellulose derivatives may show some undesirable properties with respect to manufacturing process, stability,

and performance. For example, the cellulosic fibers, when wetted, can lose resiliency and structure will collapse and therefore the rate of liquid uptake may become too low for the next liquid surges. This is one of the reasons that fibrous structures which include a mixture of two materials including both polymers derived from the renewable resources and non-renewable, fossil-based resources are produced (Weisman 2013). Moreover, it is possible to manufacture the man-made fibers such as polyester fibers with small diameter or with irregular or noncircular cross-sectional shapes (Hicks et al. 1971).

Furthermore, Addition of more absorbent materials such as absorbent gelling particles or secondary fluff results in the elevated holding capacity; however with such arrangement the desired rate of liquid uptake may not be sufficiently adequate during the successive liquid surges. Incorporation of the absorbent gelling particles between the fibers to hold them apart also result in a reduced void volume of the absorbent structure, as well as the rate of liquid uptake because of the swelling of these particles.

The most economical liquid absorbent material for use in disposable diapers is cellulosic fibers, commonly known as “fluff pulp” or simply “fluff”. Even though the batt made from these fibers have a low density and a high fluid absorbing capacity, but a much reduced wicking ability. In the poor wicking materials, gravity controls the fluid absorption; therefore the areas of greatest fluid acceptance are the areas of an absorbent fluff batt closest to the initial point of wetting or at lowest position of the structure in use in relation to gravity flow (Sigl and LaBorde 1980). Some of problems associated with the reduced wicking ability include wasting the unused fluff in dry portions of the article with unused absorbent capacity, leakage, and discomfort to the wearer.

Hsieh showed the wetting properties cotton and polyester fabrics influences on their liquid absorption capacity (Hsieh 1995). They measured the water absorption capacity of the cotton and polyester

fabrics with similar weave, weight and thickness through a mass transfer data in a vertical wicking test and using a microbalance. They found that 10% difference in cotton and polyester fibers resulted in an 18% difference in their calculated liquid absorption capacity and 23% difference in their measured liquid absorption capacity. The water retention properties of cotton fabric were found to be more than four times that of polyester fabrics. It should be noted that these differences not only comes from the greater density, better wettability, and irregular shapes of cotton fibers, but it is also affected by the methodology of performing this test. However they did not mention about it.

2.2.2 Absorbency behavior of nonwovens

Liquid absorbency behavior of nonwovens has been studied from different aspects in order to understand the wicking rate, the relationship between wicking rate and structure of nonwovens. Different characterization techniques have been used in various studies in order to quantify the absorbency behavior, as well as pore characteristics of nonwovens. In the next section first we discuss the characterization techniques for absorbency behavior and pore characteristics. Then the results from different studies are discussed.

2.2.2.1 Characterization methods: fluid absorption

The characterization techniques of absorbency measurement of the nonwovens are designed to determine the amount of liquid absorbed. The techniques can be divided into spontaneous (demand) liquid absorption and liquid retention tests. The equilibrium absorbency is reached by two different ways: absorption from dryness and exsorption from saturation. Moreover the absorbency testing system can be categorized into two categories of liquid absorption from a limited reservoir and from

an unlimited reservoir. The wicking spot test or drop test is an example of limited reservoir which is not the focus of this thesis.

There are many characterization methods for evaluating the absorption behavior of materials including the maximum absorbency and the absorption rate of a material (Harnett and Mehta 1984).

These are two main criteria that determine whether an absorbent product works well. An ideal characterization technique is the one, which exactly duplicates the actual condition of use. This principle makes some of the absorbency testing method more appropriate than the other (Larose 1942).

These testing methods include syphon test, the immersion technique, vertical wicking test, downward wicking test, the basket test, and GATS (Gravimetric Absorbency Testing System). In the following section, we are going to discuss some of the frequently used absorbency testing method.

The vertical wicking test is the Association of Nonwoven Fabrics Industry's (INDA) standard test method 10.1 (INDA WSP 10.1, n.d.). It is carried out in vertical direction. In this method a preconditioned strip of material is cut in a specific direction (machine direction or cross-direction) and one end of the strip hangs vertically down into a liquid (figure 2.12). The test determines how fast and how far the liquid goes into the fabric. The time, which is required for the liquid to reach to a given height, is recorded. Also addition of a microbalance to this system is a way to record the weight with this testing method and also to calculate the maximum absorbency in material (Hsieh 1995).

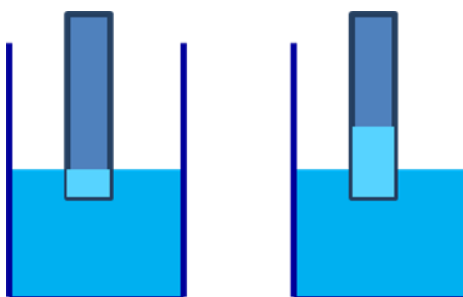


Figure 2.12: vertical wicking test

The main limitations of this method include the effect of gravity on the result, the edge effect and dependency of the result on testing direction. This method also takes a long time in case of samples with very slow wicking rate. Dependency in the testing direction is related to anisotropy of nonwoven structures. The edge effect is the effect that happens because of the equilibrium in the edge of the material when the liquid reaches there. In fact, the liquid cannot go further than those edges and this can influence in the rate of the overall velocity within the materials. It is also very important to notice that this method provides the condition for a purely capillary actions and it is not a good indicator of the amount of liquid absorbed in a certain time (Larose 1942). It was shown that the upward wicking test results in misleading results due to the effect of gravity and the fact that gravity does not have a similar proportional influence on all materials unlike the assumption in most upward wicking testing procedure (Bernard Miller 2000).

The downward wicking test is also done with a strip of the material. Comparing the vertical test method, this method tries to remove the gravity effect. In order to remove the gravity in this testing method, the strip of the material pass over a roller and actually the test is started at this point when the downward wicking begins. However the configuration starts with an initial upward wicking (figure 2.13).

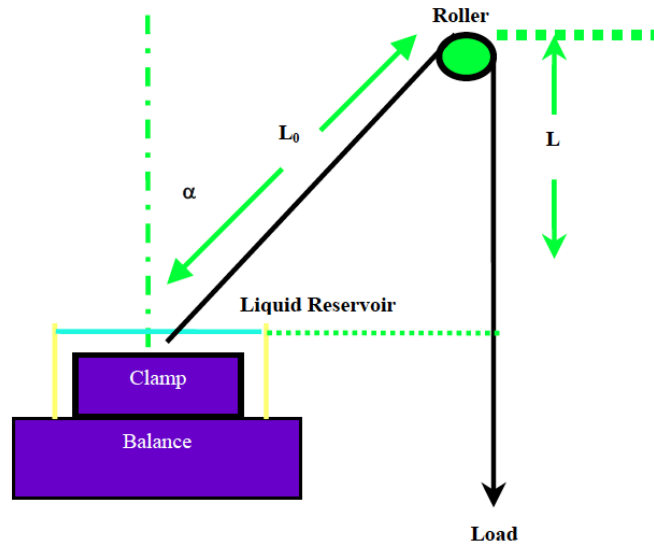


Figure 2.13: downward vertical wicking test (Konopka 2001)

In the downward wicking test, the edge effect and also dependency of testing direction are not eliminated.

The basket or sink method is also referenced in the Association of Nonwoven Fabrics Industry's (INDA) standard test method 10.1 (INDA WSP 10.1, n.d.). This method measures the total liquid uptake into a material over time. This test starts with cutting a strip of materials weighing 5 grams, then rolling the strip and placing the roll into the basket. The basket then is placed into a liquid reservoir and the time it takes for the material to sink is recorded. Moreover the weight of the absorbed liquid is recorded after letting the excess liquid to drain off. The main limitation of this method results from the rolling up the materials since the rolling effects on the amount of capillary in the structure. The extra capillaries affect the absorption behavior of the structure, also the liquid can be held through those capillaries. In this method the material is fully immersed in the liquid and the excess liquid is mostly drained under gravity effect. Since the effects of gravity on different structures

are not the same, it may mislead the measured absorption capacity. The experimental conditions are too far away from the actual condition of use (Larose 1942).

Miller developed demand wettability testing system based on a sensitive gravimetric method which was capable of measuring both the total amount of liquid uptake in the fabric through-plane direction under negative pressure gradient and absorbency rate (B. Miller and Tyomkin 1984). Demand wettability is taking up the liquid by a fabric at zero or negative driving pressure gradient, when the liquid front enters through the face of fabric unlike the wicking which happens when on edge of materials is dipped in the liquid, and the movement of the liquid is primarily in the plane of fabric. Demand wettability has the same basic mechanism as wicking, but it is not customary to call it wicking (Gagge and Gonzalez 1974).

The Gravimetric Absorbency Testing System, known as GATS method, which is a demand wettability testing system, is the other way to measure the absorption versus time. This method also is known as transverse wicking plate test in some of the older papers. In this method the absorption is done by using a porous plate that has the same dimensions as the specimen as it is shown in the figure 2.14. The sample is placed on the porous plate that is connected to liquid reservoir via a plastic tube. The plastic tube enters the plate from the bottom. The liquid is delivered to the porous plate and sample via this plastic tube and the amount of liquid absorbed by the sample is recorded by time. By equalizing the height of the liquid reservoir with that of sample holder compared to a reference point, the hydrostatic head in the system is set at a low level at the start of the experiment. The limitations involved in this test method include first, an extra capillary between the plate and the material forms because of the contact surface. This might retard the beginning of the absorption, second as the automatic start does not work, the user need to place the sample on the platform at the same time that the test is begun and this result in some errors. Another criticism is the effect of the hydrostatic head,

since the hydrostatic head decreases during the test as water wicks up through the fabric sample. This can be a significant problem with thick fabrics (Harnett and Mehta 1984).

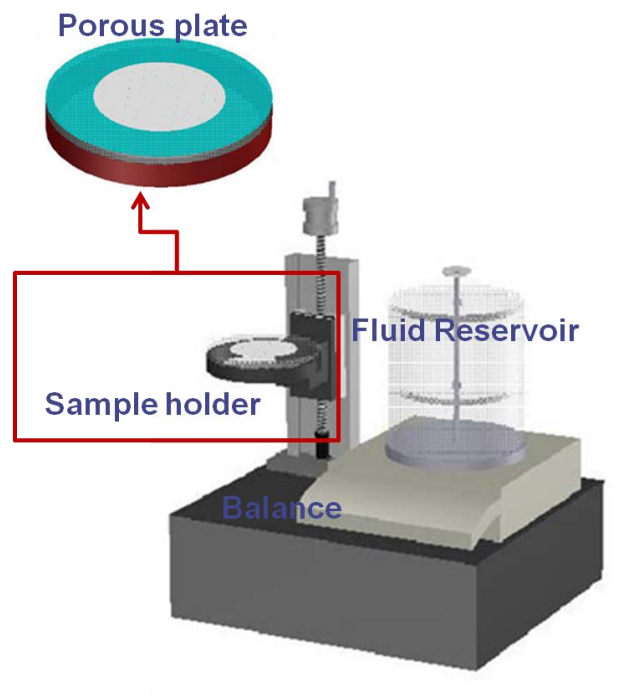


Figure 2.14: GATS (the plastic tube which connect the reservoir to the porous plate not shown)(Konopka 2001)

In the GATS arrangement, different authors have been used various kinds of sample holders including a centered single hole plate, sintered glass with fine pore (Yoo and Barker 2004). Larose found that the right degree of the wetting of the porous plate was obtained when the difference between the height of the top of the plates and the level of the water in the reservoir was from $\frac{1}{4}$ " to $\frac{5}{16}$ " (Larose 1942).

Moreover the sample might be covered by a plate, however additional room between the test sample and the cover may result in overestimation of absorption capacity of the test fabric, therefore Yoo proposed a cover with pins, so it prevents the collection of liquid between the sample and the cover

(Yoo and Barker 2004). It is noteworthy to mention that without a cover, the contact between the sample and sample holder may prevent the system to work appropriately.

A typical GATS result is shown in the figure 2.15. The information that can be obtained from the GATS result includes maximum absorbency and absorbency rate.

Regarding the calculation of absorbency rate from GATS, It has been observed that in case of smaller fiber size, the absorbed volume increases more slowly as it neared the ultimate value than the larger fiber sizes. In other word, the difference between the initial absorbency rate and absorbency rate as it nears the ultimate value is greater in case of smaller fiber sizes (Larose 1942).

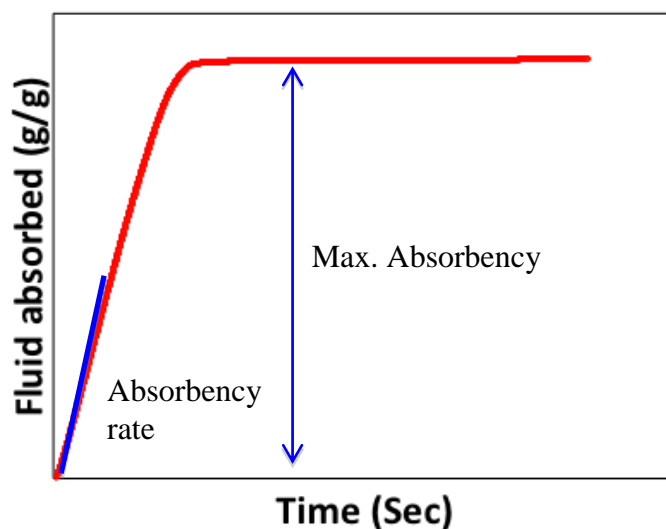


Figure 2.15: typical GATS curve

Sarkar et al. modified the transplanar wicking plate test method which is the similar system as gravimetric absorbency testing system. This mechanism was able to control the water level in the reservoir at a constant level. It means the water level is not reduced with the water transport into the fabric, and therefore the measurements are not affected by the change in the hydrostatic head.

Moreover the absorbency test may be held at different temperatures (Sarkar, Fan, and Qian 2007).

Another aspect of liquid absorption into nonwoven fabrics is mapping the liquid spreading. This has been done via different technology including discrete sensors based on conductance, thermal and optical measurements, optical imaging of liquid front, gravimetric methods, X-ray imaging and magnetic resonance imaging. Landeryou et al. described and the strength and limitation of these techniques in his work (M. A. Landeryou, Yerworth, and Cottenden 2003).

Although the techniques described in this section are being used in order to characterize the absorption capacity and rate of nonwoven such as wiping materials, none of them are able to describe the efficiency of a wipe during use. In an attempt, Oathout et al., developed a new testing methodology to determine the dynamic Wiping efficiency of fabrics representing typical manual wiping. They used a 1-kg sled where the wiping material is affixed to the bottom side and a stainless steel plate as the surface to be wipes. By pulling the sled into and through the liquid pool, a wiping speed is applied, which resemble the phenomena of wiping up real spills (Oathout 2000).

2.2.2.2 Characterization methods: nonwoven pore structure

Liquid flow characterization has been used as a techniques in order to quantify the through pore structure of fibrous materials (Hirt et al. 1987). The pore characteristics of nonwovens can be evaluated from different directions according to the way that the liquid flow happens in the structure (A. K. Jena and Gupta 1999). The techniques employed in different literature for this purpose include the capillary flow porometry, liquid porosimetry (A. Jena and Gupta 2003), in-plane flow analysis (Rebenfeld and Miller 1995), and vertical wicking. The important through pore characteristics of nonwovens include the most constricted pore diameter, the largest pore diameter, the mean pore diameter, pore volume, pore distribution, surface area, gas permeability, and liquid permeability (M. A. Landeryou, Yerworth, and Cottenden 2003).

Capillary flow porometry is a liquid extrusion technique which works based on the assumption of the so-called bundle of straight capillary tubes with no interconnectivity. This technique is founded on the Laplace equation. Laplace equation was discussed in the previous chapters

$$\Delta p = \gamma \left(\frac{1}{R_1} + \frac{1}{R_2} \right) \quad (2.33)$$

Where γ the surface tension, and R_1 , and R_2 are the principal radii of curvature of the bubble at the pore, and the largest between R_1 and R_2 controls the displacement of liquid by air. The Laplace capillary pressure is determined based on the effective radius of any pore, contact angle, and liquid surface tension. In order for the liquid to enter the pore, an external pressure difference must be applied to overcome the Laplace capillary pressure. Therefore incrementally decreasing or increasing the external applied pressure detects the information about the pore size distribution. Each pore size is sized based on its effective radius, and its contribution to the total pore volume of the porous material.

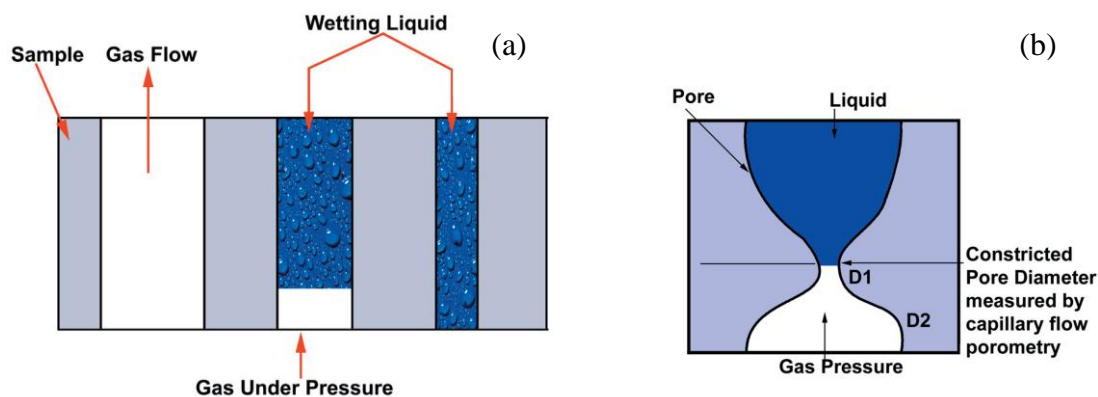


Figure 2.16: (a) principal of capillary flow porometry (b) pore diameter measured by flow porometry (A. Jena and Gupta 2003)

Capillary flow porometry measures the differential gas pressure and flow rates through wet and dry samples. A pore is detected by sensing flow through the pore. According to the Laplace equation, the required pressure is inversely proportional to the pore size. Therefore starting with a wet sample, the very first displacement of the liquid is associated with the bubble point pressure which is related to the largest detected pore diameter and in order to further displace liquid in smaller pore size, the pressure should be increased (figure 2.16 (a)). On the other hand, considering a single pore (figure 2.16(b)), the pressure would be the highest at the most constricted part of pore, and therefore the measured pressure is the required pressure to displace the liquid at the most constricted part of the pore. Consequently the pore diameter measured in this technique include the largest constricted pore diameters and smallest constricted pore diameter.

The other important measurement in this technique is the mean flow pore diameter. The mean flow pore diameter is such that fifty percent of flow is through pore larger than the mean flow pore diameter and the rest of flow is through smaller pores. For the sake of brevity, the explanation about how the mean flow pore diameter is calculated is not given here. The reader could refer to the following reference for more information (A. Jena and Gupta 2003).

Liquid Porosimetry technique is the other method to characterize the nonwoven's pore volume distribution. This technique is also based on the same assumption and is founded on the Laplace equation.

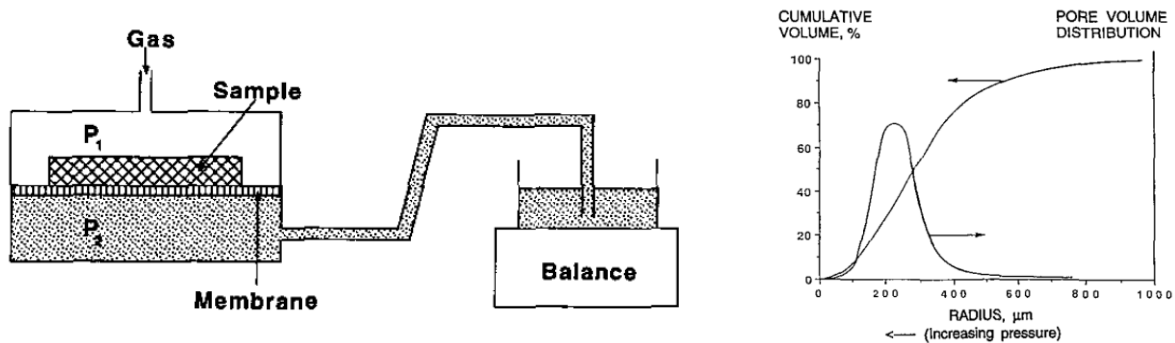


Figure 2.17: (Left) basic arrangement for liquid Porosimetry (right) prototype output for a liquid extrusion experiment (Bernard Miller and Tyomkin 1994)

The liquid Porosimetry technique can be done in two different ways. In one way, in the liquid intrusion Porosimetry, the liquid enters in the pore of an initially dry, spontaneously wettable sample. In this technique, with continuously or step-wise decrease of the external gas pressure, pores which have capillary pressure greater than the imposed external pressure will fill with the liquid. This means that the smallest pore size with higher capillary pressure fills first. This methodology is related to advancing contact angles since the liquid enters the pores. This technique measures volumes of through and blind pores (Bernard Miller and Tyomkin 1994). In the contrary, and in the other method called the liquid extrusion porosimetry, the test is done on a pre-saturated sample and the external pressure is increased and liquid will drain from the pores with lowest capillary pressure. Larger the

pore size, the capillary pressure is lower and it means the liquid drains from the largest pore size first. The receding contact angle plays a role in the later technique. The extrusion technique measures the volume of through pores only (Rebenfeld and Miller 1995). Miller introduced a new methodology, which was capable of determining the absorption/desorption hysteresis loop. In this method, the test starts with a dry material, following with a liquid intrusion, and then pressurize to produce an extrusion curve (Bernard Miller and Tyomkin 1994).

Most porous materials, in reality, do not have a constant pore size along their length but they are made of a series of interconnected contracting and enlarging voids. This fact resulted in the so called “ink-bottle” effect. According to the Young-Laplace equation, some pores must be filled by a non-wetting liquid at a given pressure, however they are not intruded in reality. This is because the pores are only connected to the fluid reservoir via some narrower pores which block the access to them. Therefore for the liquid to fill these blocked, it should first intrude the narrower pores, bottle neck, at an increased pressure. In other word, the pressure must exceed the bottle neck pressure. Therefore the large and small pores becomes filled almost at the same time and an incorrect pore volume will be assigned to a smaller pore diameter (S. Jaganathan, Vahedi Tafreshi, and Pourdeyhimi 2008b).

Jagnathan et al. showed that the ink-bottle effect is stronger in thicker samples, however the cumulative pore volume fraction is not affected by the sample thickness for the similar structures.

Greater the solid volume fraction, the pore volume distribution becomes narrower. It means the range of available pores are narrower at high solid volume fraction. However the access to larger pores is still through these very small pores causing the stronger ink-bottle effect at high SVF. Decreasing the fiber size also resulted in narrower range of available pores and similar to high SVF, the access to the larger pores is still through very small pores which results in stronger ink-bottle effect at smaller diameter. The liquid Porosimetry technique can be done through different liquids. It is noteworthy to

mention that employing the liquid with very high surface tension requires increasing the external pressure to a very high level and this may deteriorate the pore structure of the sample (S. Jaganathan, Vahedi Tafreshi, and Pourdeyhimi 2008b).

In-plane flow analysis is another methodology which provides some information about the pore structure of materials. When a fluid enters a fabric at a circular hole and it is forced to move through the samples radially, the fluid flow behavior reflects the pore structure of the sample. In order to quantify this behavior, one can obtain the radial position of fluid front as a function of time or fluid front pattern. Some of the pore characteristics that can be analyzed through the in-plane flow techniques include in-plane permeability of the fabric, anisotropy, and heterogeneities of the fabric. The isotropic flow through a homogenous fabric shows circular fluid front, which means the resistance to flow is the same in all direction. Anisotropic flow through a homogeneous fabric depicts an elliptical fluid front. It means that the resistance to flow is higher in one direction than the others. This is a typical fluid flow behavior for a fabric made of parallel fiber tows stitched together where the resistance to flow is much lower in the direction of fiber tows than the cross-direction. A particular fiber orientation such as machine direction oriented nonwoven fabric also shows an anisotropic flow behavior. Finally for a heterogeneous fabric with the lack of uniformity in the fabric structure, the point-to-point variation in the structural characteristic result in the deviation of fluid front pattern from the smooth circular or elliptical front. Some sources of heterogeneity include spatial variation in the fabric basis weight and areal density, the fiber orientation function, and variation in the fiber composition in blends (Rebenfeld and Miller 1995).

2.2.2.3 Nonwoven absorbency behavior

Improving the functionality of the absorbent articles through modification of nonwoven fabrics has been the subject of many patents for many years and the result can be found in the commercialized

products. However it did not gain enough attention from the scientific community especially with the consideration of controlling the variables. In this section, we will argue the studies in this field from both patent and paper sources. However, the use of different methods in order to determine the absorption capacity of nonwoven materials makes it difficult to compare the experimental results. For example in the methods that the sample is allowed to release the excess liquid, the samples structural parameter and condition of conducting the experiment influences on the result (A. V. Dedov 2009). It means that the absorption capacity is influenced by the liquid retention characteristics of the samples. Therefore, we will discuss various studies separately to analyze the result according to their conditions.

The wicking ability of the nonwovens is one of the key functionality in absorbent articles. One of the well-known solutions of improving the wicking ability is reduction of the pore size and improving the capillary force in order to sufficiently overcome the force of gravity. The reduced pore size is achieved in the selected localized area with increased density. One of the first to recognize this phenomenon was Heitmeyer in U.S. Pat. No. 1,863,333 which invented the pad with the zone of high compression and low compression (Heitmeyer 1932). The zone of compressed strip are used as moisture conducting channels. The number, size and position of these channels are very substantial for having an efficient product (Van Norden 1957). Different approaches of overall compression, line embossing, pattern embossing, or the like cause densification of the area. However this approach causes reduced total absorption capacity. Therefore while line-embossing is utilized to improve the liquid distribution, larger quantities of uncompressed flocky fluff are placed in the area where initial wetting takes place and where maximum capacity is most needed. This helps to diminish the effect of densification on total capacity reduction (De et al. 1973). In this case the improvement in fluid distribution is achieved at the tradeoff of an added material cost which is undesirable from an

economic standpoint. In another effort to improve the wicking ability of the absorbent pads without reducing the total absorption capacity, it has been filled to employ at least two layers of cellulosic fibers of different densities or different average pore size ranges. The higher density layers is located beneath at least a portion of lower density elements, and consequently the higher density element with lower average pore size wicks waste fluid from a lower central portion of the diapers, therefore transport the fluid upwardly and also transfer it to the lower density element with greater average pore size (Bernardin 1987). Influencing the pore size distribution and reducing maximum pore size is also achieved by stretching a fibrous structure comprising meltable fibers in one direction and freezing the deformation by heat curing. They were able to reduce the maximum pore size of the treated web to 80% of that in untreated web (Hassenboehler and Wadsworth 1993). Moreover, the capillary force is improved by producing a web containing different fibers of chemically stiffened, twisted, and curled bulking fibers, high surface area fibers, and thermoplastic binder fibers. High surface area fibers are generally small and highly conformable. They are able to provide a capillary force in excess of capillary force in the webs containing chemically stiffened, twisted, and curled bulking fibers alone (Horney and Noel 1996). Patent EP 1,573,131 B1 is about the paper products that have a fast initial fluid uptake, yet a delayed fluid strike through. Fluid strike through refers to the ability of the absorbed fluid to pass from one side of the sheet to the other side of the sheet. These paper products have been topically treated with a hydrophobic or water resistant composition in a pattern. Therefore the product includes the treated and untreated area on each side of the product and the liquid coming into contact with the paper can be easily absorbed by untreated parts (Flugge et al. 2010).

The other problem associated with the absorbent articles is to maintain the rate of liquid uptake even after successive surges and wetness of the structure. For this purpose, it was patented to provide a

surge management portion, as well as a transitional, limited time reservoir. It provides a temporary reservoir for each liquid surge occurring in the target zone, and so it leads to a slower complete release and movement of the liquid into the retention portion. This prevents the pooling of the liquid against the wearer's skin, reduces the leakage of liquid from the absorbent structure, and provides improved dryness and comfort to the wearer. The elasticized leg gathers and waist gathers are typically employed to reduce the incidence of leakage in diapers in the conventional diapers, for the mentioned invention the reliance on these parts may advantageously lessen. The surge management portion has a lower capillary pressure in comparison with the retention portion. It results in desorption of the liquid from the surge management portion into the retention part. Some of the characterization criteria for surge management portion includes a resilient structure with a selected basis weight, an appropriate amount of total fiber-surface-area within the internal structure of the fabric, a balance of wettable and non-wettable fiber-surface areas, and an appropriate distribution of the fibers within the volumetric space of the surge management portion (Latimer, Matthews, and Shershin 2002).

Moreover only 60% of the total liquid absorption capacity is being used in product such as diapers and sanitary napkin. This is due to the swelling of superabsorbent materials and consequent pore blockage. Higher degree of utilization of the total liquid absorption capacity in these products is achieved through employing superabsorbent materials having a thermos-reversible liquid absorption capacity. Constituting polymer of these materials is such that the polymer changes geometrical configuration at a certain temperature, therefore the hydrophilic and hydrophobic groups of polymer, respectively, take up another position. It results in a significant change of liquid absorption capacity of the polymer (Annergren and Wagberg 2003). Preventing the structure from bunching, densification and collapse also improve the functionality of the absorbent articles. These disadvantages basically happen through external forces. One way to achieve this goal is through better shape retention and

body contact. It was shown that this is improved by having a soft resilient member attached to the absorbent core or outside of the core. This resilient member deform, bend, or lift in a predictable manner when the external pressure is applied to the pad (Brown, Hammons, and Hines 2001).

Hirt, et al. studied the fluid flow in the fibrous structure through the radial flow of Newtonian fluid. Moreover, they obtained the liquid permeability of the fiber media from the radial spreading. By applying the law of the mass continuity to the Darcy's law, the following expression is obtained.

$$\frac{d(r^2)}{dt} = \frac{2k(p_0 - p_r)}{\epsilon\mu} \frac{1}{\ln(r/R_0)} \quad (2.34)$$

Where r is radial position of the fluid front as a function of time t , p_0 is the driving pressure at the centerhole for injection, p_r is the pressure at the moving fluid front (typically atmospheric), ϵ is the porosity of the porous material, and R_0 is the radius of the centerhole. This equation describes the pseudo-steady process of fluid spreading radially in a porous medium. Therefore the slope of plot of $\frac{d(r^2)}{dt}$ versus $\frac{1}{\ln(r/R_0)}$ can be used to calculate the permeability of fibrous structure.

$$k = \frac{S\epsilon\mu}{2(p_0 - p_r)} \quad (2.35)$$

Where S defines the slope.

In case of fiberglass nonwoven mats, they also measured the air permeability of the samples through a steady flow experiment. They found similar permeability using two different fluids of air and high viscosity liquid, and also they observed that the permeability of the fiberglass mat decreases with the compression of mat. The above-mentioned calculation is only applicable to Newtonian fluid and an isotropic spreading pattern. In contrast, in an anisotropic media the fluid front does not advance in a circle shape but in an ellipse shape. Therefore two different parameters are obtained for the in-plane permeability for the maximum and minimum flow directions. The ratio of these parameters is a measure of the anisotropy of the materials (Hirt et al. 1987).

B. S. Gupta et al. investigated the effect of various factors on absorbency behavior of nonwovens. These factors included the type of fiber, denier of fiber, blend of hydrophilic and hydrophobic fiber, environmental pressure and needling density. The experimental set-up, which was based on the gravimetric absorbency testing system, was able to record the thickness of the samples during the test period. They found that all variables produce significant effects. They observed that increasing the environmental pressure decreases both the absorbency rate and absorption capacity, and larger the fiber size the absorbency rate and absorption capacity were higher. They also observed that higher fraction of rayon fiber in the blend with polypropylene fibers reduced both the absorbency rate and absorption capacity. Increase in the needling density resulted in lower absorption capacity and higher absorbency rate. It was mentioned that increase in absorbency rate was due to the increase in the orientation of the flow channel. They observed that the thickness of the sample as a ratio of dry mass of the specimen and calculated mean pore radii was higher in case of larger fiber size and hydrophobic fibers (Gupta and Hong 1994).

You-Lo Hsieh studied the contribution of the fabric pore structure on liquid transport and retention properties in 100% cotton and polyester fibers. The results showed that the distance of liquid advancement is greater in a smaller pore due to higher capillary pressure, but the mass of liquid retained is greater in larger pores (Hsieh 1995).

Dedov studied the effect of the fiber blends and needle-punching and heat-treatment on the sorption properties of nonwovens. The result showed that nonwovens made from polyester and polypropylene fiber blend had a higher sorption capacity than the materials from polyester fiber alone. However they did not control the porosity of the sample and therefore it is not possible to make any conclusion based on this data. Moreover the result showed that additional needle-punching and heat treatment caused the decrease in the sorption capacity of nonwovens. These additional stages in the production

increase the density of the nonwoven fabrics, and therefore reduce the volume of capillaries and consequently sorption capacity (Dedov et al. 2001). In another study, Dedov showed greater the bulk density of the nonwoven materials, less the sorption capacity will be. Moreover, the importance of testing condition was shown through the influence of liquid runoff height on sorption capacity of the sample with different structural parameter (A. V. Dedov 2009).

Patanaik studied the water permeability of needle punched nonwoven fabrics. He addressed the effect of the depth on needle penetration on the water permeability of the fabrics and justified his result according to the pore size and its distribution. He observed a trend of lower water permeability values with increasing depth of needle punching. In higher depth of needle penetration, percentage of larger pores ($>300\ \mu\text{m}$) decreases because the structure is more compact. These larger pores mainly govern how easily the fluid passes through the structure. The pore size distribution of the fabrics was obtained from liquid extrusion porometry (Patanaik and Anandjiwala 2009).

Chen et al. studied the influence of fiber diameter and fiber blending of different diameter on liquid absorption behavior of nonwovens. The testing methodologies in this study were tensiometric test which calculate the vertical wicking properties and absorption capacity test based on EDANA standard WSP 10.1 (05). They confirmed that fiber fineness plays an important role in determination of absorbency behavior of nonwovens. Capillary absorption ability which was calculated based on tensiometric test, decreased with fiber size. The gravity plays an important role in the vertical wicking test. Therefore the lower capillary pressure in the samples with larger pore size leads to lower capillary absorption capacity, since the capillary pressure is the force which acts against gravity. For the same reason the liquid equilibrium height was lower in case of larger fiber sizes. Saturation time also decrease with fiber size. Moreover they determined the liquid filling ratio as the percentage of pore volume which is filled by the liquid. The result according to these two methods showed that the

nonwovens never reach their maximum absorption capacity. They found different trends in two methods. In tensiometric test, the liquid filling ratio was increased by fiber size. This might be explained by the equilibrium height which is lower in larger fiber size. It shows that larger percentages of pores are filled in the lower equilibrium height of larger fiber sizes, than in the higher equilibrium height of smaller fiber sizes. On the contrast, the opposite trend was observed in the absorption capacity ability test based on the immersion of the samples in the liquid and then drainage for a specific amount of time. The calculated liquid filling was decreased by fiber size. In this method the liquid drainage impacts on the results. Smaller fiber sizes shows higher liquid filling ratio due to higher liquid retention capability of the samples with smaller fiber size and higher capillary pressure. Regarding the blending effect, they showed that the presence of finer fibers maintained the high absorption kinetics of the coarser materials, while increasing its absorption capacity. Moreover the fiber blends showed higher liquid filling ratio than their constituent fibers. They concluded that the resulting pore structure of the blended fabrics seemed favorable to liquid diffusion (Chen et al. 2009). Li and Joo investigated the effect of pore structure on the water behavior of the needle-punched nanofiber nonwovens in order to find the nanofiber nonwovens with the best water absorption capacities and wicking behavior. Moreover a theoretical approach has been offered for calculating the channel radius in an ideal needle-punched nonwoven structure. In an ideal nonwoven structure the pore shape are cylindrical and the channels were considered as a long path from one side of nonwoven to the other. The length and radius of the channels were the same. In such a structure the average channel radius was calculated as

$$r = \sqrt{\frac{D_p^2 K a}{4L}} \quad (2.36)$$

Where K is fiber length, D_p fiber diameter, L the channel length, and a length of the nonwovens.

They showed that the alkali treatment of web of sea-island bicomponent fibers of Poly(ethylene terephthalate)/ co-(polyethylene terephthalate) results in smaller pore size so 80% of pores in treated samples are between 5 to 10 μm , whereas in the untreated samples, 60% of pores are between 40 to 80 μm . Moreover they showed that the nanofiber nonwoven possesses excellent water absorption capacities and fast wicking behavior. This is resulted from the improved capillary pressure in the nanofiber nonwovens. The liquid cannot be held in untreated samples with larger pore size due to the low capillary pressure. This resulted in that the absorbed water volume was dramatically lower than air volume in the bicomponent fibers nonwoven with the large pore diameter. In contrast in case of treated samples, the expansion of the samples after absorbing the liquid lead to the situation that the water volume absorbed in nanofiber nonwovens is much higher than the calculated air volume. Moreover they observed that increasing the punching density resulted in decrease in the value of both the absorbed water volume and the calculated air volume of the samples (Li and Joo 2012).

Das et al. studied the influence of fiber cross-sectional sizes on the capacity and rate of absorption in polyester nonwoven fabrics through gravimetric absorbency testing system. Assuming that the total surface area of all of the pores is equal to the sum of the surface area values of the fibers in nonwoven, he derived the relationship between the pore diameter (d_p) and fiber diameter (d_f) as below:

$$d_p = \frac{(1+e_p)^{1-\mu}}{(1+e_f)} \frac{1-\mu}{\mu} d_f \quad (2.37)$$

Where e_p and e_f are the pore shape factor, and fiber shape factor respectively which is equal to zero for a circular fiber and pore and as the shape of the cross section deviates from circularity, their value increases, and μ is the packing density of nonwoven. Therefore pore diameter is a function of fiber diameter, fiber shape, pore shape, and packing density based on equation 2.37. Since the geometry of

the pore cannot be identified, it must be a hypothesis for quantifying the pore shape. So the generalized form of equation 2.37 is as below

$$d_p = \frac{k}{(1+e_f)} \left(\frac{1-\mu}{\mu} \right)^m d_f \quad (2.38)$$

Where k and m are experimental constants that are needed to be determined experimentally for a nonwoven material

And then under equilibrium, based on the equality of forces that transport the liquid in the column of the pore and weight of the lifted liquid column, they derived the following expression for wicking height

$$h = \frac{4\gamma \cos \theta}{\rho g} \frac{1+e_f}{kd_f} \left(\frac{\mu}{1-\mu} \right)^m \quad (2.39)$$

Where γ is the liquid surface tension in air, θ the contact angle between fiber and liquid-air interface, ρ the liquid density, and g is the acceleration due to gravity. The absorption capacity of the nonwovens was also calculated accordingly.

They showed that the absorption capacity and the rate of absorption decrease with packing density for the needle-punched polyester fibers. Moreover, the result showed that the total absorption capacity and the rate of absorption, in general, increased with decreasing fiber diameter (Das, Pradhan, and Pourdeyhimi 2012).

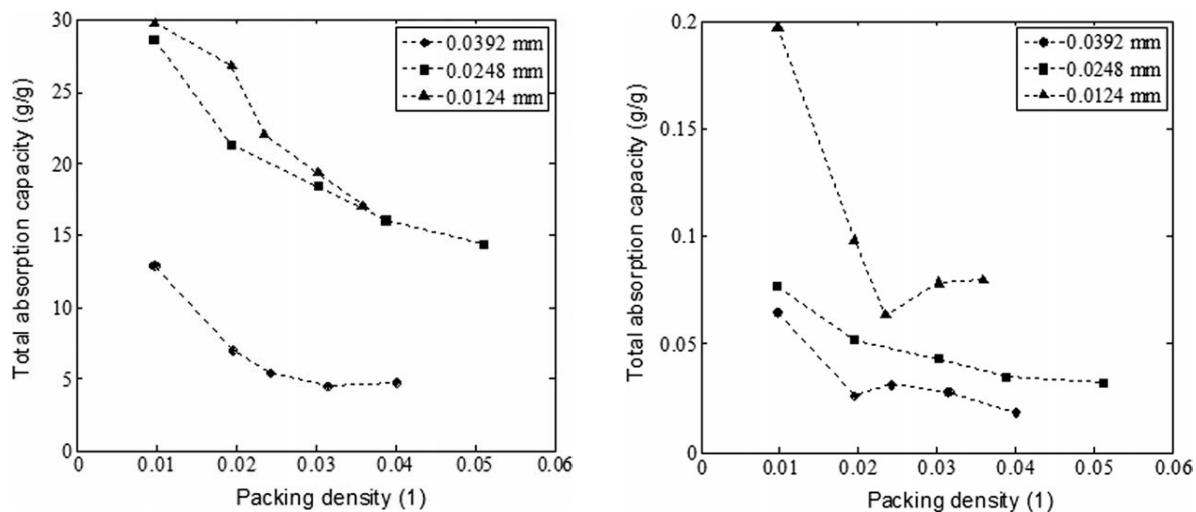


Figure 2.18: (left) plot of total absorption capacity against packing density (right) plot of the rate of absorption against packing density for different fiber diameter (Das, Pradhan, and Pourdeyhimi 2012)

Dubrovski, and Brezocnik studied the water absorption capacity of viscose/ polyester needle-punched nonwovens. Their results showed that higher water absorption capacity has been achieved in nonwoven webs with higher content of viscose fibers, higher pore volume fraction, and finer fibers. The methodology in determination of absorbency behavior of nonwovens is very important, and it should be noted that the different methods provide different information in relation to water absorbency behavior. In their work, they measured the water absorption capacity of nonwovens according to DIN 53923 as the amount of water in % that is absorbed by a nonwoven sample under standard conditions after being immersed in water. The samples were soaked in distilled water for 60 ± 3 second, and after removal from the water, they were suspended vertically for three minutes. Therefore it should be noted the result obtained from this method is biased with the amount of liquid that is released from the sample, and the liquid holding ability of the samples plays a very important role rather than that of their water absorption capacity. It is noteworthy to mention that the higher

water absorption capacity in samples containing higher percentages of viscose fibers and finer fibers is due to the higher holding capacity of these samples (Dubrovski and Brezocnik 2014).

Ashari et al. for the first time, developed a two-scale two-phase modeling methodology in order to study fluid release from saturated/unsaturated thin fibrous materials when brought in contact with a moving solid surface. In their microscale modeling, they obtained the functional relationships between the fluid saturation and capillary pressure as well as fluid saturation and relative permeability numerically. Then these relationships have been employed in their macroscale modeling which was based on Richard's equation. This two-scale modeling allows utilizing the media's internal structural parameters such as fiber diameter and fiber orientation in macroscale analysis. This is a very important capability in design and development of new products (Ashari and Vahedi Tafreshi 2009).

2.2.3 Compression of nonwovens and its impact on absorption

2.2.3.1 Compression behavior of nonwovens

Van Wyk study was one of the advanced investigations on the effect of compression pressure on solid volume fraction of fiber masses. In this study the fiber mass is considered as a system of bending unit and the fiber bending rigidity is the only fiber characteristic applied in the van Wyk equation. The van Wyk equation is appropriate for moderate degrees of compression. The fiber-friction and slippage effects are neglected in the theory of van Wyk. The relationship between the compression pressure and solid volume fraction is defined as below:

$$p = \frac{kYm^3}{\rho_w^3} \left(\frac{1}{v^3} - \frac{1}{v_0^3} \right) \quad (2.40)$$

k: a constant determined by the structure of the fiber mass

Y: Young modulus of the fibers

v_0 : fiber-mass volume at zero pressure

ρ_w : fiber density

Thickness deflection is related to the applied force on the structure of uniformly packed mass of fibers according to the distance between two contact points, fiber

Young modulus and moment of inertia of fiber cross-section. The existence of hysteresis and no initial increase in the volume on the reduction of pressure suggested that friction might be present, however it is improbable that the friction is the only cause of hysteresis. Low melt fibers as binding agent reduce the free distance and consequently improve the compressive resistance of nonwovens (van Wyk 1946).

Dunlop later found that the kY parameter is a dominating factor in characterizing the compression properties of wool samples. However it is difficult to measure that because of the different phenomena which happen during compression such as fiber slippage. It is mentioned also that the deviation from the linearity expected from van Wyk's theory in the beginning stages of increasing the force are most likely the result of fiber slippage and rearrangement (Dunlop 1974). He tried several friction models to model the compression curve of fiber assemblies. He studied the form of stress-strain curves, irrecoverable compression and hysteresis on cycling. Dunlop concluded that in order to produce all of the important features of fiber-mass compression, it is required to consider a combination of van Wyk fiber-bending theory (non-linear springs) and frictional-slippage effect. It means that the van Wyk theory might not be applicable to slow compression because of fiber slippage (Dunlop 1983).

Carnaby et al. studied the compression hysteresis of fibrous assembly at large deformation. The authors suggested that with considering the contribution of fiber viscoelasticity to the total hysteresis, an improvement could be achieved. He divided the fibers in two categories of slippage fibers and non-slippage fibers and shows that in order to predict the compressional behavior of the fibrous material is important to consider the frictional characteristics of the fibers by obtaining the

contribution of slippage and non-slippage fibers separately besides considering the bending of the fibers. The slipping contact points experience the resistance per slipping. The summation of these resistances and the average force per nonslipping contact point is equal to the external stress. In the recovery stage, there is a succession of small decrease in the value of average force per nonslipping contact point, however the behavior of the slipping contact points is subtly different during recovery. The path on the recovery differs from the compression curve because of the simultaneous effect of the reduction in net force and reduction in the critical angles and on the other hand the effect of the changing in the orientation function and existence of more fibers at a lower polar angle. In recovery, the external load is reduced to zero, while there is still some strain energy in the bent fibers. This energy is locked into the assembly because of its own internal friction. The authors of this paper considered the irreversible fiber-fiber slippage in their theory and then they derive the theoretical prediction of the full hysteresis curve for compression and recovery. In Z-direction in a 3 dimensional fibrous assembly, the critical polar angle determines whether a contacting fiber will slip on the arbitrary fiber section. The slippage is independent of the fiber orientation in XY plane. Based on the critical slipping angle, we can find the slipping contact points and non-slipping contact points. It can be concluded for example In case of wiping action, not only the polar angle is important, but also the fiber orientation distribution or azimuthal angle is important because the compression direction is not just in Z-direction. Also it should be taken into the account that the needling changes the polar angle of fibers (Carnaby and Pan 1989).

Komori and Itoh also proposed an energy-based theory for the compression deformation of a fiber mass. They considered the fiber mass as a network composed of many fiber segments in which fiber segments are bounded by two neighboring fiber contact points. They combined the individual mechanical behaviors of the segments into the total response of the mass (Komori and Itoh 1991).

The energy-based theories are founded on the fact that the compression of the assembly causes the changes in the bending energy of each fiber segment. Lee and Carnaby analyzed these changes in terms of the compressional strain and Poisson's ratio of the assembly. In the compressional studies, the authors tried to find the relationship between the fiber properties and compressional properties such as the compressional modulus, hysteresis, and bulk and so on (Lee and Carnaby 1992).

Kothari and Das studied the effect of some processing parameters on the compressional and recovery behavior of needle-punched nonwoven geotextiles. They showed that the porosity of the fabric, mode of bonding and the characteristics of constituent fibers determine their compressibility and percentage energy loss. Their results illustrate the needle-punched fabrics are more compressible than thermobonded fabrics. The adhesive-bonded fabrics also show higher compressibility. On the other hand, staple needle-punched nonwoven fabrics showed a higher percentage of energy loss than continuous-filament fabric. Due to the fact that the fibers in nonwovens fabric are bonded together with some degree of order, the equation for fiber masses is not applicable to them (Kothari and Das 1992).

Hirt et al. showed that the compressed thickness of the fiberglass mat at the same level of compression pressure is dependent on the areal density of the mats, when the greatest thickness is obtained for the sample with highest areal density. The porosity of the samples was calculated at a given compressive pressure. It was shown the porosity is independent of areal density, and fiberglass mats compress to equilibrium porosity. On the other word the compressive resistance that is the required compression in order to reach to a specific percentage of the compression is the same for these samples. It means a given compressive pressure gives rise to the same compression percentage of the samples. Since the compression percentage is the same in the entire samples, therefore the porosity is independent of the areal density. Regarding the pore volume distribution of the samples

under compression, they showed that with the compression, the distribution becomes more monodisperse and the pore size representing the largest volume of pore space decreases (Hirt et al. 1987).

2.2.3.2 Effects of compression on fluid absorption and release

In this section, first the effect of compression on the pore structure of nonwovens is discussed. The first changes after compressing the structure is the thickness reduction, however it depends on many different factors including the solidity of the structure, its initial thickness, the bending rigidity of the fibers, the bonding between fiber contact points. The thickness of a compressible and bulky nonwoven structure after subjecting to the compression pressure reduces and so the total amount of interstitial space in which the fluid can be hold reduces. The equation shows the relation between the total amount of the available space for liquid and thickness of the structure.

$$V_s = \frac{abT}{W} - \frac{1}{\rho_f} \left[\frac{cc(fluid)}{g(fiber)} \right] \quad (2.41)$$

In which V_s is the total amount of interstitial space available for holding fluid per unit dry mass of fibers, a,b and T are width, length and thickness. W is the mass of the dry web; ρ_f is the fiber density (Chatterjee and Gupta 2002).

Not only had the compression effect on the pore volume as discussed previously, the study of Jagnathan, S. et al showed that the pore size also reduced after compression (S. Jaganathan et al. 2009). As the pore size plays a key role in the absorption behavior of the materials, so this study shows the compression may effect on the absorption behavior of nonwovens. Reduction in pore size because of compression may result in increased the capillary pressure.

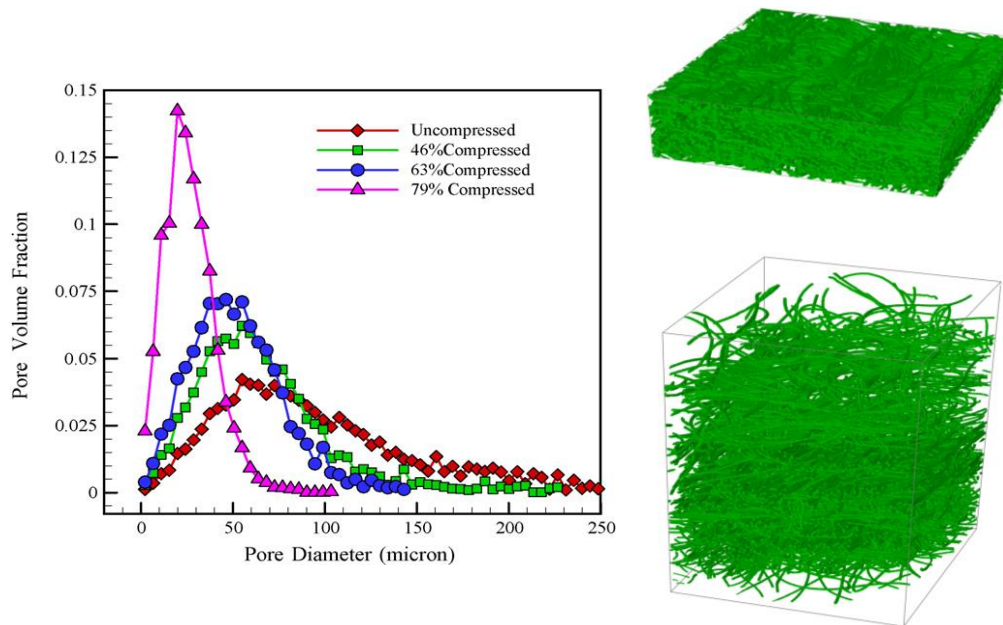


Figure 2.19: effect of compression on the geometric pore size distribution of the fibrous structure (S. Jaganathan et al. 2009).

The previous studies show the effect of compression on the pore structure of the nonwovens. Thus, it is very important to consider the factors that influence on the compression behavior of nonwovens. These factors can be divided in three main categories including fiber properties, nonwoven structure, and compression conditions. Fiber size and fiber cross-section are the influencing factors in the category of fiber properties, because they influence on the fiber bending rigidity. On the other hand, in category of the nonwoven structure, some of the main factors include fabric weight, fabric thickness, and consequently fabric packing density. Finally, the compression conditions and the way that the nonwoven is compressed might effect on the compression properties of the nonwovens. Two of important compression conditions include rate of compression and recovery, and number of compression-recovery cycles.

Larose used different weights of 35, 70, 105, and 210 gram plates in order to apply some pressure on the materials and noted that the absorption with 35 grams pressure is somewhat higher at all the times

than when no plate is used. In the case of higher weights of 70 grams and over however the higher initial rate led to higher absorption at low values, the maximum capacity was lower. The extra weight in these cases was enough to press out some of the water. When the samples are compressed the absorbency rate is constant from the beginning until the point that it reaches the ultimate value. It looks like that without compression an exponential curve best fit the curve of absorbed liquid weight versus time, however when we compressed the structure, the best fit is not anymore an exponential curve. In case of towels, they generally pressed against the objects that must be dried with a certain pressure. Rubbing also is another part of the wiping action; however according to Larose it would not affect the absorption because the purpose of rubbing is to cause the contact area between the absorbent products and object and ensure a more efficient and rapid drying action (Larose 1942). Gottlieb and coworkers showed that the volume of water absorbed into the bulk fiber system increased with the dry bulk volume, but only to a maximum value, which is the characteristic of the fiber type. At the dry bulk volume greater than the optimum, the distance between the adjacent fibers is large enough that prevent the rise of liquid to happen. They suggested that in the wet state, fibers with higher modulus are necessary if the assembly wants to hold more liquid (Gottlieb, Wakeham, and Virgin 1958).

Steiger and Kapur studied the liquid absorption of compressed fiber systems. They compressed the fiber assemblies by hydraulic pressure in order to achieve different bulk densities. Their result showed that there was a linear decreasing relationship between the weight liquid absorption capacity and bulk density for the cotton fibers. The slope of the line depended on the confining pressure. If an assembly of the fiber could be compressed to the point when its density is equal to the single fiber density, it would mean there is no capillary spaces and the absorption capacity would be equal to the uptake of swelling moisture. At this point, the environmental pressure does not affect the amount of

swelling moisture. Their result for unlubricated rayon fibers showed that the relationship between weight liquid absorption capacity and bulk density is not always linear.

The capacity per unit weight can be converted to the capacity per unit volume through below formula.

Capacity per unit weight * Original bulk density = Capacity per unit volume

It was observed that volume capacity curve versus bulk density shows a peak, while the relationship for the weight capacity curve showed a continuous decline. Their result showed that capacity exhibit an optimum with increasing the fiber size. In case of 15 denier rayon fibers, they concluded that due to the high stiffness and resistance to compression, this fiber assemblies required high compressive forces. These forces produce considerable fiber breakage. Because of the energy dissipation in the fiber disintegration process, there is no energy to perform necessary work involved in expansion of the compressed web against the confining pressure. This is the reason that 15 denier fibers showed the lowest capacity. They showed that the required pressure to reach a given bulk density is higher for the finished rayon than for unlubricated rayon. It was expected the reduction of interfiber friction due to the presence of finishes led to the less required force to reach a given degree of compaction. However at the first glance, it is opposite of what is expected, but they remarked that the reduced friction, moreover permitted greater recovery of the fiber assembly when the pressure is removed. They have concluded that the fiber properties in the dry state cannot be ignored if the assembly is going to be compressed before its use as an absorbent. They observed that depending on the bulk density of the samples, liquid surface tension, and gravitational effect, the total volume of the absorbent might reduce, not change, or increases on wetting at different dry bulk densities. The mechanism is related to the ease of introducing a new fiber, and probability of a new fiber encountering a pre-existing one. At higher densities, it is required to do more work to add new fibers. The mild distortion in the individual fibers are useful because they represent stored energy, therefore the fiber have potential

energy to uncramp on contact with the liquid, and movement of the fibers creates more room for the liquid. However when it is very difficult to add the new fiber to the system at very high densities, the greater amount of required force results in the permanent setting and damage to fibers. The increase in the total volume might be due to the swelling of fibers and/or loosening of interfiber frictional bonds, which triggers a chain of event such as curling or uncramping. In this situation, the presence of liquid surface tension makes the fiber to align into better-defined capillaries. They introduced that for the compressed absorbent product, it is beneficial that the fibers have low resilience in the dry state and high in the wet state. In this situation the desired degree of dry compaction can be achieved under the lowest possible compressional forces that lead to permanent setting and fiber damage (Steiger and Kapur 1972). Miller and Tyomkin also evaluated the effect of compression of liquid uptake parameters and observed no difference in total uptake but higher liquid uptake rate especially at the beginning of load increase (B. Miller and Tyomkin 1984).

Rebenfeld and Miller studied the pore volume distribution of glass fiber nonwovens at three different levels of compression corresponding to their thickness. They observed that the pore volume becomes smaller with the compression, also the pore volume distribution turned out to be narrower with compression and less heteroporous. Since the pore volume becomes smaller on the compression, they concluded the sorption capacity of nonwovens become less under compression. They also suggested that it is particularly important to evaluate the pore structure of nonwovens under appropriate amount of compression according to their final application (Rebenfeld and Miller 1995).

REFERENCES

- Adam, N. K. 1964. "The Chemical Structure of Solid Surfaces as Deduced from Contact Angles." In *Contact Angle, Wettability, and Adhesion*, edited by Frederick M. Fowkes, 43:52–56. WASHINGTON, D.C.: AMERICAN CHEMICAL SOCIETY.
<http://pubs.acs.org/doi/abs/10.1021/ba-1964-0043.ch002>.
- Adams, K. L., and L. Rebenfeld. 1987. "In-Plane Flow of Fluids in Fabrics: Structure/Flow Characterization." *Textile Research Journal* 57 (11): 647–54.
doi:10.1177/004051758705701104.
- Adamson, Arthur W. 1997. *Physical Chemistry of Surfaces*. 6th ed. New York: Wiley.
- Adamson, Arthur W., and Irene Ling. 1964. "The Status of Contact Angle as a Thermodynamic Property." In *Contact Angle, Wettability, and Adhesion*, edited by Frederick M. Fowkes, 43:57–73. WASHINGTON, D.C.: AMERICAN CHEMICAL SOCIETY.
<http://pubs.acs.org/doi/abs/10.1021/ba-1964-0043.ch003>.
- Annergren, J., and L. Wagberg. 2003. "Absorbent Structure with Improved Absorption Properties." EP patent 0944402B1
- Ashari, A., T.M. Bucher, H. Vahedi Tafreshi, M.A. Tahir, and M.S.A. Rahman. 2010. "Modeling Fluid Spread in Thin Fibrous Sheets: Effects of Fiber Orientation." *International Journal of Heat and Mass Transfer* 53 (9-10): 1750–58. doi:10.1016/j.ijheatmasstransfer.2010.01.015.
- Ashari, A., T.M. Bucher, and H. Vahedi Tafreshi. 2010. "A Semi-Analytical Model for Simulating Fluid Transport in Multi-Layered Fibrous Sheets Made up of Solid and Porous Fibers." *Computational Materials Science* 50 (2): 378–90. doi:10.1016/j.commatsci.2010.08.030.

- Ashari, A., and H. Vahedi Tafreshi. 2009. "A Two-Scale Modeling of Motion-Induced Fluid Release from Thin Fibrous Porous Media." *Chemical Engineering Science* 64 (9): 2067–75.
doi:10.1016/j.ces.2009.01.048.
- A. V. Dedov. 2009. "DETERMINATION OF THE SORPTION CAPACITY OF NEEDLE-PUNCH MATERIAL." *Fibre Chemistry* 41 (4): 248.
- Batra, Subhash K., and Behnam. Pourdeyhimi. 2012. *Introduction to Nonwovens Technology*. Lancaster, PA: Destech Publications.
- Bear, Jacob. 1988. *Dynamics of Fluids in Porous Media*. Dover Books on Physics and Chemistry. New York: Dover.
- Bendure, Raymond L. 1973. "Dynamic Adhesion Tension Measurement." *Journal of Colloid and Interface Science* 42 (1): 137–44. doi:10.1016/0021-9797(73)90016-7.
- Benltoufa, S., F. Fayala, and S. Ben Nasrallah. 2012. "Determination of Yarn and Fiber Diameters after Swelling Using a Capillary Rise Method." *Journal of the Textile Institute* 103 (5): 517–22. doi:10.1080/00405000.2011.589573.
- Bernardin, L. J. 1987. "Absorbent Structure Designed for Absorbing Body Fluids." US patent 4699619.
- Beuther, Paul D., Michael W. Veith, and Kenneth J. Zwick. 2010. "Characterization of Absorbent Flow Rate in Towel and Tissue." *Journal Of Engineered Fibers And Fabrics* 5 (2).
- B. Pourdeyhimi, R. Dent, and H. Davis. 1997. "Measuring Fiber Orientation in Nonwovens Part III: Fourier Transform." *Textile Research Journal* 67 (2): 143.
- Brown, R. A., J. L. Hammons, and L. M. Hines. 2001. "Disposable Absorbent Article Having a Resilient Member." EP patent 0841881B1

- Cai, Jianchao, Edmund Perfect, Chu-Lin Cheng, and Xiangyun Hu. 2014. "Generalized Modeling of Spontaneous Imbibition Based on Hagen–Poiseuille Flow in Tortuous Capillaries with Variably Shaped Apertures." *Langmuir* 30 (18): 5142–51. doi:10.1021/la5007204.
- Carnaby, G. A., and N. Pan. 1989. "Theory of the Compression Hysteresis of Fibrous Assemblies." *Textile Research Journal* 59 (5): 275–84. doi:10.1177/004051758905900505.
- Chappell, C. W., J. L. Hammons, and S. D. Keeler. 1994. Absorbent Articles Having Multiple Cores for Improved Fluid Movement." WO patent 1994005244A1
- Chatterjee, P. K., and B. S. Gupta. 2002a. *Absorbent Technology*. Amsterdam; Oxford: Elsevier Science.
- Chen, X., P. Vroman, M. Lewandowski, A. Perwuelz, and Y. Zhang. 2009. "Study of the Influence of Fiber Diameter and Fiber Blending on Liquid Absorption Inside Nonwoven Structures." *Textile Research Journal* 79 (15): 1364–70. doi:10.1177/0040517508099386.
- Corey, A. T. 1994. *Mechanics of Immiscible Fluids in Porous Media*. 3rd ed. Highlands Ranch, Colo: Water Resources Publications.
- Das, Dipayan, Arun Kumar Pradhan, and Behnam Pourdeyhimi. 2012. "Dependence of the Liquid Absorption Behavior of Nonwovens on Their Material and Structural Characteristics: Modeling and Experiments." *Journal of Applied Polymer Science* 126 (3): 1053–60. doi:10.1002/app.36635.
- Dedov, A. V., S. V. Babushkin, A. V. Platonov, A. P. Kondratov, and V. G. Nazarov. 2001. "Sorption Properties of Nonwovens Materials." *Fiber Chemistry* 33 (5): 395–97.
- De Gennes, P. 1985. "Wetting: Statics and Dynamics." *Reviews of Modern Physics* 57 (3): 827–63. doi:10.1103/RevModPhys.57.827.

- De, N. G., J. Farber, J. Glodek, and M. Higgins. 1973. "Diaper System and Absorbent Pad Therefor." US patent 3769978.
- De Schoenmaker, Bert, Lien Van der Schueren, Sander De Vrieze, Philippe Westbroek, and Karen De Clerck. 2011. "Wicking Properties of Various Polyamide Nanofibrous Structures with an Optimized Method." *Journal of Applied Polymer Science* 120 (1): 305–10. doi:10.1002/app.33117.
- Dubrovski, P. D., and M. Brezocnik. 2012. "The Modelling of Porous Properties Regarding PES/CV-Blended Nonwoven Wipes." *Fibers and Polymers* 13 (3): 363–70. doi:10.1007/s12221-012-0363-x.
- Dubrovski, P. D., and M. Brezocnik. 2014. "Prediction of the Water Absorption Capacity of VIS/PES Needle-Punched Webs Using Genetic Algorithms." *Fibers and Polymers* 15 (8): 1758–65. doi:10.1007/s12221-014-1758-7.
- Dullien, F. A. L. 1979. *Porous Media: Fluid Transport and Pore Structure*. New York: Academic Press.
- Dullien, F. A. L. 1991. *Porous Media Fluid Transport and Pore Structure*. Oxford: Elsevier Science. http://www.123library.org/book_details/?id=65038.
- Dunlop, J. I. 1974. "CHARACTERIZING THE COMPRESSION PROPERTIES OF FIBRE MASSES." *Journal of the Textile Institute* 65 (10): 532–36. doi:10.1080/00405007408630141.
- Dunlop, J. I. 1983. "On the Compression Characteristics of Fibre Masses." *Journal of the Textile Institute* 74 (2): 92–97. doi:10.1080/00405008308631770.
- Flugge, L. A., M. Higgins, J. Loritz, B. Nogaj, M. Philip, D. Radtke, B. Sarbo, and T. G. Shannon. 2010. "Paper Wiping Products Treated with a Hydrophobic Additive." EP patent 1573131B1

- Gagge, A, and R Gonzalez. 1974. "Physiological and Physical Factors Associated with Warm Discomfort in Sedentary Man." *Environmental Research* 7 (2): 230–42. doi:10.1016/0013-9351(74)90154-6.
- Ghali, K., B. Jones, and J. Tracy. 1994. "Experimental Techniques for Measuring Parameters Describing Wetting and Wicking in Fabrics." *Textile Research Journal* 64 (2): 106–11. doi:10.1177/004051759406400206.
- Gottlieb, I. M., H. Wakeham, and H. M. Virgin. 1958. "Compressional and Absorptive Behavior of Bulk Fiber Systems." *Textile Research Journal* 28 (1): 41–46. doi:10.1177/004051755802800105.
- Gouveia, Isabel C., Laura C. Antunes, and Ana P. Gomes. 2011. "Low-pressure Plasma Treatment for Hydrophilization of Poly(ethylene Terephthalate) Fabrics." *Journal of the Textile Institute* 102 (3): 203–13. doi:10.1080/00405001003616777.
- Gupta, B. S., and Cheol J. Hong. 1994. "Changes in Web Dimensions during Fluid Uptake and the Impact on Absorbency." *Tappi Journal* 77 (12): 181–88.
- Gupta, B. S, and H. S. Whang. 1999. "Surface Wetting and Energy Properties of Cellulose Acetate, Polyester and Polypropylene Fibers." *International Nonwovens Journal* 8 (1).
- Gupta, B. S. with Hyun Suk Whang. 2000. "Surface Wetting Characteristics of Cellulosic Fibers." *Textile Research Journal* 70 (4): 351–58. doi:10.1177/004051750007000412.
- Hamraoui, Ahmed, and Tommy Nylander. 2002. "Analytical Approach for the Lucas–Washburn Equation." *Journal of Colloid and Interface Science* 250 (2): 415–21. doi:10.1006/jcis.2002.8288.
- Hardy, Philip. 2009. "Baby Diaper Absorbent Cores." *Nonwovens Industry* 40 (4): 56–63.

- Harnett, P.R., and P.N. Mehta. 1984. "A Survey and Comparison of Laboratory Test Methods for Measuring Wicking." *Textile Research Journal* 54 (7): 471–78.
doi:10.1177/004051758405400710.
- Hassenboehler, C. B., and L. C. Wadsworth. 1993. "Post-Treatment of Nonwoven Webs." US patent 5244482.
- Heitmeyer, W. C. 1932. "Absorbent Pad." US patent 1863333.
- Hemmat, M., and A. Borhan. 1996. "BUOYANCY-DRIVEN MOTION OF DROPS AND BUBBLES IN A PERIODICALLY CONSTRICTED CAPILLARY." *Chemical Engineering Communications* 148-150 (1): 363–84. doi:10.1080/00986449608936525.
- Hicks, E. M., R. A. Craig, E. L. Wittbecker, J. G. Lavin, N. A. Ednie, D. E. Howe, E. D. Williams, et al. 1971. "THE PRODUCTION OF SYNTHETIC-POLYMER FIBRES." *Textile Progress* 3 (1): 1–108. doi:10.1080/00405167108688988.
- Hirt, D. E., K. L. Adams, R. K. Prud'homme, and L. Rebenfeld. 1987. "In-Plane Radial Fluid Flow Characterization of Fibrous Materials." *Journal of Building Physics* 10 (3): 153–72.
doi:10.1177/109719638701000303.
- Horney, J. C., and J. R. Noel. 1996. "Disposable Products." US patent 5549589.
- Hsieh, Y.-L. 1995. "Liquid Transport in Fabric Structures." *Textile Research Journal* 65 (5): 299–307. doi:10.1177/004051759506500508.
- Hyväluoma, J., P. Raiskinmäki, A. Jäsberg, A. Koponen, M. Kataja, and J. Timonen. 2006. "Simulation of Liquid Penetration in Paper." *Physical Review E* 73 (3).
doi:10.1103/PhysRevE.73.036705.
- Ibbett, R. N., and Y.-L. Hsieh. 2001. "Effect of Fiber Swelling on the Structure of Lyocell Fabrics." *Textile Research Journal* 71 (2): 164–73. doi:10.1177/004051750107100212.

INDA WSP 10.1. n.d. "WSP 10.1 (08) Three Standard Test Methods for Nonwoven Absorption."

Inda, Edana.

Jackson, Graham W., and David F. James. 1986. "The Permeability of Fibrous Porous Media." *The Canadian Journal of Chemical Engineering* 64 (3): 364–74. doi:10.1002/cjce.5450640302.

Jaganathan, Sudhakar. 2008. "An Investigation on Fluid Flow in Fibrous Materials via Image- Based Fluid Dynamics Simulations." PhD Dissertation, North Carolina State University.

Jaganathan, S., H. Vahedi Tafreshi, and B. Pourdeyhimi. 2008a. "A Realistic Approach for Modeling Permeability of Fibrous Media: 3-D Imaging Coupled with CFD Simulation." *Chemical Engineering Science* 63 (1): 244–52. doi:10.1016/j.ces.2007.09.020.

Jaganathan, S., H. Vahedi Tafreshi, and B. Pourdeyhimi. 2008b. "Modeling Liquid Porosimetry in Modeled and Imaged 3-D Fibrous Microstructures." *Journal of Colloid and Interface Science* 326 (1): 166–75. doi:10.1016/j.jcis.2008.07.011.

Jaganathan, S., H. Vahedi Tafreshi, E. Shim, and B. Pourdeyhimi. 2009. "A Study on Compression- Induced Morphological Changes of Nonwoven Fibrous Materials." *Colloids and Surfaces A: Physicochemical and Engineering Aspects* 337 (1-3): 173–79. doi:10.1016/j.colsurfa.2008.12.019.

Jena, Akshaya, and Krishna Gupta. 2003. "LIQUID EXTRUSION TECHNIQUES FOR PORE STRUCTURE EVALUATION OF NONWOVENS." *International Nonwovens Journal*, 45.

Jena, Akshaya K., and Krishna M. Gupta. 1999. "In-Plane Compression Porometry of Battery Separators." *Journal of Power Sources* 80 (1-2): 46–52. doi:10.1016/S0378-7753(99)00163-9.

- JUNGIL SON and GARDNERT Douglas J. 2004. "Dimensional Stability Measurements of Thin Wood Veneers Using the Wilhelmy Plate Technique." *Wood and Fiber Science* 36 (1): 98–106.
- J. W. S. Hearle and P. J. Stevenson. 1963. "Nonwoven Fabric Studies: Part III: The Anisotropy of Nonwoven Fabrics." *Textile Research Journal* 33 (11).
- Kissa, E. 1996. "Wetting and Wicking." *Textile Research Journal* 66 (10): 660–68.
doi:10.1177/004051759606601008.
- Komori, T., and M. Itoh. 1991. "Theory of the General Deformation of Fiber Assemblies." *Textile Research Journal* 61 (10): 588–94. doi:10.1177/004051759106101005.
- Konopka, Amy Elizabeth. 2001a. "The Effect of Anisotropy on In-Plane Liquid Distribution in Nonwoven Fabrics." Master of Science, North Carolina State University.
- Kothari, V.K., and A. Das. 1992. "Compressional Behaviour of Nonwoven Geotextiles." *Geotextiles and Geomembranes* 11 (3): 235–53. doi:10.1016/0266-1144(92)90002-R.
- Landeryou, M A, R J Yerworth, and A M Cottenden. 2003. "Mapping Liquid Distribution in Absorbent Incontinence Products." *Proceedings of the Institution of Mechanical Engineers, Part H: Journal of Engineering in Medicine* 217 (4): 253–61.
doi:10.1243/095441103322060703.
- Landeryou, M., I. Eames, and A. Cottenden. 2005. "Infiltration into Inclined Fibrous Sheets." *Journal of Fluid Mechanics* 529 (April): 173–93. doi:10.1017/S0022112005003356.
- Larose, P. 1942. "The Water Absorption by Towels." *American Dyestuff Reporter* 31 (6): 105–8,123–24.
- Larson, R.G., and N.R. Morrow. 1981. "Effects of Sample Size on Capillary Pressures in Porous Media." *Powder Technology* 30 (2): 123–38. doi:10.1016/0032-5910(81)80005-8.

- Latimer, M. G., B. J. Matthews, and A. M. Shershin. 2002. "Absorbent Material." EP patent 0397110B2
- Lee, Dae Hoon, and Garth A. Carnaby. 1992. "Compressional Energy of the Random Fiber Assembly Part I: Theory." *Textile Research Journal* 62 (4): 185.
- Li, Yue, and Chang Whan Joo. 2012. "Pore Structure and Liquid Behavior of Nonwovens Composed of Nanosized Fibers by Conjugate Spinning." *Journal of Applied Polymer Science* 126 (S2): E252–59. doi:10.1002/app.36627.
- Locke, E. G. 1965. "Wood and Cellulose Science. Alfred J. Stamm. Ronald, New York, 1964. X + 549 Pp. Illus. \$15." *Science* 147 (3658): 595–96. doi:10.1126/science.147.3658.595-a.
- Lu Zhu, Anne Perwuelz, Maryline Lewandowski, and Christine Campagne. 2008. "Static and Dynamic Aspects of Liquid Capillary Flow in Thermally Bonded Polyester Nonwoven Fabrics." *Journal of Adhesion Science and Technology* 22 (7): 745.
- Mao, N. 2009a. "Permeability in Engineered Non-Woven Fabrics Having Patterned Structure." *Textile Research Journal* 79 (15): 1348–57. doi:10.1177/0040517509342311.
- Mao, N. 2009b. "Unsteady-State Liquid Transport in Engineered Nonwoven Fabrics Having Patterned Structure." *Textile Research Journal* 79 (15): 1358–63. doi:10.1177/0040517509342312.
- Mao, N., and S. J. Russell. 2000a. "Directional Permeability in Homogeneous Nonwoven Structures Part II: Permeability in Idealised Structures." *Journal of the Textile Institute* 91 (2): 244–58. doi:10.1080/00405000008659503.
- Mao, N., and S. J. Russell. 2000b. "Directional Permeability in Homogeneous Nonwoven Structures Part I: The Relationship between Directional Permeability and Fibre Orientation." *Journal of the Textile Institute* 91 (2): 235–43. doi:10.1080/00405000008659502.

- Mao, N., and S. J. Russell. 2003. "Anisotropic Liquid Absorption in Homogeneous Two-Dimensional Nonwoven Structures." *Journal of Applied Physics* 94 (6): 4135. doi:10.1063/1.1598627.
- Mason, Geoffrey, and Norman R Morrow. 1991. "Capillary Behavior of a Perfectly Wetting Liquid in Irregular Triangular Tubes." *Journal of Colloid and Interface Science* 141 (1): 262–74. doi:10.1016/0021-9797(91)90321-X.
- Masoodi, Reza, and Krishna M. Pillai. 2010. "Darcy's Law-Based Model for Wicking in Paper-like Swelling Porous Media." *AICHE Journal, NA – NA*. doi:10.1002/aic.12163.
- Masoodi, Reza, Krishna M. Pillai, and Padma Prabodh Varanasi. 2007. "Darcy's Law-Based Models for Liquid Absorption in Polymer Wicks." *AICHE Journal* 53 (11): 2769–82. doi:10.1002/aic.11322.
- Masoodi, Reza, Hua Tan, and Krishna M. Pillai. 2012. "Numerical Simulation of Liquid Absorption in Paper-like Swelling Porous Media." *AICHE Journal* 58 (8): 2536–44. doi:10.1002/aic.12759.
- Miller, Bernard. 2000. "Critical Evaluation of Upward Wicking Tests." *International Nonwovens Journal* 9 (1): 35–43.
- Miller, Bernard, and Ilya Tyomkin. 1994. "Liquid Porosimetry: New Methodology and Applications." *Journal of Colloid and Interface Science* 162 (1): 163–70. doi:10.1006/jcis.1994.1021.
- Miller, B., and I. Tyomkin. 1984. "Spontaneous Transplanar Uptake of Liquids by Fabrics." *Textile Research Journal* 54 (11): 706–12. doi:10.1177/004051758405401102.
- Minor, Francis W., Anthony M. Schwartz, E.A. Wulkow, and Lawrence C. Buckles. 1959. "Part III: The Behavior of Liquids on Single Textile Fibers." *Textile Research Journal* 29 (12): 940–49. doi:10.1177/004051755902901202.

- Morehead, F. F. 1947. "Some Comparative Data on the Cross-Sectional Swelling of Textile Fibers." *Textile Research Journal* 17 (2): 96–98. doi:10.1177/004051754701700204.
- Morton, W. E, J. W. S Hearle. 2008. *Physical Properties of Textile Fibres*. Boca Raton, FL; Cambridge, England: CRC Press ; Woodhead Publishing.
- Nederveen, Cornelis J. 1994. "Absorption of Liquid in Highly Porous Nonwovens." *Tappi Journal* 77 (12): 174–80.
- Oathout, J.M. 2000. "Determining the Dynamic Efficiency With Which Wiping Materials Remove Liquids From Surfaces." *International Nonwovens Journal* 9 (1): 30–38.
- Pan, N., Phillip W. Gibson. 2006. *Thermal and Moisture Transport in Fibrous Materials*. Boca Raton, Fla.; Cambridge: CRC Press ; Woodhead Pub.
- Pan, N., and W. Zhong. 2006. "Fluid Transport Phenomena in Fibrous Materials." *Textile Progress* 38 (2): 1–93. doi:10.1533/tepr.2006.0002.
- Patanaik, A., and R. Anandjiwala. 2009. "Some Studies on Water Permeability of Nonwoven Fabrics." *Textile Research Journal* 79 (2): 147–53. doi:10.1177/0040517508091313.
- Patnaik, A., R. S. Rengasamy, V. K. Kothari, and A. Ghosh. 2006. "Wetting and Wicking in Fibrous Materials." *Textile Progress* 38 (1): 1–105. doi:10.1533/jotp.2006.38.1.1.
- Pourdeyhimi, B, B. Maze, and H. V. Tafreshi. 2006. "Simulation and Analysis of Unbonded Nonwoven Fibrous Structures." *Journal Of Engineered Fibers And Fabrics* 1 (2): 47–65.
- Pourdeyhimi, B., R. Ramanathan, and R. Dent. 1996a. "Measuring Fiber Orientation in Nonwovens: Part I: Simulation." *Textile Research Journal* 66 (11): 713–22. doi:10.1177/004051759606601107.

- Pourdeyhimi, B., R. Ramanathan, and R. Dent. 1996b. "Measuring Fiber Orientation in Nonwovens: Part II: Direct Tracking." *Textile Research Journal* 66 (12): 747–53. doi:10.1177/004051759606601202.
- Rebenfeld, L., and B. Miller. 1995. "Using Liquid Flow to Quantify the Pore Structure of Fibrous Materials." *Journal of the Textile Institute* 86 (2): 241–51. doi:10.1080/00405009508631330.
- Rengasamy, Raju Seenivasan, Vijay Kumar Kothari, Vijay S. Bele, and Rajesh Khanna. 2011. "Liquid Sorption Behaviour of Nonwovens." *The Journal of The Textile Institute* 102 (12): 1019–30. doi:10.1080/00405000.2010.529285.
- Richards, L. A. 1931. "CAPILLARY CONDUCTION OF LIQUIDS THROUGH POROUS MEDIUMS." *Physics* 1 (5): 318. doi:10.1063/1.1745010.
- Ruffo, A. P. 1970. "Absorbent Fibrous Products." US patent 3523536.
- Sarkar, Manas, Jintu Fan, and Xiaoming Qian. 2007. "Transplanar Water Transport Tester for Fabrics." *Measurement Science and Technology* 18 (5): 1465–71. doi:10.1088/0957-0233/18/5/036.
- Scheidegger, Adrian E. 1974. *The Physics of Flow through Porous Media*. 3d ed. Toronto ; Buffalo [N.Y.]: University of Toronto Press.
- Schiefer, H. F., and R. T. Kropf. 1946. "Influence of Fiber Structure of Rayon on Swelling and Radial Density." *Textile Research Journal* 16 (9): 432–37. doi:10.1177/004051754601600902.
- Schuchardt, David R., and John C. Berg. 1991. "Liquid Transport in Composite Cellulose-Superabsorbent Fiber Networks." *Wood and Fiber Science* 23 (3): 342–57.
- Sedighi Moghaddam, Maziar, Magnus E.P. Wålinder, Per M. Claesson, and Agne Swerin. 2013. "Multicycle Wilhelmy Plate Method for Wetting Properties, Swelling and Liquid Sorption of Wood." *Langmuir* 29 (39): 12145–53. doi:10.1021/la402605q.

- Seong Hun Kim, Jae Hyung Lee, Dae Young Lim, and Han Yong Jeon. 2003. "Dependence of Sorption Properties of Fibrous Assemblies on Their Fabrication and Material Characteristics." *Textile Research Journal* 73 (5): 455–60.
doi:10.1177/004051750307300514.
- Shou, Dahua, Lin Ye, Jintu Fan, and Kunkun Fu. 2014. "Optimal Design of Porous Structures for the Fastest Liquid Absorption." *Langmuir* 30 (1): 149–55. doi:10.1021/la4034063.
- Sigl, W. C., and P. A. LaBorde. 1980. "Disposable Diaper with Localized Area of Increased Density." US patent 4213459.
- Steiger, F. H., and C. Kapur. 1972. "The Absorption of Liquids by Compressed Fiber Systems." *Textile Research Journal* 42 (8): 443–49. doi:10.1177/004051757204200801.
- Szekely, J, A.W Neumann, and Y.K Chuang. 1971. "The Rate of Capillary Penetration and the Applicability of the Washburn Equation." *Journal of Colloid and Interface Science* 35 (2): 273–78. doi:10.1016/0021-9797(71)90120-2.
- Van Norden, M. G. 1957. "Disposable Absorbent Pad." US patent 2788003.
- Van Wyk, C. M. 1946. "NOTE ON THE COMPRESSIBILITY OF WOOL." *Journal of the Textile Institute Transactions* 37 (12): T285–92. doi:10.1080/19447024608659279.
- Venkatesan, Saravanan. 2013. "Adsorption." In *Separation and Purification Technologies in Biorefineries*, edited by Shri Ramaswamy, Hua-Jiang Huang, and Bandaru V. Ramarao, 101–48. Chichester, UK: John Wiley & Sons, Ltd.
<http://doi.wiley.com/10.1002/9781118493441.ch5>.
- Washburn, Edward W. 1921. "The Dynamics of Capillary Flow." *Physical Review* 17 (3): 273–83.
doi:10.1103/PhysRev.17.273.

- Weisman, P. T. 2013. "Fibrous Structures Derived from Renewable Resources." US patent 20130071630.
- Weisman, P. T., and S. A. Goldman. 1989. "High Density Absorbent Structures, Method of Their Manufacture and Absorbent Products Containing Them." EP patent 0122042B1
- Wilkes, A. G., and A. J. Bartholomew. 1995. "Extrusion through a Spinneret Defining a Plurality of Multi-Limbed Extrusion Holes into a Spin Bath of Sulfuric Acid." US patent 5458835.
- Wiryan, Surya, and John C. Berg. 1991. "The Transport of Water in Wet-Formed Networks of Cellulose Fibers and Powdered Superabsorbent." *Wood and Fiber Science* 23 (3): 457–64.
- Yong-Sung, Oh, Linda S Sites, Terry Sellers Jr., and Darrel D. Nicholas,. 2000. "Computerized Dynamic Swellometer Evaluation Of Oriented Strand Products." *Forest Products Journal* 50 (3): 35.
- Yoo, S., and R. L. Barker. 2004. "Moisture Management Properties of Heat-Resistant Workwear Fabrics-- Effects of Hydrophilic Finishes and Hygroscopic Fiber Blends." *Textile Research Journal* 74 (11): 995–1000. doi:10.1177/004051750407401110.
- Young, Wen-Bin. 2004. "Analysis of Capillary Flows in Non-Uniform Cross-Sectional Capillaries." *Colloids and Surfaces A: Physicochemical and Engineering Aspects* 234 (1-3): 123–28. doi:10.1016/j.colsurfa.2003.12.007.
- Zhong, W., X. Ding, and Z.L. Tang. 2002. "Analysis of Fluid Flow Through Fibrous Structures." *Textile Research Journal* 72 (9): 751–55. doi:10.1177/004051750207200901.
- Zisman, W. A. 1964. "Relation of the Equilibrium Contact Angle to Liquid and Solid Constitution." In *Contact Angle, Wettability, and Adhesion*, edited by Frederick M. Fowkes, 43:1–51. WASHINGTON, D.C.: AMERICAN CHEMICAL SOCIETY.
<http://pubs.acs.org/doi/abs/10.1021/ba-1964-0043.ch001>.

3 EFFECT OF BINDER FIBERS AND STRUCTURAL PARAMETERS ON COMPRESSION AND RECOVERY BEHAVIOR OF THROUGH-AIR BONDED NONWOVEN FABRICS

3.1 INTRODUCTION

Thermal bonding of fiber webs has received much attention in recent years due to its significant energy saving as compared to chemical bonding and reduced environmental impact (Russell and Textile Institute 2007). In this technique, a thermoplastic element in the form of film, powder, or fiber is integrated into the fiber web and thermal energy is used to initiate the bonding between the fibers in the web. Sufficient temperature melts the homopolymer binder fibers completely or softens the sheath in case of bicomponent fibers (Sheath/core type), and it causes the formation of bonds at the crossover point of the base, or main constituent, fibers in the fiberweb (Batra and Pourdeyhimi 2012). As a thermal bonding process, through-air bonding has been growingly penetrated in different markets for producing high bulk and heavy-weight thermally bonded nonwoven fabrics due to its versatility and ability to produce webs with good softness, drape, and re-wet. However, these structures are subjected to various levels of compression during their end-use applications. Which is why the topic of compressional behavior of these fibrous assemblies has been investigated in recent years. More specifically, it is of great importance to realize the relationships between the fiber parameters/ properties and web characteristics.

Van Wyk (1946) pioneered the study of the compressional properties of fiber masses as a system of bending units and by neglecting the effect of slippage and friction, and therefore the fiber bending characteristics, including the fiber young modulus and moment of inertia of the fiber cross-section, and the distance between two contact points known as free length are the two factors affecting on

compression behavior of fiber masses based on this theory. But he proposed that the existence of hysteresis and no initial volume increase in unloading cycle suggests that friction might be present. The microstructural characteristics of fiber assemblies including mean number of fiber contact points, mean fiber length between the contacts and the void space enclosed by adjacent fibers later was first formulated by Komory and Makishima (1977) based on fiber size, fiber packing density, and orientation density function. Although, this analysis later was modified by Pan (1993) since the prediction of compressional modulus was higher than the experimental because the prediction of the number of fiber contact point was too high, which led to much shorter mean fiber length. The van Wyk theory was modified by taking into the account the fiber slippage, its irreversible effect, and mechanical hysteresis in compression-release cycling (Dunlop 1974; Dunlop 1983). The study offered that the fiber slippage effect is much higher in the case of slow compression than fast compression. It was established that it is of significant concern to combine van Wyk fiber-bending theory and frictional-slippage effect to insure all the important features of fiber mass compression. Classifying the fibers as either slipping or non-slipping, Carnaby and Pan(1989) theoretically studied the compression hysteresis in fibrous assemblies further by determining a critical fiber polar angle as an influential factor of slippage. He suggested that the unsymmetrical value of average force per non-slipping fiber results in the different path on the recovery. On the other hand, Komori and Itoh (1991) introduced an energy-based theory for the compression deformation of a fiber mass based on the changes in the bending energy of each fiber segment. The theory incorporated the steric hindrances between fibers. Lee and Carnaby (1992) analyzed the compressional behavior in terms of the compressional strain and Poisson's ratio. The focus was to find the relationship between the fiber properties and compressional properties such as the compressional modulus, hysteresis, and bulk and so on. Beil and Roberts (2002) presented a model by first creating a single fiber model with its

realistic mechanical properties, and then computing the motions of several of these fibers together. He presented the model to bridge the gap between theory and experiment, which are because of simplifying assumptions. He reported that the nonslipping contacts are stronger than slipping contacts.

Furthermore, van Wyk (1946) addressed the relation between the pressure and packing density based on the stochastic theory of contacts between fibers and calculating the distance between the contacts. The van Wyk equation was verified for low values of packing density, but it was unrealistic for higher packing density values, when $\mu > 0.4$ due to the simplifying assumption. Neckar (1997) generalized the concept of van Wyk theory of compression by assuming that at the points where the fibers contact on another, there should be an excluded volume, therefore he considered an area contact instead of point contact and found the linear relationship between the mean volume of fibers in each contact volume and the packing density of the entire fiber formation, and based on this he modified the van Wyk relationship of pressure and packing density.

The deformation of nonwoven fabrics under compression is mainly due to fiber bending in the fibrous structures (Maze, Vahedi Tafreshi, and Pourdeyhimi 2007). Besides, in the thermal bonded structures the thermal bonds are the non-slipping contact that can transmit the compressional loads. Therefore the compressional behavior of the thermal bonded structures is highly dependent upon fiber properties, type of web structure, the fiber orientation characteristics, binder fiber characteristics, the bonding and cooling conditions (Michielsen, Pourdeyhimi, and Desai 2006). Various studies have been concentrated on formulating the relationship between fiber properties and fabric features under compression by incorporating the characteristics of nonwovens in theories of compression of fiber assemblies (Amit Rawal 2009; Amit Rawal, Mishra, and Saraswat 2012; Kothari and Das 1992; Schoppee 1998). Compression and recovery behavior have been extensively explored in the loading

and unloading cycles of needle-punched nonwovens (Kothari and Das 1992). Their study has demonstrated the dependency of compressibility and percentages energy loss on the various nonwoven structures and specifically on the basis weight, porosity of the fabric, the mode of bonding and characteristics of the constituent fibers. Having a broad range of nonwoven fabrics, it was revealed how various degrees of freedom of fiber movements influences on their compression and recovery behavior (Kothari and Das 1992). It has been observed that at the similar basis weight and thickness, larger linear densities of the both main fibers and binder fibers resulted in more compressibility and less bending resistance of the thermal-bonded nonwoven structures. The frictional losses were found to be small which suggest the good stability and elasticity of the thermal bonds (A. Rawal et al. 2007). Amit Rawal, Mishra, and Saraswat (2012) introduced a concept of compression ratio, as the ratio of fiber volume before and after application of compression strain, in predicting the fiber volume fraction at a defined level of compression strain. It has been observed that the effect of compression ratio is non-negligible which indicates the importance of methodology of compression test that is preferred to be in term of compression deformation instead of compression load. Maze, Vahedi Tafreshi, and Pourdeyhimi (2007) also discussed the compression as a result of calendaring lead to a U-shaped solid volume fraction meaning the compaction is maximum at the outer layers and minimum in the middle. However, although the compressional behavior of nonwoven fabrics has been evaluated mainly theoretically, these theories are mostly based on analytical and numerical techniques with over-simplistic and/or unrealistic assumptions and lack extensive validations due to scarceness of the experimental data on compressional behavior of nonwovens. Moreover little attention has been paid to the contribution of binder fibers.

In the present work, the compressional and recovery properties of through-air bonded nonwovens is studied for various fiber sizes, cross-sections and binder percentages. The aim of this work was to

understand the compression and recovery behavior of thermal bonded nonwoven based on their structural parameters. In this study the results are given for the compression resistance, while the controlling parameter is compression percentage, however previous studies focused on the compressibility of nonwovens at various given forces, while the controlling factor is the compression force which means the samples is compressed to a maximum force (Debnath and Madhusoothanan 2012; A. Rawal et al. 2007). The aim of this project was to understand the effect of nonwoven structural parameters on their compression and recovery behavior. To the best of author's knowledge, this study is a first attempt to investigate the effect of binder fiber percentage on the compressional behavior of thermally bonded nonwovens under defined level of compression strain.

3.2 MATERIAL AND EXPERIMENTAL

3.2.1 Description of samples

The current investigation involved series of 12 nonwoven fabrics including different fiber sizes, cross-sectional shapes, and varying binder fiber percentages to measure their compressibility and recoverability. The main fibers, provided by Barnet & Son Company, were monocomponent fibers having various linear densities of 1.5, 3, 6, and 9 denier and length of 2 inch. The binder fibers were concentric sheath/ core bicomponent fibers 2 denier* 1.5 inch Co-PET/PET with melting point of 110 °C (T 201 Provided by Fiber Innovation Technology). All the fabrics were manufactured through carding, cross-lapping, pre-needling and through air bonding processes in the Nonwovens Institute's Staple Pilot Facilities (Raleigh, North Carolina). Through air bonding was done on the temperature of 121°C and air circulation speed was 1000 RPM. Through air bonding and binder fibers were used in order to obtain a bulky structure and control solidity and keep it constant among our samples. On the other hand in order to control the compressibility of the structures, 2 different percentages of binder were used. The details of the fabrics are given in table 3.1.

Table 3.1: details of various Through-air bonded fabric

Sample no.	PET fiber size	PET fiber cross-section	Binder	Mass per unit area (g/m ²)	Thickness (mm)	Solidity
1	1.5 Denier	Round	10	229	4.52	0.0282
2	3 Denier	Round	10	221	4.48	0.0347
3	6 Denier	Round	10	223	4.83	0.0324
4	9 Denier	Round	10	234	4.94	0.0337
5	1.5 Denier	Round	20	191	3.76	0.0302
6	3 Denier	Round	20	212	4.32	0.0359
7	6 Denier	Round	20	225	4.83	0.0348
8	9 Denier	Round	20	236	5.22	0.0346
9	6Denier	4DG	10	208	3.69	0.0338
10	6Denier	4DG	20	229	3.86	0.0357
11	6Denier	Pentalobal	10	198	3.91	0.0310
12	6Denier	Pentalobal	20	195	4.06	0.0286

3.2.2 Basic web properties

Web thickness of samples was measured using an Ames Logic basic thickness gauge model no. BG1110-1-04. The presser foot diameter was 1 inch and the applied pressure was 0.6 psi. The thickness was measured for 15 different places along the fabric.

The basis weights of the samples were calculated for 18 different replicates per each sample according to equation 3.1, in which w is the mass of the sample and A is the sample area. The samples were the round samples with the cross-sectional area of 100cm².

$$\text{Basis weight} \left(\frac{g}{m^2} \right) = \frac{w (g)}{A} \quad (3.1)$$

Finally the solidity of the samples was calculated according to the equation 3.2.

$$\text{Solidity} = \frac{(w/A \times t)}{\rho} \quad (3.2)$$

Where, w: the sample mass (g)

A: sample area (cm²),

t: sample thickness (cm) and

ρ : Fiber mass density (1.37g/cm³ for polyester fibers)

3.2.3 Compression test procedure

A compressional study was carried out on an Instron 4400R, with a load cell of 1000lb and constant rate of compression of 2.5mm/min within the compression percent range of 0-40% with a pressure foot 8.89 cm diameter. For each sample, this test was done for 3 replicates and each replicate include different numbers of layers of our nonwoven sample. It was tried to keep the thickness of the sample in a specific range. Plate separation was 55 mm for all the samples. The pressure foot was brought down to reach to 40% compression based on the measured initial thickness (T_0) (figure 3.1). The initial thickness, T_0 , was measured under no compression load. The compression percent increases and corresponding compression load are recorded on the Instron. After reaching a compression percent of 40%, i.e. the final compression percent, the compression percent is gradually reduced with the same rate and corresponding compression loads are recorded in the same way during the recovery cycle. In order to maximize the accuracy of our results, the compression percentages given by the Instron were normalized according to the precise initial thickness of the samples. This testing procedure was aimed towards measuring the compressional and recovery behavior of nonwovens in terms of a constant rate of deformation.



Figure 3.1: schematic of the compression procedure on Instron

3.2.3.1 Analysis techniques of compression behavior

The compression and recovery curve was employed in order to evaluate the compressional properties of nonwoven samples. Figure 3.2 demonstrates a typical compression-recovery cycle. T_i , T_r , and T_c corresponds to the initial thickness, recovered thickness, and compressed thickness of the sample respectively. One way to evaluate the compression behavior from the compression curve is to study the compressive resistance. Compression resistance is the compression pressure required to reach a specific percent of compression.

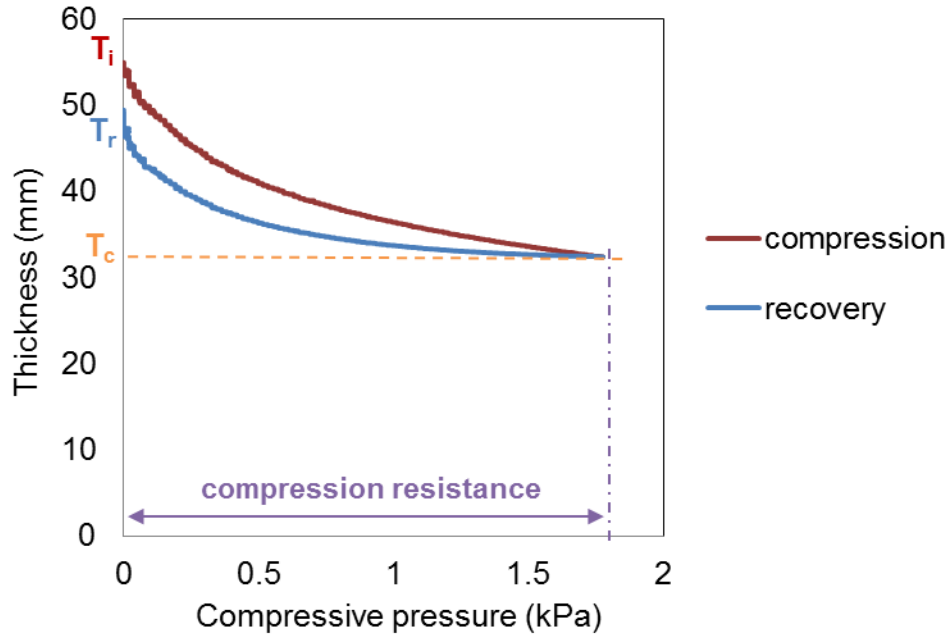


Figure 3.2: typical compression test results, compression and recovery curve

It has been shown earlier that the response of textile materials to the load is viscoelastic. The micro-level deformations such as fiber re-arrangement and fiber sliding cause the inelastic effects (Kelly, Bickerton, and Cheng 2011). When the sample is loaded, the potential bending energy is stored during the compression process, and consequently during the unloading, some part of this energy is recovered. The energy, which is stored and recovered, can be determined through the area under the curve. In order to recognize the influence of fiber size on this behavior, the energy loss percentages were calculated based on the area under the thickness versus compression pressure curve during loading and unloading according to equation 3.3. The area under the curves were measured by using the Matlab software.

$$Energy\ loss = \frac{E_l - E_u}{E_l} * 100 \quad (3.3)$$

E_i : Potential energy stored during the compression

E_u : Potential energy recovered during release of load

Recoverability determines the ability of the structure to maintain the thickness during and after loading. The recoverability was calculated based on the thickness measurement in the different situations of the samples according to equation 3.4. T_i , T_r and T_c corresponded to initial thickness, recovered thickness, and compressed thickness respectively.

$$\text{Recoverability} = \frac{T_r - T_c}{T_i - T_c} \quad (3.4)$$

3.2.3.2 Application of van Wyk theory of compression

One of the most important studies on the compression of fiber assemblies is van Wyk theory of compression (van Wyk 1946). The theory defines the relation between the pressure and volume with considering some simplifying assumption. The fiber mass is considered as a system of bending unit in this theory, and therefore the fiber bending characteristics, including the fiber young modulus and moment of inertia of the fiber cross-section, and the distance between two contact point shown as (b) are the factors affecting on compression behavior of fiber masses (Kothari and Das 1996) (figure 3.3). The mean length between the centers of two neighboring contact points shown as b in figure 3.3 is calculated for the fiber masses theoretically, and it has shown that for a given solidity, its value is proportional to the fiber diameter. The difference between the nonwoven and fiber masses is that in the fiber masses the contact properties are the same as the rest of fibers, also the contact points are not fixed, and they move under external loads (Pan 1993).

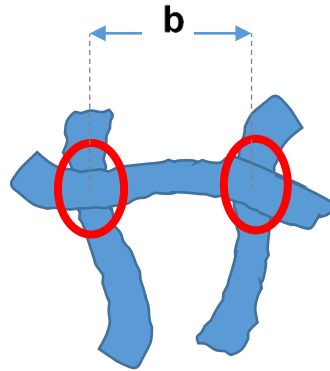


Figure 3.3: distance between two contact points in a fiber mass

According to van Wyk equation shown in equation 3.5, there is a linear relationship between the pressure load and the solid volume fraction cube in a moderately pressure load amount in the compression cycle. The slope α depends on the fiber bending rigidity and material properties based on the equation 3.6. However the compressional resistance discussed earlier is influenced by the initial solidity of the nonwoven samples, the slope α is independent of the solidity of the samples, and therefore it can be a better approach to understand the effect of fiber properties and binder percentages on the resistance to compression, especially in case of having various initial solidities.

$$P = \alpha(\mu_f^3 - \mu_{f0}^3) \quad (3.5)$$

In which P is the compression load; μ_f and μ_{f0} are solid volume fraction with and without loading and,

$$\alpha = k\tau \quad (3.6)$$

k: the van Wyk's constant (depends on material properties)

τ : the fiber bending rigidity

3.3 RESULTS AND DISCUSSION

The results are divided into two parts as follows: the effect of fiber cross-sectional size and influence of binder fibers, the effect of fiber cross-sectional shape and the influence of binder fibers. Using the analysis techniques described above, we obtained the compression resistance, recoverability, and percentage of energy loss of the various nonwoven structures. Moreover, the compressional behavior in terms of the packing density was analyzed according to van Wyk theory of compression.

3.3.1 The effect of fiber cross-sectional size on compressional behavior

Figure 3.4 shows the result of the compression and recovery curves for various fiber sizes at 2 different binder percentages. At the same compressive pressure, the compression percentages in recovery curve are higher than the compression percentage in compression curve, which means the deformation is not recovered fully. As shown in figure 3.4, the larger binder fiber percentage improve the compressive pressure at a given compression percentage at both compression and recovery curves. Moreover, the highest compressive pressure at a given compression percentage was achieved in 6 denier fibers. The highest compression pressure was about 8 kPa in the case of samples containing 10% binder fiber, however it increased up to 14 kPa in samples containing 20% more binder fibers. The results suggested that both thermal bonded structures, containing 10% and 20% binder fibers, follow the same curve at lower compression percentages, which is consistent with the results obtained in (A. Rawal et al. 2007). The more resistance to compression at samples containing 20% binder fibers compared to 10% binder fibers was shown in compression percentages as low as 3.5% for 1.5 denier fibers, however it was shifted to compression percentages of about 15% for the rest of fiber sizes.

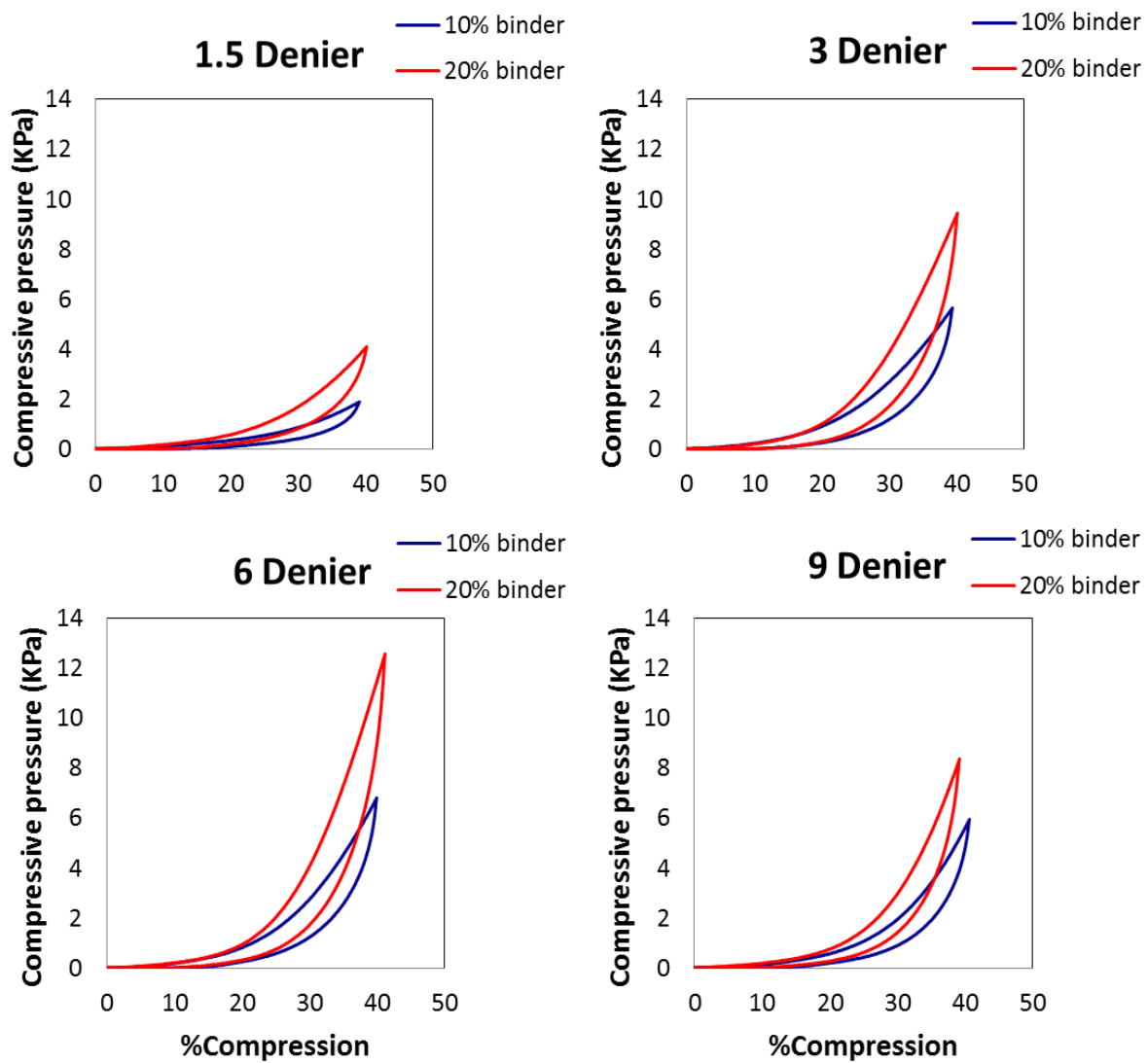


Figure 3.4: compressive pressure versus compression percentages for various fiber sizes and binder percentages

3.3.1.1 Evaluation of compressive resistance

As it was mentioned earlier, compression resistance is the compression pressure required to reach a specific percent of compression. The figure 3.5 shows the compressive resistance to reach to 10%, 20%, 30%, and 40% compression in different fiber sizes. In other words, the compressive resistance give the amount of compression pressure which if applied to the structure it will loss the given percentage of its thickness. It is observed that the required compression pressure shows a maximum by fiber linear density. It means that compressibility decrease with the increase in the fiber diameter up to a certain level and thereafter it increases with further increase in the fiber diameter. Similar trends are observed for the both binder percentages. This is explained by the effect of binders. At the same amount of binder percentages, larger fiber size might shows less resistance to the compression due to lower amount of contact points created by binders. It suggests that the binder fiber content of less than 20% is insufficient to hold the dimension of nonwovens with 9 denier fiber sizes. It is obvious that the nonwovens with higher binder percentages show higher compressive resistance, even though it seems that the larger the compression percentages, higher is the effect of binder fibers.

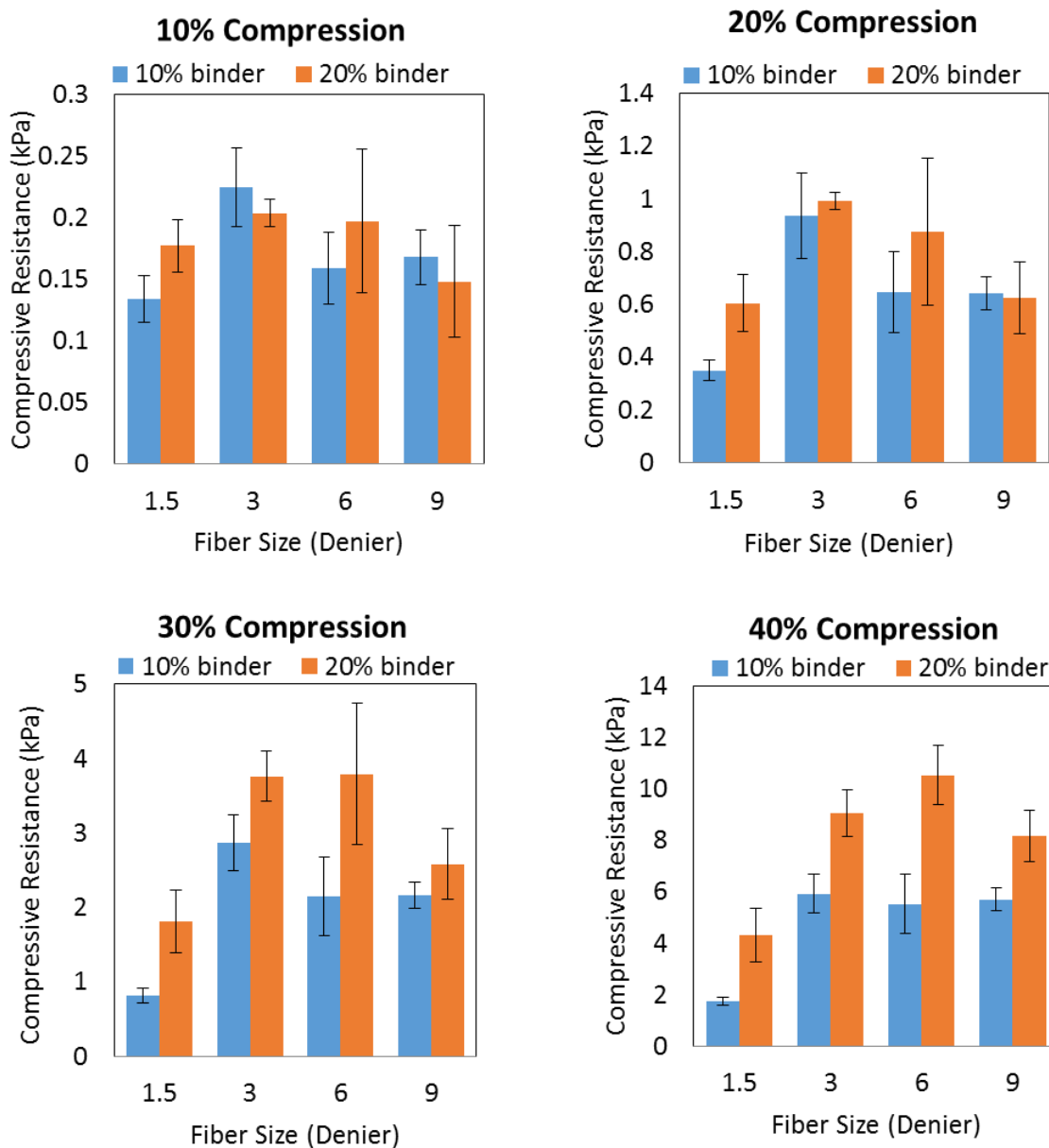


Figure 3.5: the compressive resistance in order to reach to various compression percentages for samples containing various fiber sizes and binder percentages

3.3.1.2 Evaluation of compression behavior based on van Wyk Theory

Typical curves for compressive pressure versus solidity cube is given in figure 3.6, in which Higher slope indicates higher resistance against changes in the solidity with the same amount of compression load.

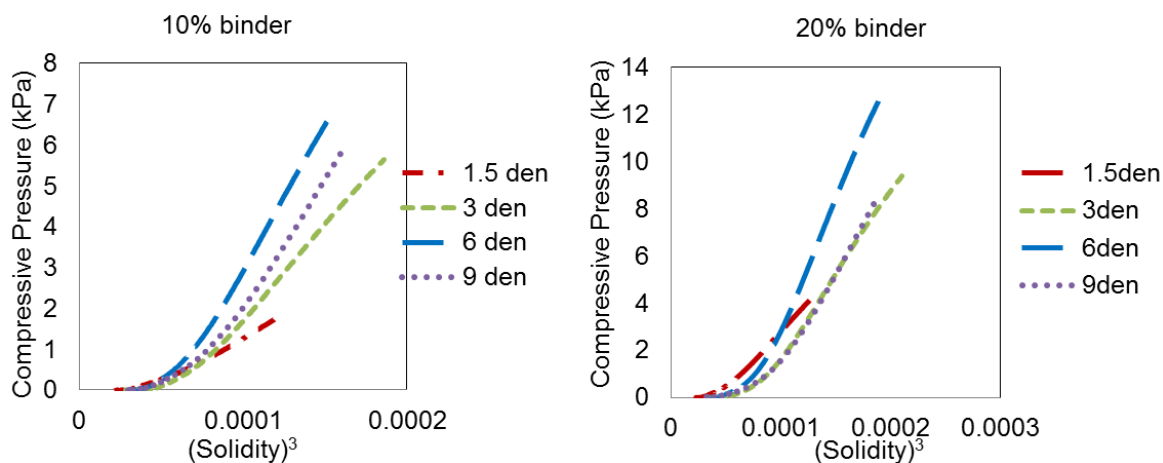


Figure 3.6: compressive pressure versus solidity cube in order to determine the resistance to compression based on van Wyks model

It is expected that the larger fiber size results in the higher slope based on van Wyk equation because of its higher bending rigidity assuming that the distance between two contact points are similar.

However, as it is observed in figure 3.7, in the presented samples, regardless of having higher bending rigidity 9 denier fibers show the lower slope than 6 denier. This is explained by the effect of binders on creating the non-slipping contact points, which suggests that the contribution of the binder fibers in creating the non-slipping contact points reduced at larger fiber sizes. However quantifying this effect is not within the scope of this study, the results suggested that binding can influence on the

slope α in nonwoven materials, which means not only the fiber diameter determines the compressibility but also the binding can influence on their compressibility. However this is of great theoretical and practical importance, unfortunately, a quantitative theory to account for this effect has not yet been formulated.

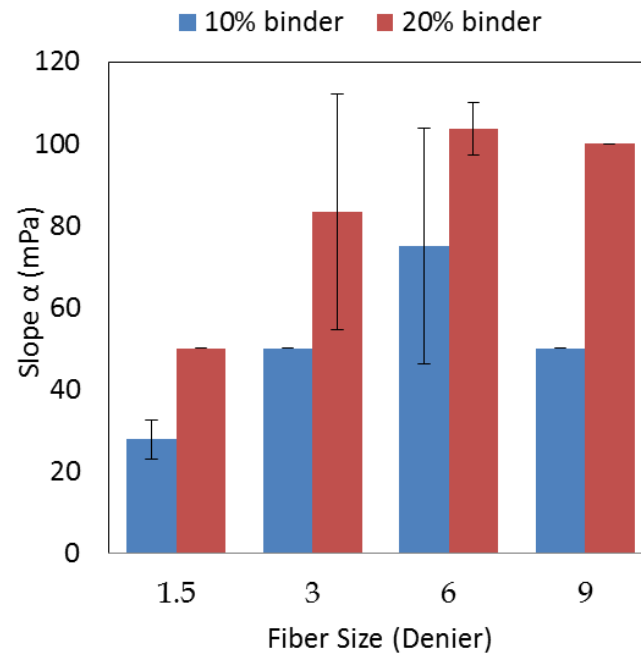


Figure 3.7: calculated slope α in order to determine the resistance to compression based on van Wyks model

3.3.1.3 Evaluation of percentage of energy loss and recoverability

The energy loss percentages results are shown in the figure 3.8 for the different samples. It was observed that without exception increase in the binder percentages result in the lower energy loss. It is due to the fact that the fiber slippage is lower in the samples with higher binder percentages, consequently the frictional effects and energy loss is lower in these samples. Energy dissipation might happen because of two reasons, the frictional loss and viscose damping. However Dunlop showed

that the hysteresis is independent of the rate of compression and it means the energy loss or dissipation is more likely because of frictional loss (Dunlop 1983). Furthermore, larger fiber sizes gave rise to smaller percentages of energy loss in general.

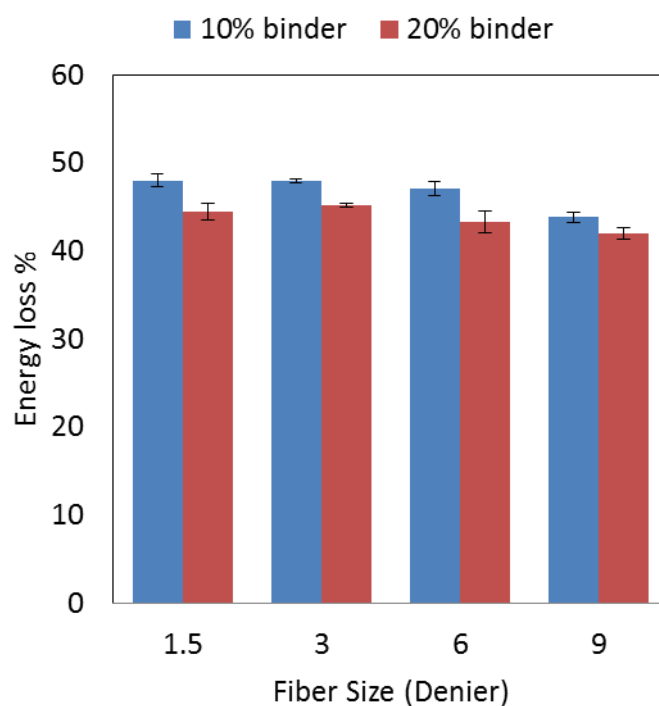


Figure 3.8: energy loss measurements in varying fiber diameter and binder percentages

Figure 3.9 shows the recoverability results. Recoverability determines the ability of the structure to maintain the thickness during and after loading and the cause of recovery is the stored energy during loading (Carnaby and Pan 1989). Therefore it is predicted that the recoverability will be higher in samples containing larger fiber sizes and 20% of binder fibers. It has been clearly observed that in majority of the cases increasing the binder percentage increases the recoverability except in 9 denier nonwovens in which there is not a significant change in recoverability. In both different binder

percentages, the recoverability shows an increase in trend with the increase in the fiber diameter. This is in agreement with the results obtained from energy loss percentages.

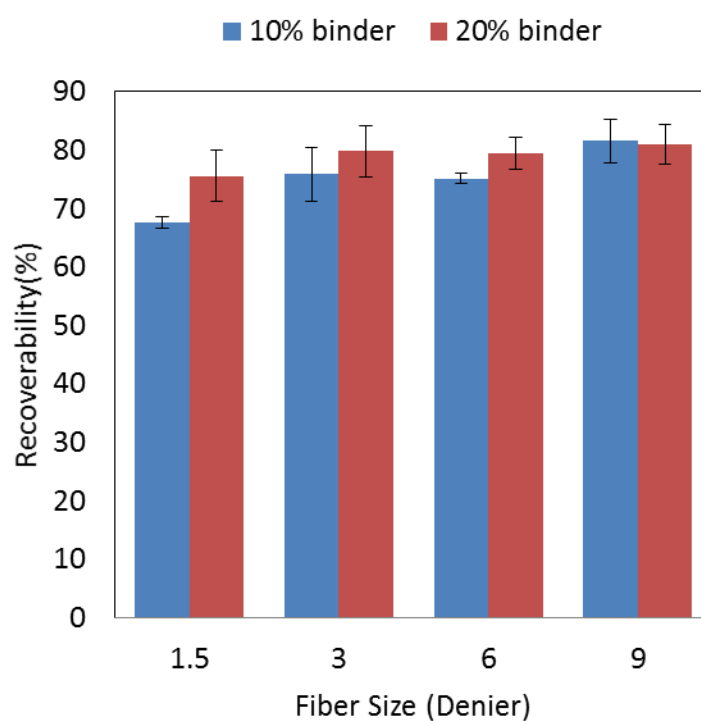


Figure 3.9: recoverability measurements in varying fiber diameter and binder percentages

3.3.2 The effect of fiber cross-sectional shape on compressional behavior

As outlined in the introduction, we sought to understand the effect of structural parameters of nonwovens on their compression behavior, therefore the effect of fiber cross-sectional shape was also studied. The compression result for nonwoven materials with different fiber cross-sectional shape has

been shown in figure 3.10 at different binder percentages. The graphs show that 4DG and Pentalobal fibers behave in a different manner than round fibers with the same fiber diameter, which refutes the conclusion given by Pan (1993).

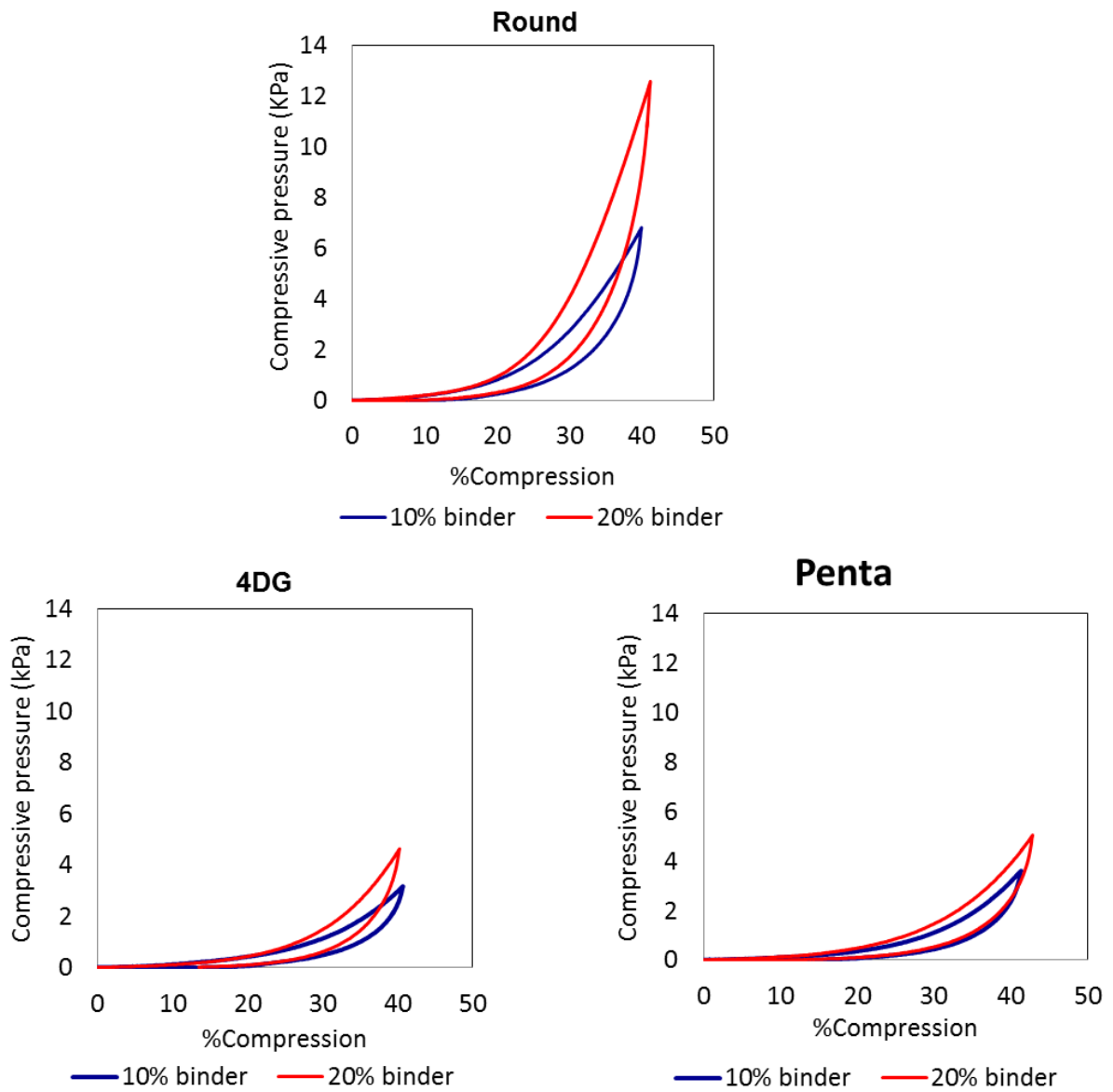


Figure 3.10: compression pressure vs. compression percent, different fiber cross-section at various binder percentages

3.3.2.1 Evaluation of compressive resistance

The compressive resistance at various compression levels was measured for different fiber cross-sections as can be seen in figure 3.11. Without exception, round fiber cross-section exhibits significantly higher compressive resistance than 4DG and pentalobal fiber cross-sections. However the compressive resistance values are dependent on the initial solidity of the samples (Neckár 1997). Therefore the slight differences between the 4DG and pentalobal fibers might come from the variation in their initial solidities. The compression resistance was invariably observed to be higher in samples of round and 4dg fiber cross-sections containing 20% of binder fibers than 10% binder fibers, but it was not seen in case of Pentalobal fibers. The compression resistance, therefore, was studied by van Wyk theory of compression, in order to eliminate the impact of initial solidity.

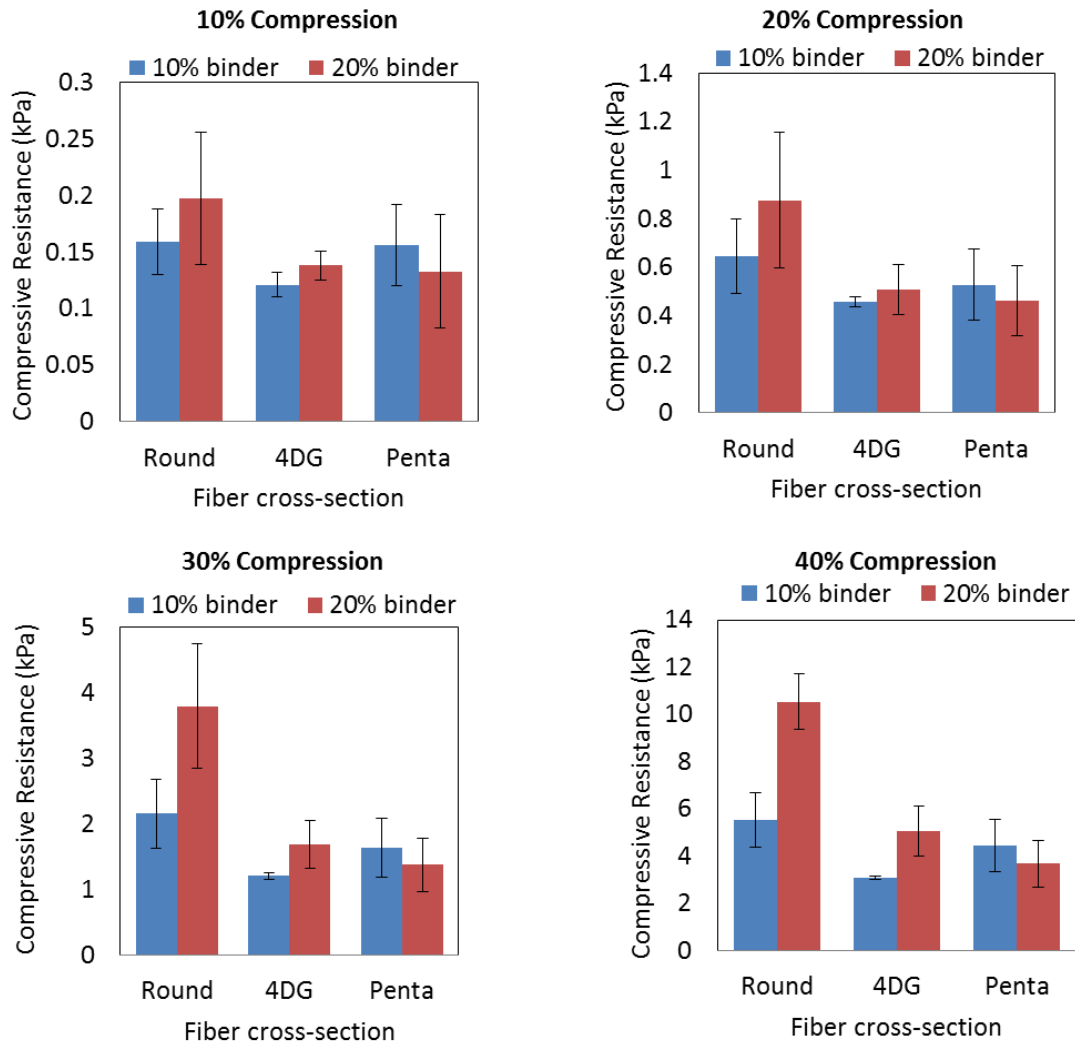


Figure 3.11: compressive resistance for different fiber cross-sections at various compression levels

3.3.2.2 Evaluation of compression behavior based on van Wyk theory

Figure 3.12 displays the typical compressive pressure versus solidity cube for different fiber cross-sections. As it was mentioned earlier, higher slope of the linear part indicate the higher resistance against changes in solid volume fraction of the samples with the same amount of compression load.

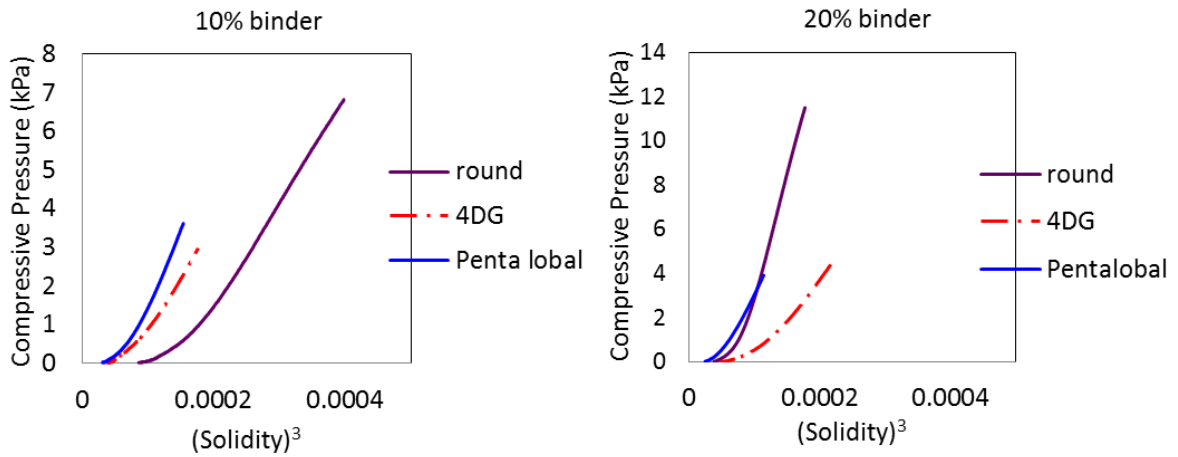


Figure 3.12: compressive pressure vs. cube solidity in different fiber cross-sections

The slope α is calculated for different fiber cross-sections and is shown in figure 3.13. It can be observed that round fiber shows higher slope than non-round fiber cross-section which is as expected because of their higher bending rigidity due to their higher moment of inertia of the round shapes. Moreover as anticipated, nonwoven materials containing 20% binder exhibit larger slope since the binder fibers makes some non-slipping contact point and larger the percentages of the binder fibers, the number of bonded contact points are increased (Pan 1993).

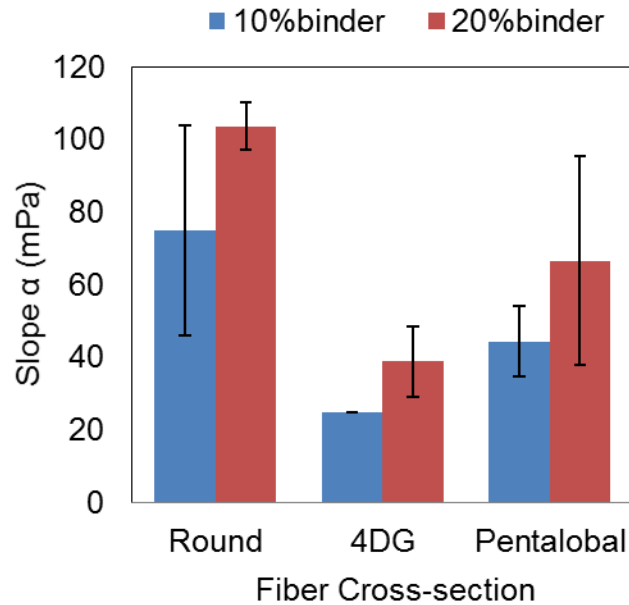


Figure 3.13: calculated slope α based on van Wyk equation.

3.3.2.3 Evaluation of energy loss percentage and recoverability

The energy loss percentages were measured for fibers of various fiber cross-sections at different binder fiber percentages as indicated in figure 3.14. The round fibers exhibited slightly lower percentages of energy loss. This might be due to the different packing behavior of fibers which therefore the round fibers can better hold the dimension of the nonwoven and so the energy loss is lower. As it was stated earlier, smaller percentage of energy loss gives rise to higher recoverability percentages. The measured recoverability, which can be found on figure 3.15, supports this statement.

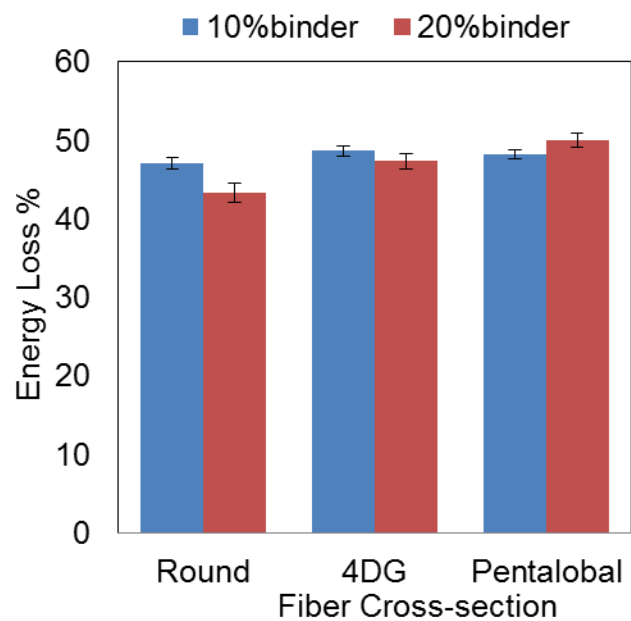


Figure 3.14: percentage of energy loss in samples of various fiber cross-section and binder percentages

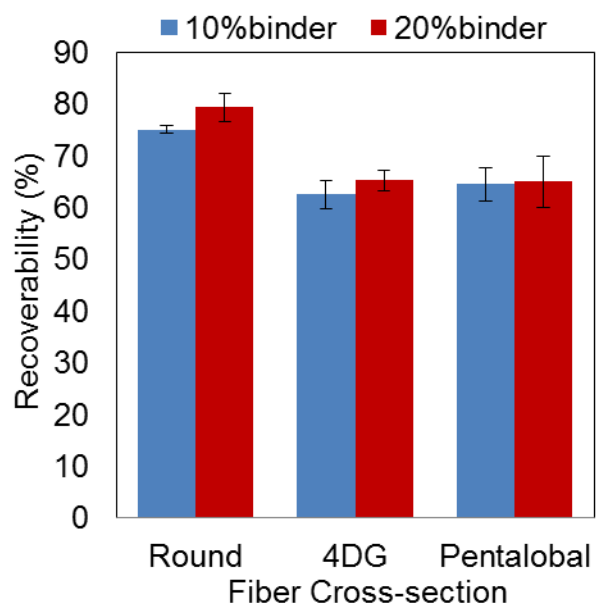


Figure 3.15: recoverability measurements in varying fiber cross-section and binder percentage

3.4 CONCLUSION

In this paper, compression and recovery behavior of through-air bonded nonwoven fabrics was studied. The compressional behavior of nonwovens was evaluated in terms of their structural parameters including fiber size, fiber cross-sectional shape, and binder percentages. To the best of author's knowledge, for the first time, the testing methodology was established in terms of constant rate of elongation. Compressive resistance, percentage of energy loss, and recoverability were evaluated. Our results indicate that all the fiber size, fiber cross-section and binder percentages influence on the compressional and recovery behavior of nonwovens. At the similar percentage of the same binder fibers, the compressive resistances show an increase and then decrease by the fiber size. Larger binder percentages improve both the compressive resistance and recoverability of the through-air bonded nonwovens. Moreover, the larger fiber linear densities and also round fiber cross-section improve the recoverability of the nonwoven fabric. The packing density of the nonwovens at various compression levels was also studied based on van Wyk theory. The results showed the linear relationship between the compressive pressure and cube of solidity at the middle range of compression.

REFERENCES

- Batra, Subhash K., and Behnam. Pourdeyhimi. 2012. *Introduction to Nonwovens Technology*. Lancaster, PA: Destech Publications.
- Beil, N. B., and W. W. Roberts. 2002. "Modeling and Computer Simulation of the Compressional Behavior of Fiber Assemblies: Part I: Comparison to van Wyk's Theory." *Textile Research Journal* 72 (4): 341–51. doi:10.1177/004051750207200411.
- Carnaby, G. A., and N. Pan. 1989. "Theory of the Compression Hysteresis of Fibrous Assemblies." *Textile Research Journal* 59 (5): 275–84. doi:10.1177/004051758905900505.
- Debnath, Sanjoy, and M. Madhusoothanan. 2012. "Studies on Compression Properties of Polyester Needle-Punched Nonwoven Fabrics under Dry and Wet Conditions." *Journal of Industrial Textiles* 41 (4): 292–308.
- Dunlop, J. I. 1974. "CHARACTERIZING THE COMPRESSION PROPERTIES OF FIBRE MASSES." *Journal of the Textile Institute* 65 (10): 532–36. doi:10.1080/00405007408630141.
- Dunlop, J.I. 1983. "On the Compression Characteristics of Fibre Masses." *Journal of the Textile Institute* 74 (2): 92–97. doi:10.1080/00405008308631770.
- Kelly, Piaras Alphonsus, Simon Bickerton, and Jonathan Cheng. 2011. "Transverse Compression Properties of Textile Materials." *Advanced Materials Research* 332-334 (September): 697–701. doi:10.4028/www.scientific.net/AMR.332-334.697.
- Komori, Takashi, and Kunio Makishima. 1977. "Numbers of Fiber-to-Fiber Contacts in General Fiber Assemblies." *Textile Research Journal* 47 (1): 13–17.
- Komori, T., and M. Itoh. 1991. "Theory of the General Deformation of Fiber Assemblies." *Textile Research Journal* 61 (10): 588–94. doi:10.1177/004051759106101005.

- Kothari, V.K., and A. Das. 1992. "Compressional Behaviour of Nonwoven Geotextiles." *Geotextiles and Geomembranes* 11 (3): 235–53. doi:10.1016/0266-1144(92)90002-R.
- Kothari, V. K., and A. Das. 1996. "An Approach to the Thoery of Compression of Nonwoven Fabrics." *Indian Journal of Fiber and Textile Research* 21 (December): 235–43.
- Lee, Dae Hoon, and Garth A. Carnaby. 1992. "Compressional Energy of the Random Fiber Assembly Part I: Theory." *Textile Research Journal* 62 (4): 185.
- Maze, Benoit, Hooman Vahedi Tafreshi, and Behnam Pourdeyhimi. 2007. "Geometrical Modeling of Fibrous Materials under Compression." *Journal of Applied Physics* 102 (7): 073533. doi:10.1063/1.2794476.
- Michielsen, Stephen, Behnam Pourdeyhimi, and Prashant Desai. 2006. "Review of Thermally Point-Bonded Nonwovens: Materials, Processes, and Properties." *Journal of Applied Polymer Science* 99 (5): 2489–96. doi:10.1002/app.22858.
- Neckár, Bohuslav. 1997. "Compression and Packing Density of Fibrous Assemblies." *Textile Research Journal* 67 (2): 123–30.
- Pan, Ning. 1993. "A Modified Analysis of the Microstructural Characteristics of General Fiber Assemblies." *Textile Research Journal* 63 (6): 336–45. doi:10.1177/004051759306300605.
- Rawal, A., S. Lomov, T. Ngo, I. Verpoest, and J. Vankerrebrouck. 2007. "Mechanical Behavior of Thru-Air Bonded Nonwoven Structures." *Textile Research Journal* 77 (6): 417–31. doi:10.1177/0040517507081313.
- Rawal, Amit. 2009. "Application of Theory of Compression to Thermal Bonded Non-Woven Structures." *Journal of the Textile Institute* 100 (1): 28–34. doi:10.1080/00405000701592975.

- Rawal, Amit, Puneet Kumar Mishra, and Harshvardhan Saraswat. 2012. "Modeling the Compression-Induced Morphological Behavior of Nonwoven Materials." *Journal of Materials Science* 47 (5): 2365–74. doi:10.1007/s10853-011-6055-x.
- Russell, S. J., Textile Institute, eds. 2007. *Handbook of Nonwovens*. Woodhead Publishing Series in Textiles 58. Boca Raton: CRC Press [u.a.].
- Schoppee, M. M. 1998. "A Poisson Model of Nonwoven Fiber Assemblies in Compression at High Stress." *Textile Research Journal* 68 (5): 371–84. doi:10.1177/004051759806800507.
- Van Wyk, C. M. 1946. "NOTE ON THE COMPRESSIBILITY OF WOOL." *Journal of the Textile Institute Transactions* 37 (12): T285–92. doi:10.1080/19447024608659279.

4 INVESTIGATION OF EFFECT OF STRUCTURAL PARAMETERS ON ABSORPTION AND RELEASE PROPERTIES OF NONWOVENS- PART I: FIBER SIZE STUDY

4.1 INTRODUCTION

Nonwovens are fiber assemblies, which are bonded by mechanical, thermal or chemical means. They are a particular type of porous structure with high porosities. Absorbency is one of the key properties required in major nonwoven applications including baby diapers, personal hygiene products, wipes and medical fabrics (Hardy 2009). The functionality of the absorbent products is related to receiving, absorbing, retaining or releasing of the liquid depending on their final applications (Tirimacco, Goulet, and Veith 2008; Roque et al. 2011; Ikezawa, Watanabe, and Yamada 1997; Chappell, Keeler, and Hammons 1994). Improving the functionality of the absorbent products through modification of nonwoven fabrics has been the subject of many patents for many years and the result can be found in the commercialized products. Some of the fundamental practices by industry include the reduction of the pore size and improving the capillary force by trying various approaches such as overall compression, line embossing, and pattern embossing (Heitmeyer 1932; De et al. 1973), employing layers of various densities of average pore size ranges (Bernardin 1987), stretching a fibrous structure comprising meltable fibers in one direction and freezing the deformation by heat curing in order to reduce the pore size (Hassenboehler and Wadsworth 1993), producing a web containing different fibers of chemically stiffened, twisted, and curled bulking fibers, high surface area fibers, and thermoplastic binder fibers in order to improve the capillary forces (Horney and Noel 1996). However systematic investigation of the absorption behavior of nonwovens did not gain enough attention from the scientific point of view especially with the consideration of controlling the different variables including structural parameters and materials.

Even absorbency of materials have been studied extensively in various fields, absorbency behavior of nonwoven products are complex and have not fully understood (Cueto et al. 2009; Yun et al. 2009; Ashari and Vahedi Tafreshi 2009a; Chatterjee and Gupta 2002; Tracy, Ghali, and Jones 1994; Ashari and Vahedi Tafreshi 2009b). Absorption in nonwovens is a process in which water molecules enter the bulk volume of nonwovens. Several fundamental physical phenomena are included in this process including the wetting of fiber surfaces, transport of liquid into the porous structure of nonwovens by capillary forces or external forces, adsorption of liquid on the fiber surfaces, and the diffusion of liquid into the interior of fibers. Wetting of the fiber surface depends on the surface energy of the fibers, as well as liquid properties (Kissa 1996; Patnaik et al. 2006; Richards 1931). On the other hand, the transport of liquid into the porous structure not only is related to Interaction of fibers and liquids through the resulted contact angle and the liquid properties but to the geometric configuration of porous structure as well (Pan and Zhong 2006; Adamson 1997). The influence of pore characteristics on the liquid transport behavior has been extensively studied by modeling the simple pore structures, as well as more complicated structures using Laplace equation (Chatterjee and Gupta 2002), Lucas-Washburn equation (Washburn 1921) and Hegan-Poiseuille equation for examples in (Shou, Ye, Fan, and Fu 2014; Shou, Ye, Fan, Fu, et al. 2014; Figliuzzi and Buie 2013; Mason and Morrow 1991; Young 2004; Szekely, Neumann, and Chuang 1971; Hamraoui and Nylander 2002; Masoodi, Pillai, and Varanasi 2007; Hemmat and Borhan 1996). Therefore geometrical aspects of the structure and the material properties are, along with finish, major contributors to absorption and release behavior of nonwovens.

The structural parameters of nonwovens, including the fiber geometry, fiber orientation, and web solidity define the pore characteristics of nonwovens, Moreover the external factors such as external forces and swelling may influence on the pore characteristics. When it comes to the nonwoven

materials, the effect of fiber orientation on both the pore characteristics, as well as absorption properties has been widely recognized through theoretical, as well as empirical evaluations (Konopka 2001; Mao and Russell 2003; Mao 2009; Ashari, Bucher, and Vahedi Tafreshi 2010). It is well-known that the anisotropy of liquid absorption is influenced by the fiber orientation distribution in fabric plane. Furthermore it is well documented that the pore characteristics, mainly porosity, play a significant role on the absorption properties of nonwovens (Raju Seenivasan Rengasamy et al. 2011; Das, Pradhan, and Pourdeyhimi 2012; R.S. Rengasamy, Das, and Praba Karan 2011). Other researches have also investigated the effect of the construction parameters of nonwovens and fiber materials simultaneously (Dubrovski and Brezocnik 2014; Dedov et al. 2001; Dubrovski and Brezocnik 2012) which is why it is difficult to make any conclusion based on their results.

In order to characterize the absorption behavior of nonwovens, it is important that the absorbency behavior is measured in conditions similar to those found in real situation. The gravimetric absorbency testing system has the most advantages in this regard (Seong Hun Kim et al. 2003), whereas many of the researches on absorption behavior of nonwovens are based on vertical wicking test or weight gain method where the results are highly influenced by the testing situation (X. Chen et al. 2009). Finally, to the best of author's knowledge, the release properties of nonwovens remains unstudied experimentally and there is little available on numerical simulation (Ashari and Vahedi Tafreshi 2009a), moreover little work has been done on the influence of compression on the pore characteristics, as well as absorption behavior, although these studies carries practical importance in many applications. The Purpose of this study is to scientifically examine the absorbency and release behavior of nonwovens by decoupling the effect of structural parameters and material properties, considering the impact of compression and flow direction. In the current paper we focus on the

structural parameters evaluation by emphasizing on the influence of fiber cross-sectional size on the pore characteristics, absorption and release properties of nonwovens under compression.

4.2 MATERIAL AND EXPERIMENTAL

4.2.1 Description of samples

In this work, eight different types of fabrics, as shown in Table 4.1 as group A and group B, were produced in order to study the effect of fiber size, and percentages of binder fibers. Group A fabrics were 90%PET, 10% binder fiber, made of four different fiber linear densities; Group B fabrics were 80% PET, 20% Co-PET fiber. Both group A and B has round fiber cross-section. The binder fibers were concentric sheath/ core Co-PET /PET bicomponent fibers with the linear density of 2 denier and 1.5 inch. Melting point of co-PET sheath component is 110 °C (T201 Provided by Fiber Innovation Technology). All the fabrics were manufactured through carding, cross-lapping, pre-needling and through air bonding processes in the Nonwovens Institute's Staple Pilot Facilities (Raleigh, North Carolina). Through air bonding was done on the temperature of 121°C.

Table 4.1: sample details

Group code	Sample #	PET fiber size (denier)	PET fiber diameter (µm)	PET fiber cross-section	% Binder	%PET
A	1	1.5	13	Round	10	90
	2	3	19	Round	10	90
	3	6	28	Round	10	90
	4	9	33	Round	10	90
B	1	1.5	13	Round	20	80
	2	3	18	Round	20	80
	3	6	27	Round	20	80
	4	9	33	Round	20	80

4.2.2 Basic web properties

Thickness of samples was measured using an Ames Logic basic thickness gauge model no. BG1110-1-04. The presser foot diameter was 1 inch and the applied pressure was 0.6 psi. The thickness was measured for 15 different places along the fabric.

The basis weights of the samples were calculated for 18 different replicates per each sample according to equation 4.1, in which w is the mass of the sample and A is the sample area. The samples were the round samples with the area of 100cm^2 .

$$\text{Basis weight } \left(\frac{\text{g}}{\text{m}^2} \right) = \frac{w (\text{g})}{A} \quad (4.1)$$

Finally the solidity of the samples was calculated according to the equation 4.2.

$$\text{Solidity} = \frac{(w/A/t)}{\rho} \quad (4.2)$$

Where, w : sample mass (g)

A : sample area (cm^2),

t : sample thickness (cm) and

ρ : fiber mass density ($1.37\text{g}/\text{cm}^3$ for polyester fibers)

4.2.3 Pore size measurement - porometry technique

The mean flow pore diameter of the nonwoven samples was measured using a capillary flow porometer (CFP-1100-AA, PMI, New York, USA) according to the principle of liquid extrusion technique. The samples were fully wetted with a fluid in the name of Galwick and surface tension of $15.9 \text{ Dynes}/\text{cm}$.

4.2.4 Pore size measurement of compressed samples- porosimetry technique

The PMI liquid extrusion porosimeter (LEP-1100AX) was employed to measure the median pore size (according to through-pore volume) at various compression levels. This technique was performed on

the nonwoven samples containing 6-denier fiber in order to measure the porous parameters of the nonwoven samples under various levels of compression of 0, 20, 30, and 40% compression. The samples were wetted with water with surface tension of 72 Dynes/cm.

4.2.5 Through-plane absorbency testing under compression

The Gravimetric Absorbency Testing System (GATS) is the system that widely used in many industries (Chatterjee and Gupta 2002). In a typical setup of this system, the liquid is delivered to the sample by the capillary pressure of the sample's porous structure, the amount of liquid absorbed by the sample is recorded against time, and then the data is graphed based on the weight of absorbed liquid versus time. The graph is then used to measure the maximum capacity of absorption and the rate of absorption. In order to remove the effect of sample's weight, the maximum absorption and absorbency rate is reported per each gram of fabric. The height of the test plate and the height of liquid in the reservoir kept at the same level in order to provide zero hydrostatic pressure. This provides the situation in which the liquid is taken up solely on demand by material. A compression foot, having a diameter slightly larger than the samples, was added to this set-up. A linear actuator controlled the compression foot in order to control the samples thickness. Samples were compressed to 0, 10, 20, 30, and 40 % of initial thickness and their absorbency was measured. Figure 4.1 shows the schematic of the modified GATS. The samples are placed on a metal mesh where the whole area of the samples was in contact with the liquid. Modified GATS is capable of measuring maximum capacity of absorption, as well as the rate of absorption under varied static compression level and in the through-plane direction.

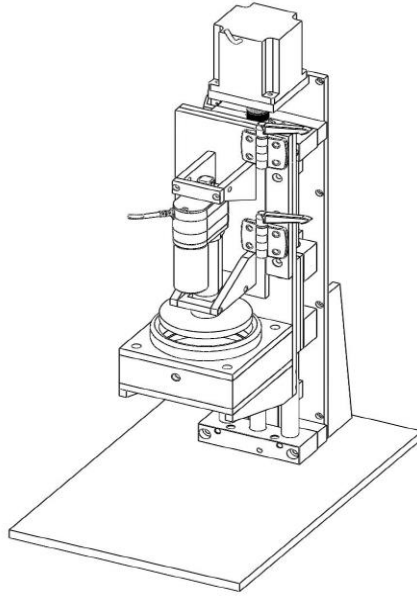


Figure 4.1: modified NWI GATS (compression GATS)

Figure 4.2 shows a typical testing result on modified GATS. The information obtained from the GATS results includes maximum absorbency and absorbency rate as shown in the figure 4.2. The absorbency is the ratio of the weight of liquid absorbed by the samples to the dry weight of the nonwoven materials. The curve consists of fast initial liquid uptake followed by plateaus, which indicate it reach maximum absorption capacity of samples. The slope of the liquid rise in the beginning of the test determines the absorbency rate.

The nonwoven materials were tested with the modified gravimetric absorbency testing systems (GATS) under 0, 10, 20, 30, 40% compression level. The 0.1% Triton-X100 solution was selected as the testing liquid to achieve complete wetting of fibers. Samples were cut to round sample with diameter of 8.89 cm. All the finishes and impurities were removed through washing the samples with

distilled water 50°C for 6 hours. The distilled water was replaced 3 times per 6 hours. 3 replicates per each treatment were tested, and their average and standard deviation are reported.

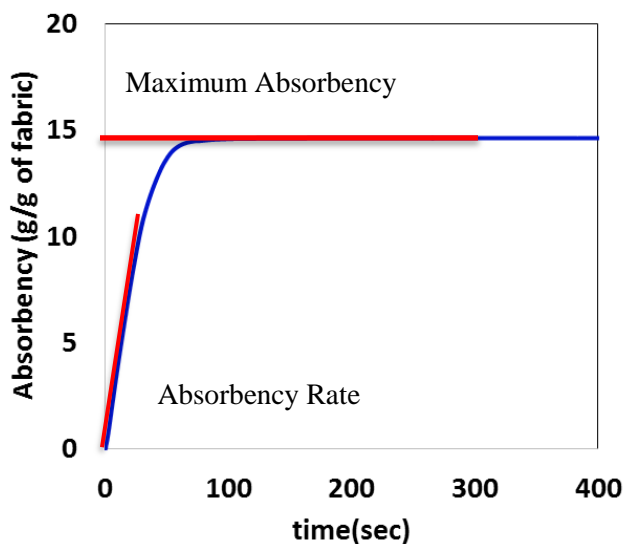


Figure 4.2: typical GATS curve

4.2.6 In-plane wicking measurement

In order to study the wicking behavior of samples in-plane direction, a point wicking test were performed on the entire samples. In the in-plane wicking test, we replaced the metal mesh sheet on the top of the samples holder with a Teflon plate, which was hollowed in the center in GATs system previously described. Figure 4.3 shows the schematic of the Teflon plate. The hollow cylinder in the middle of the plate is where the liquid is delivered to the sample. To hold the sample tightly on the plate for testing, a hoop was used to tight the sample in the horizontal plane. The test was stopped when the liquid reaches the inner edge of the hoop.



Figure 4.3: schematic of the Teflon plate for the in-plane wicking testing system

The nonwoven samples were tested for their in-plane wicking properties under zero compression percentages. The 0.1% Triton-X100 solution was selected as the testing liquid to achieve complete wetting of the samples. A 4 inches hood was employed for holding the samples tight. Samples were cut with an area of 100 cm^2 . The test was done under a slightly negative pressure head, since otherwise the liquid does not had enough pressure to move through the hollow cylinder in the middle of the plate. All samples were washed prior to the test and were free of finishes.

4.2.7 Vertical wicking measurement

In order to study the absorption behavior of nonwoven samples in the vertical direction, the vertical wicking test was performed in accordance with the Association of Nonwoven Fabrics Industry's (INDA) standard test method 10.1 (INDA WSP 10.1). In this method a preconditioned strip of material was cut in a machine direction with the dimension of 1 inch by 6 inch and one end of the strip hanged vertically down into a liquid. The first 60 minutes of the experiment was recorded in a video format and afterwards the picture was taken in order to record the liquid penetration at various times. Imagej software was employed to measure how fast and how far the liquid goes into the fabric during the vertical wicking.

The liquid used for the vertical wicking measurements was 0.1% Triton-X100 solution. All the samples were washed prior to the test and were free of finishes. For observing the height of water wicked into the fabric, a mentioned solution of 0.00126% navy acid blue dye was used.

4.2.8 Evaluation of liquid holding capacity under compression

Two different methodologies were employed in order to study the release behavior of saturated samples at different compression levels. In the first methodology, the sample is saturated on the GATS under no compression, and then in a separate set-up, the samples were loaded to different levels of compression consecutively and the amount of liquid release in each step is recorded. Figure 4.4 shows the schematic of desorbency testing system under compression. The required loading weight in order to reach to the specific amount of compression percentages is calculated based on the compression result of the samples on the Instron, and the area of the samples. From the compression result (Chapter 3), the compressive pressure required to reach a compression percentages is known, and the compression pressure is converted to the required loading weight by knowing the samples area.

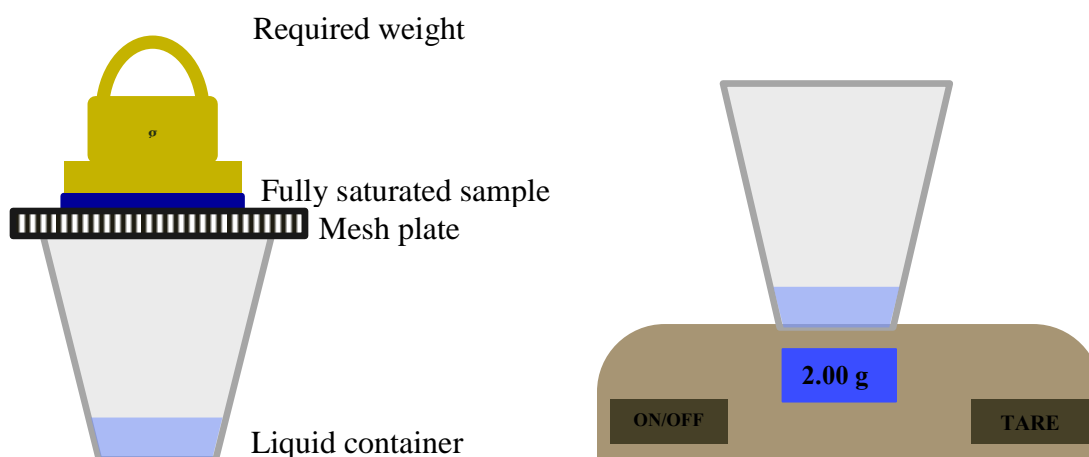


Figure 4.4: desorbency testing set up under compression based on GATS

In the second methodology, first the basket test (Edana WSP 10.1 (08)) is done on the samples with some modification for the purpose of completely wetting the sample. In contrast with the standard, in this method, different layers of the each sample are stacked in the basket and after completing the basket test, with the same procedure mentioned earlier, the required loading weight is calculated and the amount of liquid released from the sample is calculated. The schematic is shown in figure 4.5.

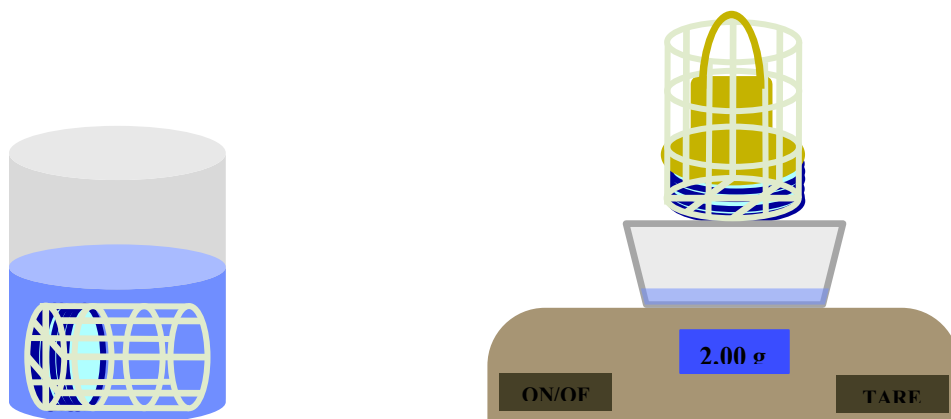


Figure 4.5: desorbency testing system under compression based on Basket test

The nonwoven materials were tested with desorption testing system based on both GATS and basket test under 0, 10, 20, 30, 40% compression level. The 0.1% Triton-X100 solution was selected as the testing liquid to achieve complete wetting of fibers. Samples for the testing methodology based on GATS were cut to round sample with diameter of 8.89 cm. For the testing methodology based on basket test different layers of the samples with the diameter of 6.35 cm were cut in order to reach to the weight range on 5 ± 0.2 g. It should be noted that a new basket with larger dimensions were made for this purpose. 2 replicates per each treatment were tested, and their average and standard deviation are reported.

Liquid holding capacity of the samples was calculated for both methodology explained earlier through the equation 4.3.

$$W_{rt} = \frac{(W_s - W_{rl})}{W_s} \times 100 \quad (4.3)$$

Where W_{rt} is the percentage of the liquid retained by the sample, W_s the mass of liquid absorbed by the samples at saturation, and W_{rl} the mass of liquid released by the sample.

It should be noted that the mass of liquid absorbed by the sample at saturation is calculated based on the maximum absorption of liquid from GATS result, or the absorption capacity calculated from basket test.

4.2.9 Theoretical determination of maximum absorption capacity of nonwovens

Assuming all the pores are filled with the liquid, so the whole amount of interstitial space inside the nonwoven fabrics is a key factor, which determines the maximum absorption capacity. Thus maximum absorption capacity of the samples with this assumption that all the pores are filled with water was calculated according to below relationship between solidity and the maximum absorbency. The solidity of the samples at that specific amount of compression load was obtained based on the dimensions of the samples after compression. The relation between the maximum absorbency, C_{max} can be calculated theoretically as shown in equation 4.4.

$$C_{max} = \left(\frac{1}{s} - 1\right) \cdot \frac{1}{\rho_{fiber}} \quad (4.4)$$

Where s is the solid volume fraction, and

$$\rho_{fiber} = \rho_{PET} = 1.37 \text{ g/cm}^3$$

4.3 RESULTS AND DISCUSSION

4.3.1 Thickness and solid volume fraction

The thickness and solid volume fraction of the samples are listed in table 4.2. Generally speaking, the thickness and solidity of the samples are consistent in a reasonable range. However it was observed that the samples containing smaller fiber size appeared to have slightly lower solidity. Moreover in general, larger binder percentages gave rise to slightly higher solidity. But these small variations are inevitable and hard to control. This means that employing the binder fibers and through-air bonding is a reliable technique in order to have control over the solidity of the samples containing various fibers. In this study, it was attempted to consider the influence of these small variations by discussing the results according to the solidity of the samples.

Table 4.2: structural characteristics of nonwoven samples

Samples code	Basis weight (g/m ²)	Thickness (mm)	Initial Solidity
A1	218	5.01	0.032
A2	210	4.35	0.035
A3	212	4.45	0.035
A4	222	4.78	0.034
B1	182	4.06	0.033
B2	202	4.11	0.036
B3	214	4.25	0.037
B4	224	4.81	0.034

4.3.2 Pore diameter

Our purpose was to investigate the absorbency behavior of nonwovens according to their pore characteristics; therefore the pore diameter and its distribution were experimentally determined with a capillary flow porometer. The values of the smallest and largest detected pore diameter, as well as mean flow pore diameter were graphed in the figures 4.6 and 4.7. All the values measured in this

technique are related to the most constricted pore diameter; also the mean flow pore diameter is such that 50% of flow happened through the pores larger than this value, and the rest of the flow is through smaller pores (Akshaya Jena and Gupta 2003). It is obvious from the figures that larger fiber size creates the structure with larger pore size. The porometer did not provide the pore size information for the 9 denier samples with the composition of 90% PET and 10% Co-PET. It is because of the large size of pores in this structure, which are behind the scope of the instrument. Moreover, it is observed that samples with 20 % binder fibers have smaller pores. This is especially obvious at samples containing larger fiber sizes.

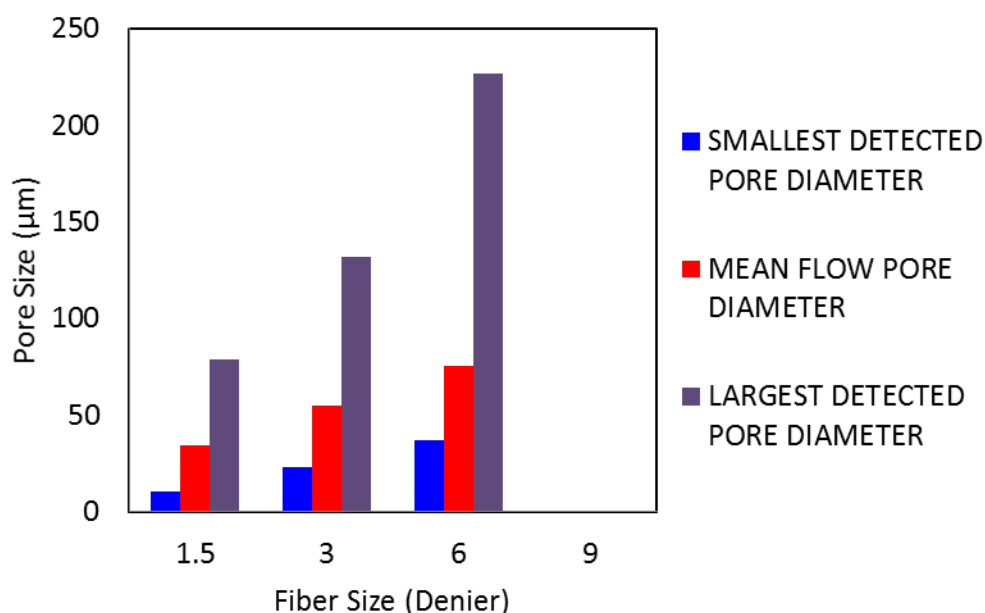


Figure 4.6: experimental result for pore diameter for 90%PET-10%Co-PET

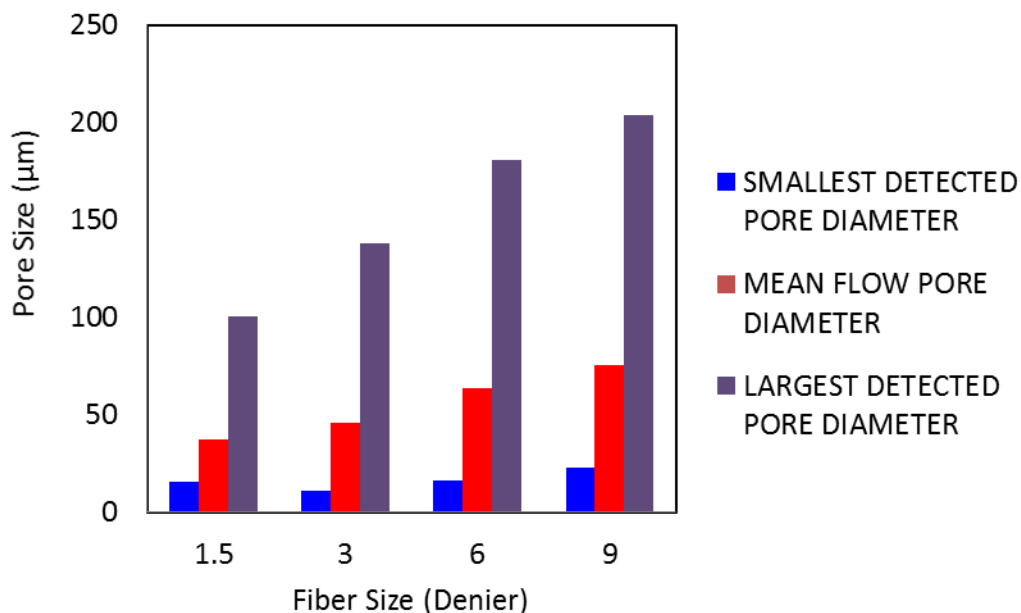


Figure 4.7: the experimental result for pore diameter for 80%PET-20%Co-PET

4.3.3 Absorption properties

In this section, the liquid absorption behavior of the nonwovens materials with different fiber sizes and different binder percentages are discussed. To understand the effect of compression, samples were compressed to different compression percentages of 0, 10, 20, 30, and 40 % based on their initial thickness. Plot of GATS absorbency are shown in figures 4.8 and 4.9 for different fiber sizes and binder percentages at various compression levels. The overall response was that the maximum absorption of the material was decreased with compression. Moreover it was observed that the rates of absorption varies at various fiber sizes and compression levels, however in the GATS results shown here the variation in rate is not clear. Plots of GATS absorbency for samples containing 20%

of binder percentages is shown in figure 4.9. Similar behavior is observed in these samples. In the following sections, the maximum absorption and absorbency rate were discussed separately.

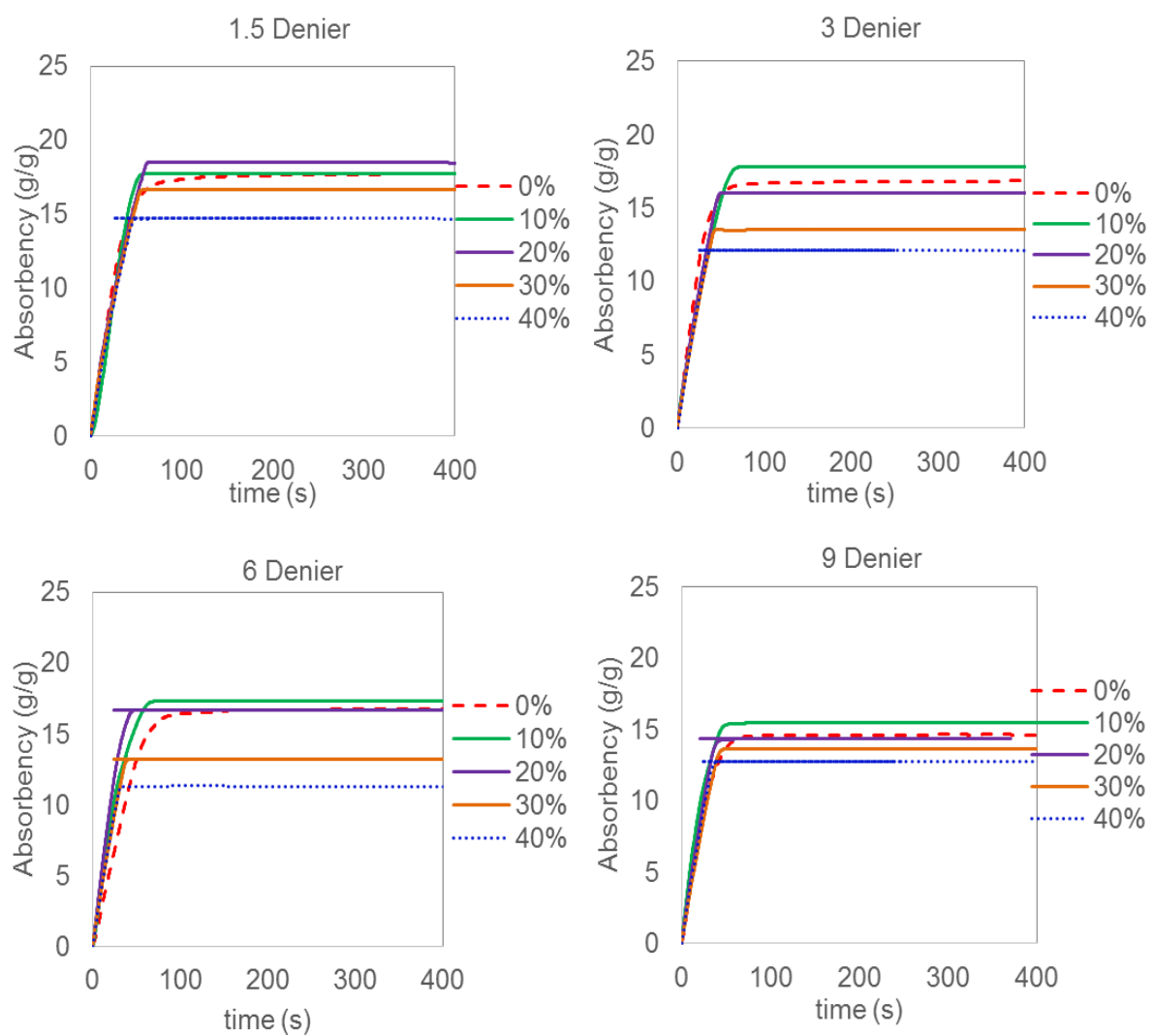


Figure 4.8: the GATS results for different fiber diameter- 90% PET-10% Co-PET- at various compression levels

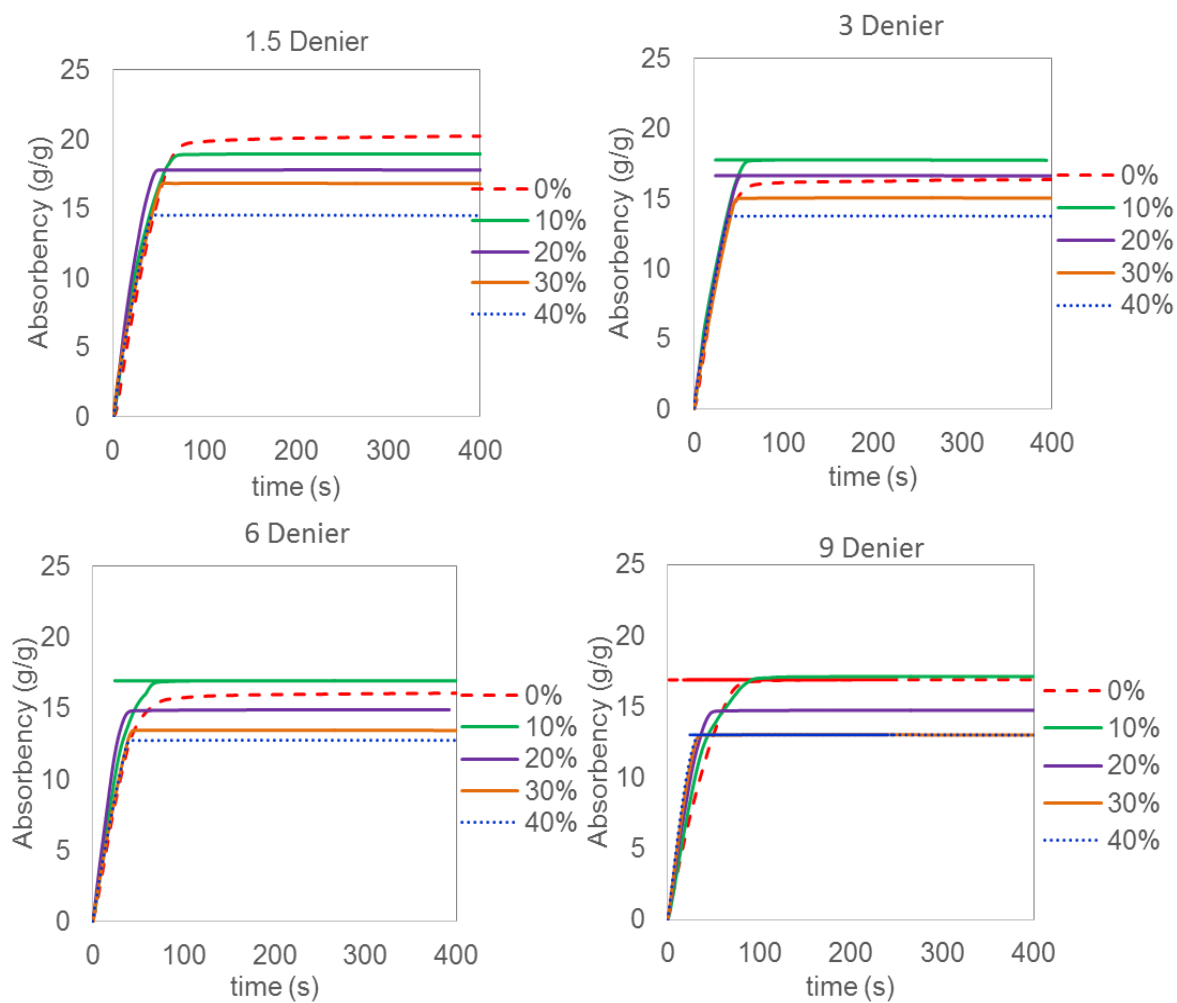


Figure 4.9: the GATS results for different fiber diameter- 80% PET-20% Co-PET- at various compression levels

4.3.3.1 Maximum absorption

The maximum absorption of the samples were measured under no compression for the samples containing various fiber sizes through two different techniques, basket and GATS. The basket or sink method is referenced in the Association of Nonwoven Fabrics Industry's (INDA) standard test method 10.1 (INDA WSP 10.1). Figure 4.10 demonstrates the absorbency values measured by these techniques and under no compression. It is evident that the absorbency value obtained in both techniques are lower than the anticipated value according to solidity of the samples, which means samples were not fully saturated in any of the techniques under no compression. Furthermore however the results obtained by these techniques are in good agreement in general, but looking at the results for 20% binder confirms that the GATS results are more consistent with the theory, and less affected by the fiber size. Basket results are highly affected by the retention property of the structure, which is why larger fiber sizes showed smaller absorbency amount disregarding of their solidity.

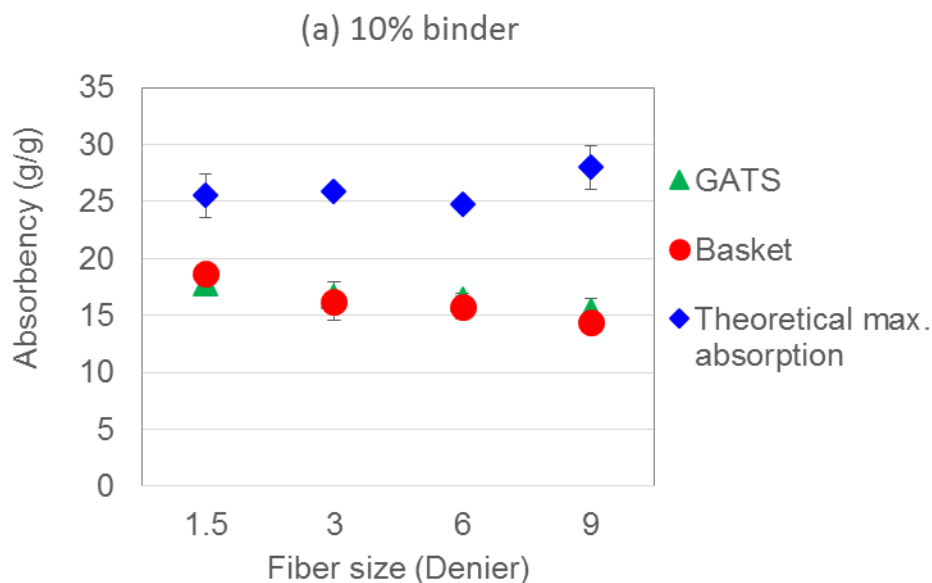
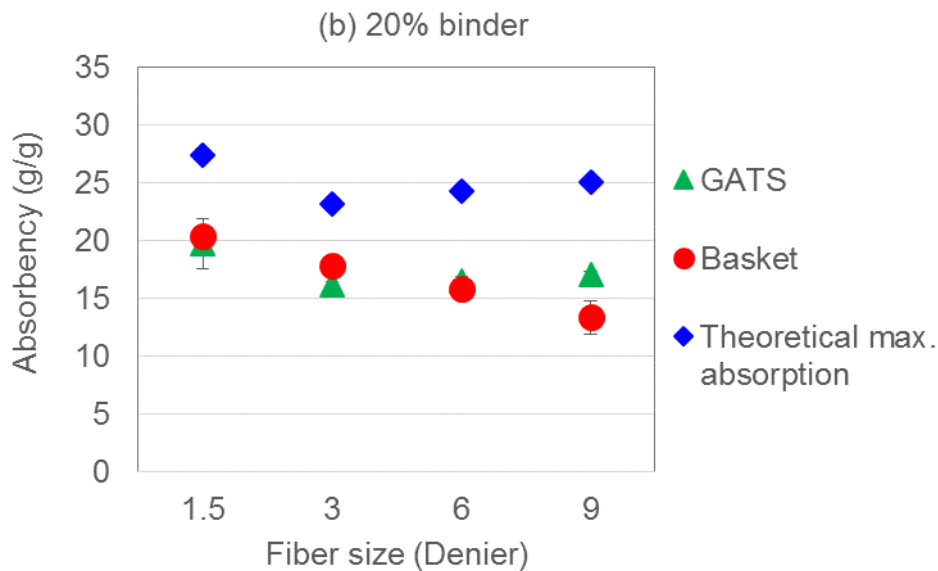


Figure 4.10: the maximum absorption results for different fiber diameters measured via different methods- (a) 90% PET-10% Co-PET (b) 80% PET-20% Co-PET



4.3.3.1.1 Effect of compression

Figure 4.11 illustrates the maximum absorption for samples of different fiber sizes and various binder percentages at diverse compression level. On the whole, it can be observed that maximum absorption is reduced by compression as anticipated. By contrast, slight increase in the maximum absorption is observed at 10% of compression level for 3, 6, and 9 denier fiber sizes. This could be explained as a consequence of imperfect contact between the sample and sample holder, which is unavoidable. Also our results suggest that the effect of imperfect contact between the sample and sample holder is more significant in case of samples of larger fiber sizes. Moreover, as evident from the figure 4.11, the maximum absorption was unaffected by binder percentages.

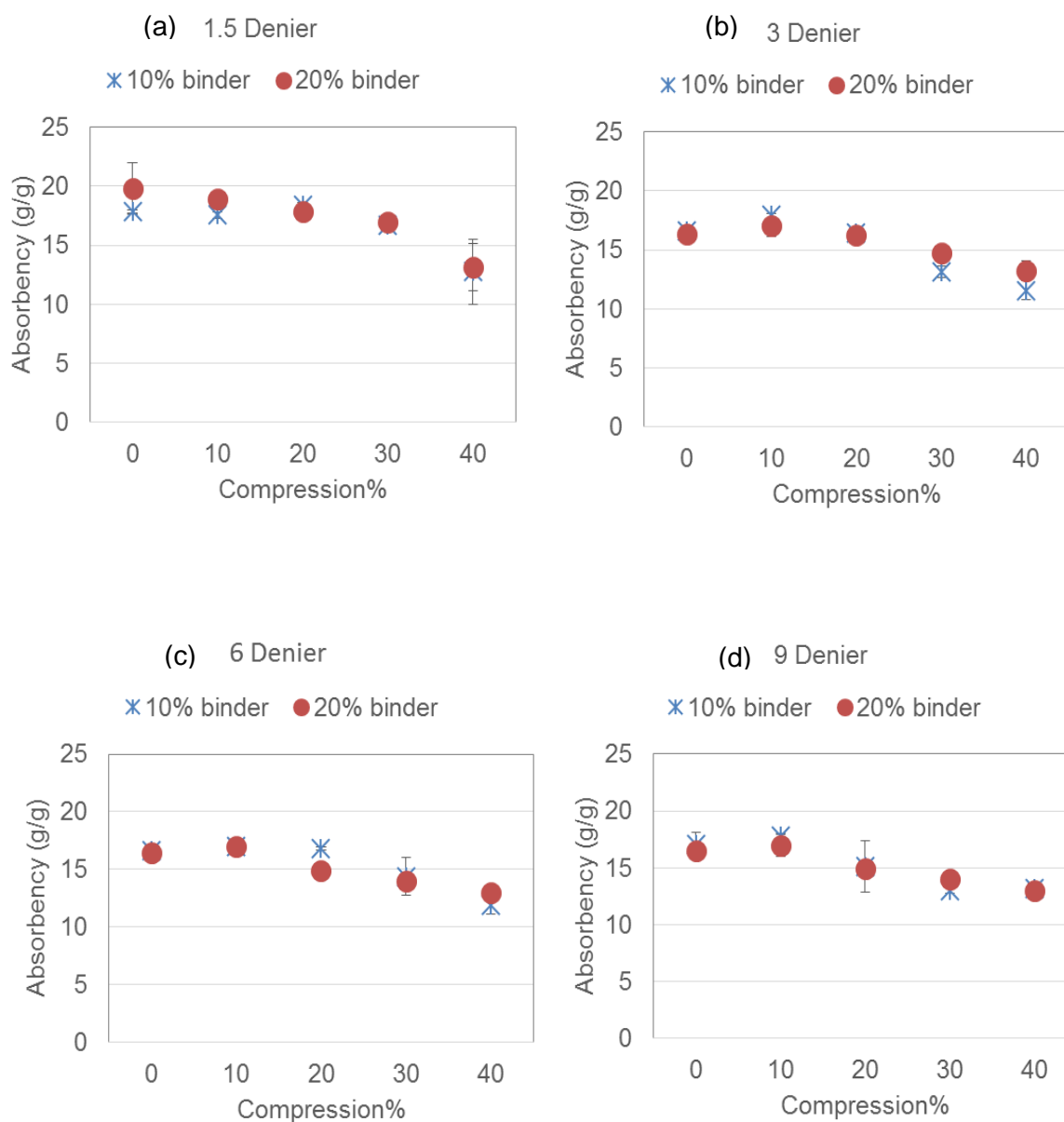


Figure 4.11: the GATS maximum absorption results for different fiber diameter under different compression level- (a) 1.5 denier (b) 3 denier (c) 6 denier (d) 9 denier

The relation between the absorption capacity and porosity or solidity of the nonwoven samples has established in the equation 4.4. In our study, various levels of solidity were obtained using compression of the samples to different levels and greater the compression percentages, higher are the solidity. Therefore the theoretical maximum absorption capacity for the given range of solidities

calculated based on equation 4.4 was compared with actual maximum absorption measured by GATS. Figure 4.12 displays the results for various fiber sizes and binder percentages. As can be seen, the absorbency was lower at higher solidity, which is consistent with the theoretical calculation. The lowest solidity values are in correspondence with the absorption results under no compression, which was discussed in the previous section. The samples were not fully saturated, which is why there is a gap between experimental and theoretical results. However for the rest of our data, the experimental data are above the predicted values. This may happen due to the possibility of trapping the liquid between the sample and top compressing plate, which is inevitable. This possibility is linked to the existence of capillary between the sample and top plate. In addition in a general trend, smaller fiber sizes show slightly higher absorption value at similar solidity. This may be interpreted by the higher capillary forces of smaller pore sizes according to Laplace equation (Chatterjee and Gupta 2002) and therefore their higher capability to overcome the gravity force that acts against the capillary force as a driving force. On the whole, it can be concluded based on our results that the main factor determining the maximum absorbency of the nonwovens is the available pore volume which is determined based on solidity or porosity. But other factors such as pore size have some effect on how much it is possible to actually fill the available pores.

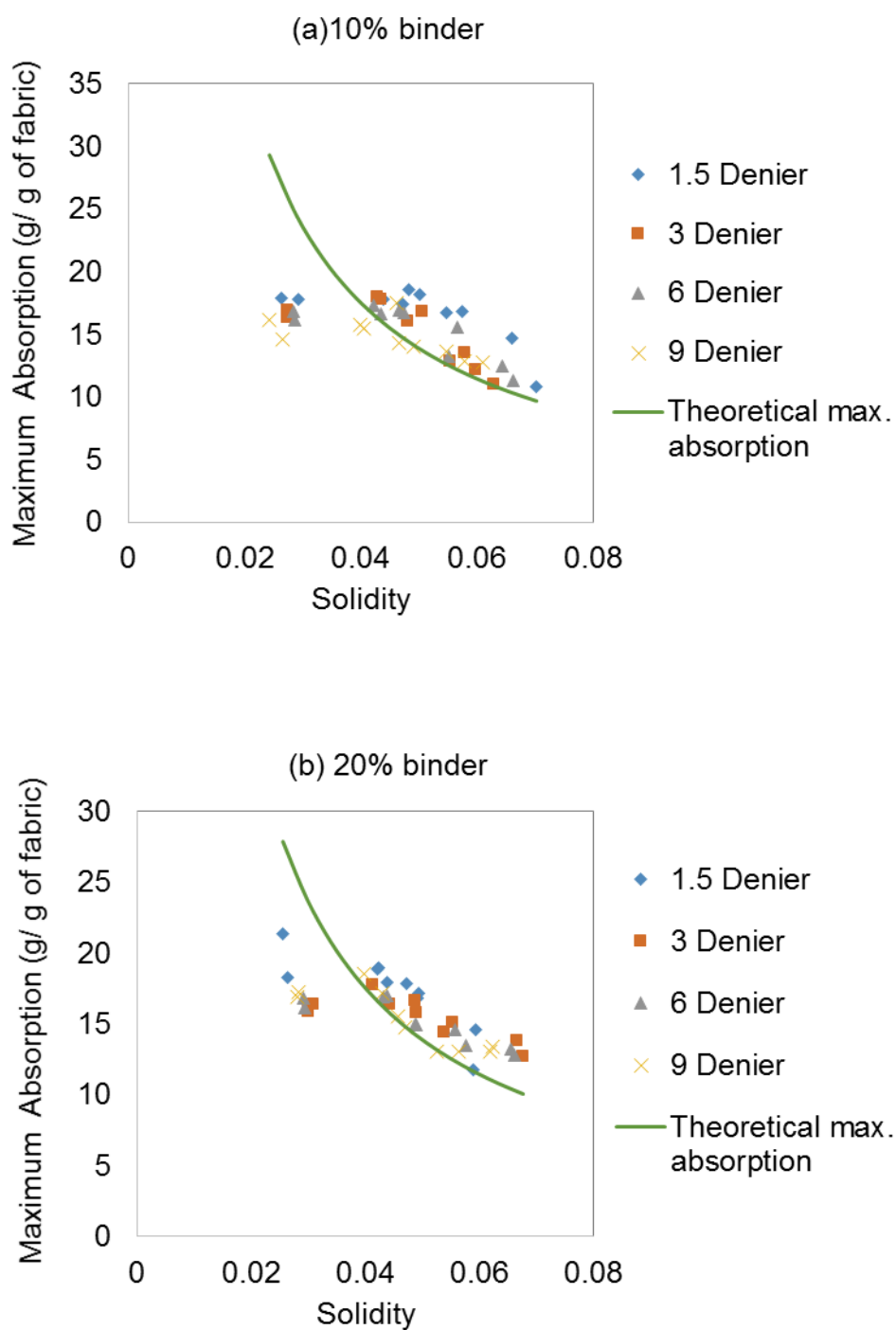


Figure 4.12: maximum absorbency (Theory, GATS) versus solidity (a) 10% binder (b) 20% binder- solid line shows the theoretical results and dots show the experimental result

4.3.3.2 Absorbency rate-through-plane direction

4.3.3.2.1 Effects of fiber size (or pore size)

In this section, we evaluated the absorbency rate in through-plane direction for the samples containing different fiber sizes and binder percentages at varied compression levels. The absorbency rate was measured based on GATS results, which was discussed in section 4.2.5. Figure 4.13 shows the rate of absorption at no compression level. As can be seen in this figure, in general both the fiber sizes and binder percentages impacts on the rate of absorption. The rate increased and then decreased by fiber size. Moreover the rate is somewhat decreased at samples containing larger binder percentages in all the different fiber sizes. Based on the pore size of the samples shown in figures 4.6 and 4.7, structures with larger fiber size give rise to structures with larger pore sizes. In the situations that there is no externally applied pressure, so fluid penetration occurs due to capillary pressure while gravitational forces may hinder it. The capillary pressure, which is driving force behind spontaneous fluid infiltration into nonwoven materials, has an inverse relationship with the radius of capillary tube according to Laplace equation. Simplifying the nonwoven structure, the pore size plays the same role as the radius of capillary tube. It is concluded that magnitude of the capillary pressure is greater in smaller pore sizes. In the case of upward infiltration, the gravity force opposes the fluid infiltration. Moreover the samples containing 20% binders shows smaller rate of absorption. From the pore size calculation, it was observed that these samples have smaller pore size compared to samples containing 10% binder. Therefore the smaller rate of absorption can be explained through Washburn equation.

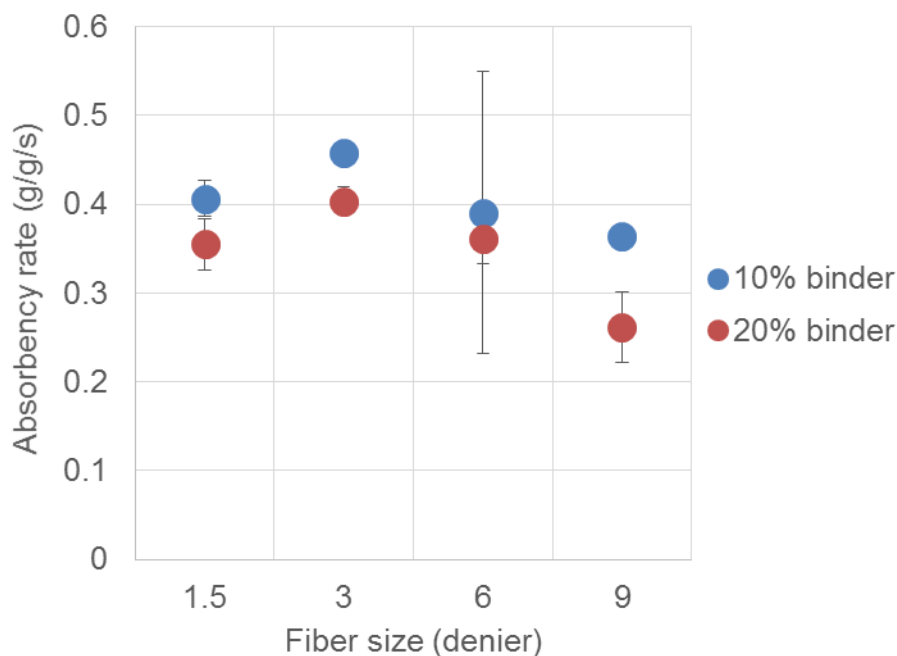


Figure 4.13: through-plane absorbency rate at various fiber sizes and binder percentages

In order to establish the relationship between the rates and pore characteristics, the rate of absorption at various fiber sizes were graphed based on their mean flow pore diameter, furthermore the above-mentioned Washburn equation for vertical situation was employed to calculate the rate of absorption theoretically. Lucas-Washburn equation deals with the wicking or the rate of liquid penetration into the capillaries when they are under capillary pressure and flow happens from a saturated reservoir. This equation determines the variation of liquid height as a function of time in a one direction. In case of vertical wicking where the flow is resisted by gravity, the rate of liquid penetration is defined as

$$\frac{dl}{dt} = \frac{r^2}{8\eta l} \left(\frac{2\gamma \cos \theta}{r} - \rho gl \right) \quad (4.5)$$

Where l is Height of liquid at time t , r the capillary (pore) radius, γ the surface tension of liquid, η the viscosity of the liquid, g the gravitational acceleration and θ is the contact angle between liquid and fiber. In order to solve the equations, the contact angle was assumed to be zero considering the complete wetting is achieved by the aforementioned liquid. The surface tension of the liquid was measured by tensiometer and it was 31 mN/m and finally the liquid viscosity was assumed to be equal with water liquid viscosity which is 8.9×10^{-4} Pa.s or 8.9×10^{-3} dyn.s/cm² at about 25°C.

Figure 4.14 demonstrated the results. Inspection of this figure indicates that a maximum value of the absorbency rate was obtained at the mean flow pore sizes of about 50 to 60 micrometer at both the samples containing 10% and 20% binder, which is consistent with results obtained by Washburn equation. However, the complex geometry of nonwoven fabrics hinder the applicability of Washburn equation to the nonwoven materials, they can explicate our observation in the through-plane rate of absorption with the vertical situation. Our results revealed that the pore size plays an important role in determining the absorbency rate of the nonwoven samples. Furthermore, there are optimum pore size ranges in order to achieve the maximum absorbency rate.

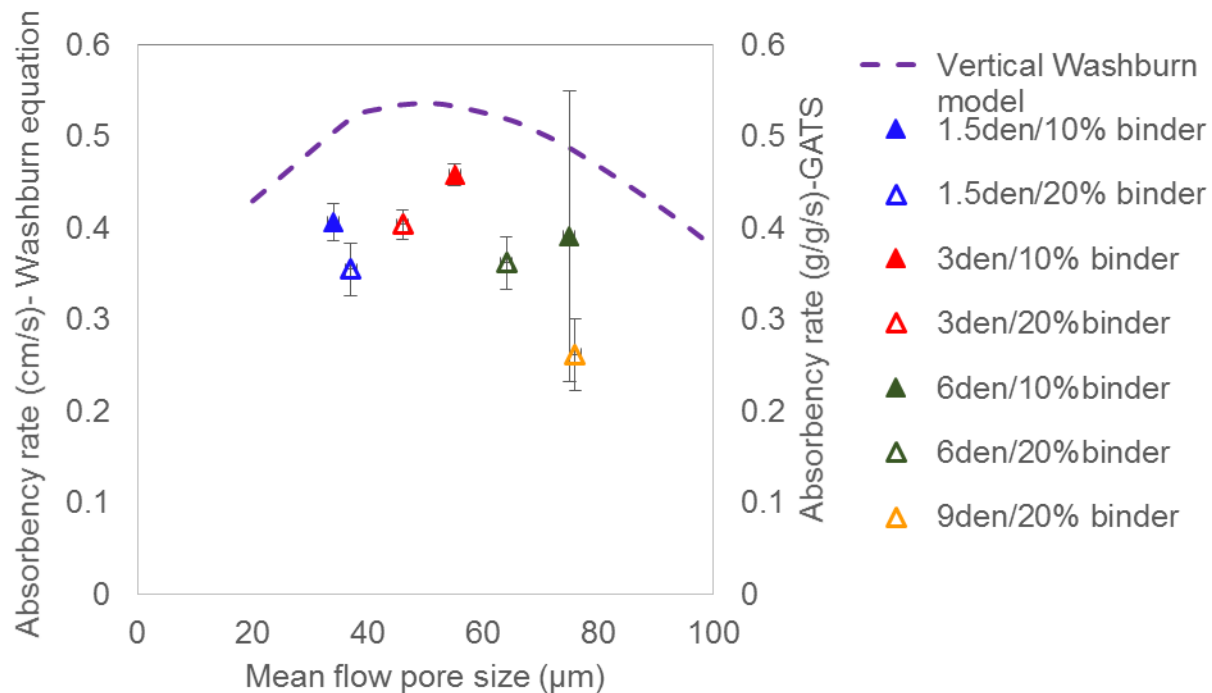


Figure 4.14: through-plane absorbency rate for various fiber sizes and binder percentages according to their mean flow pore sizes- line shows the theoretical results built on left vertical axis, and dots show the experimental result built on right vertical axis

4.3.3.2.2 Effects of compression

It is important to reiterate that the aim of this study was to evaluate the effect of structural characteristics on the absorbency behavior of nonwovens. In this section, we evaluate the absorbency rate of entire samples at varied compression levels, in order to further evaluate the effect of structure on the absorbency rate of nonwovens, also to comprehend the effect of compression on it. The figure 4.15 corresponds to the absorbency rate at varied level of compression. The Figure shows that the absorbency rate is influenced by compression and it increased and then decreased by the compression.

Although samples containing 10% binder and 20% binder shows similar trend with compression, the differences shown in their absorbency rates at different compression level is smaller compared to the samples containing 20% compression. It might be due to the fact that samples with lower percentage of binders easily collapses with compression, and their structure is deformed with the compression easier.

The maximum rate of absorption was associated with larger compression percentages at larger fiber sizes and this may be attributed to larger initial pore sizes. However, 1.5 denier fibers did not follow this. It may be due to the dissimilar packing behavior of the small fiber sizes (Langston, Kennedy, and Constantin 2015). Assuming that the mean pore diameter of nonwoven is reduced by the compression, as it was discussed by Jagnathan, et al. (Jaganathan et al. 2009), it could be inferred therefore that larger pore sizes were required to be compressed to a higher level in order to reach to the desirable range of pore sizes for obtaining the maximum absorbency rate.

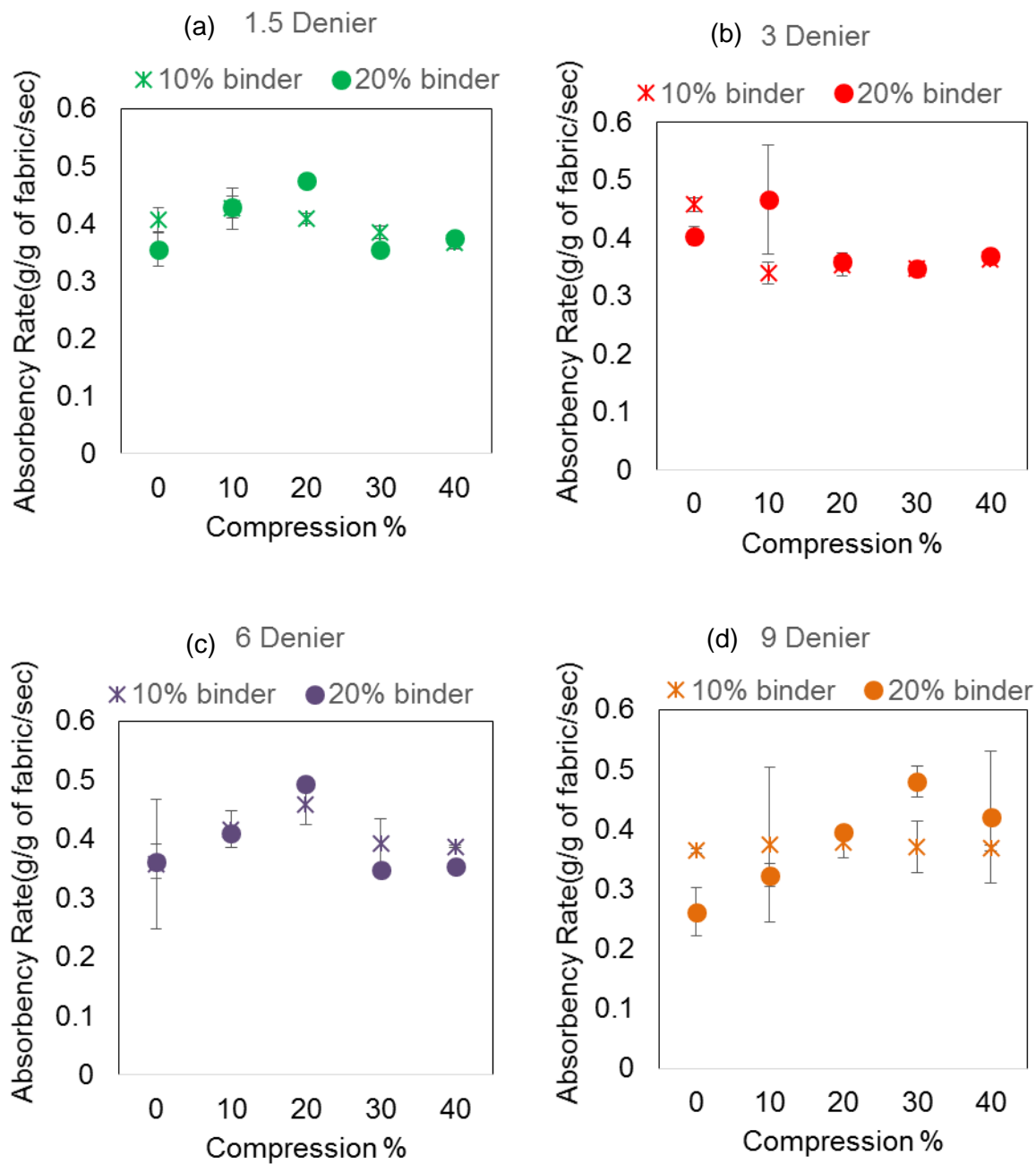


Figure 4.15: absorbency rate for (a) 1.5 Denier (b) 3 Denier (c) 6 Denier and (d) 9Denier structures @ 0,10,20,30, and 40 % compression levels

In order to examine the above-mentioned hypothesis, the pore characteristics of the 6-denier samples were measured by compression porosimetry technique at compression levels of 0, 20, 30, and 40%. Figure 4.16 displays the median pore size of 6 denier samples at varied compression level. On the whole, the median pore size was reduced by the compression, which is in line with the result obtained by Jagnathan et al. (Jaganathan et al. 2009). It should be noted that porosimetry techniques for characterizing the pore under compression is different from the porometry technique used in aforementioned discussion on the effect of fiber size. In general, the porometry technique measure the constricted pore diameter based on flow characteristics, although the porosimetry technique measures the pore volume (A. Jena et al. 2001) and it underestimates the volume of larger pore sizes due to ink-bottle effect (Jaganathan, Vahedi Tafreshi, and Pourdeyhimi 2008). The mean flow pore diameter given by porometry technique is a smaller value than the median pore diameter based on volume obtained by porosimetry technique. Since the porosimetry technique characterizes the pore structure and its anisotropy level (Gribble et al. 2011), it can be speculated that the difference between the values achieved by these techniques is larger at higher level of tortuosity.

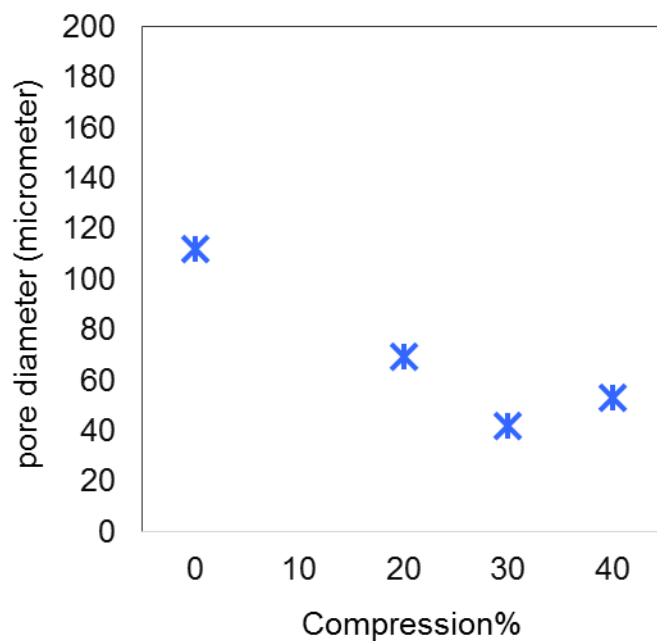


Figure 4.16: median pore size measured by compression Porosimetry technique for samples of 6 denier fibers at varied compression level

Subsequently, the absorbency rate of 6-denier fiber samples was graphed versus the median pore size at different compression levels. As evident from the figure 4.17 the absorbency rate showed a maximum with median pore sizes achieved at a specific level of compression. According to this, the maximum rate was achieved at the median pore sizes of around 70 Micrometer. This observation was consistent with our previous discussion on the effect of pore size at varied fiber sizes.

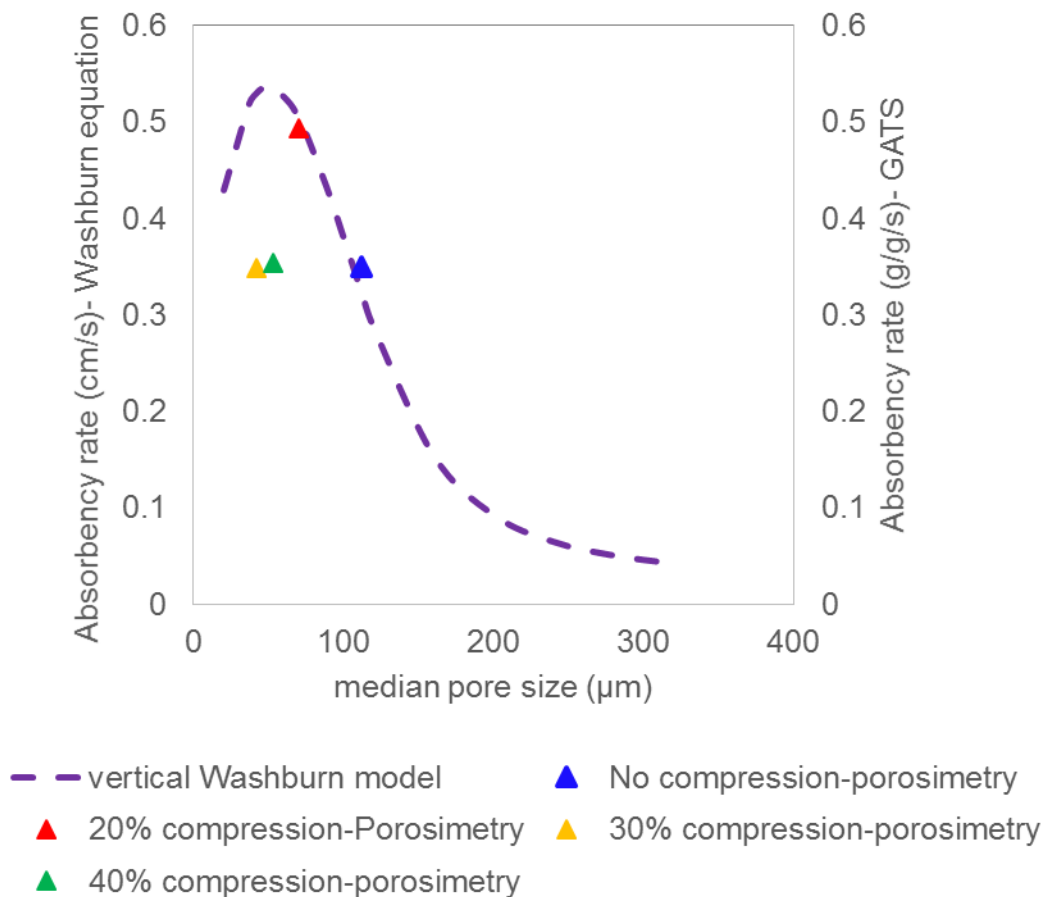


Figure 4.17: through-plane absorbency rate for 6-denier fiber sizes (20% binder percentages) according to their median flow pore sizes- line shows the theoretical results built on left vertical axis, and dots show the experimental result built on right vertical axis

4.3.3.3 In plane absorbency rate

The nonwoven fabrics are highly anisotropic and the previous study has shown that the in-plane liquid spreading is driven by structure anisotropy (Ashari et al. 2010; Kim and Pourdeyhimi 2003). Hence the In-plane absorbency rate of the entire samples was measured through point wicking test. The gravity does not significantly influence on the results and hence the results were compared with the horizontal Washburn equation. Figure 4.18 shows the results for group A of the fabric with

different fiber size and binder fiber percentages. The result shows a considerable increase in the in-plane absorbency rate with increasing the fiber size from 1.5 denier to 3 denier in both binder percentages. However further increase in the fiber denier did not changes the in-plane absorbency rate of the samples containing 10% binder and small decrease in the rate was happened for the samples containing 20% binders. The decrease in the larger fiber sizes at samples containing 20% binder implied that the gravity effect were not negligible.

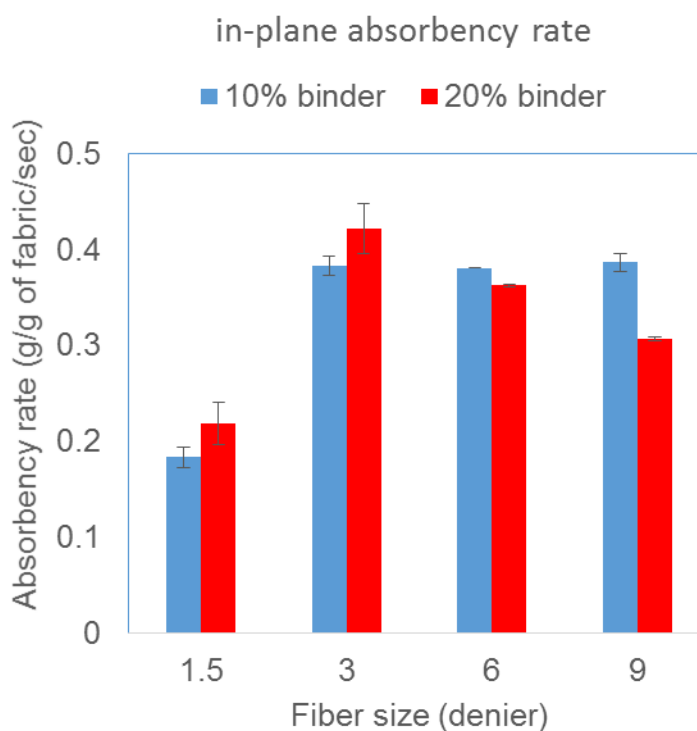


Figure 4.18: in-plane absorbency rate of samples- Fiber size effect

According to Washburn equation, rate of liquid penetration into a horizontal capillary and under the capillary pressure is defined as:

$$\frac{dl}{dt} = \frac{r \gamma \cos \theta}{\eta 4l} \quad (4.6)$$

Where l is Height of liquid at time t , r the capillary (pore) radius, γ the surface tension of liquid, η the viscosity of the liquid and θ is the contact angle between liquid and fiber (Washburn 1921).

In order to solve the equations, the contact angle was assumed to be zero considering the complete wetting is achieved by the aforementioned liquid. The surface tension of the liquid was measured by tensiometer and it was 31 mN/m and finally the liquid viscosity was assumed to be equal with water liquid viscosity which is $8.9 \cdot 10^{-4}$ Pa.s or $8.9 \cdot 10^{-3}$ dyn.s/cm² at about 25°C.

In the horizontal situation, for instance in in-plane direction, according to the equation 4.6 larger pore size basically results in faster rate of liquid penetration. As shown in figure 4.19, our results were in good agreement with the Washburn equation theory for horizontal situation, however it should be noted that the pore size value measured by porometry technique is related to the through-plane direction, and the pore sizes in in-plane direction may be different.

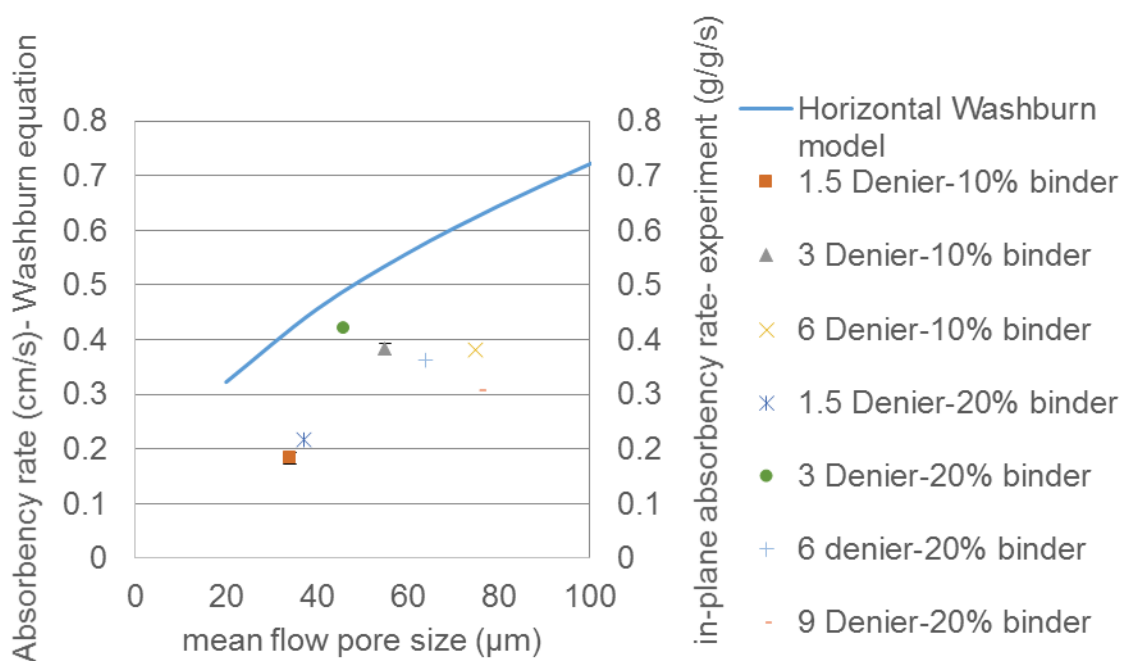


Figure 4.19: in-plane absorbency rate of samples vs. mean flow pore size- Fiber size effect

4.3.3.4 Vertical wicking rate

Vertical wicking provides the condition for a purely capillary action and it is not a good indicator of the amount of liquid absorbed in a certain time (Larose 1942). Therefore it has been employed in the researches to model the fluid flow according to the capillary pressure provided by the porous structure based on Lucas-Washburn and Laplace equations (Chatterjee and Gupta 2002). One of the challenges in using these equations is the estimation of the capillary radius. Due to the tortuous fluid path in real porous media which is in contrast with the assumption of the aligned capillary tubes supposed in these equation, it is required to estimate the “equivalent capillary radius” for a real porous media. The previous data has shown that the most accurate for estimating the equivalent capillary radius is the vertical- wicking test (Masoodi and Pillai 2010), in which the capillary pressure is balanced with the gravitational potential energy. In order to obtain a better understanding of the pore structure, therefore the vertical wicking test was done on the samples containing 20% binder fibers. Figure 4.20 shows the results obtained by vertical wicking test. The initial rate of liquid penetration was measured as 8.0, 12.2, 7.0, and 6.4 mm/s for the samples containing 1.5, 3, 6, and 9 denier fibers respectively. The highest initial rate of liquid penetration was observed in case of samples containing 3 denier fibers which is again in a good agreement with the vertical Washburn equation previously discussed. Furthermore the liquid penetration distance was measured after 42 hours given in table 4.3. It showed that the 1.5 denier samples had the highest liquid penetration distance following by 3, 6, and 9 denier fibers respectively, which accounts for their smaller pore size and higher capillary pressure. Figure 4.21 displays the corresponding photo after 42 hours.

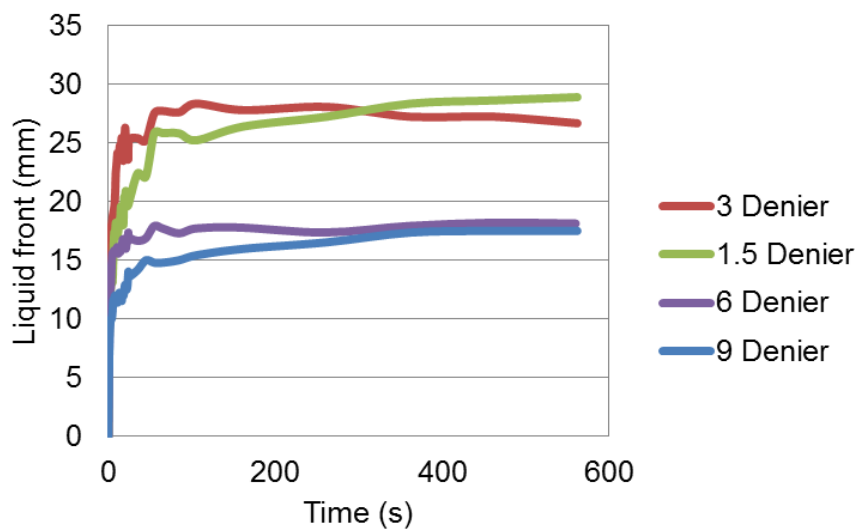


Figure 4.20: vertical wicking test results for various fiber sizes for the samples containing 20% binder fibers

Table 4.3: liquid penetration rate and distance in vertical test-various fiber sizes

fiber size(denier)	Initial Rate of liquid penetration (mm/s)	Liquid front (mm) after 42 hours
1.5	8.0	31.8
3	12.2	24.2
6	7.0	18.3
9	6.4	16.2

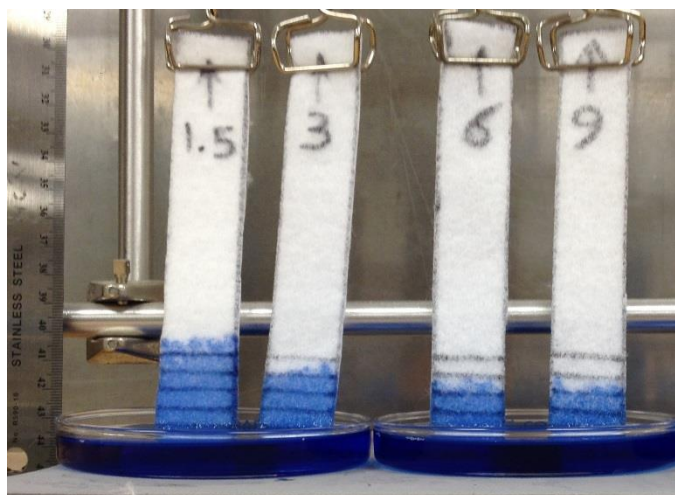


Figure 4.21: the vertical wicking experiments after 42 hours

4.3.4 Release properties

As outlined in the introduction, most of the published works on the liquid handling of the porous media is only concerned with liquid absorption with no attention to the fluid release. In this section, we evaluate the release behavior of the entire nonwoven samples at various compression levels in regard to their fiber size and pore characteristics.

4.3.4.1 Liquid holding capacity

Liquid holding capacities were measured for the samples with different fiber sizes. Figure 4.22 shows the result for the liquid holding capacity under no compression. As evident from the figure, liquid holding capacity of the samples containing 10% binder fibers reduced by increasing the fiber sizes, however it remained constant in case of samples containing 20% of binder percentages. The capillary pressure of the pore is the force, which retains the liquid in the pores. Smaller the pore size, higher the capillary pressure according to Laplace equation. This means that the samples with smaller fiber size were able to retain higher percentage of the absorbed liquid because of higher capillary pressure. Moreover smaller the fiber size, higher is the surface area of the structure. Higher surface area may also lead to higher retention capability of the samples.

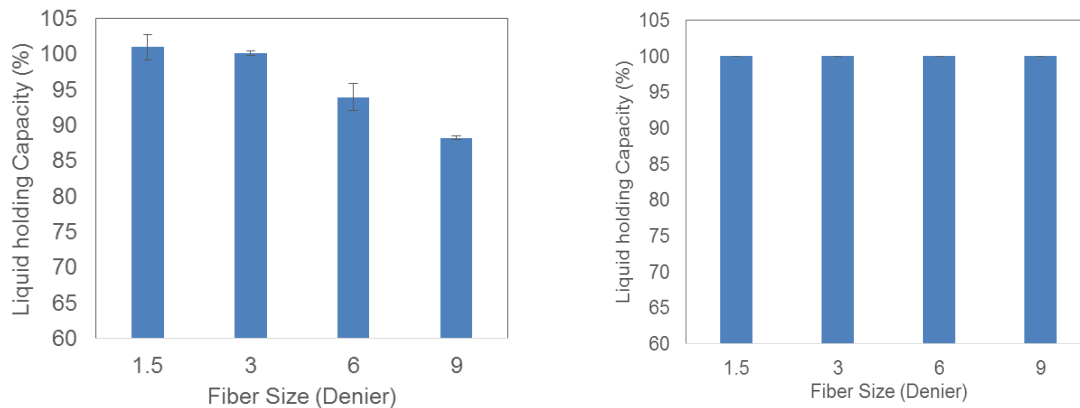


Figure 4.22: liquid holding capacity of the samples with different fiber sizes at no-compression (Left) 90% PET-10% Co-PET (Right) 80%PET-20% Co-PET

Figure 4.23 displays the liquid holding capacity of the samples under compression. It is obvious that compression reduces the liquid holding capacity of the samples. However reduction in the liquid holding capacity is different for various fiber sizes. In case of larger fiber size, it is seen that after initial release of the liquid under no compression, the rest of liquid can be held by the structure up to higher compression percentages. When the sample with the larger fiber size and larger pore sizes are compressed, the liquid is transported from the larger pore sizes to smaller pore size. On the other hand the pore size becomes smaller with the compression and therefore higher capillary pressure of the pores can hold the liquid inside the pores.

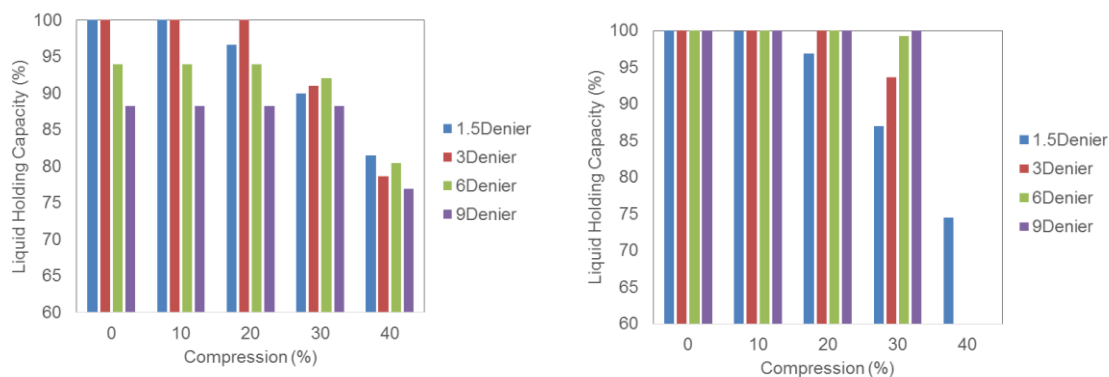


Figure 4.23: liquid holding capacity of the samples with different fiber sizes-compression effect (Left) 90% PET, 10% Co-PET (Right) 80% PET, 20% Co-PET

The graphs in the right side of figure 4.23 shows the results for samples containing higher percentages of the binder fibers. Since these samples have originally smaller pore sizes, it is observable that they start to release the liquid at higher compression percentages. Due to high resistance of these samples, it was not possible to reach to 40% of compression at samples of larger fiber size than 1.5 denier. The liquid retention capacity was studied according to their solidity at varied compression levels. Generally speaking, the retention capacity of the nonwovens is reduced at higher solidities as expected. Figures 4.24 and 4.25 illustrated the liquid retention capacity at varied levels of solidity for samples containing 10% and 20% binder fibers. As it can be observed, while the samples were not fully saturated, shown in the areas that there is a gap between the liquid retention capacities and theoretical maximum absorption, which represents there is a fraction of empty pores, achieving higher solidities by compression only redistribute the liquid from larger pores to smaller pore with higher capillary pressure, and therefore the liquid were not releases. However after achieving the fully saturated samples, the further increase in solidity led to liquid release and reduction in liquid retention capacity.

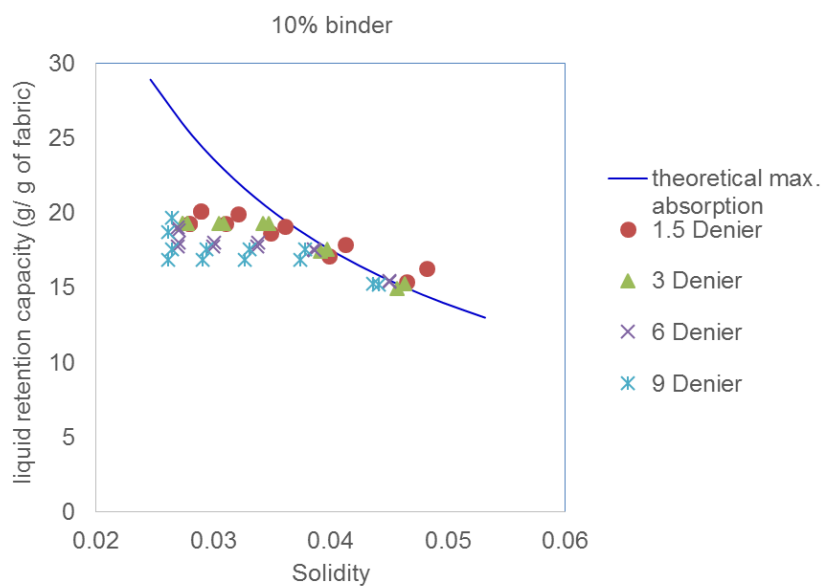


Figure 4.24: liquid retention capacity of samples of various fiber sizes, containing 10% binder fibers at varying solidity levels

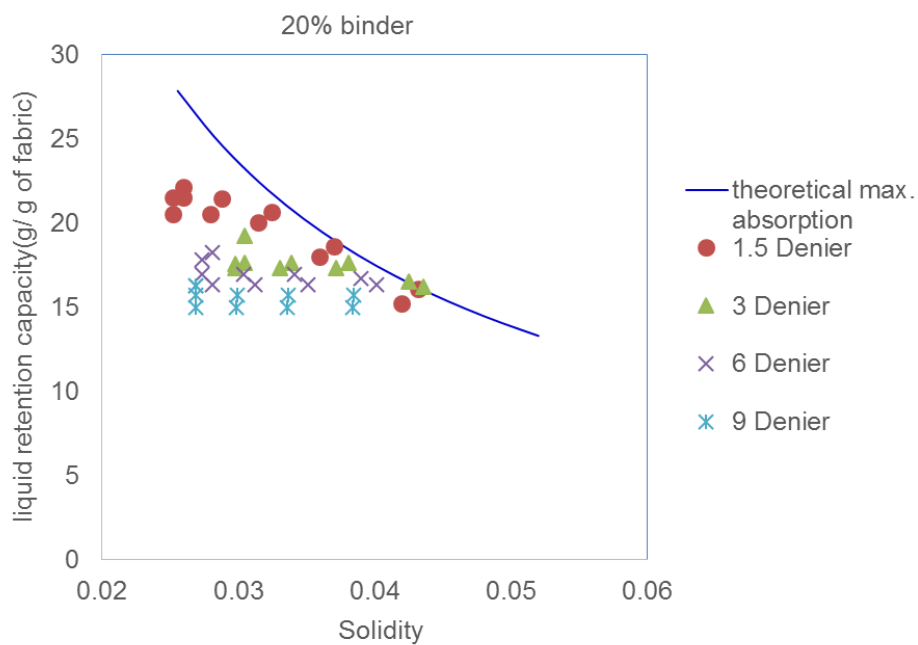


Figure 4.25: liquid retention capacity of samples of various fiber sizes, containing 20% binder fibers at varying solidity levels

4.4 CONCLUSION

In this study we evaluated the absorbency and release properties of nonwovens, including their absorption capacity, absorbency rate, and retention capacity according to their structural parameters covering solidity and pore size. We found that in the case of samples containing various fiber sizes, and binder percentages, the maximum absorption of nonwovens is governed by the solidity; the absorbency rate is dictated by the pore size; and the retention capacity of the nonwoven samples is defined based on their saturation levels, pore size, and solidity. Our results provide compelling evidence that the maximum rate of absorption can be achieved in a given range of pore sizes, which can be obtained by the choice of fiber size or a specific level of compression depending on the original pore size. These findings therefore reveal how the structural parameters of nonwovens determine their absorption behavior with the focus on the influence of fiber size and compression. The finding of this study appears to be valuable in the engineering of the fabric structural architecture in absorbent products such as hygiene products and wipes. Furthermore, the Washburn equation was employed as the theoretical model and our results were in perfect agreement with the theoretical model. Our results are encouraging and should be explored in other fiber sizes and compression levels, since we just tested the pore structure of 6-denier fibers at various compression levels. Moreover, it would be beneficial to investigate the packing behavior of various fiber sizes under compression in order to understand their pore characteristics with the compression.

REFERENCES

- Adamson, Arthur W. 1997. *Physical Chemistry of Surfaces*. 6th ed. New York: Wiley.
- Ashari, A., T.M. Bucher, H. Vahedi Tafreshi, M.A. Tahir, and M.S.A. Rahman. 2010. "Modeling Fluid Spread in Thin Fibrous Sheets: Effects of Fiber Orientation." *International Journal of Heat and Mass Transfer* 53 (9-10): 1750–58. doi:10.1016/j.ijheatmasstransfer.2010.01.015.
- Ashari, A., T.M. Bucher, and H. Vahedi Tafreshi. 2010. "A Semi-Analytical Model for Simulating Fluid Transport in Multi-Layered Fibrous Sheets Made up of Solid and Porous Fibers." *Computational Materials Science* 50 (2): 378–90. doi:10.1016/j.commatsci.2010.08.030.
- Ashari, A., and H. Vahedi Tafreshi. 2009a. "A Two-Scale Modeling of Motion-Induced Fluid Release from Thin Fibrous Porous Media." *Chemical Engineering Science* 64 (9): 2067–75. doi:10.1016/j.ces.2009.01.048.
- Ashari, A., and H. Vahedi Tefreshi. 2009b. "General Capillary Pressure and Relative Permeability Expressions for through-Plane Fluid Transport in Thin Fibrous Sheets." *Colloids and Surfaces A: Physicochemical and Engineering Aspects* 346 (1-3): 114–22. doi:10.1016/j.colsurfa.2009.06.001.
- Bernardin, L. J. 1987. "Absorbent Structure Designed for Absorbing Body Fluids." US Patent 4699619.
- Chappell, C. W., S.D. Keeler, and J.L. Hammons. 1994. "Absorbent Articles Having Multiple Cores for Improved Fluid Movement", WO patent 1994005244A1
- Chatterjee, P. K., and B. S Gupta. 2002. *Absorbent Technology*. Amsterdam; Oxford: Elsevier Science. <http://www.sciencedirect.com/science/book/9780444500007>.

- Chen, X., P. Vroman, M. Lewandowski, A. Perwuelz, and Y. Zhang. 2009. "Study of the Influence of Fiber Diameter and Fiber Blending on Liquid Absorption Inside Nonwoven Structures." *Textile Research Journal* 79 (15): 1364–70. doi:10.1177/0040517508099386.
- Cueto, N., D. Benavente, J. Martínez-Martínez, and M.A. García-del-Cura. 2009. "Rock Fabric, Pore Geometry and Mineralogy Effects on Water Transport in Fractured Dolostones." *Engineering Geology* 107 (1-2): 1–15. doi:10.1016/j.enggeo.2009.03.009.
- Das, Dipayan, Arun Kumar Pradhan, and Behnam Pourdeyhimi. 2012. "Dependence of the Liquid Absorption Behavior of Nonwovens on Their Material and Structural Characteristics: Modeling and Experiments." *Journal of Applied Polymer Science* 126 (3): 1053–60. doi:10.1002/app.36635.
- Dedov, A.V., S.V. Babushkin, A.V. Platonov, A.P. Kondratov, and V.G. Nazarov. 2001. "Sorption Properties of Nonwovens Materials." *Fiber Chemistry* 33 (5): 395–97.
- De, N. G., J. Farber, J. Glodek, and M. Higgins. 1973. "Diaper System and Absorbent Pad Therefor." US patent 3769978.
- Dubrovski, P. D., and M. Brezocnik. 2012. "The Modelling of Porous Properties Regarding PES/CV-Blended Nonwoven Wipes." *Fibers and Polymers* 13 (3): 363–70. doi:10.1007/s12221-012-0363-x.
- Dubrovski, P. D., and M. Brezocnik. 2014. "Prediction of the Water Absorption Capacity of VIS/PES Needle-Punched Webs Using Genetic Algorithms." *Fibers and Polymers* 15 (8): 1758–65. doi:10.1007/s12221-014-1758-7.
- Figliuzzi, B., and C. R. Buie. 2013. "Rise in Optimized Capillary Channels." *Journal of Fluid Mechanics* 731 (September): 142–61. doi:10.1017/jfm.2013.373.

- Gribble, Christopher M., Graham Peter Matthews, Giuliano M. Laudone, Andrew Turner, Cathy J. Ridgway, Joachim Schoelkopf, and Patrick A.C. Gane. 2011. "Porometry, Porosimetry, Image Analysis and Void Network Modelling in the Study of the Pore-Level Properties of Filters." *Chemical Engineering Science* 66 (16): 3701–9. doi:10.1016/j.ces.2011.05.013.
- Hamraoui, Ahmed, and Tommy Nylander. 2002. "Analytical Approach for the Lucas–Washburn Equation." *Journal of Colloid and Interface Science* 250 (2): 415–21. doi:10.1006/jcis.2002.8288.
- Hardy, Philip. 2009. "Baby Diaper Absorbent Cores." *Nonwovens Industry* 40 (4): 56–63.
- Hassenboehler, C. B., and L. C. Wadsworth. 1993. "Post-Treatment of Nonwoven Webs.", US patent 5244482.
- Heitmeyer, W. C. 1932. "Absorbent Pad." US patent 1863333.
- Hemmat, M., and A. Borhan. 1996. "BUOYANCY-DRIVEN MOTION OF DROPS AND BUBBLES IN A PERIODICALLY CONSTRICTED CAPILLARY." *Chemical Engineering Communications* 148-150 (1): 363–84. doi:10.1080/00986449608936525.
- Horney, J. C., and J. R. Noel. 1996. "Disposable Products." US patent 5549589.
- Ikezawa, Hideo, Shinobu Watanabe, and Shunichi Yamada. 1997. "Process for Producing Wiping Nonwoven Fabric.", EP patent 0560556B1
- INDA WSP 10.1. n.d. "WSP 10.1 (08) Three Standard Test Methods for Nonwoven Absorption." Inda, Edana.
- Jaganathan, S., H. Vahedi Tafreshi, and B. Pourdeyhimi. 2008. "Modeling Liquid Porosimetry in Modeled and Imaged 3-D Fibrous Microstructures." *Journal of Colloid and Interface Science* 326 (1): 166–75. doi:10.1016/j.jcis.2008.07.011.

- Jaganathan, S., H. Vahedi Tafreshi, E. Shim, and B. Pourdeyhimi. 2009. "A Study on Compression-Induced Morphological Changes of Nonwoven Fibrous Materials." *Colloids and Surfaces A: Physicochemical and Engineering Aspects* 337 (1-3): 173–79.
doi:10.1016/j.colsurfa.2008.12.019.
- Jena, Akshaya, and Krishna Gupta. 2003. "LIQUID EXTRUSION TECHNIQUES FOR PORE STRUCTURE EVALUATION OF NONWOVENS." *International Nonwovens Journal*, 45.
- Jena, A., H. Sanders, J. Miller, and R. Wimberly. 2001. "Comparison of Mercury Porosimetry and Flow Porometry for the Testing of Battery Separator Materials." In , 71–75. IEEE.
doi:10.1109/BCAA.2001.905102.
- Kim, H. S., and B Pourdeyhimi. 2003. "In-Plane Liquid Distribution In Nonwoven Fabrics: Part 2 — Simulation." *International Nonwovens Journal Summer* (2): 29–33.
- Kissa, E. 1996. "Wetting and Wicking." *Textile Research Journal* 66 (10): 660–68.
doi:10.1177/004051759606601008.
- Konopka, Amy Elizabeth. 2001. "The Effect of Anisotropy on in-Plane Liquid Distribution in Nonwoven Fabrics." Master Thesis, North Carolina State University.
- Langston, Paul, Andrew R. Kennedy, and Hannah Constantin. 2015. "Discrete Element Modelling of Flexible Fibre Packing." *Computational Materials Science* 96 (January): 108–16.
doi:10.1016/j.commatsci.2014.09.007.
- Larose, P. 1942. "The Water Absorption by Towels." *American Dyestuff Reporter* 31 (6): 105–8,123–24.
- Mao, N. 2009. "Unsteady-State Liquid Transport in Engineered Nonwoven Fabrics Having Patterned Structure." *Textile Research Journal* 79 (15): 1358–63. doi:10.1177/0040517509342312.

- Mao, N., and S. J. Russell. 2003. "Anisotropic Liquid Absorption in Homogeneous Two-Dimensional Nonwoven Structures." *Journal of Applied Physics* 94 (6): 4135. doi:10.1063/1.1598627.
- Mason, Geoffrey, and Norman R Morrow. 1991. "Capillary Behavior of a Perfectly Wetting Liquid in Irregular Triangular Tubes." *Journal of Colloid and Interface Science* 141 (1): 262–74. doi:10.1016/0021-9797(91)90321-X.
- Masoodi, Reza, and Krishna M. Pillai. 2010. "Darcy's Law-Based Model for Wicking in Paper-like Swelling Porous Media." *AICHE Journal, NA – NA*. doi:10.1002/aic.12163.
- Masoodi, Reza, Krishna M. Pillai, and Padma Prabodh Varanasi. 2007. "Darcy's Law-Based Models for Liquid Absorption in Polymer Wicks." *AICHE Journal* 53 (11): 2769–82. doi:10.1002/aic.11322.
- Pan, N., and W. Zhong. 2006. "Fluid Transport Phenomena in Fibrous Materials." *Textile Progress* 38 (2): 1–93. doi:10.1533/tepr.2006.0002.
- Patnaik, A., R. S. Rengasamy, V. K. Kothari, and A. Ghosh. 2006. "Wetting and Wicking in Fibrous Materials." *Textile Progress* 38 (1): 1–105. doi:10.1533/jotp.2006.38.1.1.
- Rengasamy, Raju Seenivasan, Vijay Kumar Kothari, Vijay S. Bele, and Rajesh Khanna. 2011. "Liquid Sorption Behaviour of Nonwovens." *The Journal of The Textile Institute* 102 (12): 1019–30. doi:10.1080/00405000.2010.529285.
- Rengasamy, R.S., Dipayan Das, and C. Praba Karan. 2011. "Study of Oil Sorption Behavior of Filled and Structured Fiber Assemblies Made from Polypropylene, Kapok and Milkweed Fibers." *Journal of Hazardous Materials* 186 (1): 526–32. doi:10.1016/j.jhazmat.2010.11.031.
- Richards, L. A. 1931. "CAPILLARY CONDUCTION OF LIQUIDS THROUGH POROUS MEDIUMS." *Physics* 1 (5): 318. doi:10.1063/1.1745010.

- Roque, Caroline, Peyras-Carratte Jeremie, Guillaume Martins, and Christian Larcheron. 2011. "Wipe Materials Comprising Regenerated Plant-Protein Fibres.", US patent 20110236665
- Seong Hun Kim, Jae Hyung Lee, Dae Young Lim, and Han Yong Jeon. 2003. "Dependence of Sorption Properties of Fibrous Assemblies on Their Fabrication and Material Characteristics." *Textile Research Journal* 73 (5): 455–60.
doi:10.1177/004051750307300514.
- Shou, Dahua, Lin Ye, Jintu Fan, and Kunkun Fu. 2014. "Optimal Design of Porous Structures for the Fastest Liquid Absorption." *Langmuir* 30 (1): 149–55. doi:10.1021/la4034063.
- Shou, Dahua, Lin Ye, Jintu Fan, Kunkun Fu, Maofei Mei, Hongjian Wang, and Qing Chen. 2014. "Geometry-Induced Asymmetric Capillary Flow." *Langmuir* 30 (19): 5448–54.
doi:10.1021/la500479e.
- Szekely, J, A.W Neumann, and Y.K Chuang. 1971. "The Rate of Capillary Penetration and the Applicability of the Washburn Equation." *Journal of Colloid and Interface Science* 35 (2): 273–78. doi:10.1016/0021-9797(71)90120-2.
- Tirimacco, Maurizio, Mike Thomas Goulet, and Michael William Veith. 2008. "Paper Towel with Superior Wiping Properties", US patent 7462258
- Tracy, J., K. Ghali, and B. Jones. 1994. "Experimental Techniques for Measuring Parameters Describing Wetting and Wicking in Fabrics." *Textile Research Journal* 64 (2): 106–11.
doi:10.1177/004051759406400206.
- Washburn, Edward W. 1921. "The Dynamics of Capillary Flow." *Physical Review* 17 (3): 273–83.
doi:10.1103/PhysRev.17.273.

Young, Wen-Bin. 2004. "Analysis of Capillary Flows in Non-Uniform Cross-Sectional Capillaries."

Colloids and Surfaces A: Physicochemical and Engineering Aspects 234 (1-3): 123–28.

doi:10.1016/j.colsurfa.2003.12.007.

Yun, Tae Sup, Guillermo A. Narsilio, Olivier Buzzi, Stephen Fityus, and David W. Smith. 2009.

"Upscaling of Navier–Stokes Equations in Porous Media: Theoretical, Numerical and Experimental Approach." *Computers and Geotechnics* 36 (7): 1200–1206.

doi:10.1016/j.compgeo.2009.05.006.

5 INVESTIGATION OF EFFECT OF STRUCTURAL PARAMETERS ON ABSORPTION AND RELEASE PROPERTIES OF NONWOVENS UNDER COMPRESSION- PART II: FIBER CROSS-SECTIONAL SHAPE STUDY

5.1 INTRODUCTION

Fiber cross-sectional shape is one of determining factor of the geometric configuration of nonwoven's pore structure. A remarkable variety of non-circular cross-section fiber has been designed in recent years. These attention-grabbing fibers have typically focused on providing high surface area and surface capillary (Yoeng-Beek and Joon-Young 2002; Yeom and Pourdeyhimi 2011; Vaughn and Carman 2001; Pourdeyhimi, Chappas, and Barnes 2013). Some of the benefits of the non-circular cross-sectional shaped fibers includes but not limited to fluid movement, high bulk (Thompson 1997; Wilkes and Bartholomew 1995), insulation properties, tactile, and visual aesthetics (Dalton and Phillips 1998; Largman, Gefri, and Mares 1991). The use of the non-circular shaped fibers in absorbent products has been pointed out in many patents (Phillips et al. 1990; Meirowitz et al. 1993; Waxman and LIEN 2014; Bernt et al. 2014), also it experienced a steady increase in recent years. However, little work has been done on evaluating the influence of the cross-sectional shape of fibers on absorbency behavior of nonwovens. In order to recognize their role, it is necessary to realize their effect on the pore characteristics of nonwovens.

Meirowitz, et al. exhibited that the samples containing the non-circular shaped fibers had enhanced fluid distribution ability (Meirowitz et al. 1993). Furthermore, Nguyen, et al. found that incorporation of an effective amount of non-limbed cellulosic fibers into the limbed cellulosic fibers have enhanced the specific absorption capacity of the nonwoven beyond that of a nonwoven containing only the multi-limbed cellulosic fibers. The limbed fibers have some projected wings coming out from the

core part of the fibers and generally symmetrical cross-sectional shape, e.g., Y, X, H, or T-shaped (Nguyen, Martens, and Garbolino 1998). On the other hand, the non-circular shaped cross-sections have been used in the form of bicomponent fibers in that one component has the lower melting temperature. It can be used as a binder fiber to bond the fiber intersections, which are in the form of channels in case of non-circular shaped cross-sections. Due to those bonded point, this configuration led to a resilient fluid transporting network (Thompson 1997). Waxman and Lien also claimed that the improvement of moisture absorption and dispersion can be achieved in a needle-punched nonwoven fabric which comprises a mixture of circular cross-sectional shape hydrophobic fibers (60-65%) and non-circular cross-sectional shape hydrophilic fibers (35-40%) in comparison with the hydrophobic/hydrophilic blend where both fibers have a circular cross-sectional shape (Waxman and LIEN 2014). However, although the utilization of the non-circular cross-sectional fibers has been presented in numerous patent applications, little study has been conducted on the role of these fibers in absorbent products.

The purpose of this study is to describe and examine the role of fiber cross-sectional shape on the structural characteristics of nonwovens and their absorption and release properties in regard to the effect of compression and flow direction. This work continues our previous work in which we studied the effect of structural parameters with the focus on the effect of fiber cross-sectional size (the reader may refer to chapter 5 of this dissertation).

5.2 MATERIAL AND EXPERIMENTAL

5.2.1 Description of the samples

In this work, six different types of fabrics, as shown in Table 5.1 as group C and group D, were produced in order to study the effect of fiber cross-sectional shape, and percentage of binder fibers. Group C fabrics were 90%PET, 10% binder fiber, made of 6 denier fiber of three different fiber cross-sectional shape; Group D fabrics were 80% PET, 20% binder fibers, also made of 6-denier fibers of the same three different fiber cross-sectional shape. The entire main fibers have similar length of 2 inches. The binder fibers were concentric sheath/core Co-PET/PET bicomponent fibers with the linear density of 2 denier and 1.5 inch. Melting point of Co-PET sheath component is 110 °C (T201 Provided by Fiber Innovation Technology). All the fabrics were manufactured through carding, cross-lapping, pre-needling and through air bonding processes in the Nonwovens Institute's Staple Pilot Facilities. Through air bonding was done on the temperature of 121°C. The schematic of fiber cross-sectional shapes is given in figure 5.1.

Table 5.1: sample details

Group code	Sample #	PET fiber size (denier)	PET fiber cross-section	% Binder	%PET
C	1	6	Round	10	90
	2	6	Pentalobal	10	90
	3	6	4DG	10	90
D	1	6	Round	20	80
	2	6	Pentalobal	20	80
	3	6	4DG	20	80

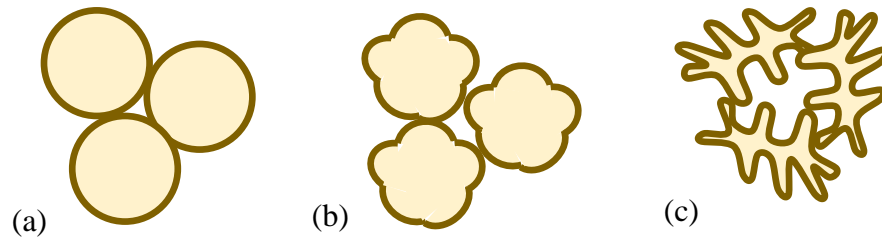


Figure 5.1: schematic of various fiber cross-sectional shape (a) round (b) pentalobal (c) 4DG

5.2.2 Basic web properties

Web thickness of samples was measured using an Ames Logic basic thickness gauge model no. BG1110-1-04. The presser foot diameter was 1 inch and the applied pressure was 0.6 psi. The thickness was measured for 15 different places along the fabric.

The basis weights of the samples were calculated for 18 different replicates per each sample according to equation 5.1, in which w is the mass of the sample and A is the sample area. The samples were the round samples with the cross-sectional area of 100cm^2 .

$$\text{Basis weight} \left(\frac{\text{g}}{\text{m}^2} \right) = \frac{w (\text{g})}{A} \quad (5.1)$$

Finally the solidity of the samples was calculated according to the equation 5.2.

$$\text{Solidity} = \frac{(w/A/t)}{\rho} \quad (5.2)$$

Where, w : sample mass (g)
 A : sample area (cm^2),
 t : sample thickness (cm) and
 ρ : fiber mass density (1.37g/cm^3 for polyester fibers)

5.2.3 Pore size measurements- porometry technique

The porous parameters of the nonwoven samples were measured using a capillary flow porometer (CFP-1100-AA, PMI, New York, USA) according to the principle of liquid extrusion technique. The samples were fully wetted with a fluid in the name of Galwick and surface tension of 15.9 Dynes/cm.

5.2.4 Pore size measurement of compressed samples- porosimetry technique

The PMI liquid extrusion porosimeter (LEP-1100AX) was employed to measure the median pore size (according to through-pore volume) at various compression levels. This technique was performed on the nonwoven samples containing 6-denier fiber in order to measure the porous parameters of the nonwoven samples under various levels of compression of 0, 20, 30, and 40% compression. The samples were wetted with water with surface tension of 72 Dynes/cm.

5.2.5 Experimental technique for absorption and release properties

The techniques and protocols were developed in order to analyze the absorption and release properties of nonwovens at various compression levels. The absorption properties were evaluated in various flow directions including through-plane, horizontal in-plane, and vertical in-plane direction. The techniques were discussed comprehensively in our previous paper (Chapter 4 of this dissertation).

5.3 RESULTS AND DISCUSSION

5.3.1 Thickness and solid volume fraction

The web structural characteristics of the entire nonwoven samples are given in table 5.2. Generally speaking, the basis weight of the samples was in a reasonable range around 200 g/m². However employing 4DG fibers resulted in the nonwoven samples with smaller thickness and consequently greater solidities value. On the other hand, the samples containing 10% binder fibers and pentalobal fibers also gave rise to the samples of slightly lower thickness and greater solidity values. This is attributed to the packing behavior and low resistance of non-circular fiber cross-section which led to the samples of higher solid volume fraction during the nonwoven production. In case of the pentalobal fiber, the results shows that 10% binder fibers is not sufficient to maintain the solid volume fraction of the sample compared to that of round cross-sectional shaped fibers. The compression properties of various fiber cross-sectional shapes and binder percentages were discussed in chapter 4 of this dissertation.

Table 5.2: basic web characteristics

Samples code	Basis weight (g/m ²)	Thickness (mm)	Initial Solidity
C1	212	4.45	0.035
C2	210	3.92	0.039
C3	217	3.69	0.043
D1	214	4.25	0.037
D2	202	4.06	0.036
D3	236	3.86	0.044

5.3.2 Pore diameter

In order to evaluate absorbency behavior of nonwovens containing various fiber cross-sectional shapes according to their structural properties, first we measured the pore characteristics of nonwovens through porometry technique via a capillary flow porometer. The values of smallest and

largest detected pore diameter, as well as mean flow pore diameter has displayed in figure 5.2 for samples containing various binder percentages. The smallest pore size for pentalobal samples containing 10% binder fibers were not detected by the porometry technique. It is evident from the results that 4DG fiber cross-section shape led to smaller pore size values which is ascribed to their higher solidity values. The round and pentalobal fiber cross-sections exhibited almost identical pore sizes values. On the other hand, samples containing 20% binder fibers exhibit smaller pore sizes in different fiber cross-sections as a rule. Similar trend was observed in case of samples of various fiber cross-sectional size.

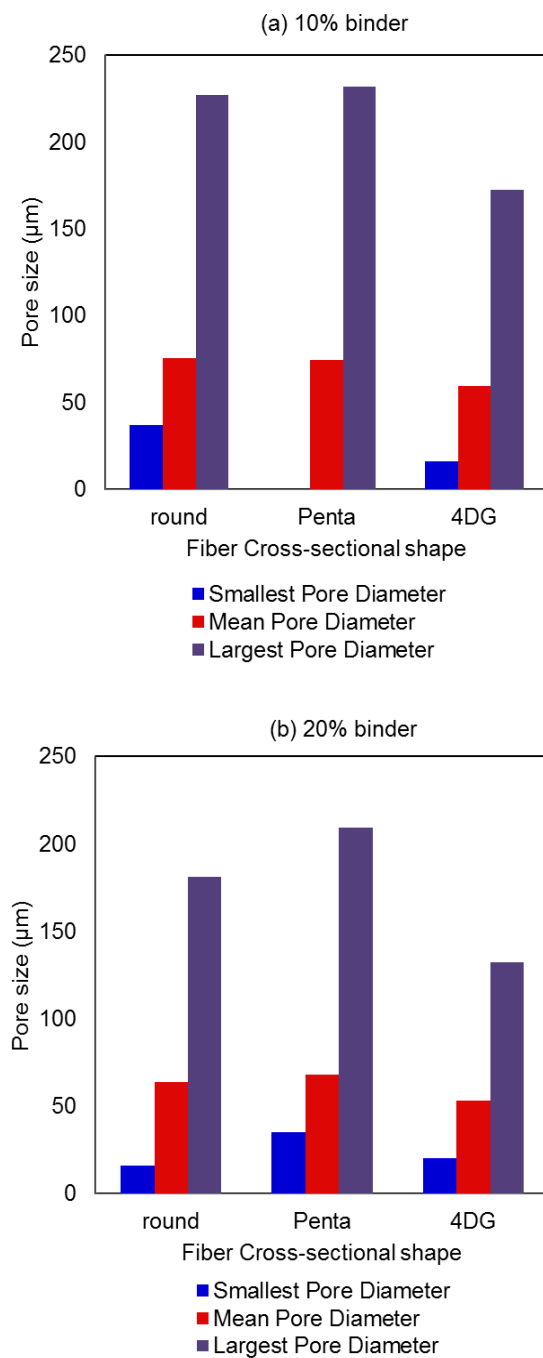


Figure 5.2: the porometer results for various fiber cross-sectional shape (a) 10% binder (b) 20% binder

5.3.2.1 Pore characteristics on compression

As mentioned previously, our purpose was to study the absorption behavior of nonwoven considering the influence of compression and in relation to their structural characteristics. In this section we evaluated the pore size of various fiber cross-sectional shapes at different compression levels. Figure 5.3 demonstrates the median pore diameter based on pore volume measured by porosimetry technique. These values correspond to the pore size in which 50% of pore volume is accounted for the smaller pore sizes and the remaining 50% pore volume is accounted for the larger pore sizes, however it should be noted that this technique underestimates the volume of larger pore sizes due to ink-bottle effect (Jaganathan, Vahedi Tafreshi, and Pourdeyhimi 2008). First of all, it should be noted that the trend obtained among various fiber cross-sectional shaped obtained based on median pore diameter measured by porosimetry technique were not similar to that of mean flow pore diameter measured by porometry technique. As it was mentioned earlier, since the porosimetry technique characterizes the pore structure and its anisotropy level (Gribble et al. 2011), it can be speculated that the difference between the median pore diameter and mean flow pore diameter achieved by these techniques is larger at higher level of tortuosity. It could be interpreted as the tortuosity is greatest in samples of 4DG fibers following with the samples of round fibers. According to our results, the minimum tortuosity was observed in pentalobal fibers since the mean flow pore size and median pore diameter displayed the minimum difference. From figure 5.3 it can also be seen that the trend of the median pore diameter with compression was not similar for the circular cross-sectional shaped fibers and non-circular cross-sectional shaped fibers. Even though, the observed trend of reduction in median pore sizes with the compression in case of round fiber cross-section was as anticipated and in line with those of Jaganathan et al. (Jaganathan et al. 2009), a striking difference was noted when the fiber cross-sectional shape was deviated from the circular shape. It can be observed that 4DG and

pentalobal fibers revealed substantial rise in median pore diameter with compression at some levels of compression. The surprising behavior of non-circular cross-sectional fibers may be the consequence of their packing manner.

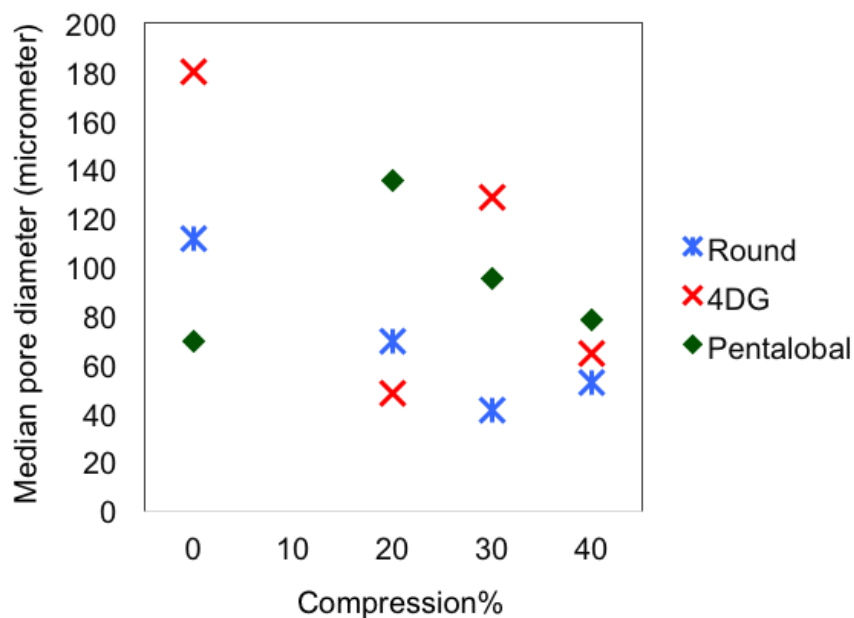


Figure 5.3: the median pore diameter measured by porosimetry technique at varied compression levels

It was predicted that the pore size distribution of nonwovens became narrower with the compression. Table 5.3 lists the pore size distribution of various fiber cross-sections at different compression levels. On the whole the pore size distribution in case of round fiber cross-section became narrower relatively, however it was not seen in case of the non-circular fiber cross-sections. It can be observed that there was a surprising change in the pore size distribution of non-circular fiber cross-sections where a percentage of pore volume was attributed to the pore sizes larger than 500 micrometer with

the compression. It is seen that the fibers show a bi-modal pore distribution under no compression, in which a fraction of pores are smaller than 50 micrometer and the rest are attributed to the larger pores. This feature is specifically observed in case of 4DG fibers. This is ascribed to two different kinds of pores that are available in the samples containing 4DG fibers. The smaller pores are created due to the channels formed by the irregular fiber cross-sectional shapes as shown in figure 5.1 and the larger ones take place between the fibers themselves. The smaller pores disappear under the compression due to the packing of the fibers and distortion of fiber cross-sectional shapes. Then the non-circular fiber cross-sections packed very closely in some adjacent, creating fiber bundles, where larger pore sizes occur in their vicinity.

Table 5.3: the pore size distribution of nonwovens containing round, pentalobal, and 4DG fiber cross-sections at no compression and under 20%, 30%, and 40% compression

fiber cross-section	Pore size range (μm)	Compression %			
		0%	20%	30%	40%
Round	<50	4	25	52	39.5
	50-70	30	63	44.5	53.5
	70-100	9	6.5	3	3
	100-200	40.5	4.5	0.5	4
	200-300	15	1	0	0
	300-500	1.5	0	0	0
Pentalobal	<50	24.18	2.185	10	13
	50-70	34	13	19.5	36
	70-100	17	24	28	12
	100-200	24	28	18	17
	200-300	1	20	5	5
	300-500	0	9	1.5	4
	500-2000		3	18	3
	>2000				10
4DG	<50	11.34	46.7	5.5	13
	50-70	0.759	32	19	66
	70-100	3.037	21	4	5
	100-200	55	0.3	38.5	15
	200-300	16.5	0	2	1
	300-500	8	0	1.5	
	500-2000			20.5	
	>2000			9	

5.3.3 Absorption properties

The main purpose of this study was to recognize the influence of structural factors on the absorption properties of nonwovens. In chapter 4, the effect of fiber cross-sectional size was evaluated using compression GATS, In-plane absorbency testing system, and vertical wicking test. Fiber cross-sectional shape is the other important fiber properties, which dictate the web structural characteristics of nonwovens. In this section the absorption behavior of the nonwoven materials is discussed for three different fiber cross-sectional shapes. Figure 5.4 and 5.5 demonstrated the GATS absorbency behavior of these samples at various levels of compression for samples containing 10% and 20% binder fibers respectively. Generally speaking the overall response of various fiber shapes were identical to the compression. As expected, the maximum absorption of the samples dropped by compression for the entire samples; also the absorbency rate was changed at various degree of compression. In the following section, these parameters are discussed in more details.

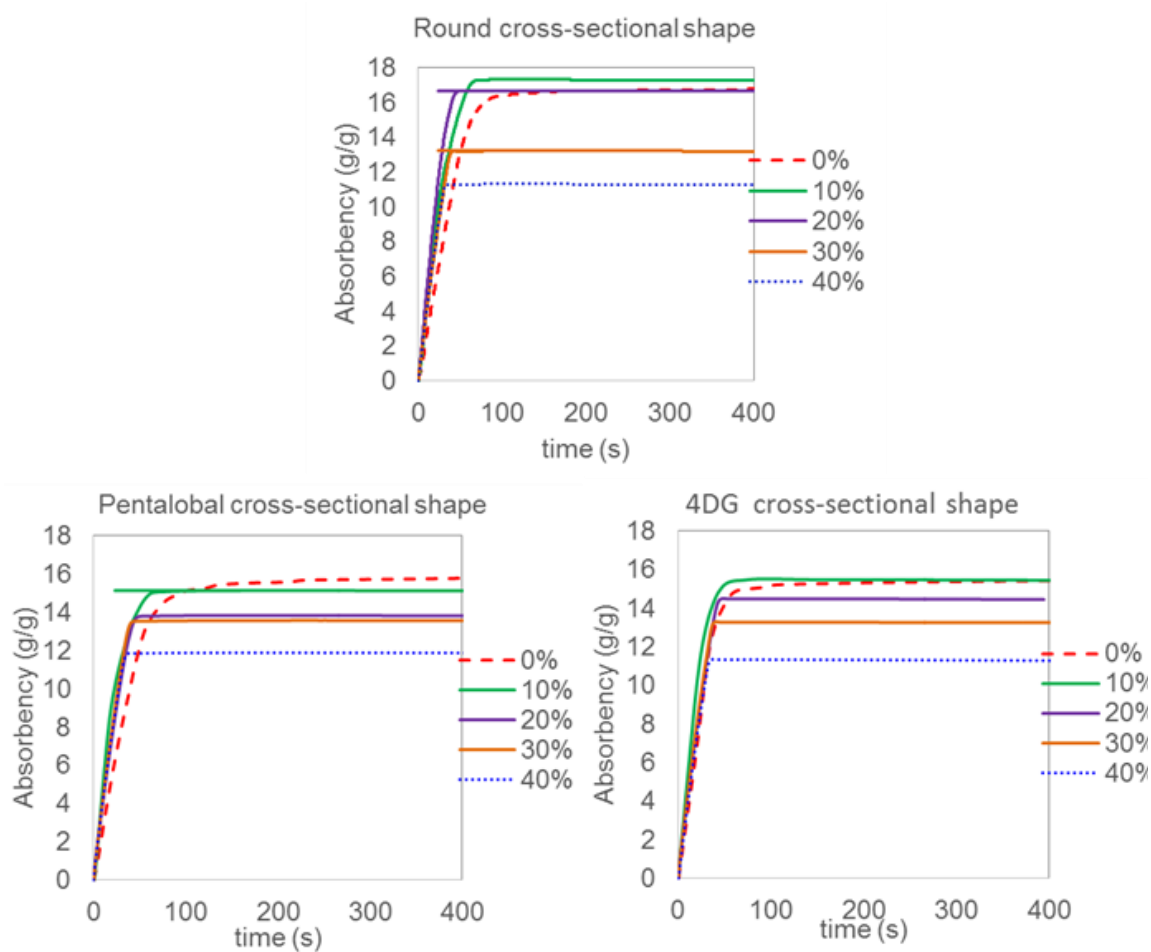


Figure 5.4: the GATS results for different fiber cross-sectional shape- 90% PET-10% Co-PET- at various compression levels

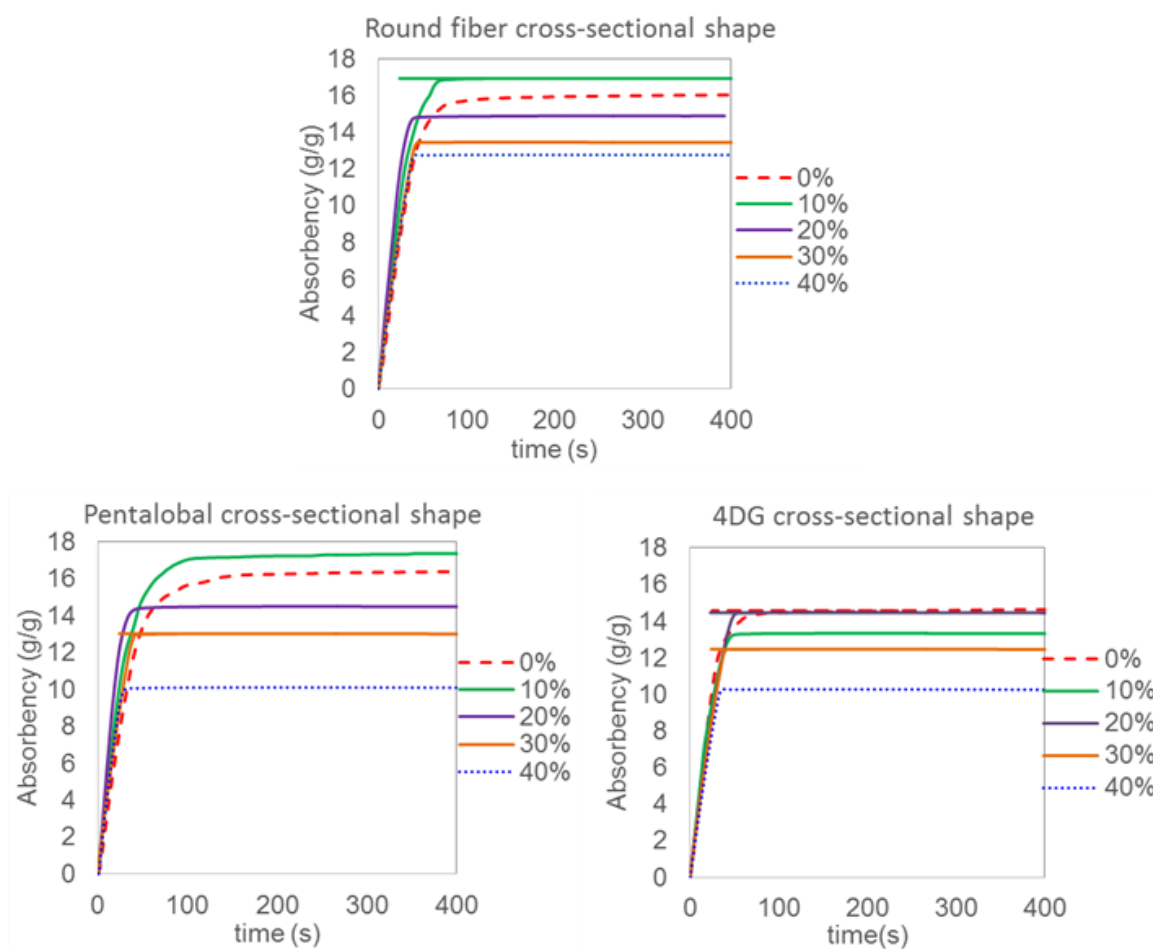


Figure 5.5: the GATS results for different fiber cross-sectional shape- 80% PET-20% Co-PET- at various compression levels

5.3.3.1 Maximum Absorption

Maximum absorption was measured experimentally through compression GATS absorbency curve. Figure 5.6 shows the results for different fiber cross-sectional shapes, different binder percentages and under varied compression percentages. The graph exhibited the overall reduction in maximum absorption with compression, however the maximum absorption was unaffected by small compression. This is due to the imperfect contact between the sample and sample holder, which was explained in the previous chapter.

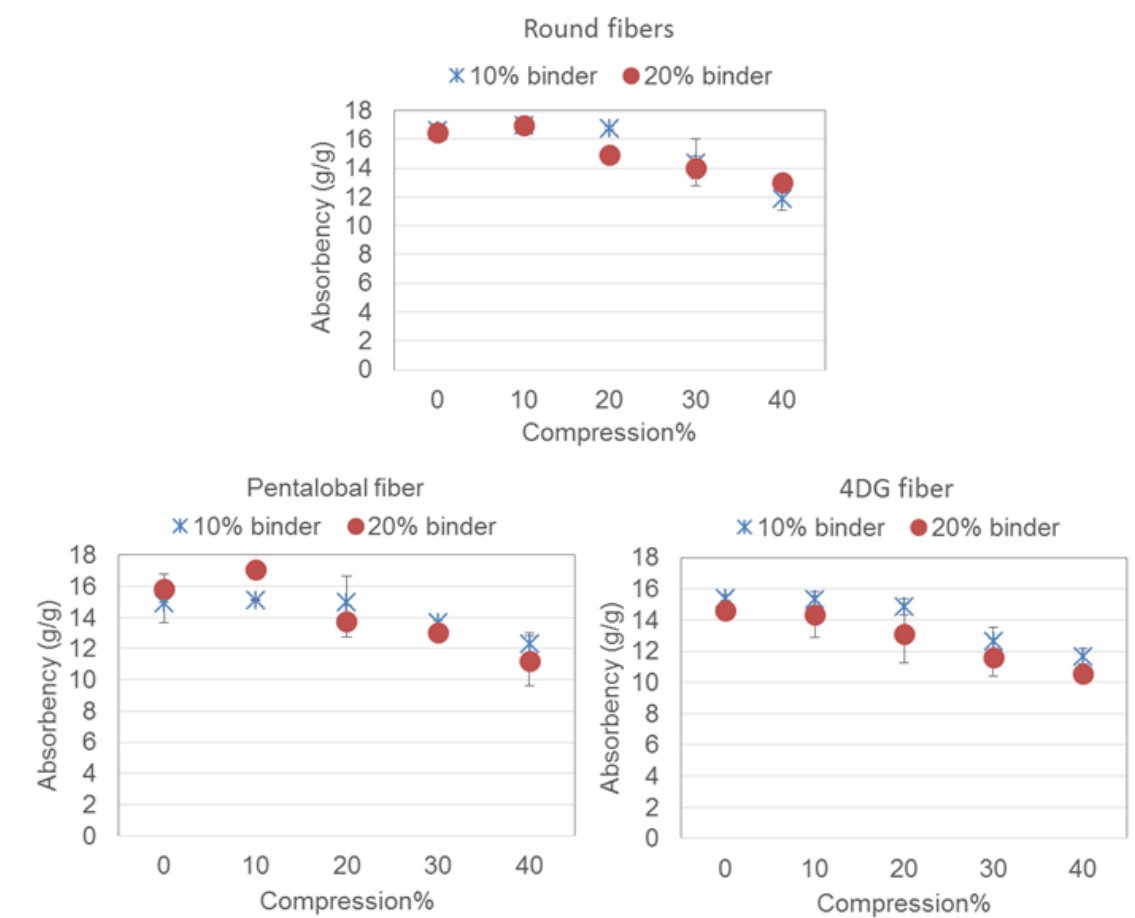


Figure 5.6: the GATS maximum absorption for various fiber cross-sectional shape and binder percentages at varied compression levels

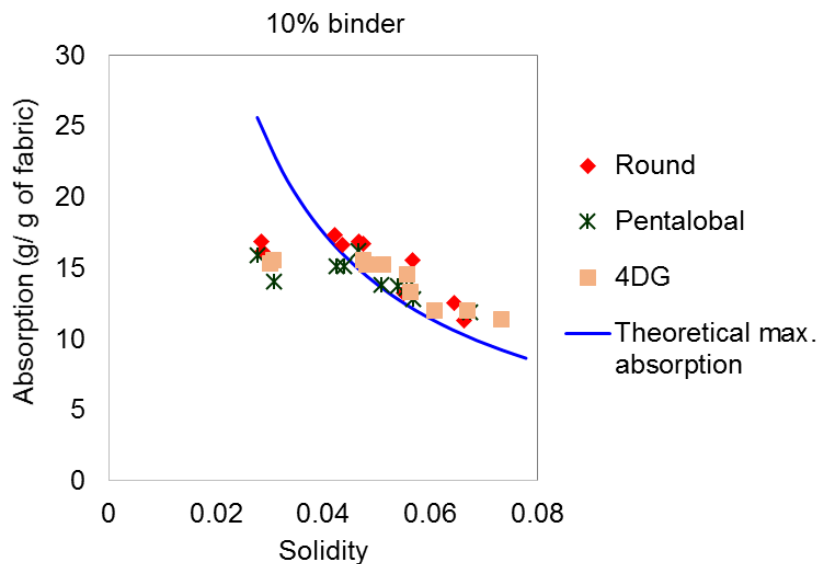


Figure 5.7: the GATS maximum absorption results vs. solidity for different fiber cross-sectional shape of nonwoven samples containing 90% PET-10% Co-PET

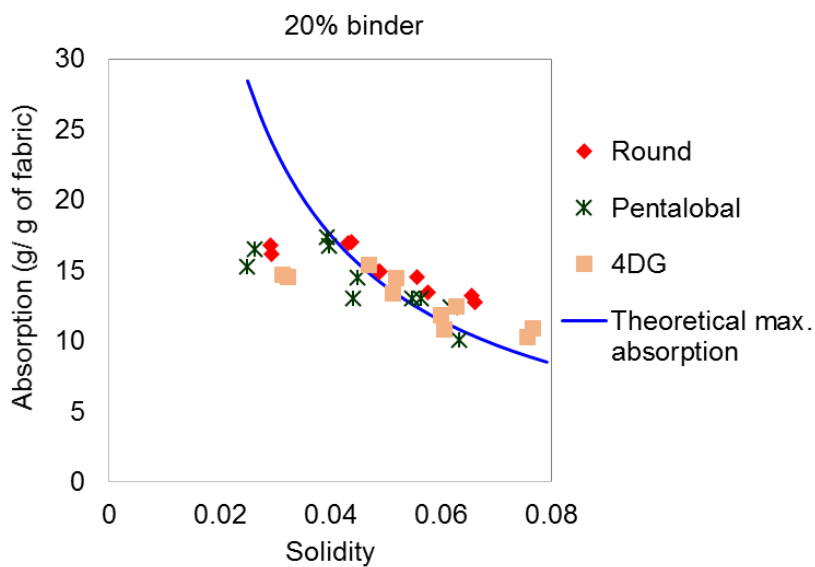


Figure 5.8: the GATS maximum absorption results vs. solidity for different fiber cross-sectional shape of nonwoven samples containing 80% PET-20% Co-PET

In order to realize the relationship between the maximum absorption and the structural parameter of nonwovens, the experimental maximum absorption is graphed versus solidity of the samples as shown in figures 5.7 and 5.8. The figures illustrate both the theoretical and GATS maximum absorption of samples at various solidity achieved at different compression levels. As expected, the maximum absorption is mainly governed by solidity of the samples and it was reduced with the solidity. The results show that the fiber cross-sectional shape has negligible impact on the maximum absorption of the nonwoven samples. The smallest solidity values are attributed to the non-compression situation where the contact between the sample and samples holder is imperfect. This caused the difference between the theoretical and experimental values since the samples were not fully saturated. These behaviors have already observed in the investigation of samples with different fiber sizes in previous sections.

5.3.3.2 Absorbency Rate

The relationship between the absorbency rate and the nonwoven structure is very complicated and not fully agreed (Mao and Russell 2003; Das, Pradhan, and Pourdeyhimi 2012). In this work, our aim was to establish this relationship by methodological design of nonwoven structure. Our way to achieve the various structural designs was to produce nonwoven fabrics of similar porosity and various pore shapes via various fiber cross-sectional shapes. The other goal was to understand the changes in absorption behavior of nonwovens. Moreover the anisotropic nature of nonwoven structures consequences on having different pore structures in through plane and in plane directions. Therefore, in this section the absorbency rate of samples is discussed in terms of various fiber cross-sectional shape, compression levels, and flow direction.

5.3.3.2.1 Through-plane direction

In this work, we sought to comprehend the influence of fiber cross-sectional shape on the absorbency behavior experimentally in various flow directions. In this section, the results for through-plane direction are being discussed. Figure 5.9 demonstrated the results for various fiber cross-sectional shape and binder percentages. It was seen that the effect of binder percentages was insignificant under no compression. The data shown in this figure hardly confirm any significant effect of the fiber cross-sectional shape on the absorbency rate in through-plane direction.

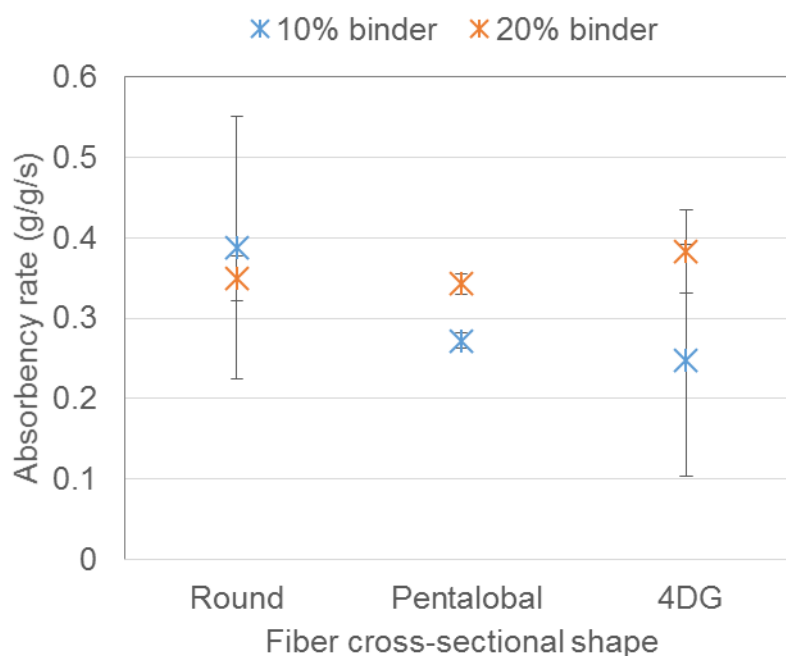


Figure 5.9: the GATS absorbency rate in through-plane direction for various fiber cross-sectional shape and binder percentages

Figures 5.10 and 5.11 displays the results at varied compression level. It can be identified from these figures that the absorbency rate increased initially, showed a maximum and then decreased in all

samples regardless of fiber cross-sectional shape. On the other hand, no specific trend was observed among the samples of various fiber cross-sectional shapes. However, it is noteworthy to mention that at 20% compression levels, pentalobal fibers show the highest absorbency rate in both two different binder percentages. Comparing the pore size distribution of the various samples given in table 5.3 shows that in case of pentalobal samples containing 20% binder fibers, 52% of their pore volume was in the range of 70-200 micrometer at 20% compression, while it was reduced to 11% and 21.3% for round and 4DG fiber cross-section respectively. The higher absorbency rate may be attributed to the difference between the pore size distributions of the samples. This result is in line with our finding in chapter 4 where the median pore sizes in range of 70-100 micrometer illustrated the highest absorbency rate.

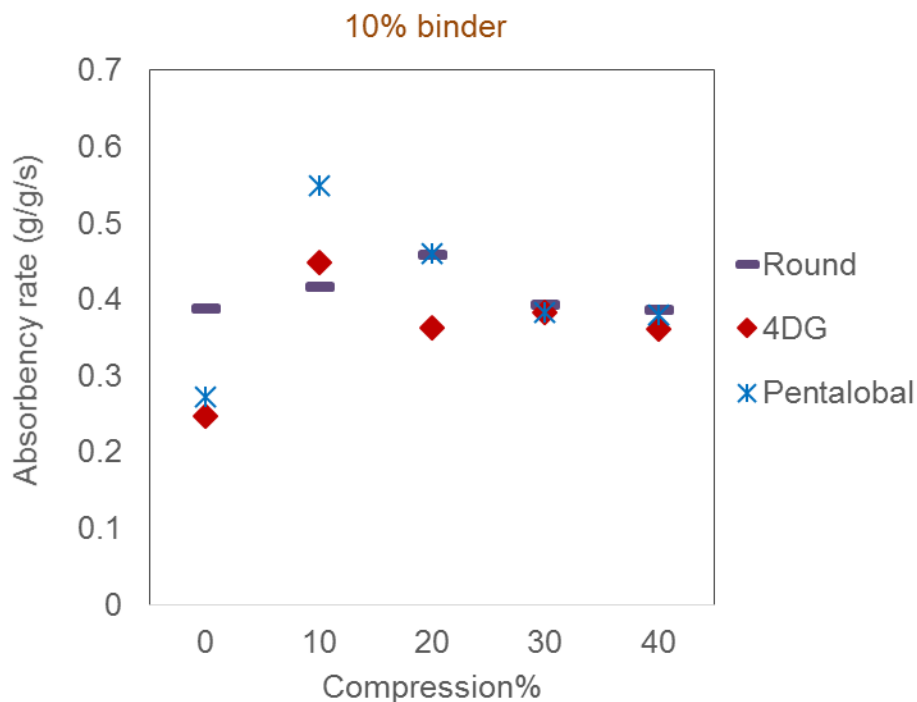


Figure 5.10: the GATS absorbency rate in through-plane direction at varied compression levels for various fiber cross-sectional shapes of the nonwoven samples containing 90% PET-10% Co-PET

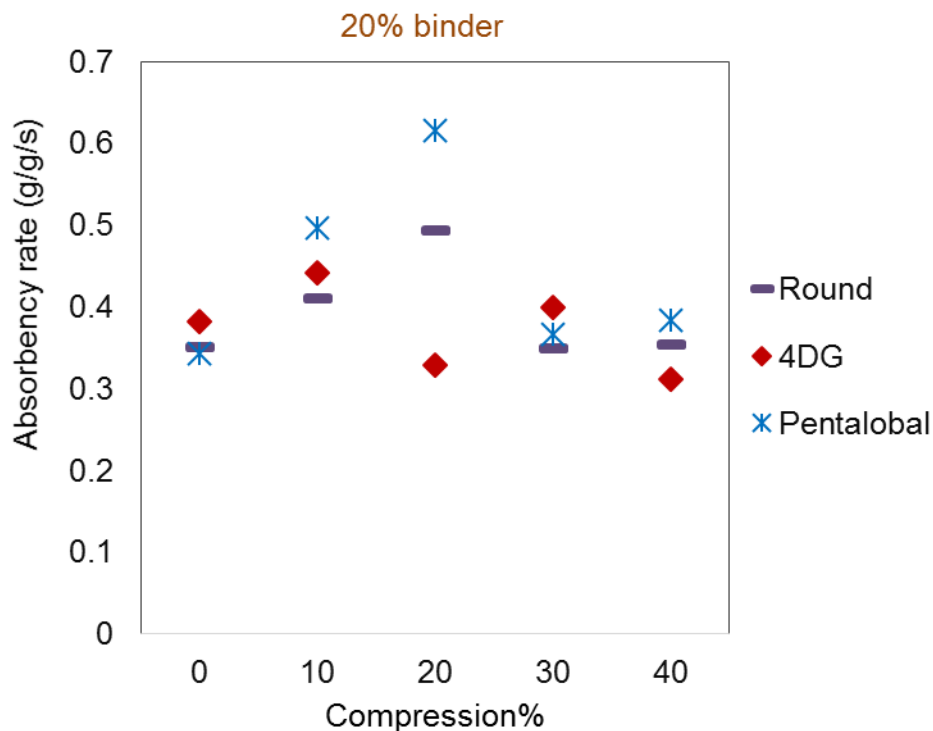


Figure 5.11: the GATS absorbency rate in through-plane direction at varied compression levels for various fiber cross-sectional shapes of the nonwoven samples containing 80% PET-20% Co-PET. As it was mentioned earlier there are two types of pores, and consequently two types of liquid spreading, first the liquid spreading which happens between the fibers or pore structures, and the liquid spreading through the fiber surface morphology. The liquid spreading through the pore structure or between the fibers does not affected by the fiber cross-sectional shape unless the sample is compressed or fibers are highly packed. On the other hand, the spreading through the fiber surface highly depends on the fiber cross-sectional shapes, however this always follow the fiber direction. In case of the samples used in this study, where the samples are carded, cross-lapped, and pre-needled, most of the fibers are oriented in in-plane direction, and the fraction of fibers oriented in through-plane directions are very limited. Therefore the fiber-cross sectional shape does not have a significant influence on the rate of absorption in through plane direction.

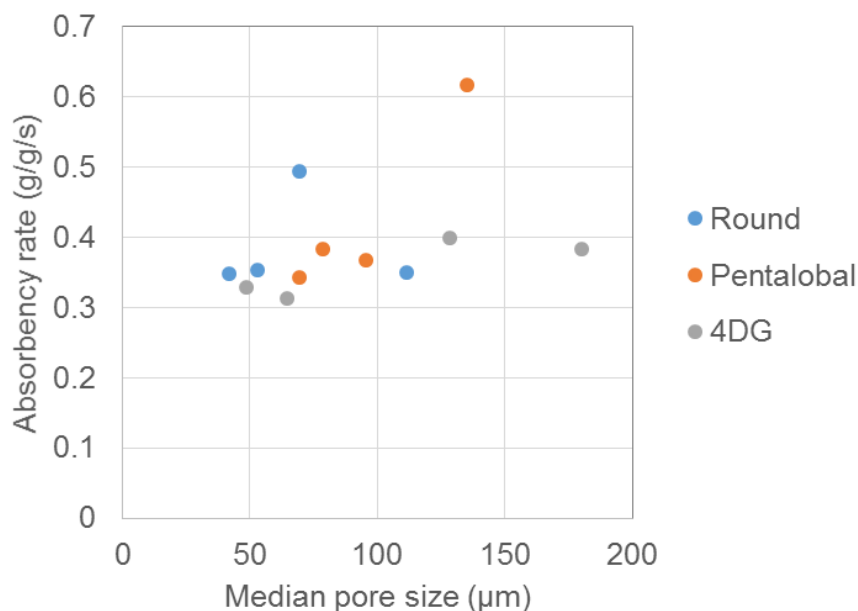


Figure 5.12: absorbency rate vs. median pore size for different fiber cross-sectional shapes for nonwoven samples containing 80% PET-20% Co-PET

In order to realize the relationship between the absorbency rates and pore size, figure 5.12 displays the absorbency rate versus the median pore size at various fiber cross-sectional shapes. It can be observed from this figure, while the absorbency rate of circular fiber cross-section samples exhibited a maximum value with the median pore size in the range of 70 micrometer, this behavior was not seen in case of non-circular fiber cross-section including both pentalobal and 4DG fibers. On contrast, the rate of absorption showed an increasing trend with the pore size in non-circular fiber cross-sections. These results were not in agreement with the vertical Washburn equation in which the absorbency rate gives rise to a maximum with the pore size (the reader may refer to chapter 4 of this dissertation for more information). It may be explained by the fact that the groove shaped pore spontaneously transports the liquid with a significantly faster rate in horizontal plane than in vertical direction.

Therefore, even though the flow happens in a through-plane direction, the absorption is occurred in both vertical and horizontal direction, while the rate in horizontal direction is much higher than the rate in vertical direction (figure 5.13).

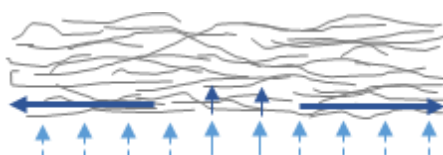


Figure 5.13: schematic view of through-plane absorptivity of nonwoven samples containing non-circular fiber cross-sectional shape

5.3.3.2.2 In-plane absorptivity rate

The nonwoven fabrics are highly anisotropic and the previous study has shown that the in-plane liquid spreading is driven by structure anisotropy (Ashari et al. 2010; Kim and Pourdeyhimi 2003). Hence the In-plane absorptivity rate of the entire samples was measured through point wicking test. The gravity does not significantly influence on the results and hence the results were compared with the horizontal Washburn equation. Figure 5.14 displays the result for in-plane absorptivity rate of the entire samples. The result shows that the in-plane absorptivity rate of 4DG fiber cross-section is the highest and then the pentalobal fibers shows higher in-plane absorptivity rate than round fibers. The result shows that the specific fiber-cross sectional shapes accelerate the absorptivity rate in the in-plane direction since the fibers in carded, cross-lapped web are mainly oriented in x-y plane rather than in z-direction. This is attributed to the fiber surface texture or the grooves formed by the non-circular fiber cross-sectional shapes (2001 Vaughn).

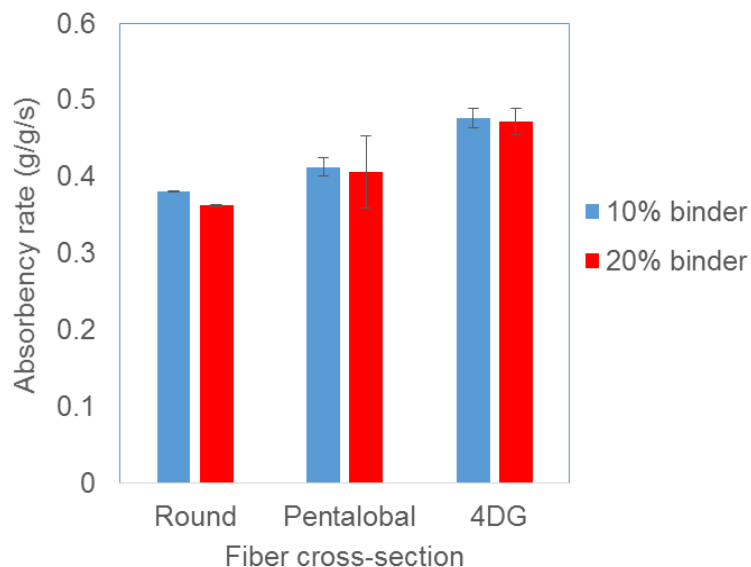


Figure 5.14: the GATS in-plane absorbency rate for various fiber cross-sectional shape and binder percentages

5.3.3.2.3 Vertical wicking rate

Vertical wicking has been used in the researches to model the fluid flow according to the capillary pressure provided by the porous structure based on Lucas-Washburn and Laplace equations (Chatterjee and Gupta 2002), because it provides the condition for a purely capillary action (Larose 1942). One of the challenges in using these equations is the estimation of the capillary radius. Due to the tortuous fluid path in real porous media, which is in contrast with the assumption of the aligned capillary tubes supposed in these equations, it is required to estimate the “equivalent capillary radius” for a real porous media. The previous data has shown that the most accurate for estimating the equivalent capillary radius is the vertical- wicking test (Masoodi and Pillai 2010), in which the capillary pressure is balanced with the gravitational potential energy. In order to obtain a better

understanding of the pore structure, therefore the vertical wicking test was done on the samples containing 20% binder fibers. Figure 5.16 shows the results obtained by vertical wicking test. The initial rate of liquid penetration was measured as 7.0, 9.1 and 15 mm/s for the samples containing round, pentalobal, and 4DG fibers respectively. As anticipated, the results showed that non-circular fibers led to higher vertical wicking rate, however 4DG fiber also displayed significantly greater initial rate than pentalobal fibers. It could be speculated from these results that the flow direction plays an important role in order to achieve the elevated absorbency rate in non-circular fiber cross-sectional shapes. The results also were in agreement with the in-plane absorbency rate. This is because the grooves are highly oriented in in-plane direction rather than through-plane direction. The liquid penetration distance was measured at 42 hours as shown in table 5.4. It showed that the 4DG fiber samples had considerably greater liquid front than pentalobal and round fibers. It could be concluded that 4DG fiber provided significantly greater capillary pressure in in-plane direction than round and pentalobal fibers due to the smaller pore size, however it was not observed according to pore size distribution measured in porosimetry technique given in table 5.3, even though it should be noted the measured pore size distribution corresponds to through-plane direction rather than the in-plane direction which is flow direction in vertical wicking test.

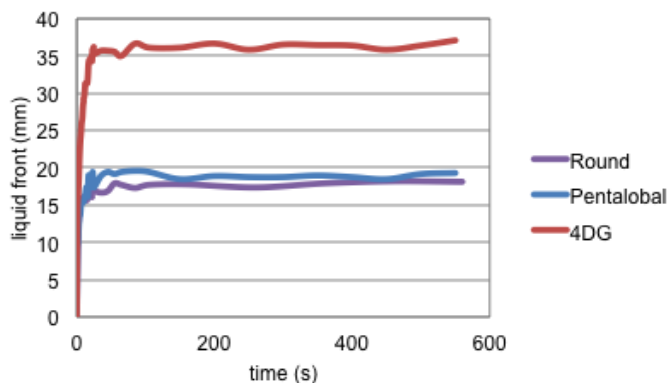


Figure 5.15: vertical wicking result, liquid front distance vs. time for various fiber cross-sectional shapes of nonwoven samples containing 90% PET-10% Co-PET fiber

5.3.4 Release properties

In this section, the release properties of the entire nonwoven samples is discussed by measuring their liquid holding capacity at various compression levels. Moreover their holding behavior is related to their pore characteristics including their solidity and pore shapes.

The liquid holding capacity of the samples with different fiber cross-sections and binder percentages is shown in figure 5.16. This figure shows the result for the samples under no compression. It can be observed in the figure that even though round and pentalobal fibers released a fraction of absorbed liquid under no compression, the 4DG fibers has the capability to hold the entire liquid absorbed by the samples. Then, the 4DG fibers showed the highest liquid holding capacity under no compression.

Table 5.4: the liquid front rate and distance for various fiber cross-sectional shape- vertical wicking test

Fiber cross-sectional shape	Rate (mm/s)	Liquid front after 42 hours (mm)
Round	7.0	18.301
Pentalobal	9.1	18.947
4DG	15	107.39

This is because of the higher capillary pressure due to the presence of the groove on the cross-section of the fibers and their smaller pore sizes which was discussed in the previous section. These grooves

act as smaller pore size with higher capillary pressure, therefore they can retain the liquid. Moreover, as mentioned in the introduction, the non-circular shaped fiber provides structure with higher surface area and it can help to retain more liquid inside the pores. The results also exhibited that the round fiber cross-section and pentalobal fiber cross-section have approximately similar capability to hold the liquid at no compression in the samples containing 10% binder fibers, nevertheless the pentalobal fibers displayed higher holding capacity in the samples containing 20% binder fibers. It is thought that the smaller pore sizes in the samples containing 20% binder fibers led to higher capillary pressure.

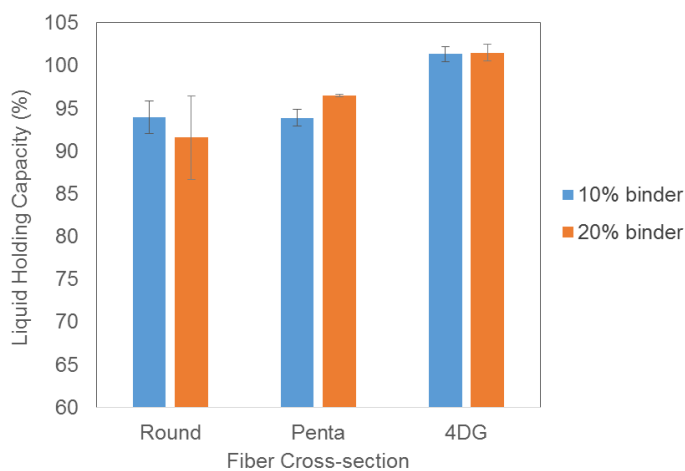


Figure 5.16: liquid holding capacity of samples with different fiber cross-section and binder percentages

Figure 5.17 and 5.18 demonstrated the liquid holding capacity of the entire samples at various compression levels for samples containing 10% and 20% binder fibers respectively. It was not possible to reach the 40% of compression in round fiber samples containing 20% binder fibers according to the release methodology employed in this study due to high resistance of these samples to compression. After their initial release, the round fibers start to release the liquid at lower compression percentages and with higher rate than pentalobal and 4DG fibers. Therefore it is observed that even though pentalobal and round fibers did not exhibit a very significant difference in their liquid holding capacity at no compression, pentalobal fibers were capable of considerably retaining more percentages of liquid than the round fibers at higher compression. Since the obtained results are influenced by the solidity of the samples, the retention properties of the samples is studied according to their solidity in the following discussion.

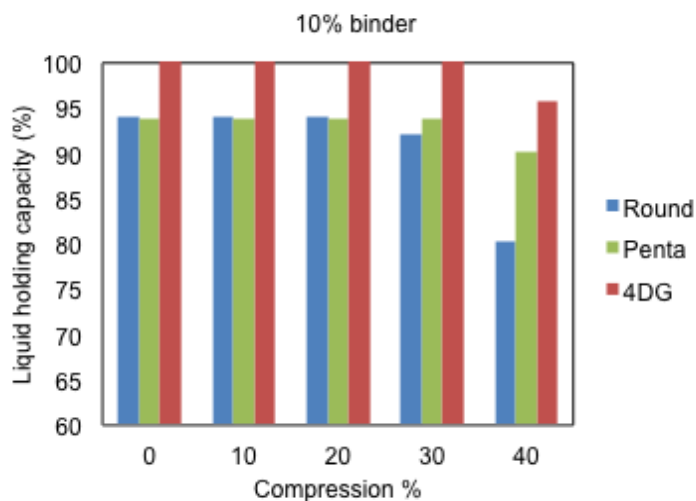


Figure 5.17: Liquid holding capacity of samples with different fiber cross-sectional shape at varied compression levels for the samples containing 90% PET,10% Co-PET

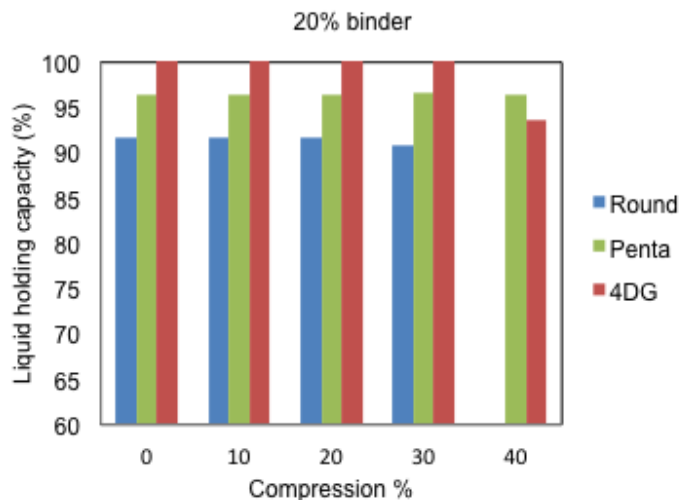


Figure 5.18: Liquid holding capacity of samples with different fiber cross-sectional shape at varied compression levels for the samples containing 80% PET, 20% Co-PET

In this work, we sought to establish the relationship between the retention properties and the structural parameter of nonwovens. Therefore the liquid retention capacity of the samples was examined based on their solidity values achieved at varied compression levels as shown in figures 5.19 and 5.20. As indicated in these figures, the liquid retention of the entire samples remained

constant as long as the samples are not fully saturated disregarding the solidity values. The unsaturated samples appeared in those areas that there was a gap between the retention capacities and theoretical maximum absorption. The existence of the gap confirms that a fraction of the pore volume is not filled with the liquid. Achieving the greater solidity values due to the compression on those areas brought about the redistribution of liquid from larger pores to smaller pores, where the capillary pressure is higher according to Laplace equation, and therefore it is harder for the liquid to be released. Nonetheless, in the solidity levels where the samples were fully saturated, the further increase in solidity value led to the liquid release and liquid retention drop. Since for the entire samples containing various fiber cross-sectional shape, the same behavior was observed, it could be inferred therefore that the cross-sectional shape did not have a significant effect on the liquid retention of the samples under compression and the influencing factor is the saturation level of the samples at various solidity values.

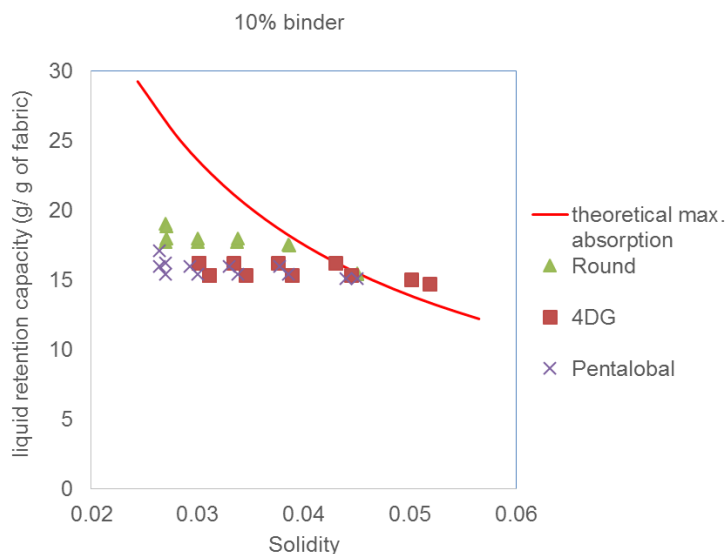


Figure 5.19: liquid retention capacity vs. solidity value for the samples of various fiber cross-sectional shape, containing 90% PET,10% Co-PET fibers

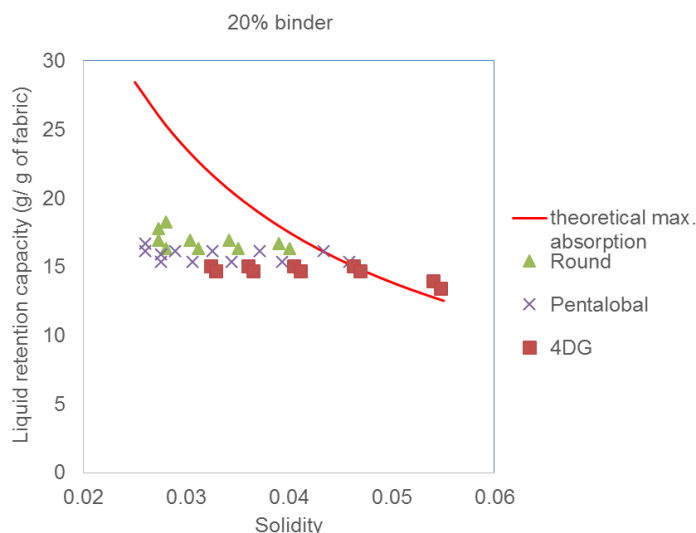


Figure 5.20: liquid retention capacity vs. solidity value for the samples of various fiber cross-sectional shape, containing 80% PET,20% Co-PET fibers

5.4 CONCLUSION

Previous attempts have been reported the significance of the fiber cross-sectional shape in improving the absorbency behavior of nonwovens. However the evaluating role of the fiber cross-sectional shapes on the structural parameters of nonwovens demanded clarification. In this study, we examined the absorption and release properties of nonwovens with the focus on the impact of fiber cross-sectional shape in regard to the pore characteristics. In order to obtain various structures, the study was done at different levels of compressions and binder percentages. The nonwovens were made of various fiber cross-sectional shape including round, pentalobal and 4DG fibers.

It was found that the benefit gained by the non-circular or shaped fiber cross-sectional shape highly depends on the flow direction. This is attributed to the direction of promoting channels, which are in the same direction as fiber direction. This gave rise to the highest rate of 4DG and pentalobal fibers nonwovens in in-plane absorption and vertical wicking. Moreover although the median pore size of

the nonwoven containing circular fibers was reduced under the compression as anticipated, the non-circular fiber cross-section did not behave the same. A remarkable increase in the median pore size was observed in case of pentalobal and 4DG fiber nonwovens with the compression. On the whole, it was observed that greater the median pore size, the rate of absorption was faster in case of pentalobal and 4DG fiber nonwovens. This was not in line with the results for the round cross-sectional fibers in which the absorbency rate showed a maximum with pore size. Furthermore, it was observed that the retention capacity of the nonwovens sample under no compression is governed by the fiber cross-sectional shape and in general the non-circular fiber cross-section resulted in greater retention capacity, however the retention capacity is dictated by their saturation levels and solidity under compression and it is not affected by the fiber cross-sectional shapes.

REFERENCES

- Ashari, A., T.M. Bucher, H. Vahedi Tafreshi, M.A. Tahir, and M.S.A. Rahman. 2010. "Modeling Fluid Spread in Thin Fibrous Sheets: Effects of Fiber Orientation." *International Journal of Heat and Mass Transfer* 53 (9-10): 1750–58. doi:10.1016/j.ijheatmasstransfer.2010.01.015.
- Bernt, Ingo, Matthew North, Reinhold Röthenbacher, Walter Roggenstein, and Roland Scholz. 2014. "Regenerated Cellulose Fiber." US patent 20140147616
- Chatterjee, P. K, and B. S Gupta. 2002. *Absorbent Technology*. Amsterdam; Oxford: Elsevier Science. <http://www.sciencedirect.com/science/book/9780444500007>.
- Dalton, J. Nelson, and Bobby M. Phillips. 1998. "Process of Making a Non-Circular Cross Sectional Fiber." US patent 5753166
- Das, Dipayan, Arun Kumar Pradhan, and Behnam Pourdeyhimi. 2012. "Dependence of the Liquid Absorption Behavior of Nonwovens on Their Material and Structural Characteristics: Modeling and Experiments." *Journal of Applied Polymer Science* 126 (3): 1053–60. doi:10.1002/app.36635.
- Gribble, Christopher M., Graham Peter Matthews, Giuliano M. Laudone, Andrew Turner, Cathy J. Ridgway, Joachim Schoelkopf, and Patrick A.C. Gane. 2011. "Porometry, Porosimetry, Image Analysis and Void Network Modelling in the Study of the Pore-Level Properties of Filters." *Chemical Engineering Science* 66 (16): 3701–9. doi:10.1016/j.ces.2011.05.013.
- Jaganathan, S., H. Vahedi Tafreshi, and B. Pourdeyhimi. 2008. "Modeling Liquid Porosimetry in Modeled and Imaged 3-D Fibrous Microstructures." *Journal of Colloid and Interface Science* 326 (1): 166–75. doi:10.1016/j.jcis.2008.07.011.
- Jaganathan, S., H. Vahedi Tafreshi, E. Shim, and B. Pourdeyhimi. 2009. "A Study on Compression-Induced Morphological Changes of Nonwoven Fibrous Materials." *Colloids and Surfaces A:*

- Physicochemical and Engineering Aspects 337 (1-3): 173–79.
doi:10.1016/j.colsurfa.2008.12.019.
- Kim, H. S., and B Pourdeyhimi. 2003. “In-Plane Liquid Distribution In Nonwoven Fabrics: Part 2 — Simulation.” *International Nonwovens Journal Summer* (2): 29–33.
- Largman, Theodore, Fred J. Gefri, and Frank Mares. 1991. “Filaments Having Trilobal or Quadrilobal Cross-Sections.” US patent 5057368
- Larose, P. 1942. “The Water Absorption by Towels.” *American Dyestuff Reporter* 31 (6): 105–8, 123–24.
- Mao, N., and S. J. Russell. 2003. “Anisotropic Liquid Absorption in Homogeneous Two-Dimensional Nonwoven Structures.” *Journal of Applied Physics* 94 (6): 4135. doi:10.1063/1.1598627.
- Masoodi, Reza, and Krishna M. Pillai. 2010. “Darcy’s Law-Based Model for Wicking in Paper-like Swelling Porous Media.” *AIChE Journal*, NA – NA. doi:10.1002/aic.12163.
- Meirowitz, Randy Emil, Sriram Padmanabhan, Robert John Phelan, and Kim Te Tang. 1993. “Absorbent Structure for Masking and Distributing a Liquid.” CA patent 2076416A1
- Nguyen, Hien, Nicolas Martens, and Glenn Garbolino. 1998. “Absorbent Body.” US patent 5750446
- Phillips, Bobby Mal, Shriram Bagrodia, William Alston Haile, Harry Probert Hall, and David Augustus Casey. 1990. “Fibers Capable of Spontaneously Transporting Fluids.” EP patent 0391814A2
- Pourdeyhimi, Behnam, Walter Chappas, and Harry M. Barnes. 2013. “Articles Containing Woven or Non-Woven Ultra-High Surface Area Macro Polymeric Fibers.” US patent 20130133980
- Thompson, Hugh A. 1997. “Resilient Fluid Transporting Network for Use in Absorbent Articles. US patent 5628736

- Vaughn, Edward A., and Brent G. Carman. 2001. "Expanded Surface Area Fibers: A Means for Medical Product Enhancement." *Journal of Industrial Textiles* 30 (4): 303.
- Waxman, David M., and Shih-Kuang LIEN. 2014. "Absorbent Article Containing Structured Fibers." US patent 8629316
- Wilkes, Andrew G., and Alan J. Bartholomew. 1995. "Process of Making Viscose Staple Fibers. US patent 5458835
- Yeom, Bong Yeol, and Behnam Pourdeyhimi. 2011. "Web Fabrication and Characterization of Unique Winged Shaped, Area-Enhanced Fibers via a Bicomponent Spunbond Process." *Journal of Materials Science* 46 (10): 3252–57. doi:10.1007/s10853-010-5212-y.
- Yoeng-Beek, Choi, and Yoon Joon-Young. 2002. "A Non-Circle Cross Section Fiber with Excellent Absorption and Dry." WO patent 2002070794A1

6 INVESTIGATION OF EFFECT OF STRUCTURAL PARAMETERS ON ABSORPTION PROPERTIES OF NONWOVENS UNDER COMPRESSION- PART III: HETEROGENEOUS LAYERED STRUCTURE STUDY

6.1 INTRODUCTION

Absorbency is one of the key properties required in major nonwoven applications including baby diapers, personal hygiene products, wipes and medical fabrics (Hardy 2009). Geometrical aspects of the structure and the material properties are, along with finish, major contributors to absorbency behavior of nonwovens. Even absorbency of materials have been studied extensively in various fields, absorbents behavior of nonwoven products are complex and have not been fully understood (Cueto et al. 2009; Yun et al. 2009; Ashari and Vahedi Tafreshi 2009a; Chatterjee and Gupta 2002; Tracy, Ghali, and Jones 1994; Ashari and Vahedi Tafreshi 2009b). With a given liquid, the nonwoven structural parameters play an important role on the absorption properties of nonwovens. The structural characteristics are affected by fiber geometry including both of the size and shape of fiber, nonwoven structure which can be solidity or packing density and fiber orientations, and finally by the external factors such as compression. Moreover, the different cross-sections along the absorption direction influences the liquid absorbency behavior significantly (Young 2004).

A few analytical researches examined the liquid absorption rate in heterogeneous capillary tubes (Reyssat et al. 2008; Shou, Ye, Fan, and Fu 2014; Shou, Ye, Fan, Fu, et al. 2014; Erickson, Li, and Park 2002). The simulation and modeling revealed that the any deviation in capillary diameter tends to slow the liquid wetting speed (Erickson, Li, and Park 2002). Shou et al. analyzed the liquid absorption in tubes having non-uniform cross-section along their length and showed that the liquid can pass more readily through a reduction of cross-sectional width than an expansion of cross-

sectional width (Shou, Ye, Fan, Fu, et al. 2014). The previous studies on the non-uniform cross-sectional capillaries are limited to the numerical studies in case of capillary tubes. While the previous researches on the absorbency behavior of nonwovens were concentrated on the homogenous mono-layered nonwoven fabrics (Das, Pradhan, and Pourdeyhimi 2012; Chen et al. 2009), many of absorbent articles, in particular diapers and sanitary pads, are highly engineered structures that contains various layers. Obtaining a pore size gradient has been pointed out in some of the patents in order to improve the absorbency behavior of absorbent articles (Potts et al. 2002; Jackson et al. 1997; Scheubel et al. 2000). The purpose of utilizing multiple layers is to improve the fluid movement and facilitate the faster flow. It is necessary to understand the liquid absorption as a function of pore size gradient in order to obtain the best design and optimization of the engineered absorbent articles. Furthermore, the absorbent articles are subjected to varying degrees of compression during their end-use applications. The applied compression carries practical importance due to their impact on the structural deformations.

In the present study, we examined the absorption behavior of nonwoven samples owning heterogeneous layered structures in regards to different compression levels. For this purpose, the heterogeneous structure was produced by layering of nonwoven web layers, the layers of which has an average pore size different from the average pore sizes of other nonwoven web layers.

6.2 MATERIAL AND EXPERIMENTAL

6.2.1 Description of the samples

To study the absorbency behavior in layered structure, four different types of fabric, as shown in table 6.1, were produced. This set of fabrics are made of four different fiber linear densities and contain 80%PET, and 20% binder fibers. For the entire samples, the binder fibers were concentric sheath/

core bicomponent fibers 2 denier* 1.5 inch Co-PET/PET with melting point of 110 °C (Provided by Fiber Innovation Technology). The fabrics were manufactured through carding, cross-lapping, Pre-needle punching and through air bonding processes in the Nonwovens Institute's Staple Pilot Facilities (Raleigh, North Carolina). Through air bonding was done on the temperature of 121°C. Through air bonding and binders were used in order to control solidity and keep it constant among our samples.

Table 6.1: sample details

Group code	Sample #	PET fiber size (denier)	PET fiber cross-section	% Binder	%PET
E	1	3	Round	20	80
	2	6	Round	20	80
	3	9	Round	20	80
	4	15	Round	20	80

The nonwoven fabrics in group E were used to achieve various layered structures. The samples contain 4 different layers in order to achieve a basis weight of about 200 gm⁻². The structures were made according to both pore size expansion and pore size reduction. The experiments were performed on the control samples containing 4 similar layers, 2 layers of 3 denier fiber on bottom and 2 layers of the other fiber sizes on top (in order to reach pore size expansion in flow direction), and 2 layer of 3 denier fiber on top and 2 layers of the other fiber sizes on bottom (in order to reach pore size reduction in flow direction). The layered samples went through the through-air bonding twice after positioning the layers on the specific order. Through air bonding was done on the temperatures of 130 and 141 °C respectively.

6.2.2 Basics web properties

Thickness of samples was measured using an Ames Logic basic thickness gauge model no. BG1110-1-04. The presser foot diameter was 1 inch and the applied pressure was 0.6 psi. The thickness was measured for 15 different places along the fabric.

The basis weights of the samples were calculated for 18 different replicates per each sample according to equation 6.1, in which w is the mass of the sample and A is the sample area. The samples were the round samples with the area of 100cm^2 .

$$\text{Basis weight } \left(\frac{\text{g}}{\text{m}^2} \right) = \frac{w \text{ (g)}}{A} \quad (6.1)$$

Finally the solidity of the samples was calculated according to the equation 6.2.

$$\text{Solidity} = \frac{(w/A/t)}{\rho} \quad (6.2)$$

Where, w : sample mass (g)

A : sample area (cm^2),

t : sample thickness (cm) and

ρ : Fiber mass density ($1.37\text{g}/\text{cm}^3$ for polyester fibers)

6.2.3 Compression testing procedure

A compressional study was carried out on an Instron 4400R, with a load cell of 1000lb and constant rate of compression of $2.5\text{mm}/\text{min}$ within the compression percent range of 0-40% with a pressure foot 8.89 cm diameter. For each sample, this test was carried out for 2 replicates and each replicate

include different numbers of layers of our nonwoven sample. It was tried to keep the thickness of the sample in a specific range. Plate separation was 55 mm for all the samples. The pressure foot was brought down to reach to 40% compression based on the measured initial thickness (T_0) (figure 6.1). The initial thickness, T_0 , was measured under no compression load. The compression percent increases and corresponding compression load are recorded on the Instron. After reaching a compression percent of 40%, i.e. the final compression percent, the compression percent is gradually reduced with the same rate and corresponding compression loads are recorded in the same way during the recovery cycle. At the end, the load-deformation results were used to determine the compressive resistivity, as well as recoverability.



Figure 6.1: the schematic of the compression procedure on Instron

6.2.4 Experimental technique for absorption testing under compression

The Gravimetric Absorbency Testing System (GATS) is the system that widely used in many industries (Chatterjee and Gupta 2002). In a typical setup of this system, the liquid is delivered to the sample by the capillary pressure of the sample's porous structure, the amount of liquid absorbed by the sample is recorded against time, and then the data is graphed based on the weight of absorbed liquid versus time. The graph is then used to measure the maximum capacity of absorption and the rate of absorption. In order to remove the effect of sample's weight, the maximum absorption and absorbency rate is reported per each gram of fabric. The height of the test plate and the height of

liquid in the reservoir kept at the same level in order to provide zero hydrostatic pressure. This provides the situation in which the liquid is taken up solely on demand by material. A compression foot, having a diameter of slightly larger than samples, was added to the set-up, while a linear actuator controlled it. Then the samples were compressed to 10,20,30,40 % of their initial thickness and absorbency of compressed samples was measured. The samples are placed on a metal mesh where the whole area of the samples was in contact with the liquid. Figure 6.2 shows the schematic of the modified GATS. Modified GATS is capable of measuring maximum capacity of absorption, as well as the rate of absorption under varied static compression level and in the through-plane direction.

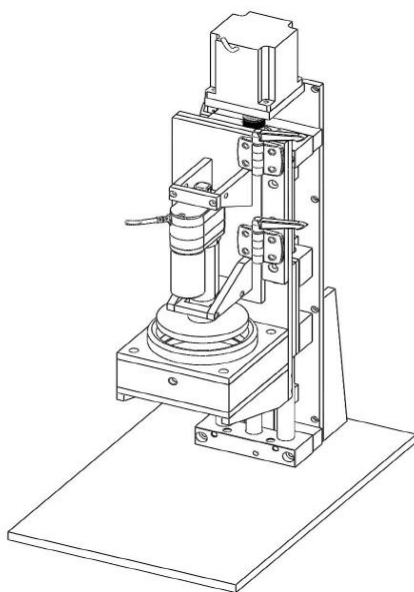


Figure 6.2: the modified NWI GATS (Compression GATS)

Figure 6.3 shows a typical testing result on modified GATS. The information obtained from the GATS results includes maximum absorbency and absorbency rate as shown in the figure 6.3. The absorbency is the ratio of the weight of liquid absorbed by the samples to the dry weight of the nonwoven materials. The curve consists of fast initial liquid uptake followed by plateaus, which

indicate it reach maximum absorption capacity of samples. The slope of the liquid rise in the beginning of the test determines the absorbency rate.

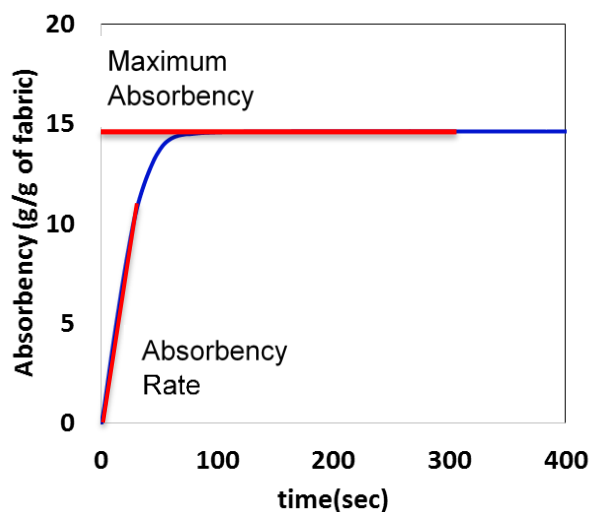


Figure 6.3: typical GATS curve

6.2.5 Theoretical determination of maximum absorption capacity of nonwovens

Assuming all the pores are filled with the liquid, so the whole amount of interstitial space inside the nonwoven fabrics is a key factor, which determines the maximum absorption capacity. Thus maximum absorption capacity of the samples with this assumption that all the pores are filled with water was calculated according to below relationship between solidity and the maximum absorbency. The solidity of the samples at that specific amount of compression load was obtained based on the dimensions of the samples after compression. The relation between the maximum absorbency, C_{max} can be calculated theoretically as shown in equation 6.3.

$$C_{\max} = \left(\frac{1}{S} - 1\right) \cdot \frac{1}{\rho_{\text{fiber}}} \quad (6.3)$$

Where s is the solid volume fraction, and

$$\rho_{\text{fiber}} = \rho_{\text{PET}} = 1.37 \text{ g/cm}^3$$

6.3 RESULTS AND DISCUSSION

6.3.1 Thickness and solid volume fraction

The thickness and solid volume fraction of the samples are listed in table 6.2. Generally speaking, the basis weight of the samples is consistent in a reasonable range and about 50 g/m^2 in each layers.

However it was observed that the samples containing 3 denier and 6 denier fiber size appeared to have somehow lower thickness and higher solidity values. But the small variations are inevitable and hard to control. In this study, it was attempted to consider the influence of these small variations by discussing the results according to the solidity of the samples.

Table 6.2: structural characteristics of separate layers

Group code	Sample #	Basis weight (g/m^2)	Thickness (mm)	Initial Solidity
E	1	51	1.48	0.0250
	2	51	1.48	0.0250
	3	58	1.86	0.0229
	4	57	1.99	0.0211

6.3.2 Compression properties

In this section, the compression properties of the layered structures are discussed. The typical compression-recovery curves were shown in figure 6.4 for the heterogeneous layered structures and the control layered structures of constituent fibers. It is obvious that for the various heterogeneous layered structures, the compression-recovery curves of these structures places in between of the control layered structures of constituent fibers. While the larger fiber sizes displayed the higher resistance to compression compared to the smaller fiber sizes, the heterogeneous layered structures illustrated a resistance to compression, which is in between of those observed in larger fiber sizes and smaller fiber sizes. This trend was observed in the entire heterogeneous layered structures.

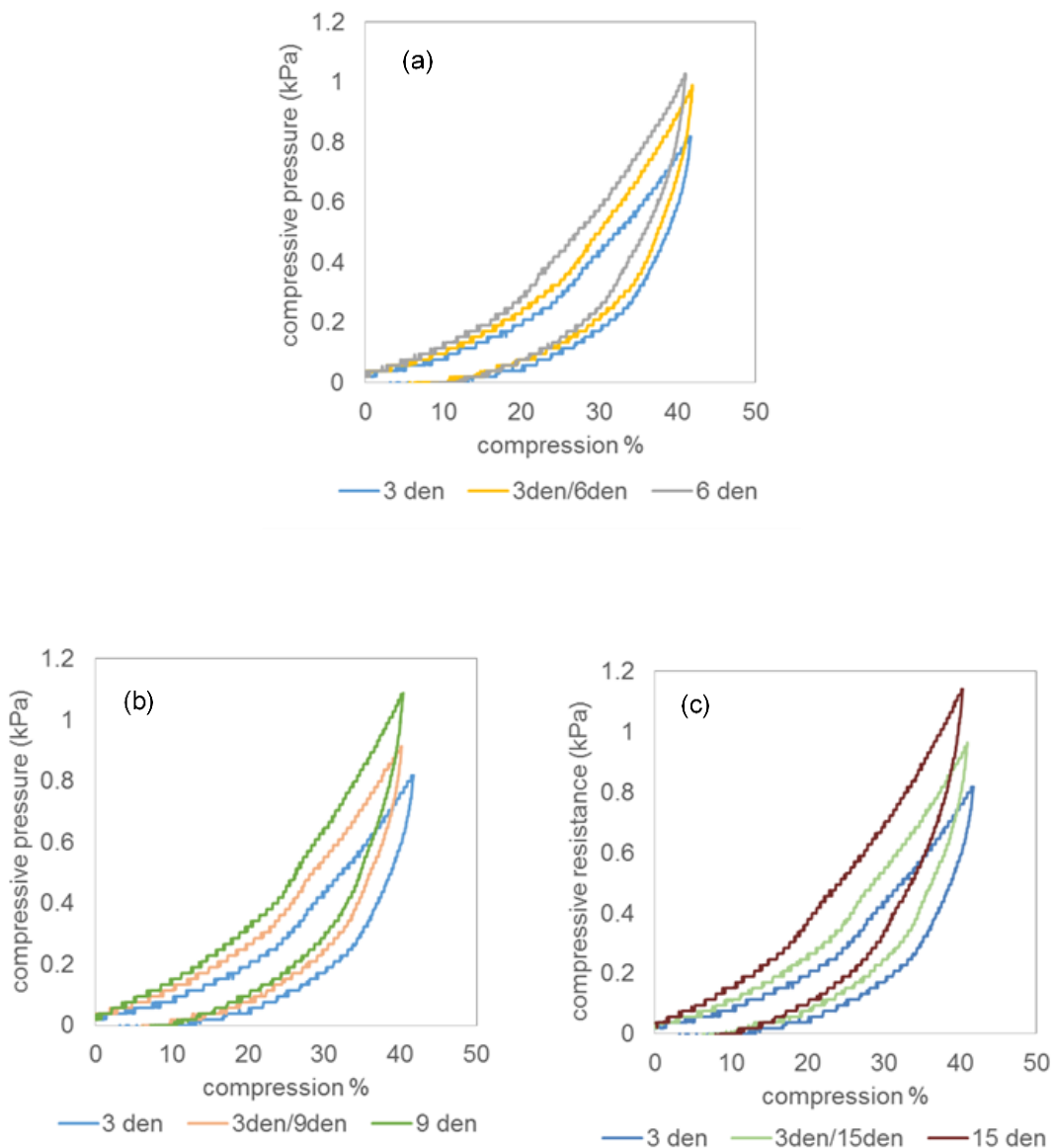


Figure 6.4: typical curves of compression pressure vs. compression percentages during loading and unloading (a) 3den, 3den/6den, 6den (b) 3den, 3den/9den, 9den (c) 3den, 3den/15den, 15den

The resistance to compression was quantified in two ways, first the resistance to compression was found at 40% compression according to compression curves, also the slope α was calculated according to van Wyk theory (for the sake of brevity, the equation is not given here, the reader could

refer to chapter 3 of this dissertation for the details). The results were shown in figure 6.5. It can be seen that on the whole, heterogeneous layered structures displays a resistance to compression and slope α , which is in the middle range of those related to their constituent fibers structures.

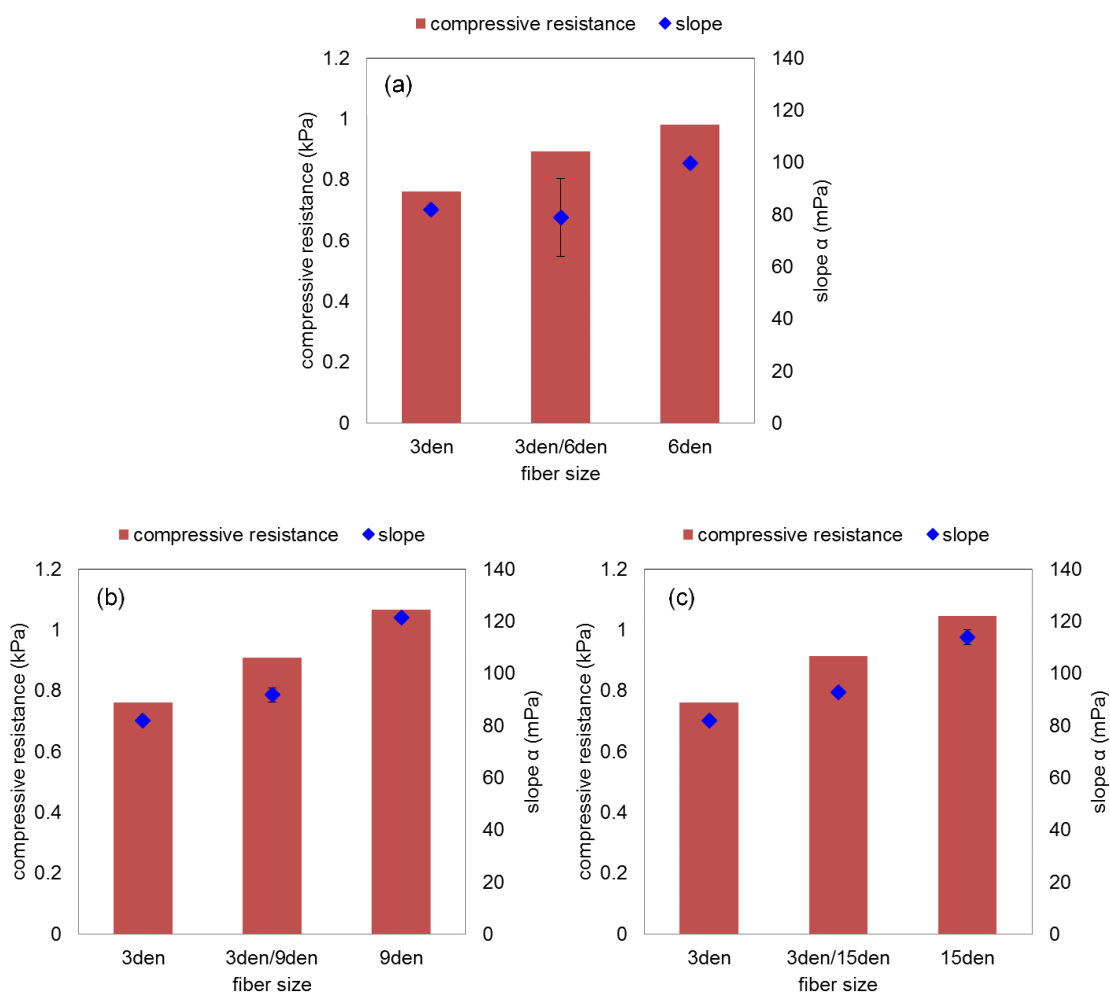


Figure 6.5: compressive resistance at 40% compression and slope alpha according to van Wyk equation for (a) 3den, 3den/6den, 6den (b) 3den, 3den/9den, 9den (c) 3den, 3den/15den, 15 den

The thickness recoverability was measured for the control samples, as well as heterogeneous structures. The results were shown in figure 6.6. As anticipated, the control samples containing larger fiber sizes gave rise to larger recoverability percentages. The effect of fiber size on the recoverability was discussed in chapter 3 of this dissertation. On the whole, the recoverability has been improved in the heterogeneous layered structures compared to the recoverability of control samples containing smaller fiber sizes. The recoverability of the heterogeneous layered structure was observed to be in the range of recoverability of the control samples containing larger fiber sizes.

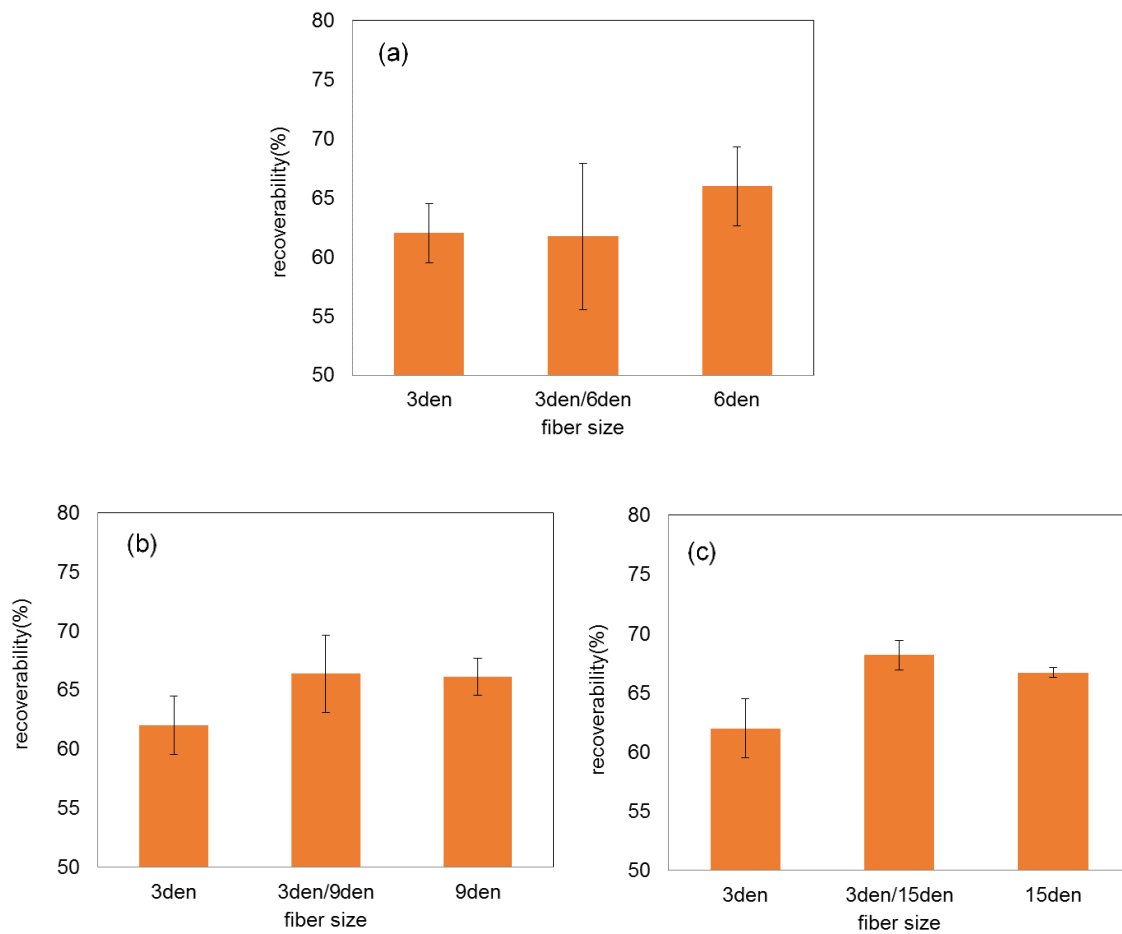


Figure 6.6: thickness recoverability for homogenous and heterogeneous layered nonwoven samples (a) 3den, 3den/den, 6den (b) 3den, 3den/9den, 9den (c) 3den, 3den/15den, 15den

6.3.3 Absorption properties

In this section, we evaluate the influence of heterogeneous structures on absorption properties of the nonwoven samples. As it was discussed both the pore size expansion and reduction was achieved by layering of nonwoven fabrics containing various fiber sizes of 3, 6, 9, and 15 denier. The solidity was kept unchanged for the various layers in a reasonable range. The control samples were obtained in homogeneous layered structures of similar nonwoven fabrics. The typical GATS curves at various compression levels are illustrated in figure 6.7 for control samples. As it can be seen from the figure, both the absorption capacity and absorbency rate is affected by the compression in control samples. The effect of compression is more significant in case of layered structures containing larger fiber sizes, this is due to their initial larger pore sizes, which brings about higher structural modifications under compression. The absorbency showed a maximum with the compression in the entire control samples. This was in line with the results obtained for homogenous non-layered structures. The maximum absorbency was achieved at higher compression levels at larger fiber sizes. On the whole, the absorbency rate showed an increasing trend with compression.

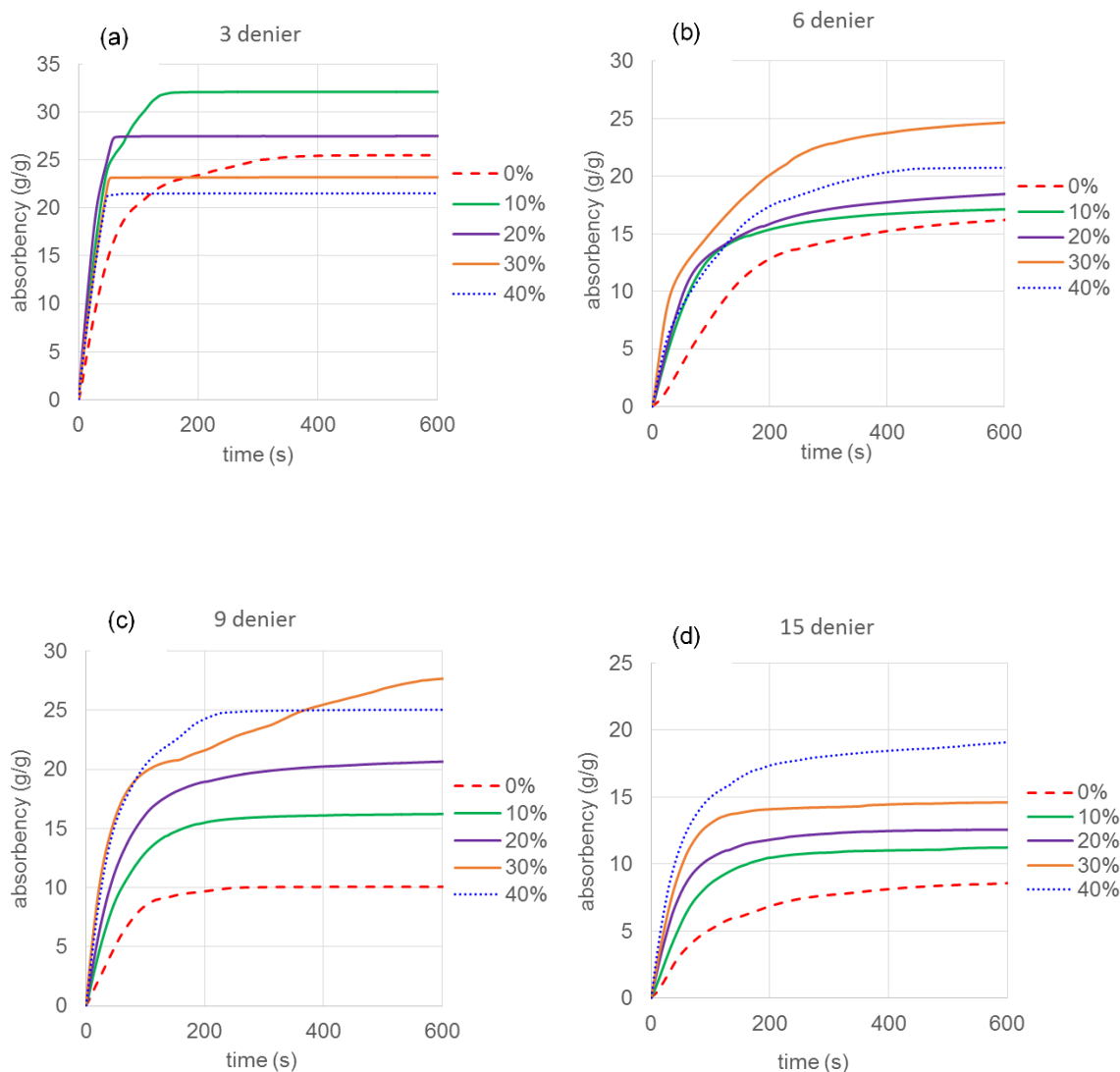


Figure 6.7: typical GATS curve for homogeneous layered structures (a) 3den (b) 6den (c) 9den (d) 15 den

Figures 6.8 and 6.9 give the typical GATS curve for pore size expansion and pore size reduction respectively. It was found that the absorbency behavior is less affected by the compression in the samples containing pore size expansion, on the contrary to samples of pore size reduction. When the structures with pore size reduction is subjected to various degrees of compression, they provide a wide range of maximum absorption and time to reach to that maximum. This observation may benefit

the design of absorbent products. In the following section, we are going to discuss the maximum absorption and absorbency rate considering the effect of pore size heterogeneity and compression.

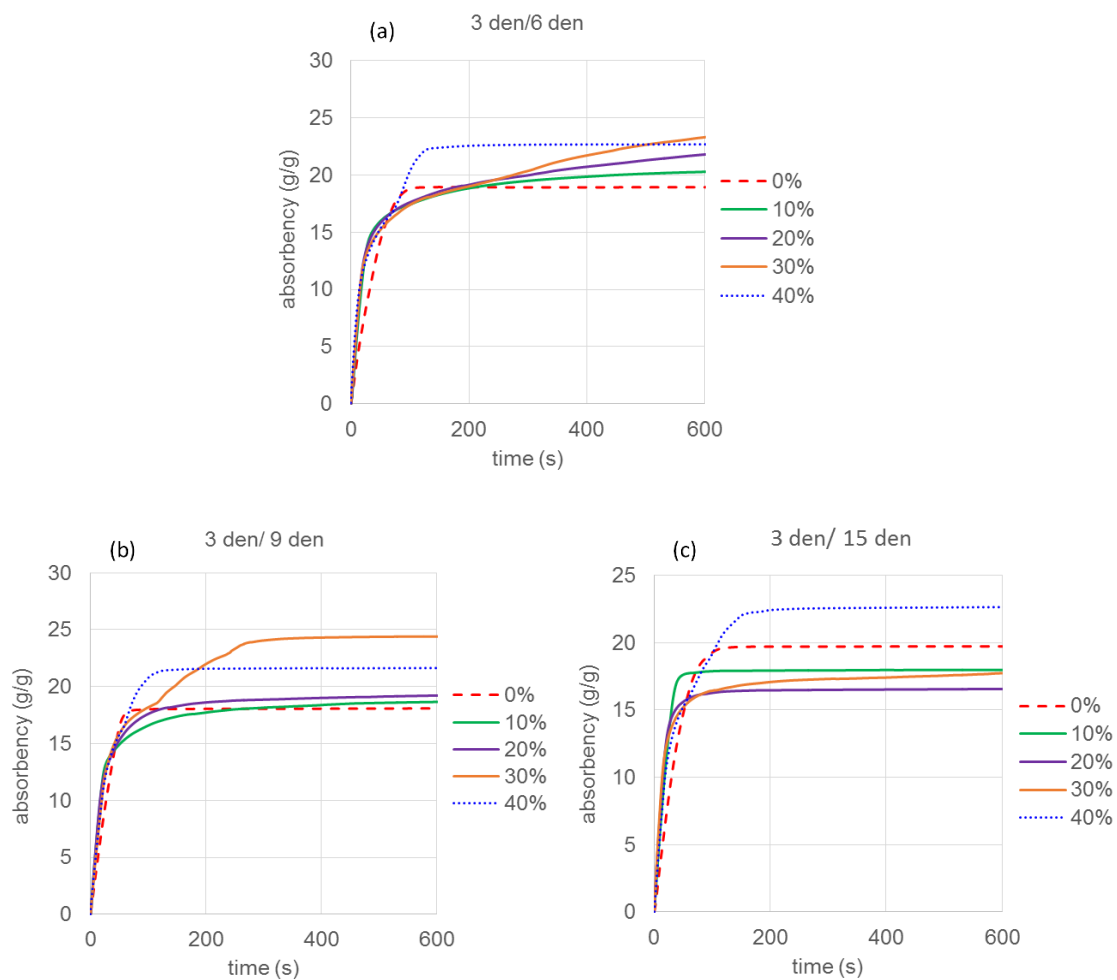


Figure 6.8: typical GATS curve for the nonwoven structures having a pore size expansion (a) 3den/6den (b) 3den/9den (c) 3den/15den

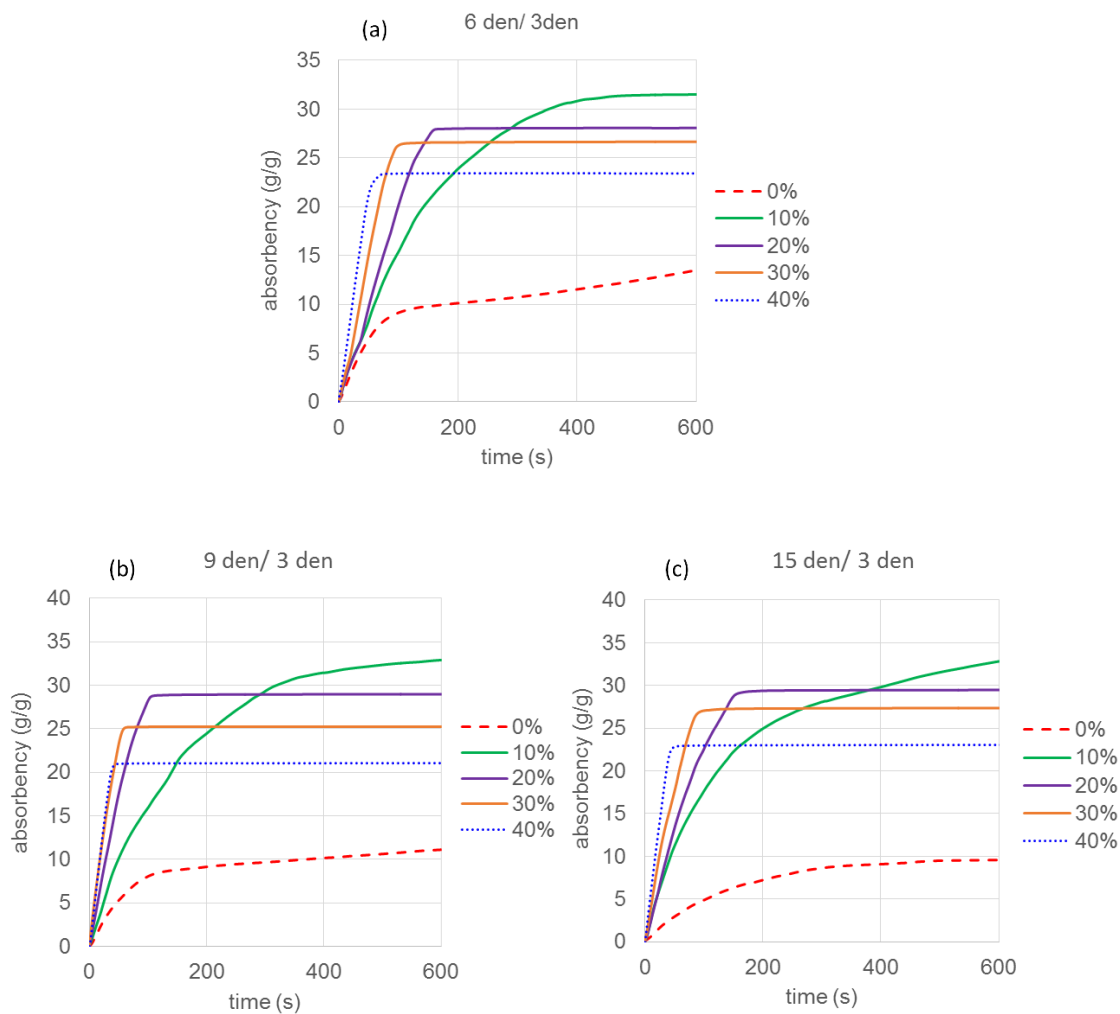


Figure 6.9: typical GATS curve for the nonwoven structures having a pore size reduction (a) 6den/3den (b) 9den/3den (c) 15den/3den

6.3.3.1 Maximum absorption

It was confirmed that the maximum absorption amount obtained through GATS is highly governed by the solidity of the samples, which means the maximum absorption is changed significantly with slight changes in the solidities. Therefore in this section, the absorbency is discussed in term of solidity of the samples. The various solidity values were obtained by compressing the structures to different levels. Figure 6.10 presented the absorbency amount in the control layered structure. As detailed in the figure, the maximum absorption initially increased, showed a maximum and decreased with the solidity in the control samples. The maximum absorption capacity was also calculated theoretically according to equation 6.3. The smooth line in the figure shows the theoretical maximum absorption. It is evident that a fraction of the available pores are not filled with the liquid. This observation was happened due to insufficient capillary pressure; therefore it cannot overcome the gravitational forces through the entire sample thickness. The lack of capillary pressure has a more remarkable effect on the layered structures because the capillaries are not oriented through the entire sample thickness. The capillary pressure is the driving force of the liquid absorption and gravitational forces act against capillary pressure and hinder the absorption. The capillary pressure is defined based on Laplace equation and it depends on the pore size for a specific fiber and a given liquid. According to Laplace equation, the capillary pressure is lower at larger pore sizes (the reader refers to chapter 2 for further information). This means the gravitational forces have a more significant influence on hindrance of the liquid wicking. On the other hand, the greater solidity values gave rise to smaller pore sizes due to the compression. Therefore, it provides higher capillary pressure and consequently the liquid may wick to a larger fraction of the available pore volume and despite the decrease in the available pore volume, the experimental maximum absorption is increased initially. The results confirmed at a specific solidity values, the samples are fully saturated. After that specific solidity values, there is a

perfect agreement between the experimental and theoretical maximum absorption, where further increase in solidity value is accompanied with the maximum absorption reduction.

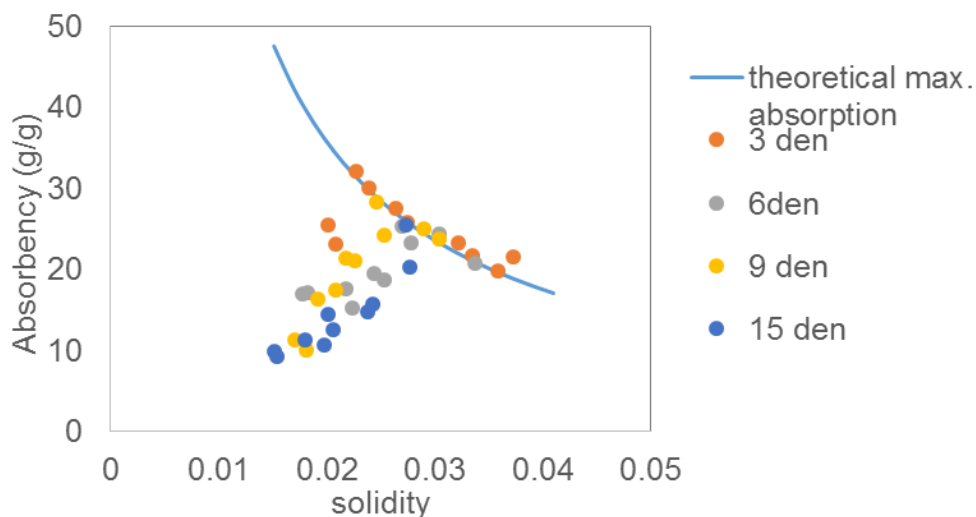


Figure 6.10: absorbency vs. solidity for homogenous layered nonwovens (control samples)

The absorbency amount was also measured in the samples having a pore size reduction in which the larger fiber sizes are in contact with the liquid. In these structures, the liquid is penetrated from the larger fiber sizes to smaller fiber sizes. Figure 6.11 displays the results for 3 various negative pore size gradients. The overall response was that the experimental absorbency amount is in good agreement with the theoretical maximum absorption. It could be concluded that the structure with pore size reduction achieves the maximum absorption capacity. It implies that the liquid may transfer from the larger pore sizes to the smaller one. The discrepancy was observed in case of lowest solidity values where the absorption happens under no compression.

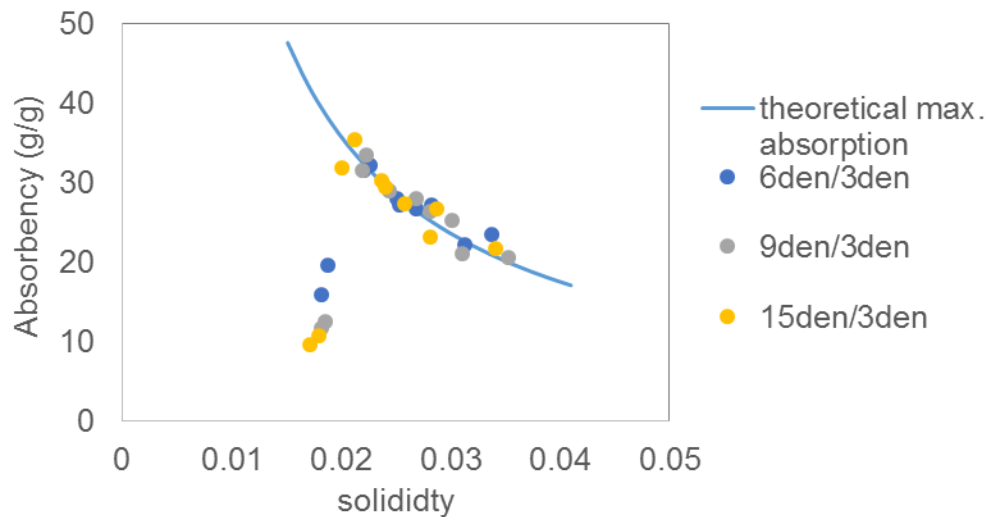


Figure 6.11: absorbency vs. solidity for heterogeneous layered structures having pore size reduction

Figure 6.12 Corresponds to absorbency amount in samples having a pore size expansion in which the smaller fiber sizes are in contact with the liquid. The liquid is transported from the smaller fiber sizes to larger fiber sizes. It is apparent that these samples cannot reach to their maximum absorption, which means a fraction of the available pores may not be filled with the liquid. It indicates that the liquid was not transported through the thickness of the sample or it is blocked in the bottom layered with smaller pore size. This is attributed to the higher capillary pressure in the bottom layers with smaller pore size. Then the capillary pressure in the top layers with larger pore size is not sufficient to wick the liquid. The pore sizes becomes smaller in the entire layers by the compression, however it should be noted that the smaller fiber sizes are compressed to a higher level than the larger fiber sizes due to their lower resistance to compression. It means the absorbency amount may not be improved significantly even under compression. This is in contrary to what it was observed in case of control samples with larger fiber sizes and lower capillary pressure. This is because the capillary pressure is

always higher in the bottom layers with smaller pore sizes, and therefore the liquid is blocked in the bottom layers.

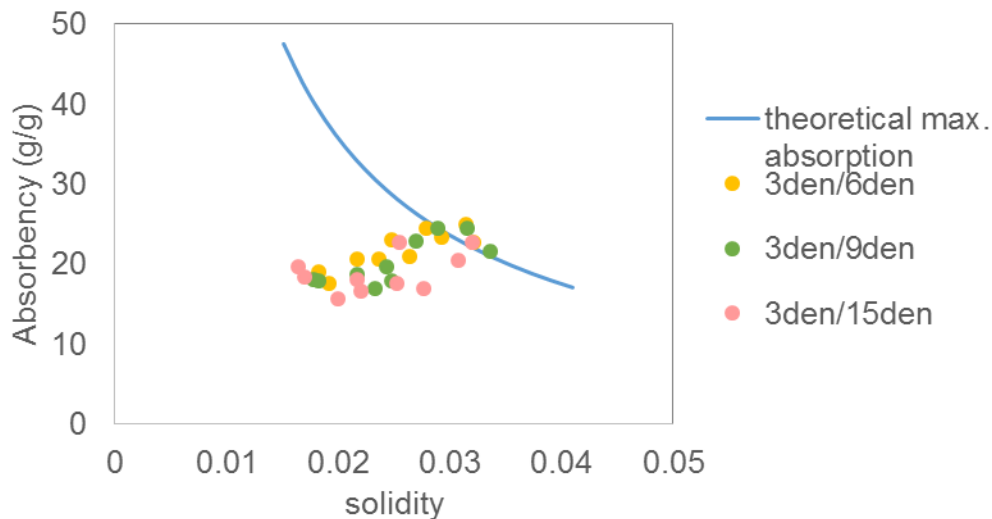


Figure 6.12: absorbency vs. solidity for heterogeneous layered structures having pore size expansion

6.3.3.2 Absorbency rate

Figure 6.13 shows the absorbency rate at different compression levels in the layered structures having similar pore size through the thickness of the samples (control samples) for different fiber sizes. As expected, the absorbency rate is lower at higher the fiber size. This is due to the fact that larger pore sizes have lower capillary pressure and therefore capillary pressure cannot overcome the gravity force and this decelerates the rate of liquid penetration. On the whole, the absorbency rate shows an increasing trend with compression. In case of 3 denier fibers, the absorbency rate initially increases and then decreases with the compression. The effect of fiber size and consequently pore sizes were discussed in chapter 4 of this dissertation.

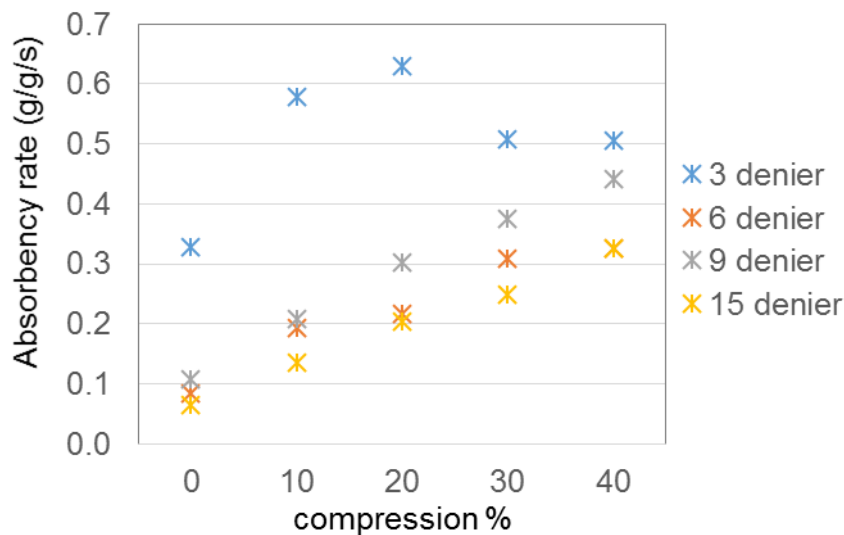


Figure 6.13: absorbency rate at different compression levels for homogeneous layered structures (control samples)

In this section, the effect of pore size heterogeneity on the absorbency rate is discussed. Figure 6.14 demonstrates the rate of absorption at different compression levels in layered structure with various pore size expansions in which the smaller fiber sizes, 3 denier fibers, are in contact with the liquid. The absorbency rate is also shown for the control samples containing 3 denier fibers. The results show that the absorbency rate for the control sample and various pore size expansions are in a similar range at different compression levels. Therefore it could be inferred that the initial liquid uptake rate is mainly governed with the layer that is in contact with the liquid.

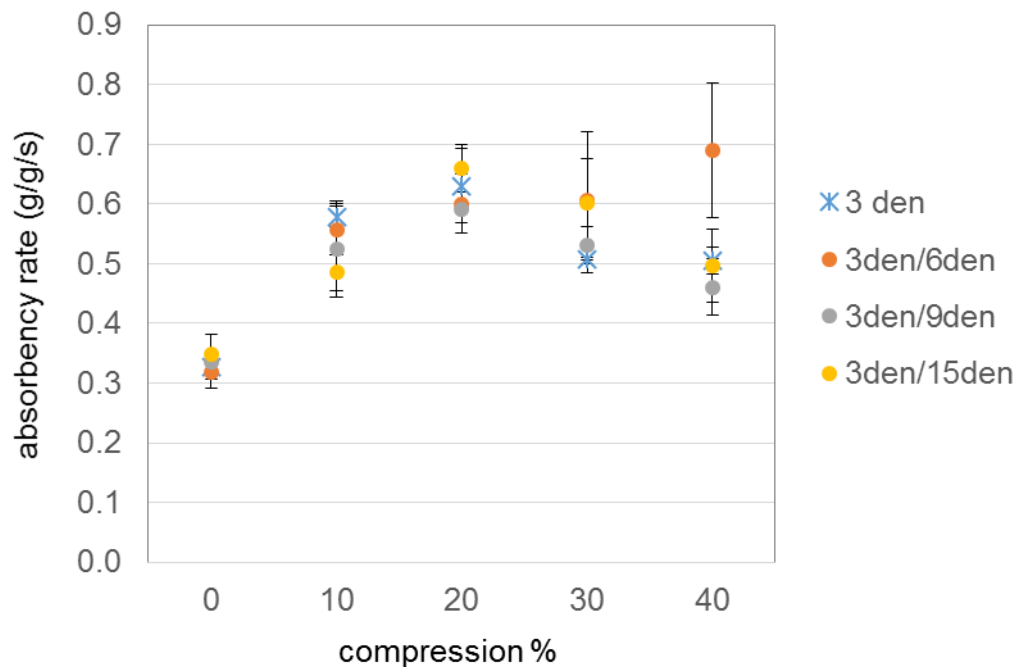


Figure 6.14: absorbency rate at different compression levels for heterogeneous layered structure having pore size expansion (the results for the control samples of 3 denier fibers is given)

The absorbency rate was plotted for the various samples of pore size reduction in figure 6.15. The larger fiber sizes are in contact with the liquid in these samples. The absorbency rate also was shown for the control samples containing the larger fiber sizes. As it can be seen, the absorbency rate of these structures is primarily dictated by the larger fiber sizes, which are in contact with the liquid. However it is also observed that having the smaller fiber sizes on top of the larger fiber sizes may slightly improve the initial rate of absorption especially in case of larger pore size reduction and at higher compression levels.

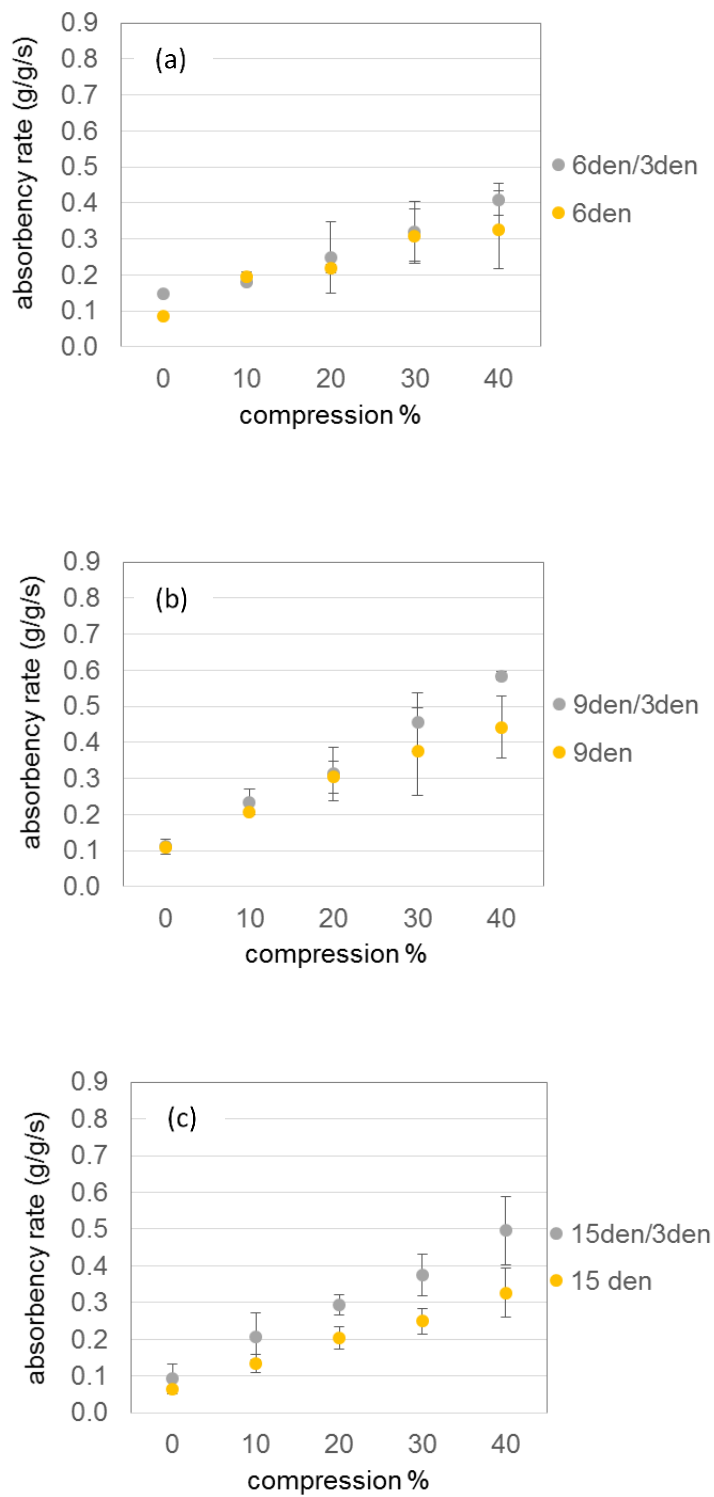


Figure 6.15: absorbency rate for structures having pore size reduction at different compression levels (a) 6den/3den, 6den (b) 9den/3den, 3den (c) 15den/3den, 3den

6.4 CONCLUSION

In this work, we analyzed the compression and absorption behavior of heterogeneous nonwoven having a layered structure. These structures were achieved by positioning of the layers of various fiber sizes. The asymmetric liquid transport is examined in both the pore size expansion and reduction structures. The absorbency behavior of heterogeneous nonwoven structures was compared to that of a uniform medium of constituting fibers, which is employed as control samples.

The compression resistivity of the heterogeneous layered structures was found to be in the middle of the range of those for the control samples of the constituent fibers. Although the recoverability was observed to be improved towards that of the control samples of the larger fiber sizes. It was found that although the maximum absorption is mainly governed by the solidity in heterogeneous nonwoven fabrics having a pore size reduction, it is different in the layered structures having a pore size expansion. Liquid is blocked in the section with the smaller pore sizes and higher capillary pressure, therefore the liquid cannot be transported from the bottom layers to the top layers in the structures having a pore size expansion. It was not achievable to reach to the theoretical maximum absorption in pore size expanded structures except at very high compression percentages. The initial liquid uptake rate is mainly governed by the pore size of the layer, which is in contact with the liquid. Although it was seen that the absorbency rate slightly improve in pore size reduced structures by positioning of the smaller pore sizes on top of larger pore sizes, especially at larger pore size differences and higher compression percentages. This study provides an initial exploration of asymmetric nonwoven structure, and insights gained from this work offers some solutions to more complex layered structures in order to have better absorbent product designs.

REFERENCES

- Ashari, A., and H. Vahedi Tafreshi. 2009a. "A Two-Scale Modeling of Motion-Induced Fluid Release from Thin Fibrous Porous Media." *Chemical Engineering Science* 64 (9): 2067–75.
doi:10.1016/j.ces.2009.01.048.
- Ashari, A., and H. Vahedi Tafreshi. 2009b. "General Capillary Pressure and Relative Permeability Expressions for through-Plane Fluid Transport in Thin Fibrous Sheets." *Colloids and Surfaces A: Physicochemical and Engineering Aspects* 346 (1-3): 114–22.
doi:10.1016/j.colsurfa.2009.06.001.
- Chatterjee, P. K., and B. S Gupta. 2002. *Absorbent Technology*. Amsterdam; Oxford: Elsevier Science. <http://www.sciencedirect.com/science/book/9780444500007>.
- Chen, X., P. Vroman, M. Lewandowski, A. Perwuelz, and Y. Zhang. 2009. "Study of the Influence of Fiber Diameter and Fiber Blending on Liquid Absorption Inside Nonwoven Structures." *Textile Research Journal* 79 (15): 1364–70. doi:10.1177/0040517508099386.
- Cueto, N., D. Benavente, J. Martínez-Martínez, and M.A. García-del-Cura. 2009. "Rock Fabric, Pore Geometry and Mineralogy Effects on Water Transport in Fractured Dolostones." *Engineering Geology* 107 (1-2): 1–15. doi:10.1016/j.enggeo.2009.03.009.
- Das, Dipayan, Arun Kumar Pradhan, and Behnam Pourdeyhimi. 2012. "Dependence of the Liquid Absorption Behavior of Nonwovens on Their Material and Structural Characteristics: Modeling and Experiments." *Journal of Applied Polymer Science* 126 (3): 1053–60.
doi:10.1002/app.36635.
- Erickson, D., D. Li, and C.B. Park. 2002. "Numerical Simulations of Capillary-Driven Flows in Nonuniform Cross-Sectional Capillaries." *Journal of Colloid and Interface Science* 250 (2): 422–30. doi:10.1006/jcis.2002.8361.

- Hardy, Philip. 2009. "Baby Diaper Absorbent Cores." *Nonwovens Industry* 40 (4): 56–63.
- Jackson, Wanda Walton, Monica Signoret Diaz, Cheryl Anne Perkins, Dawn Marie Huffman, Wendy Louise Bush, Cheryl Ann Mocadlo, and Richard John Birtwell. 1997. "Apertured Film/nonwoven Composite for Personal Care Absorbent Articles and the like." US patent 5643240A
- Potts, David, Jack Lindon, Emmanuelle Damay, Dmitry Yavich, and Matthew Young. 2002. "Absorbent Article with Fluid Treatment Agent." US patent 20020065495 A1
- Reyssat, Mathilde, Laurent Courbin, Etienne Reyssat, and Howard A. Stone. 2008. "Imbibition in Geometries with Axial Variations." *Journal of Fluid Mechanics* 615 (November): 335. doi:10.1017/S0022112008003996.
- Scheubel, Gerard, Xiaolan Shen, Ervin Dan, and Ian Cheyne. 2000. "Three Dimensional Needled Non-Woven Absorbent Composites." CA patent 2268344 A1
- Shou, Dahua, Lin Ye, Jintu Fan, and Kunkun Fu. 2014. "Optimal Design of Porous Structures for the Fastest Liquid Absorption." *Langmuir* 30 (1): 149–55. doi:10.1021/la4034063.
- Shou, Dahua, Lin Ye, Jintu Fan, Kunkun Fu, Maofei Mei, Hongjian Wang, and Qing Chen. 2014. "Geometry-Induced Asymmetric Capillary Flow." *Langmuir* 30 (19): 5448–54. doi:10.1021/la500479e.
- Tracy, J., K. Ghali, and B. Jones. 1994. "Experimental Techniques for Measuring Parameters Describing Wetting and Wicking in Fabrics." *Textile Research Journal* 64 (2): 106–11. doi:10.1177/004051759406400206.
- Young, Wen-Bin. 2004. "Analysis of Capillary Flows in Non-Uniform Cross-Sectional Capillaries." *Colloids and Surfaces A: Physicochemical and Engineering Aspects* 234 (1-3): 123–28. doi:10.1016/j.colsurfa.2003.12.007.

Yun, Tae Sup, Guillermo A. Narsilio, Olivier Buzzi, Stephen Fityus, and David W. Smith. 2009.

“Upscaling of Navier–Stokes Equations in Porous Media: Theoretical, Numerical and Experimental Approach.” *Computers and Geotechnics* 36 (7): 1200–1206.

doi:10.1016/j.compgeo.2009.05.006.

7 INVESTIGATION OF EFFECT OF FIBER ABSORBENCY ON ABSORPTION AND RELEASE PROPERTIES OF NONWOVENS UNDER COMPRESSION

7.1 INTRODUCTION

A major current focus in design of engineered absorbent nonwoven fabrics is how to ensure their suitable functionality in fluid handling depending on their final applications. For this purpose, mixture of absorbent and non-absorbent has been extensively practiced in potential applications (Anjur, Shah, and Wisneski 1997; Welchel, Kepner, and Leach 2000; Shipley 1997; Chen and Dilnik 1997). For examples Shipley claimed that addition of a layer of non-absorbent fiber to absorbent fiber core improves the water retention of the absorbent articles by impeding the pooling of the liquid in absorbent fibers (Shipley 1997). The liquid transport and retention in nonwoven fabrics is a complex and intricate phenomena, in which the fiber properties plays a significant role. The factors which influence on the absorption properties of fibers include their intrinsic surface energy and wettability (Hsieh, Miller, and Thompson 1996; Hsieh, Thompson, and Miller 1996; Gupta and Hong 1994), as well as diffusion of the liquid into the fibers (Kawase et al. 1986; Topgaard and Söderman 2001). Although the empirical published studies are limited to the products and specific experimental conditions (Ashari, Bucher, and Vahedi Tafreshi 2010), without comprehending the impact of various dominant parameters (Nederveen 1994; Gupta and Hong 1994), therefore their results are not applicable to the product development in general.

Surface energy and wettability of the textile fibers has been extensively studied for many years (Patnaik et al. 2006; Pan and Zhong 2006). Kealble studied the wettability of the fibers in terms of their dispersion-polar interactions across the liquid-solid interface by introducing an indirect method to estimate the dispersion and polar parts of the surface energy of the fibers. They confirmed the

importance of these parameters in the wettability behavior of fibers (Kaelble 1970; Kaelble and Uy 1970). Whang & Gupta analyzed the surface wetting characteristics of various fibers through Wilhelmy technique considering the contribution of dispersion and polar parts of surface energy (Gupta and Whang 1999; Whang and Gupta 2000). Hsieh also examined the importance of wetting and capillary theories to analyze the liquid transport in 100% cotton and polyester woven fabrics. By considering the contribution of fiber surface properties and pore structure and geometry, he pointed out that decoupling the contribution of these parameter is critical in design and evaluation of fibrous materials for application in absorbent articles (Hsieh 1995a).

The liquid diffusion into the fibers depends strongly on their chemical structure and morphology, including the extent of fiber crystallinity and porosity. The liquid diffusion depends on the ability of chemical groups on the fiber to make hydrogen bond with the water molecule. Li, et al. investigated the water diffusion into cellulose fibers through different techniques in regard the molecular structure of these fibers ((Li, Häggkvist, and Ödberg 1997; Li et al. 1992). They found that the diffusional motion of water in pores is anisotropic. This indicated that the pores are oriented along the fiber axis having length ranging from a few micrometers up to 20 micrometer (Li et al. 1992). Topgaard and Soderman evaluated the diffusion of water absorbed in cellulose fiber through H-NMR technique in order understand the water-cellulose interaction. They showed that the diffusion rate is very sensitive to the moisture content and more water leads to faster diffusion (Topgaard and Söderman 2001). The absorption process is kinetically quite different when capillary penetration is accompanied by diffusion of the liquid into the fibers or into a finish on the fibers (Patnaik et al. 2006). Kawase et al., studied the capillary spreading when liquid is diffused into cotton fibers. They found that liquid diffusion into the fibers greatly influence on the liquid drop spreading rate, and on the whole it reduces the spreading rate in case of cotton and rayon fibers (Kawase et al. 1986).

Swelling is a consequence of liquid diffusion into the fiber. In the swelling fibers, the fluid not only is able to fill the pores created between the fibers which are in micrometer-sized ranges, but also can enter the nano-sized pores inside the fibers (Chatterjee and Gupta 2002). Swelling of textile fibers has been the focus of many researches from several decades ago by employing various techniques (Schiefer and Kropf 1946; Morehead 1947; Preston, Nimkar, and Gundavda 1951; Morehead 1952; Schuchardt and Berg 1991; Wiryana and Berg 1991). It is generally accepted that the cross-sectional swelling is more than the longitudinal swelling in most of fibers (Morton, Hearle, and Textile Institute (Manchester 2008). Preston, et al., examined the centrifugal technique in order to measure the weight swelling of the fibers, and showed that this technique is influenced by both the imbibed and the capillary water retained by the fibers, which is why even when the fiber is impermeable to liquid, for example glass fiber, considerable amount of the liquid were retained in the capillary spaces even after centrifuging at 1000 G (Preston, Nimkar, and Gundavda 1951). Schiefer and Kropf displayed that as the rayon fiber density increases the swelling decreases, also repeated drying of staple rayon caused the smaller swelling effect (Schiefer and Kropf 1946).

Apart from that swelling changes the structural characteristics of the nonwoven fabrics, and therefore the parameters such as porosity and pore size, which are governing factor of absorbency, is changing in the course of swelling and are function of time. In other word, the liquid sorption into the fibers decreases the volume of the liquid flowing in the capillary spaces, and reduces the available pore volume between the fibers for capillary penetration. Consequently the capillary pressure depends on both time and space (Schuchardt and Berg 1991). Therefore the absorbency behavior has been shown to be different in the nonwoven containing swelling fibers. Some analytical and modeling studies in recent years has focused on absorption properties of fibrous materials containing swelling fibers. Much of the studies used the vertical wicking technique in order to study the swelling properties

(Masoodi and Pillai 2010; Benltoufa, Fayala, and Nasrallah 2012; Masoodi and Pillai 2012; Mullins and Braddock 2012). In the Wilhelmy technique, which is based on vertical wicking experiment, a tensiometer detects the surface energy forces that is related to the perimeter of the fibers, therefore, the swelling may evaluated by recoding the force since the swelling may alters the perimeter. This technique is a reliable technique in case of circular fiber cross-sections. In another study, Ashari, et al. simulated the fluid absorption and release properties in composite multi-layered fibrous fabrics made of swelling and non-swelling fibers through a semi-analytical techniques in which they employed the vertical height rise experiments in order to experimentally reflect the swelling effect on their simulation (Ashari, Bucher, and Vahedi Tafreshi 2010). However, the relation between the wicking rate, wicking time, and liquid characteristics has been thoroughly described in the previous works, the relation between the wicking rate and the structural characteristics is very challenging and needs clarification. It becomes more complicated in case of fibrous structure containing swelling fibers since the swelling alter the structural configuration. One approach to establish this relation is to analyze the wicking rate in the samples containing various percentages of rayon fibers.

While much qualitative study has been successfully practiced in absorbent articles production, a considerate and systematic approach is demanded for the in-depth understanding of the relationship among material properties, fiber swelling, and liquid transport behavior in nonwovens fabrics containing absorbent fibers. Furthermore, since many absorbent articles are subjected to various degrees of loading, it is necessary to comprehend the absorption and release properties of nonwovens under compression. In the first phase of this research, we studied the effect of pore characteristics on the fluid absorption and release properties of the nonwovens by employing the impermeable fiber incapable of absorbing and/or storing the fluid in their internal structure (non-swelling) and in the following, we are going to discuss the effect of materials properties and compression percentages

considering the swelling effect by producing the samples containing various degrees of swelling and non-swelling fibers.

7.2 MATERIAL AND EXPERIMENTAL

7.2.1 Description of the samples

In this study, 5 different types of fabrics as shown in table 7.1 were produced in order to study the effect of fiber absorbency. The binder percentages, PET and rayon fiber size and fiber cross-sectional shape is the same in this group fabric.

For the entire samples, the binder fibers were concentric sheath/core bicomponent fibers 2 denier* 1.5 inch Co-PET/PET with melting point of 110 °C (Provided by Fiber Innovation Technology). All the fabrics were manufactured through carding, cross-lapping, pre-needle punching and through air bonding processes in the Nonwovens Institute's Staple Pilot Facilities. Through air bonding was done on the temperature of 121°C and air circulation speed was 1000 RPM. Through air bonding and binders were used in order to achieve the highest possible control over the sample's solidity and keep it constant as much as it was possible.

Table 7.1: samples characteristics

Group code	Rayon fiber size (denier)	PET fiber size (denier)	Rayon fiber cross-section	PET fiber cross-section	% Rayon	% PET	% Binder
80R	3	3	trilobal	Round	80	0	20
64R	3	3	trilobal	Round	64	16	20
40R	3	3	trilobal	Round	40	40	20
16R	3	3	trilobal	Round	16	64	20
0R	3	3	trilobal	Round	0	80	20

7.2.2 Basic web properties

Web thickness of samples was measured using an Ames Logic basic thickness gauge model no. BG1110-1-04. The presser foot diameter was 1 inch and the applied pressure was 0.6 psi. The thickness was measured for 15 different places along the fabric.

The basis weights of the samples were calculated for 18 different replicates per each sample according to equation 7.1, in which w is the mass of the sample and A is the sample area. The samples were the round samples with the cross-sectional area of 100cm².

$$\text{Basis weight } \left(\frac{\text{g}}{\text{m}^2} \right) = \frac{w(\text{g})}{A} \quad (7.1)$$

Finally the solidity of the samples was calculated according to the equation 7.2.

$$\text{Solidity} = \frac{(w/A/t)}{P\rho_p + R\rho_r} \quad (7.2)$$

Where, w : the sample mass (g)

A : sample area (cm²),

t : sample thickness (cm) and

ρ_p : Fiber mass density (1.37g/cm³ for polyester fibers)

ρ_r : Fiber mass density (1.50 g/cm³ for rayon fibers)

P : fraction of polyester fibers and binder fibers

R : fraction of rayon fibers

7.2.3 Pore size measurement

The porous parameters of the nonwoven samples were measured using a capillary flow porometer (CFP-1100-AA, PMI, New York, USA) according to the principle of liquid extrusion technique. The samples were fully wetted with a fluid in the name of Galwick and surface tension of 15.9 Dynes/cm.

7.2.4 Compression properties measurement

The compressional study was carried out on an Instron 4400R, with a load cell of 1000lb and constant rate of compression of 2.5 mm/min in the compression percent range of 0-40% with a pressure foot

8.89 cm diameter. The presser foot is brought down to reach to 40% compression based on the initial thickness. The initial thickness, T_0 , is measured under no compression load. The compression percent increases and corresponding compression load are recorded on the Instron after each increase in compression percent. After reaching a compression percent of 40%, i.e. the final compression percent, the compression percent is gradually reduced with the same rate and corresponding compression loads are recorded in the same way during the recovery cycle. For each sample, this test was carried out for 3 replicates and each replicate include different number of layers of our nonwoven sample. It was tried to keep the thickness of the sample in a specific range of 50 ± 2 mm. Plate separation was 55 mm for all the samples.

7.2.5 Swelling characteristics

To estimate the swelling of rayon fiber, cross-sectional area of rayon fibers were measured in dry and wet condition using an optical microscope for 25 different points. Proper precautions were taken in the illumination of the microscope for maximum optical performance. The measurements were conducted using the ImageJ software package. The area swelling percentage of the fibers was calculated according to the mean value for the wet and dry cross-sectional area and according to below equation:

$$\% \text{ swelling} = \frac{\text{wet area} - \text{dry area}}{\text{dry area}} * 100 \quad (7.3)$$

7.2.6 Experimental technique for absorption and release properties

The techniques and protocols was developed in order to analyze the absorption and release properties of nonwovens at various compression levels. The absorption properties were evaluated in various flow directions including through-plane, horizontal in-plane. The techniques were discussed

comprehensively in our previous paper (Chapter 4 of this dissertation). For the sake of brevity, they are not mentioned here again. It is noteworthy to mention that in theoretical calculation of the maximum absorption, the fiber mass density for each sample were calculated based on the weight fraction of each fiber as below

$$\rho_{\text{fiber}} = \text{fraction of PET and binder fibers} * \rho_{\text{PET}} + \text{fraction of rayon fibers} * \rho_{\text{rayon}} \quad (7.4)$$

PET fiber and Rayon fiber mass density were considered 1.37 g/cm^3 , and 1.5 g/cm^3 respectively.

Furthermore the basket test was performed with a non-swelling liquid (n-octane) in order to find out the effect of swelling on the absorption capacity of the samples. The use of n-octane as a non-swelling liquid for the cellulosic fibers has been referenced in many researches including (Schuchardt and Berg 1991).

7.3 RESULTS AND DISCUSSION

7.3.1 Basic web characteristics

The web structural characteristics of the entire nonwoven samples are shown in table 7.2. On the whole, the basis weight of the samples was in a reasonable range around 200 g/m^2 . The samples containing 80% and 0% rayon fibers exhibited the lower basis weight, lower thickness and greater solidity, while the web characteristic were almost identical in the rest of the samples that contain various percentages of Rayon and PET fibers.

Table 7.2: web structural characteristics

Group code	Basis weight (g/m ²)	Thickness (mm)	Initial Solidity
80R	183	2.95	0.0660
64R	234	4.76	0.0531
40R	222	4.68	0.0525
16R	213	4.59	0.0525
0R	187	3.57	0.0599

7.3.2 Pore diameter

The pore diameter and its distribution were experimentally determined with a capillary flow porometer. The values of the mean flow pore diameter for the wet samples were graphed in figure 7.1. It confirmed that the swelling happens instantaneously in cellulosic fibers (Schuchardt and Berg 1991), also the samples were wet while their mean flow pore diameter was measured in porometer, therefore it can be speculated that the given data for the pore diameter reflect the effect of swelling. It is seen that with increasing the rayon percentages the mean flow pore diameter is decreased. This is mainly because of the rayon fibers are packed very well and higher the percentages of the rayon fibers, higher the packing density or solidity of the structure will be (Table 7.2). With the same basis weight, high solidity of the structure resulted in the less distance between the fibers and smaller mean pore sizes. In case of absorbent fibers such as rayon fibers, swelling also reduces the distance between the fibers and resulted in smaller pore sizes.

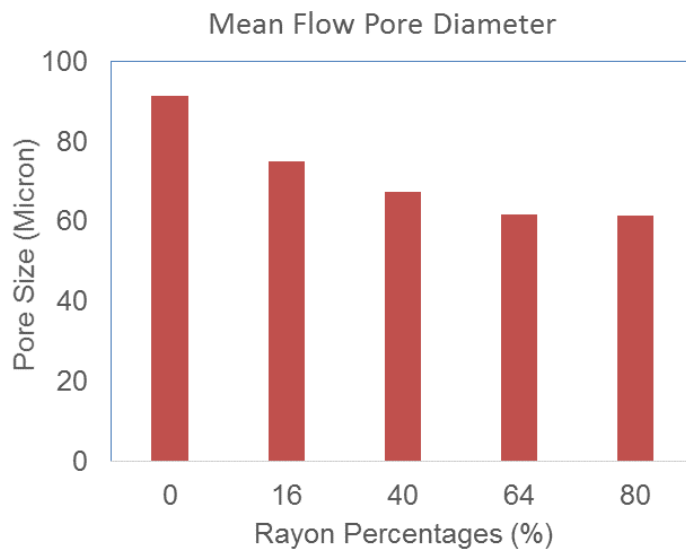


Figure 7.1: mean flow pore diameter of the samples with different rayon percentages

7.3.3 Compression properties

The compression result for nonwoven materials with different percentages of rayon fiber has been shown in figure 7.2. The graphs show that samples containing 80% of rayon fibers are highly resistant to compression. It is because of the very compact structure of the samples containing 80% rayon fibers. The fibers are highly packed in these samples and they have higher initial solid volume fraction than the rest of samples.

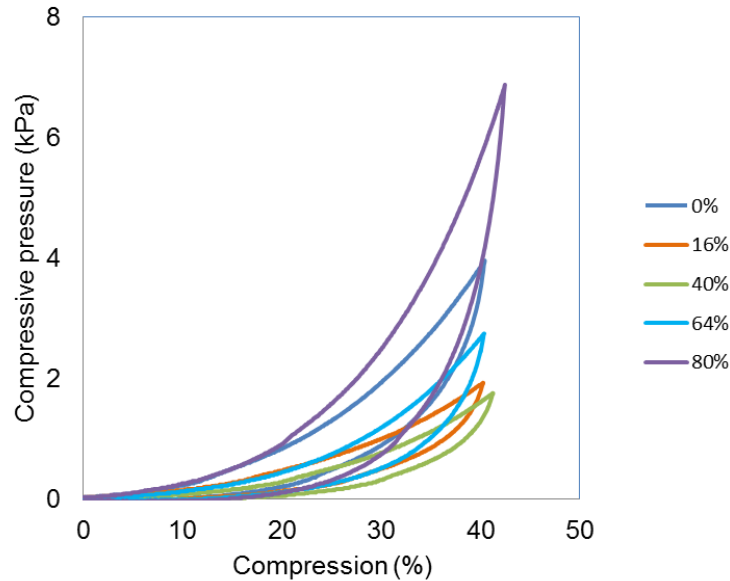


Figure 7.2: compression pressure vs. compression percent, different rayon fiber percentages (legend shows the rayon fiber percentages)

Compressive resistance evaluation is one way to evaluate the compression properties of the nonwovens. Compressive resistance is the compression pressure required to reach a specific percent of compression. The compressive resistance at 40% compression level is shown in figure 7.3 for samples containing different rayon percentages. Since the compression resistance is influenced by the solid volume fraction of the samples, the solid volume fraction is shown in the graph as well. Samples containing 0, and 80% of rayon fibers with higher solidity show higher compressive resistance because of their more compacted structure. However for the sample containing 16, 40, and 64% of rayon fibers with the same solidity, increasing the rayon percentages resulted in higher compressive resistance. The compressive resistance of the nonwoven samples also resulted from the bending rigidity of the samples. The bending rigidity is determined based on the fiber size, fiber cross-section and young modulus of the fibers.

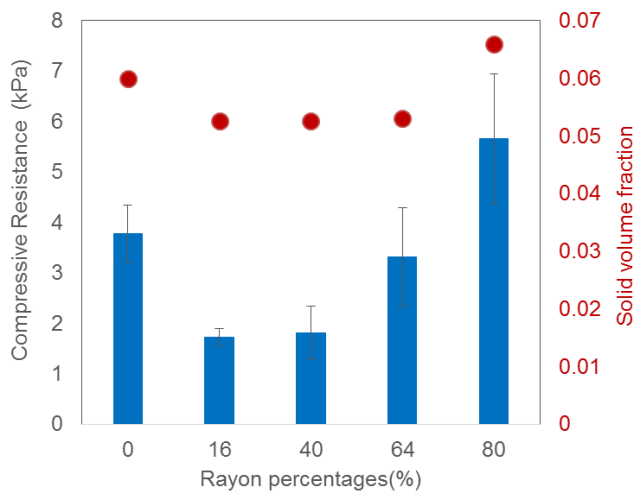


Figure 7.3: compressive resistance at 40% compression- different rayon fiber percentages

Moreover, the compression properties of fiber assemblies were studied by van Wyk (van Wyk 1946). The van Wyk work focused on finding the relationship between the compressive pressure and solid volume fraction of the samples with considering some simplifying assumption. According to the van Wyk equation shown as equation 7.5, there is a linear relationship between the compressive pressure and the solid volume fraction cube in a moderately pressure load amount in the compression cycle. Figure 7.4 shows a typical compressive pressure versus solidity cube for different samples. Higher slope of the linear part indicate the higher resistance against changes in solid volume fraction of the samples with the same amount of compression load.

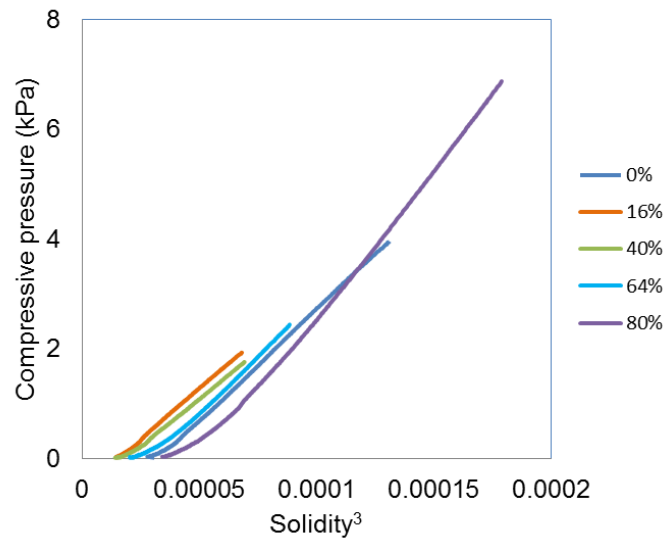


Figure 7.4: compressive Pressure vs. cube solidity in samples containing different rayon fiber percentages

$$P = \alpha(\mu_f^3 - \mu_{f0}^3) \quad (7.5)$$

In which P is the compression load; μ_f and μ_{f0} are solid volume fraction with and without loading and,

$$\alpha = k\tau \quad (7.6)$$

k: the van Wyk's constant (depends on material properties)

τ : the fiber bending rigidity

The slope α as shown in equation 7.6 depends on the fiber bending rigidity and material properties.

Based on this equation, the slope α is calculated for different rayon content and is shown in figure 7.5.

It can be observed that samples containing higher rayon percentages shows higher slope, which indicates their higher bending rigidity. In this way of comparing the resistance to compression is not influenced by the initial solid volume fraction of the sample and it is observed that without

considering the effect of initial solidity, samples with 64% and 80% of rayon fibers shows similar resistance to compression.

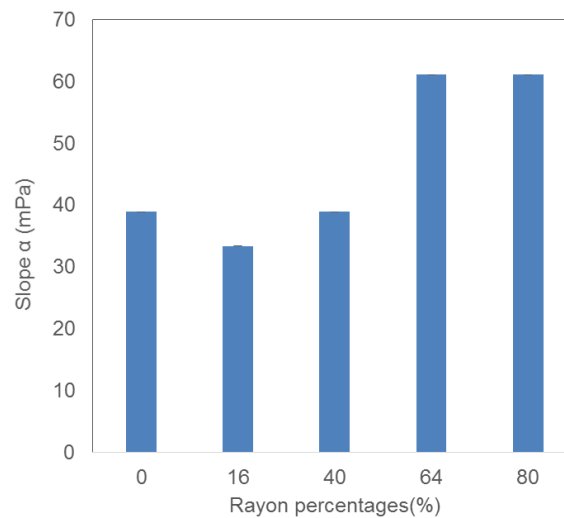


Figure 7.5: calculated slope α based on van Wyk equation

Recoverability determines the fraction of the thickness, which is recovered after the compression. The recoverability is calculated based on the initial thickness (T_i), recovered thickness (T_r), and compressed thickness (T_c) according to equation 7.7.

$$\text{Recoverability} = \frac{T_r - T_c}{T_i - T_c} \quad (7.7)$$

The recoverability of the samples with different percentages of rayon fibers were calculated and shown in figure 7.6.

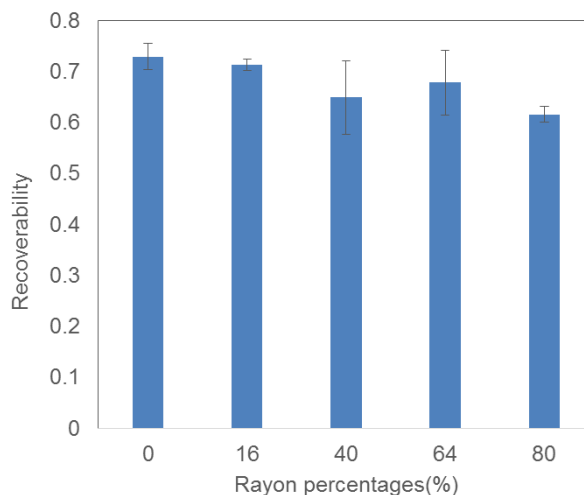


Figure 7.6: recoverability measurements in varying rayon fiber percentages

It can be observed from figure 7.6 that higher the rayon percentages, lower the recoverability is. This is attributed to the way the rayon fibers with trilobal cross-sectional shape are packed due to compression. The low stiffness of the trilobal fiber cross-sectional shapes gives rise to the compact packing of rayon fibers, and consequently higher friction among the fibers which makes it harder for the fiber to recover to their original thickness after unloading.

7.3.4 Swelling properties

As mentioned earlier, the swelling properties of cellulosic fibers has been studied for several decades and through different techniques (Karlsson et al. 1998, 1949; Preston and Nimkar 1949). Figure 7.7 displays the cross-section of the rayon fiber used in our study. Cross-sectional area of the rayon fibers were measured in dry and wet situation. The measured cross-sectional area were 120 (± 10) and 260 (± 50) for dry and wet rayon fibers respectively. According to these data the area swelling percentages in trilobal shaped rayon fibers were 116%, by contrary, the area swelling percentage of in

regular crenulated rayon fibers has been reported to be around 65% (Preston and Nimkar 1949; Morton, Hearle, and Textile Institute (Manchester 2008)). This may be attributed to the greater surface area of trilobal fibers because a greater fraction of the fiber wall is exposed to the liquid. The swelling reduces the available pore volume between the fibers, therefore the capillary pore becomes narrower. Since the absorbency rate of the nonwovens samples are affected by the pore size, the swelling alters the rate of absorption in nonwovens.

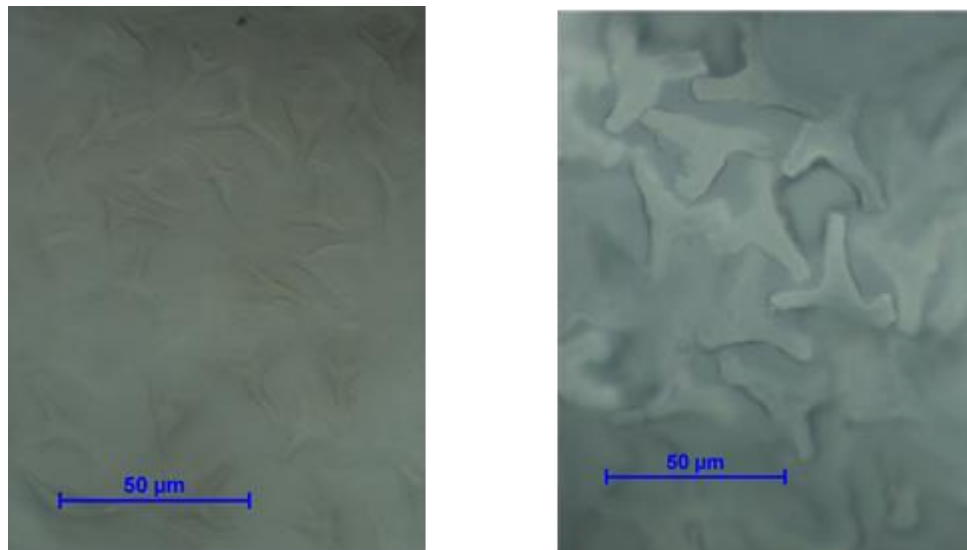


Figure 7.7: cross-sectional images of trilobal rayon fibers (left) dry (right) wet-instantaneously

7.3.5 Absorption

In this section, we are going to evaluate the liquid absorption behavior of the nonwovens materials containing different rayon fiber percentages. To understand the effect of compression, samples were compressed to different compression percentages of 0, 5, 10, 20, 30, and 40 % based on their initial thickness. Figure 7.8 exhibited the typical GATS absorbency plot for the entire samples. It is

observed that the absorbency behavior of the samples is influenced by their constituent fibers and their percentages. These plots show that for the whole samples, the maximum absorption of the material decreased with comparison. The rate of absorption is influenced by the compression. This relationship had been predicted from other considerations, but had never been proved. The proof provided by these results should therefore be of special interest. In the following section, we are going to discuss the changes in absorbency behavior of the samples according to their pore characteristics at different compression level.

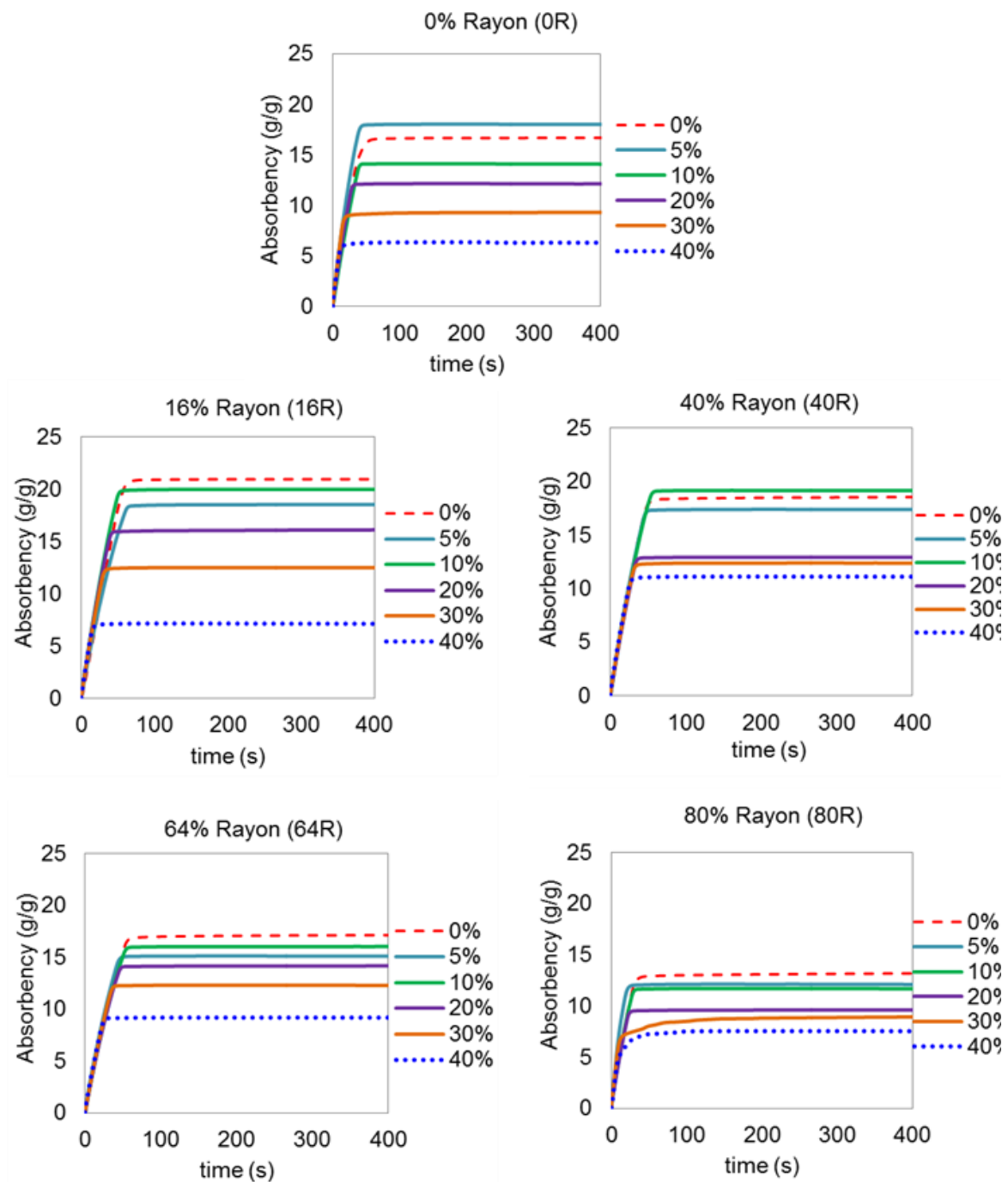


Figure 7.8: typical GATS absorbency curve for samples containing various fractions of rayon fiber at different levels of compression

7.3.5.1 Maximum absorption

The general purpose of this research was to study the influence of fiber materials on the absorbency behavior of the nonwoven. In our study, the maximum absorbency amount was measured for the samples containing the various percentages of PET fibers, rayon fibers, and binder. Figure 7.9 illustrated the results obtained by through-plane GATS technique. As evident from the figure, the maximum absorbency was not remained constant among the samples containing various percentages of fibers. The figure also show the general trend of reduction in maximum absorption with compression as predicted. Although it should be noted that in small compression percentages, the maximum absorbency is not affected by the compression in some of the samples. On the other hand, the data exhibited that the differences among the maximum absorption in various rayon fiber percentages becomes less at higher compression percentages. The variation among the result may also come from their initial solidity or the available pore volume. In the following, the absorbency amount is discussed according to their solidities at various compression levels. This discussion is of great advantage, since it removes the influence of the initial solidity.

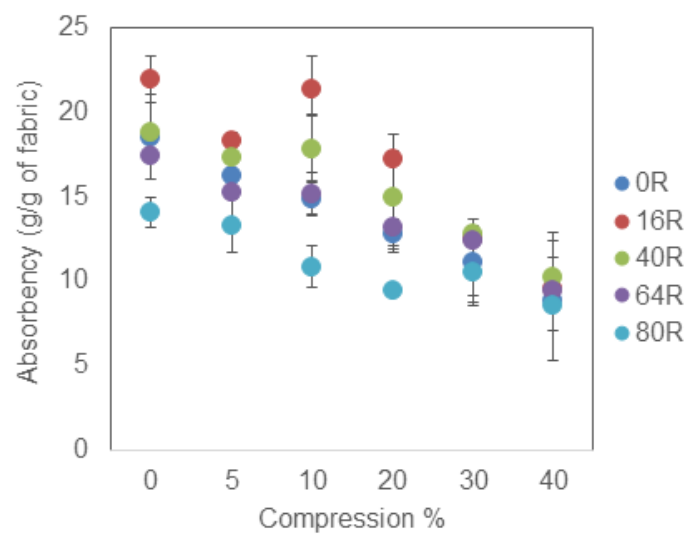


Figure 7.9: the GATS maximum absorption results under different compression levels for samples containing various rayon fiber percentages

The aforementioned theory (equation 4.4- chapter 4) about the absorption capacity of the nonwoven samples predicts the maximum absorption of the nonwoven according to their solidity and fiber density of the sample. The theoretical maximum absorption was calculated for the entire samples at different solidity levels. Figure 7.10 displays the results. Figures suggest that the experimental maximum absorption are in good agreement with the theory, which means the absorption capacity of the nonwoven sample is mainly governed by their solidity and fiber density of the samples. Although, it was infrequently observed that deviation from the theory was not infinitesimal at very high compression. This might be due to the fiber breakage at higher compression, which bring about the collapse of the fabric structure, and hence they loss a bigger portion of the available pore. It is noteworthy to mention that the imperfect contact between the samples and sample holder cause the initial deviation from theory in the entire samples. Slight compression of the samples was solved the issue of the contact at higher solidities. The result were inconsistent with the claims about the influence of the pore size distribution on the absorption capacity of the nonwoven samples (Barnholtz, Trokhan, and Suer 2011).

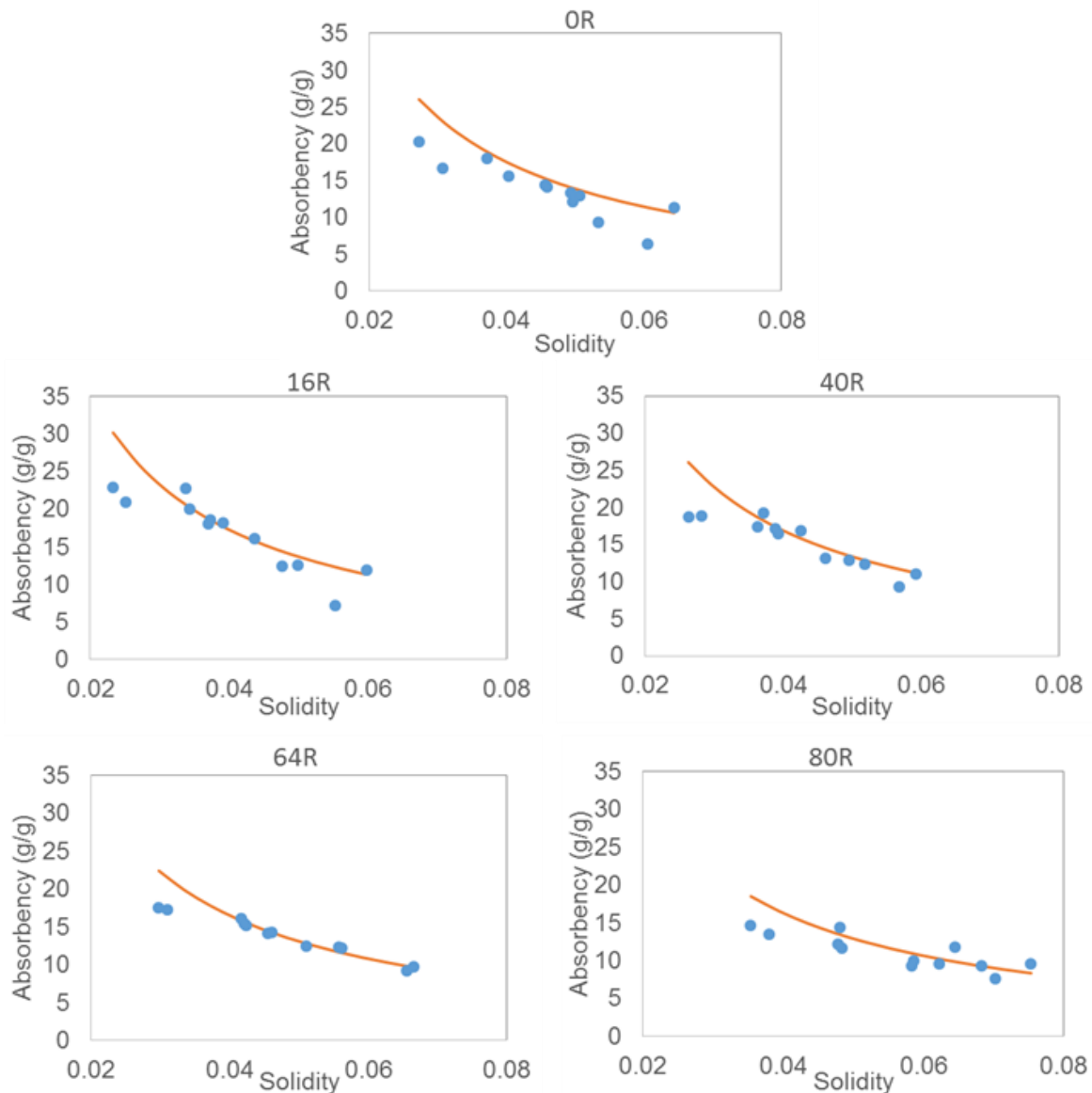


Figure 7.10: maximum absorbency (theory, GATS) versus solidity for the samples containing various rayon percentages- solid lines shows the theoretical results and dots show the experimental result

In order to examine the effect of swelling, we also examined the maximum absorption of the samples with a non-swelling liquid. In our study, n-octane was chosen as the non-swelling liquid which was according to the references (Schuchardt and Berg 1991). Then the basket test was performed on the

samples with both of liquids. As indicated in figure 7.11, the data did not show a remarkable difference between the results achieved by two liquids. However, it is observed that n-octane absorption exhibited slightly lower value, but it looks like, it was in the range of experimental error and the variation in the solidity of the sample. As we discussed in the previous section, it is certain that the swelling takes place in the fibers, which means the liquid is diffused into the fiber themselves. Therefore it can be inferred that swelling did not have a significant influence on the absorption capacity of the samples, the only difference is that part of the liquid is absorbed into the intra-fiber pores instead of the inter-fiber pores. It is evident that a fiber swells mainly by exchanging the fiber volume with fluid volume. It should, however, be noted that the test was performed under no compression.

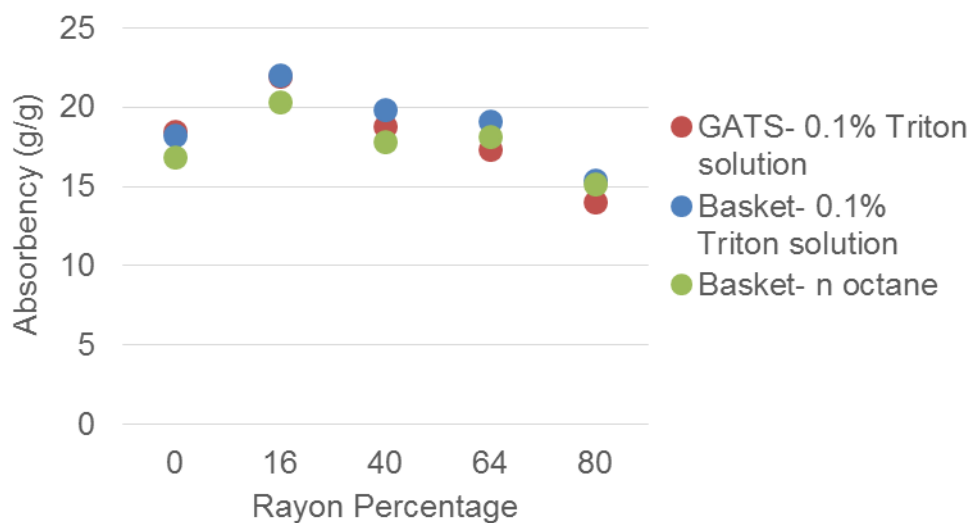


Figure 7.11: absorbency with 0.1% triton solution (non-swelling liquid) and n-octane (swelling liquid)

7.3.5.2 Absorbency rate

In this section, we sought to understand the absorbency rate of nonwoven samples containing various percentages of PET fiber and rayon fibers, considering the influence of the intrinsic material properties such as their surface energy, the swelling properties, their pore characteristics, and compression. The absorbency test was performed in two different flow directions including through-plane and in-plane direction. The results were also compared with the Washburn equation for the vertical and horizontal situations. It should, however, be noted that all the samples were washed and dried in order to remove all the finishes and impurities. This might slightly alter the structural parameters of the samples. In order to assure that the changes are insignificant, the thickness of the samples was measured before and after washing. The changes in the samples thickness in the entire samples were less than 10%. Although, the wetting and drying also influence on the shape of pores or open spaces (Schuchardt and Berg 1991; Wiryana and Berg 1991). The changes in the shape of open pores were not explored in this study. In future, it is advised that the changes in pore shape of the samples containing swelling fiber is further studied.

7.3.5.2.1 Through-plane absorbency rate

The absorbency rate of the samples containing the blend of PET fibers, Rayon fibers, and binder fibers at different percentages were measured at different compression levels. Figure 7.12 shows the result of absorbency rate of the samples in through-plane direction and at no compression. It can be identified in figure 7.12 the absorbency rate exhibited a minimum with the rayon percentages at the samples containing 64% rayon fibers, while the highest level of absorption rate was observed at samples containing 80% of rayon fibers. Comparing the surface energy of the PET fibers and Rayon fibers (Gupta and Whang 1999; Gupta with Hyun Suk Whang 2000), it is known that the trilobal

rayon fibers not only have substantially higher surface energy than PET fibers, but also the majority of the surface energy is attributed to the polar contribution, in contrast to PET fibers in which the majority of the surface energy is due to the dispersion contribution. Increased surface polar groups led to improved polarity and hydrogen bonding capacity with the water-based solution. Hence, the highest absorbency rate may be associated with this surface properties of the samples containing 80% of rayon fiber. On the other hand, it is known from the literature that the wetting and drying of the samples of swelling fibers alter the open pore shapes or the orientation of the flow channels. This is because the fibers are swelled during wetting and shrinkage happens after drying. It is likely that the greater absorbency rate of 80R samples is due to the possible alteration in the flow channels. This needs to be further explored. Furthermore, it was shown that the mean flow pore size is reduced at the samples containing larger rayon fiber percentages. The results show that the absorbency rate is reduced at the samples of the smaller pore sizes. This is further discussed in the following.

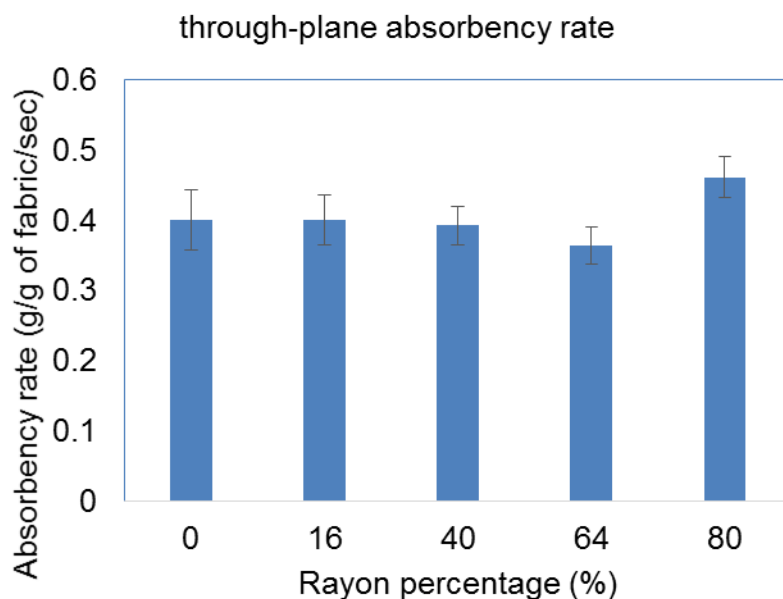


Figure7.12: through plane absorbency rate of samples containing different rayon fiber percentages

The overall response was that the rate of absorption is reduced in the samples containing both rayon and PET fiber (16R, 40R, and 64R) in comparison to the samples containing only PET fibers (0R). It can be found from the figure that the samples containing 16% and 40% rayon fibers exhibited higher absorbency rate in the mixture of the rayon fibers and PET fiber. This is in line with the suggested percentages of rayon fiber for use in an extra wicking layer employed in an absorbent article in US patent no. 8466336 (Carlucci et al. 2013).

In earlier studies attempts were made to examine the influence of swelling on the absorbency rate by performing the vertical wicking test on fibrous structures made of swelling fibers with various degrees of swelling. The results in previous studies, using a vertical wicking, indicated that the Lucas-Washburn provides a good description of wicking flow when fiber swelling is not extensive and occurs rapidly (Schuchardt and Berg 1991; Wiryana and Berg 1991). On the other hand, it has been shown that the swelling happens spontaneously in case of cellulosic fibers. In our study, the through-plane absorbency rate results were analyzed according the pore size of the samples and also compared with the vertical Washburn equation, where the gravity effect is taken to the account. Figure 7.13 indicated the results. There was not observed an agreement between the experimental and theoretical results obtained from vertical wicking test. It is noteworthy to mention that larger the rayon percentage, smaller was the pore size, which means smaller absorbency rate according to the vertical Washburn equation. On the other hand, the possibility of the swelling increases at larger the rayon percentage. Assuming that swelling hinder the liquid flow, our results suggest that the swelling has the more significant effect on the through-plane absorbency rate than the pore size because excluding the 80R samples, the absorbency rate increased in the samples containing smaller rayon percentages. It can be concluded that the vertical Washburn equation cannot predict the through-plane absorbency

rate in samples containing both absorbent and non-absorbent fibers, by considering their swollen pore size.

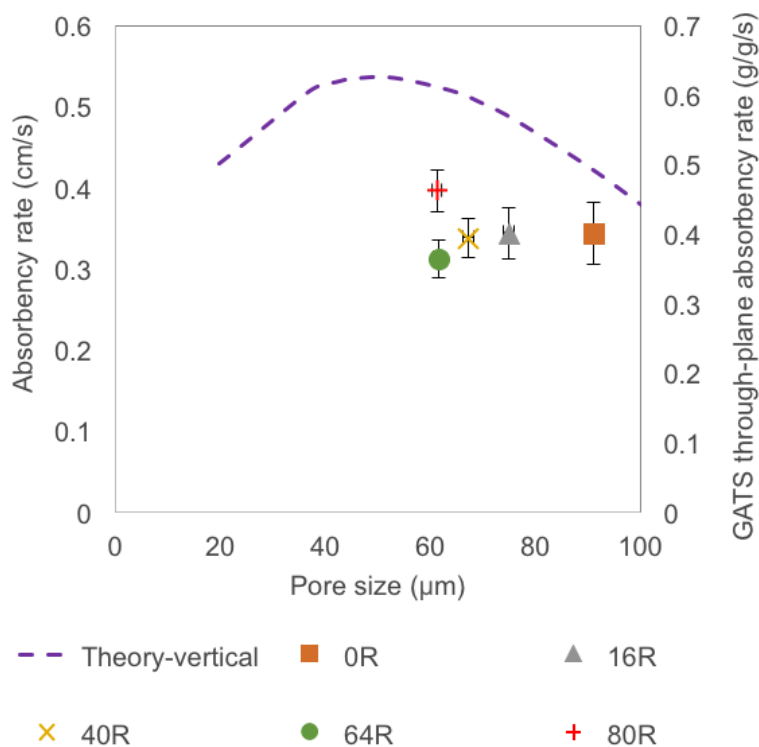


Figure 7.13: through-plane absorbency rate versus pore size for the samples containing various percentages of rayon fibers

Figure 7.14 shows the absorbency rate of the samples at different compression level. The general trend of increase in absorbency rate was observed with the compression. However as displayed in the figure, the samples containing 16, 40, and 64% of rayon fibers are less influenced by the compression. It indicates that the through-plane absorbency rate is less affected by the structural parameter such as pore size in these samples. On the other hand, it suggests that a neutralizing

interaction between the effect of compression on the pore structure, and the fiber materials and consequent swelling under compression. This interaction may bring about an almost constant absorbency rate at different levels of compressions. In the absorbency rate of samples containing both absorbent fibers and non-absorbent fibers, all of the pore structural parameters, diffusion of liquid into the intrafiber pores and swelling are the determining parameters for the absorbency rate. The diffusion of the liquid into the intrafiber pores may accelerate the liquid uptake by the structure; however swelling may cause the liquid flow hindrance especially at higher compression percentages.

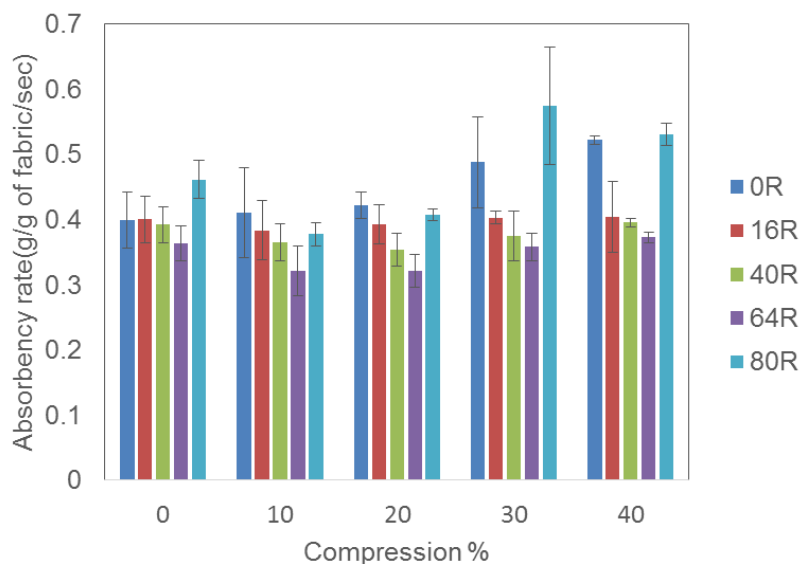


Figure 7.14: absorbency rate of samples containing various percentages of rayon fibers at different compression levels

7.3.5.2.2 In-plane absorbency rate

In-plane absorbency rate was measured for the entire sample while the only contributing force to the flow was in-plane capillary pressure. Figure 7.15 illustrates the results. It shows that the in plane absorbency rate increases with increasing the rayon fiber percentages from 0 to 16 percentages, and

then decreases at higher percentages of rayon fibers. The initial increase in the absorbency rate is because of addition of absorbent fibers with higher surface energy. For the samples containing the rayon fibers, the results showed that larger rayon percentages gave rise to smaller rate.

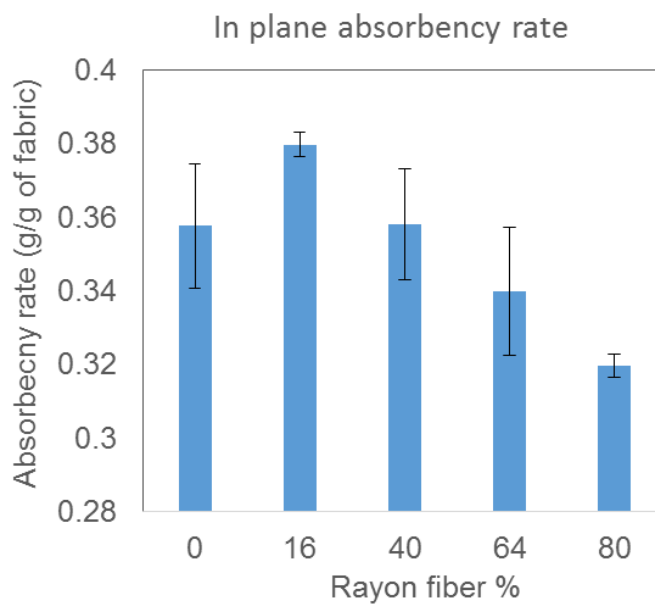


Figure 7.15: in plane absorbency rate of samples containing different rayon fiber percentages

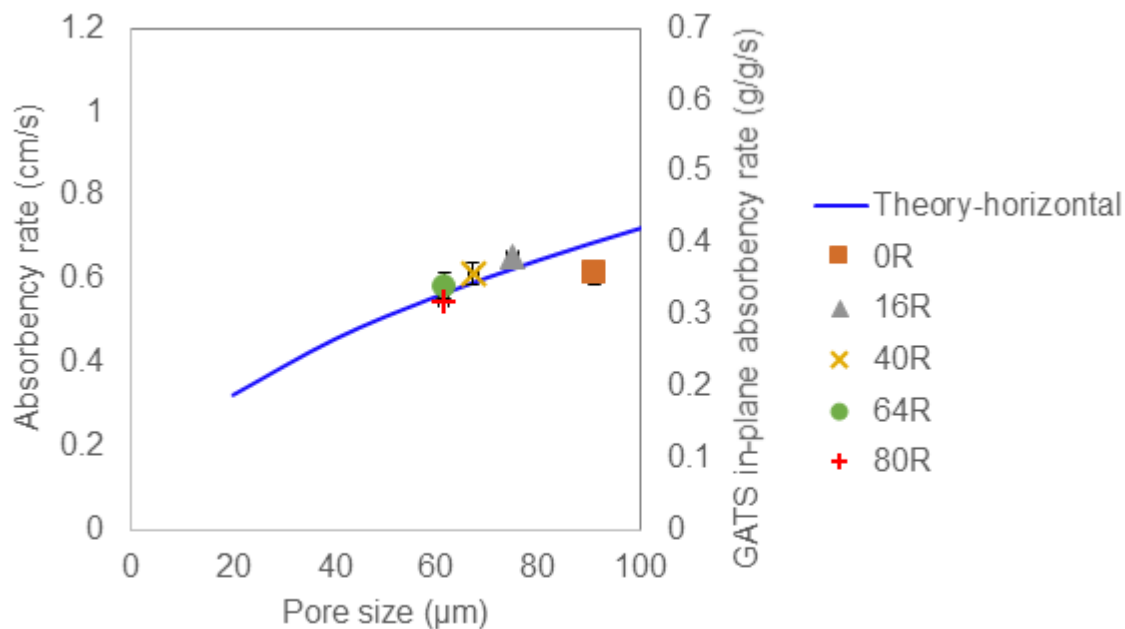


Figure 7.16: in-plane absorbency rate versus pore size for the samples containing various percentages of rayon fibers

In order to examine the influence of pore size, the rate of absorption was graphed versus pore size in figure 7.16. Moreover, the experimental results were compared with the theoretical values calculated based on in-plane absorbency rate. It is evident from the figure that there is a good agreement between the theoretical and experimental results among the samples containing rayon fibers. In contrary to the through-plane absorbency rate, it appears that the in-plane absorbency rate can be smoothly predicted in sample according to their swollen pore size. It is indicated that 0R sample is categorized in a different group than the other samples, due to their different material properties.

7.3.6 Release properties

Liquid holding capacity of samples containing different blend of PET fibers and rayon fibers were measured at different compression through the loading of the fully saturated samples taken from the GATS. It is important to mention that the majority of the samples absorbed some liquid by separating them from the GATS sample holder. As it was discussed earlier, the samples are not fully saturated while there is no compression. This suggests that a fraction of the available pore volume is empty and ready to absorb liquid. It seems the movement of the sample brought about this opportunity for the samples. On the other hand the recoverability of the samples may also be of great advantages to this situation. The amount of liquid absorbed by the samples was significant in most of the samples, therefore this was discussed in advance. Figure 7.17 displays the results for the amount of liquid absorbed while the samples on GATS, and the amount of liquid held by the samples after removing from the GATS by filled and empty icons respectively. All the results were given versus the solidity of the samples. First of all, the figure confirms the substantial influence of the solidity of the samples on their liquid retention capacity. It implies it is not beneficial to compare the liquid retention capacity of the samples without considering the solidity. Furthermore, it is obvious that the samples of 80R, 64R, and 16R have absorbed an appreciable amount of liquid after separating them from the GATS. This value was observed to be infinitesimal in case of 40R and 0R samples. It is thought that various reasons may cause this behavior in 40R and 0R samples. The recoverability of the samples was discussed in previous section. It seems that the obtained result for 40R samples is due to their lower recoverability, although the 0R samples cannot hold the liquid due to their non-absorbing nature.

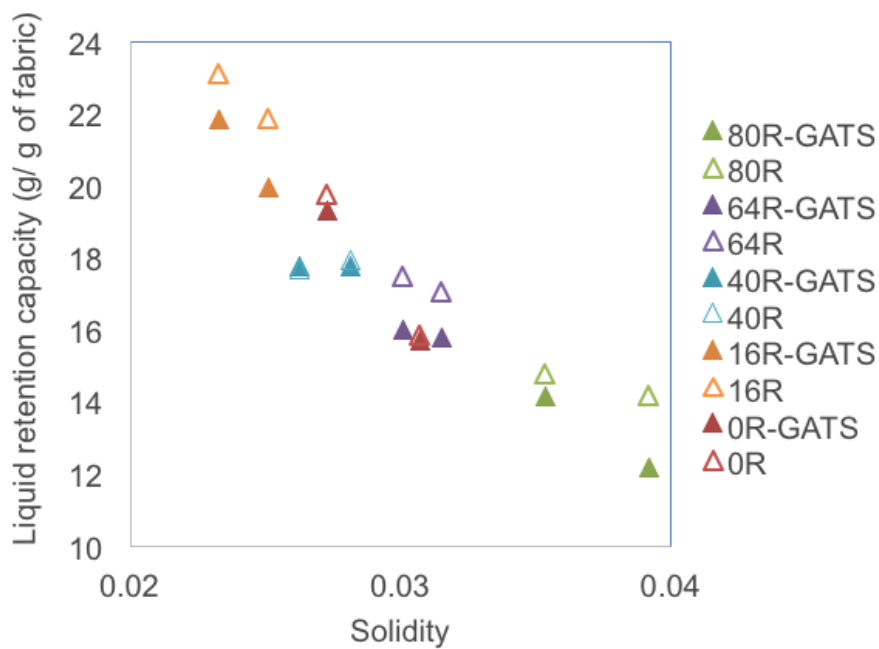


Figure 7.17: comparison between the amount of liquid retention of the samples on the GATS and after removing from the GATS

Figure 7.18 shows the liquid holding capacity of the samples under no compression. Since the fluid holding capacity is measured according to the maximum weight of liquid absorbed by the samples from the GATS results, those samples that absorb the liquid after removing the samples from the top of sample holder shows liquid holding capacity higher than 100%. In the other, as long as the liquid holding capacity is equal to 100%, it means that nor the sample released any liquid, neither it absorbed any liquid, which is the case for 0R, and 40R samples. Although, the liquid holding capacity of greater than 100% suggested that the sample absorbed some liquid. This behavior was observed for 16R, 64R, and 80R. In general, it was observed that samples with higher percentages of rayon fibers have higher liquid holding capacity. The reason is that in the case of rayon fibers due to their

hydrophilic nature, water molecules penetrate into the fibers and be absorbed into the amorphous part of cellulosic fibers, and the water molecules absorbed in this level cannot be easily drained. Moreover liquid retention happens in the intrafiber nano-sized pores of rayon fibers, with very high capillary pressure.

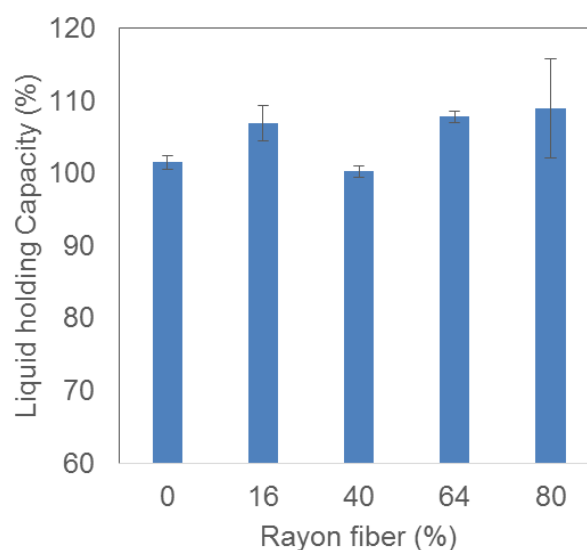


Figure 7.18: liquid holding capacity of samples with different rayon fiber percentages at no compression after removing from the GATS

Figure 7.19 shows the liquid holding capacity of the sample under compression. It shows that the liquid holding capacity reduces with compression. However the compression percentage at that the reduction in the liquid holding capacity begins, varies at samples with different percentages of rayon fiber. We were not able to reach to 40% of compression in case of samples with 80% of rayon fibers due to its high resistance to compression, which was discussed on the evaluation of compression properties of the samples.

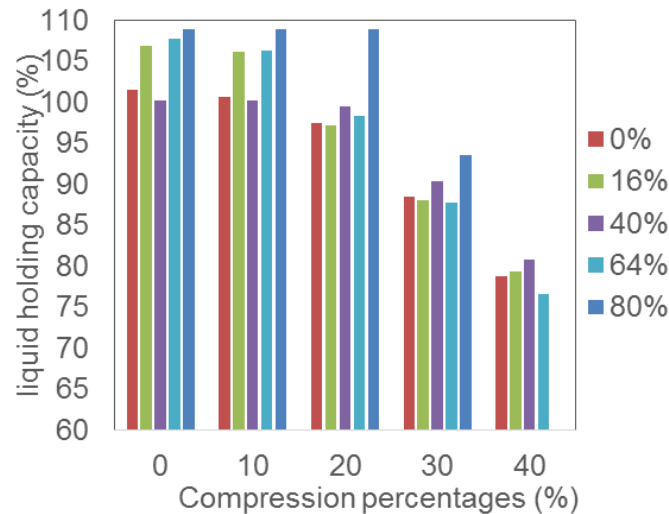


Figure 7.19: liquid holding capacity of samples with different rayon percentages under various compression percentages

So far, liquid holding capacity of the samples was discussed as the percentage of the liquid, which is held by the samples at various compression percentages, compared to the saturated value. This value is unit less and does not affected by the solidity of the samples. Although as it was mentioned earlier, the liquid retention capacity of the samples, which is measured based on the mass of liquid retained by the samples per dry mass of the samples, needs to be discussed according to the solidity of the samples. In the following, we sought to understand the liquid retention capacity of the samples at various degrees of solidity achieved by compression of the samples. As detailed in figure 7.20, on the whole, the liquid retention capacity is reduced by the solidity. Generally speaking in samples containing higher percentages of rayon fibers, the lower liquid retention capacity is the consequence of greater solidity of the samples. Further inspection of the figure indicates that the liquid retention capacity remains constant at lower levels of the solidity invariably. Nevertheless, the reduction in

liquid retention capacity is varied for different samples. In spite of difficulty in comparing the results for the samples containing various rayon fiber percentages due to the initial variation in their solidity values, in the middle range of solidity represented in figure 7.20, it can be found that the liquid retention capacity is decreased by rayon fiber percentage at a given solidity value to some extent. This is related to the low wet modulus of the rayon fibers. Rayon fiber loses its modulus when wet, therefore it tends to collapse under compression especially in wet situation, and to lose a remarkable fraction of its pore volume (Hsieh 1995b; Steiger and Kapur 1972). This may contribute to the collapse of the structure and pore volume, which leads to lower liquid retention capacity at a given solidity. Nonetheless, different degrees of compression are required in order to obtain a constant solidity among the various samples. The pore size and its distribution is evidently not constant among the samples at various degrees of compression. Unfortunately, the pore size and its distribution is not available for these samples in this study. Future work should therefore include the effect of pore size and its distribution as well.

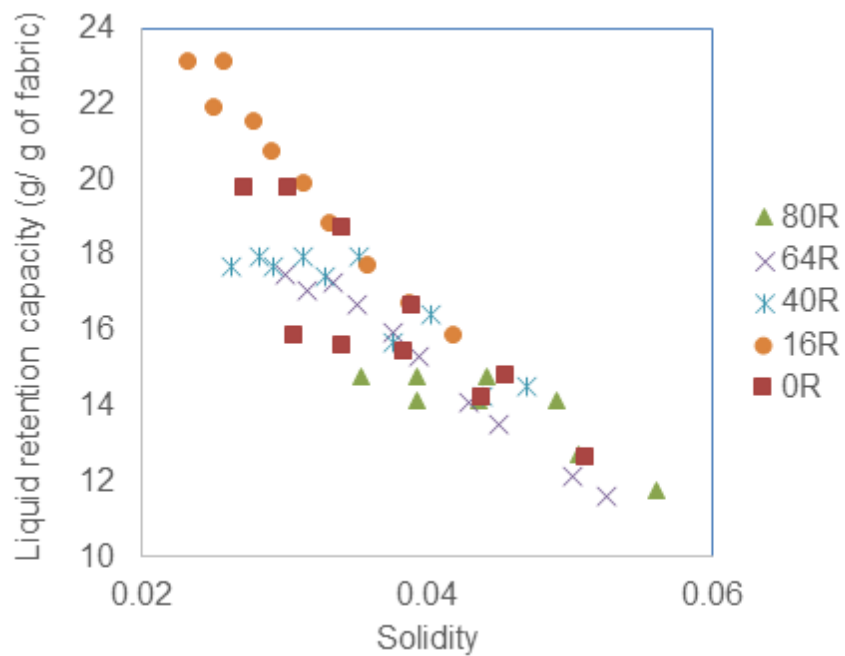


Figure 7.20: liquid retention capacity versus solidity for the samples containing various rayon fiber percentages

To realize the liquid retention behavior of the samples based on their solidity value and also their maximum absorption capacity at a given solidity, the maximum absorption capacity of the samples was calculated based on equation 4.4- chapter 4, It can be identified from figure 7.21 that the reduction in the liquid retention did not initiate by achieving the higher solidity through compression of the structure, as long as liquid retention does not meet the maximum absorption capacity of the sample at the given solidity. The similar behavior was observed in samples of non-absorbent fibers discussed in chapter 4 and 5. As discussed in those chapter, this phenomena is ascribed to the redistribution of the liquid from larger pore sizes to smaller pore sizes that is brought by the compression of the structure at higher solidities. In general, after the reduction took place at a specific

solidity, the liquid retention capacity exhibited a good agreement with the maximum absorption capacity.

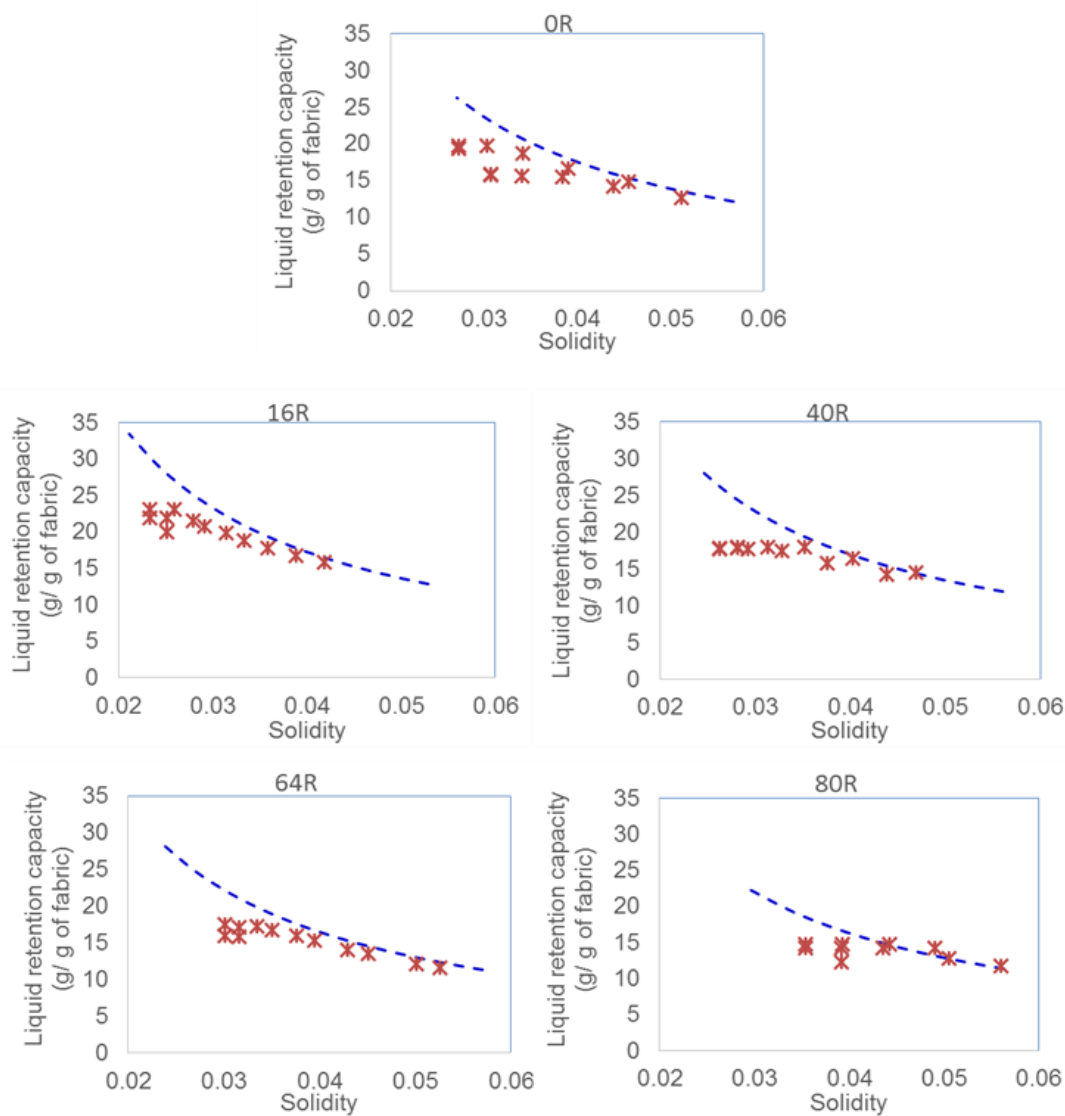


Figure 7.21: liquid retention capacity versus solidity for the samples containing various rayon percentages- solid line shows the theoretical maximum absorption capacity results and cross symbols show the experimental result

7.4 CONCLUSION

The previous studies have documented the surface energy and wettability of various textile fibers, their swelling properties, as well as the wicking properties of the fibrous materials containing swelling fibers. However the absorption and release properties of nonwoven fabrics remained unstudied for the nonwoven samples containing both swelling and non-swelling fibers. In this study, we figured out the absorption and release properties of nonwoven samples containing various degree of rayon, PET, and binder fibers at various compression levels. The focus of this research was to provide insight into the absorption and release properties of nonwoven, based on their material properties, as well as the structural parameters including solidity and pore size.

The swelling properties were examined for trilobal rayon fibers. The cross-sectional area swelling percentages was more than that reported in literature for regular rayon fiber with crenulated cross-sectional shape. However, it was realized that the swelling of rayon fibers did not influence the maximum absorbency. Absorbency rate was tested in both in-plane and through-plane direction. Greater absorbency rate was achieved in samples of larger pore sizes in in-plane direction regardless of the composition of the samples, which were analogues to the horizontal Washburn equation. The through-plane absorbency rate exhibited a minimum with rayon fiber percentages. Through-plane absorbency rate was analyzed based on the pore size of the samples. The results were inconsistent with the vertical Washburn equation. It could be speculated that swelling led to more complicated consequences in through-plane direction than in in-plane direction. The percentage liquid holding capacity tended to be greater in samples containing greater percentages of rayon fibers. Liquid retention was found to depend greatly on the solidities of the samples; hence it was difficult to draw any definite conclusion about the impact of rayon fiber percentages on the liquid retention capacity due to the discrepancy in the solidity values. Yet, it was observed that the larger solidity values did

not give rise to reduction in liquid retention capacity as long as the unfilled pores were available in the structure.

REFERENCES

- Anjur, Sriram Padmanabhan, Ketan Narendra Shah, and Anthony John Wisneski. 1997. "Elastomeric Absorbent Structure." US patent 5645542
- Ashari, A., T.M. Bucher, and H. Vahedi Tafreshi. 2010. "A Semi-Analytical Model for Simulating Fluid Transport in Multi-Layered Fibrous Sheets Made up of Solid and Porous Fibers." *Computational Materials Science* 50 (2): 378–90. doi:10.1016/j.commatsci.2010.08.030.
- Barnholtz, Steven Lee, Paul Dennis Trokhan, and Michael Donald Suer. 2011. "Fibrous Structures and Methods for Making Same." US patent 20110209840
- Benltoufa, S., F. Fayala, and S. Ben Nasrallah. 2012. "Determination of Yarn and Fiber Diameters after Swelling Using a Capillary Rise Method." *Journal of the Textile Institute* 103 (5): 517–22. doi:10.1080/00405000.2011.589573.
- Carlucci, John, Maurizio Tamburro, Alessandro Gagliardini, Evelina Toro, and Pancrazio Veronese. 2013. "Thin Absorbent Core Substantially Free of Cellulose Fibers." US patent 8466336
- Chatterjee, P. K., and B. S Gupta. 2002. *Absorbent Technology*. Amsterdam; Oxford: Elsevier Science. <http://www.sciencedirect.com/science/book/9780444500007>.
- Chen, Fung-Jou, and Rebecca Lyn Dilnik. 1997. "Absorbent Article Having a Cellulosic Transfer Layer." WO patent 1997017925A1
- Gupta, B. S, and Cheol J. Hong. 1994. "Changes in Web Dimensions during Fluid Uptake and the Impact on Absorbency." *Tappi Journal* 77 (12): 181–88.
- Gupta, B. S, and H. S. Whang. 1999. "Surface Wetting and Energy Properties of Cellulose Acetate, Polyester and Polypropylene Fibers." *International Nonwovens Journal* 8 (1).
- Gupta, B. S. with Hyun Suk Whang. 2000. "Surface Wetting Characteristics of Cellulosic Fibers." *Textile Research Journal* 70 (4): 351–58. doi:10.1177/004051750007000412.

- Hsieh, Y.-L. 1995a. "Liquid Transport in Fabric Structures." *Textile Research Journal* 65 (5): 299–307. doi:10.1177/004051759506500508.
- Hsieh, Y.-L., A. Miller, and J. Thompson. 1996. "Wetting, Pore Structure, and Liquid Retention of Hydrolyzed Polyester Fabrics." *Textile Research Journal* 66 (1): 1–10. doi:10.1177/004051759606600101.
- Hsieh, Y.-L., J. Thompson, and A. Miller. 1996. "Water Wetting and Retention of Cotton Assemblies as Affected by Alkaline and Bleaching Treatments." *Textile Research Journal* 66 (7): 456–64. doi:10.1177/004051759606600707.
- Kaelble, D. H. 1970. "Dispersion-Polar Surface Tension Properties of Organic Solids." *The Journal of Adhesion* 2 (2): 66–81. doi:10.1080/0021846708544582.
- Kaelble, D. H., and K. C. Uy. 1970. "A Reinterpretation of Organic Liquid-Polytetrafluoroethylene Surface Interactions." *The Journal of Adhesion* 2 (1): 50–60. doi:10.1080/0021846708544579.
- Karlsson, J.O., M. Andersson, P. Berntsson, T. Chihani, and P. Gatenholm. 1998. "Swelling Behavior of Stimuli-Responsive Cellulose Fibers." *Polymer* 39 (16): 3589–95.
- Kawase, T., S. Sekoguchi, T. Fuj, and M. Minagawa. 1986. "Spreading of Liquids in Textile Assemblies: Part I: Capillary Spreading of Liquids." *Textile Research Journal* 56 (7): 409–14. doi:10.1177/004051758605600702.
- Li, Tie-Qiang, Mats Häggkvist, and Lars Ödberg. 1997. "Porous Structure of Cellulose Fibers Studied by Q-Space NMR Imaging." *Langmuir* 13 (13): 3570–74. doi:10.1021/la970045m.
- Li, Tie-Qiang, Ulf Henriksson, Tomas Klason, and Lars Ödberg. 1992. "Water Diffusion in Wood Pulp Cellulose Fibers Studied by Means of the Pulsed Gradient Spin-Echo Method." *Journal of Colloid and Interface Science* 154 (2): 305–15. doi:10.1016/0021-9797(92)90145-C.

- Masoodi, Reza, and Krishna M. Pillai. 2010. "Darcy's Law-Based Model for Wicking in Paper-like Swelling Porous Media." *AICHE Journal*, NA – NA. doi:10.1002/aic.12163.
- R. Masoodi, Pillai, K.M., 2012. "A GENERAL FORMULA FOR CAPILLARY SUCTION-PRESSURE IN POROUS MEDIA." *Journal of Porous Media* 15 (8): 775–83.
doi:10.1615/JPorMedia.v15.i8.60.
- Morehead, F. F. 1947. "Some Comparative Data on the Cross-Sectional Swelling of Textile Fibers." *Textile Research Journal* 17 (2): 96–98. doi:10.1177/004051754701700204.
- Morehead, F.F., 1952. "A Method for Studying the Effect of Humidity on the Cross-Sectional Swelling of Some Common Fibers." *Textile Research Journal* 22 (8): 535–39.
doi:10.1177/004051755202200807.
- Morton, W. E, J. W. S Hearle, and England) Textile Institute (Manchester. 2008. *Physical Properties of Textile Fibres*. Boca Raton, FL; Cambridge, England: CRC Press ; Woodhead Publishing.
- Mullins, Benjamin J., and Roger D. Braddock. 2012. "Capillary Rise in Porous, Fibrous Media during Liquid Immersion." *International Journal of Heat and Mass Transfer* 55 (21-22): 6222–30.
doi:10.1016/j.ijheatmasstransfer.2012.06.046.
- Nederveen, Cornelis J. 1994. "Absorption of Liquid in Highly Porous Nonwovens." *Tappi Journal* 77 (12): 174–80.
- Pan, N., and W. Zhong. 2006. "Fluid Transport Phenomena in Fibrous Materials." *Textile Progress* 38 (2): 1–93. doi:10.1533/tepr.2006.0002.
- Patnaik, A., R. S. Rengasamy, V. K. Kothari, and A. Ghosh. 2006. "Wetting and Wicking in Fibrous Materials." *Textile Progress* 38 (1): 1–105. doi:10.1533/jotp.2006.38.1.1.

- Preston, J. M., and M. V. Nimkar. 1949. "MEASURING THE SWELLING OF FIBRES IN WATER." *Journal of the Textile Institute Proceedings* 40 (7): P674–88.
doi:10.1080/19447014908664692.
- Preston, J. M., M. V. Nimkar, and S. P. Gundavda. 1951. "4—Capillary and Imbibed Water in Assemblies of Moist Fibres." *Journal of the Textile Institute Transactions* 42 (2): T79–90.
doi:10.1080/19447027.1951.10750259.
- Schiefer, H. F., and R. T. Kropf. 1946. "Influence of Fiber Structure of Rayon on Swelling and Radial Density." *Textile Research Journal* 16 (9): 432–37. doi:10.1177/004051754601600902.
- Schuchardt, David R., and John C. Berg. 1991. "Liquid Transport in Composite Cellulose-Superabsorbent Fiber Networks." *Wood and Fiber Science* 23 (3): 342–57.
- Shipley, Arthur Roger. 1997. "Absorbent Article Containing Absorbent and Non-Absorbent Fibers." WO patent 1997005839A1
- Steiger, F. H., and C. Kapur. 1972. "The Absorption of Liquids by Compressed Fiber Systems." *Textile Research Journal* 42 (8): 443–49. doi:10.1177/004051757204200801.
- Topgaard, Daniel, and Olle Söderman. 2001. "Diffusion of Water Absorbed in Cellulose Fibers Studied with H-NMR." *Langmuir* 17 (9): 2694–2702. doi:10.1021/la000982l.
- Van Wyk, C. M. 1946. "NOTE ON THE COMPRESSIBILITY OF WOOL." *Journal of the Textile Institute Transactions* 37 (12): T285–92. doi:10.1080/19447024608659279.
- Welchel, Debra Nell, Eric Scott Kepner, and Crystal Sutphin Leach. 2000. "Hydroentangled Nonwoven Composites." US patent 6022818
- Wiryan, Surya, and John C. Berg. 1991. "The Transport of Water in Wet-Formed Networks of Cellulose Fibers and Powdered Superabsorbent." *Wood and Fiber Science* 23 (3): 457–64.

8 CONCLUSIONS AND RECOMMENDATIONS

8.1 CONCLUSIONS

The current research is focused on investigation of absorption and release properties of nonwovens under compression, considering the influence of the structural parameters and fiber absorbency properties. The investigated parameter are divided into structural parameters including fiber cross-sectional size, namely 1.5,3,6, and 9 deniers, fiber cross-sectional shape, that is to say round, pentalobal, and 4DG, heterogeneous layered structures having a pore size expansion and reduction, as well as fiber absorbency properties including varying percentages of absorbent and non-absorbent fibers. In order to understand the influence of compression, which is of practical importance, the various degree of compression were applied in the investigational study of these parameters. Furthermore, various techniques were employed to consider the effect of flow direction. The absorption and release properties explored in this project consist of maximum absorbency, rate of absorption, and liquid retention. The purpose of this research is to establish the structure-property relationship of absorption and release properties. Then the analysis is based on the pore characteristics of the nonwoven samples including pore size and solidity. This information was utilized in order to understand the absorption and release behavior of nonwovens at various degrees of compression. The finding of this study appears to be valuable in the design of absorbent products from the materials and structural point of view. Notable findings of this study are summarized below:

- 1- Fiber size effect (Pore size effect): the maximum absorbency of the nonwovens is mainly governed by the available pore volume, porosity or solidity, however the fiber size may influence on how much of the available pore is filled with the liquid. The absorbency rate of nonwovens is governed by their pore size and a given range of pore size results in the

maximum absorbency rate. This specific range of pore size was achieved by the choice of fiber size (3 denier fibers) or a specific level of compression depending on the original pore size. The pore characteristics of 6 denier round fiber was measured at different levels of compression and it was observed that the median pore sizes decreases with compression. The absorbency rate is also influenced by the flow directions, due to the fiber orientation, as well as the effect of gravity in through-plane direction and vertical direction. The Washburn equation was employed as the theoretical model and our results were in perfect agreement with the theoretical model.

- 2- Fiber cross-sectional shape: maximum absorption was not influenced by the fiber cross-sectional shape and it governs generally by the solidity of the samples. The absorbency rate is influenced by the fiber cross-sectional shape in a specific way. The specific fiber cross-sectional shape such as 4DG fibers, which creates the groove in the fiber surface, benefited the absorbency rate in two situations, when the grooves are oriented in the flow direction or the samples are highly compressed. The 4DG fibers showed a bi-modal pore size distribution, which attributed to the smaller pore created by the groove on the fiber surface and the larger pores between the fibers. A remarkable increase in the median pore size was observed in case of pentalobal and 4DG fiber nonwovens with the compression. On the whole, it was observed that greater the median pore size, the rate of absorption was faster in case of pentalobal and 4DG fiber nonwovens. This was not in line with the results for the round cross-sectional fibers in which the absorbency rate showed a maximum with pore size.
- 3- Heterogeneous layered structure: The maximum absorbency is affected by the structural heterogeneity. While the maximum absorbency in the layered structure having a pore size reduction is mainly governed by the available pore volume, it is different in the pore size

expanded structures. This is due to the fact that the liquid cannot be transported from the smaller pore size attaining higher capillary pressure to the larger pore size creating less capillary pressure. The initial liquid uptake rate is mainly governed by the pore size of the layer which is in contact with the liquid, in other words, the heterogeneity in pore size was not observed to have a significant effect on the initial rate of absorption. Although it was seen that the absorbency rate slightly improves in the samples of pore size reduction, where the smaller pore sizes are placed on top of the larger pore sizes. This was observed especially at larger pore size differences and at higher compression percentages.

- 4- Fiber absorbency: The swelling properties of trilobal rayon fibers were measured. The maximum absorbency of the samples was measured by n-octane, which is a non-swelling liquid. It was realized that the swelling of rayon fibers did not influence the maximum absorbency. Absorbency rate was tested in both in-plane and through-plane direction. Greater absorbency rate was achieved in samples of larger pore sizes in in-plane direction regardless of the composition of the samples, which were analogues to the horizontal Washburn equation. The through-plane absorbency rate exhibited a minimum with rayon fiber percentages. Through-plane absorbency rate was analyzed based on the pore size of the samples. The results were inconsistent with the vertical Washburn equation. It could be speculated that swelling led to more complicated consequences in through-plane direction than in in-plane direction.

8.2 RECOMMENDATIONS

The results of this research suggest that the average pore size, the pore size distribution, and pore volume, as well as their reaction to the compression are the main contributing factors on the

absorption and release behavior of nonwovens at different compression levels. Below is the list of our recommendations according to this study observation:

- 1- The fiber sizes chosen for this research were 1.5, 3, 6, and 9 denier in order to understand the effect of structural parameter on absorption properties of nonwovens under compression. The results obtained for 1.5 denier fibers have suggested that the packing behavior of smaller fiber size might be different from the larger one. Therefore it is recommended to conduct this study in smaller fiber size.
- 2- The applied compression was in static mode, due to the limitation of the developed compression GATS. In order to simulate the real situation, however, it is required to consider the dynamic situation, by applying a cyclic compression and decompression. In this situation, the recovery behavior of the samples also plays a critical role in determination of available pore volume, as well as pore size.
- 3- The absorption properties of the nonwovens having a pore size gradient were evaluated at different compression levels. In order to better realize the effect of gradient structure, further research should further examine how the compression influences on the pore characteristics of various layers. This study leads to more valuable information for the improved design of absorbent products.
- 4- The rayon fiber was used for conducting the initial experiments on the influence of swelling on the pore characteristics of nonwovens and consequently on their absorption properties. Now that the initial groundwork for understanding the influence of swelling has been established, it would be of interest to investigate the effect of superabsorbent materials that may be of more interest on the absorbent product development

- 5- The pore size distribution of nonwovens containing non-circular fiber cross-sectional shapes revealed some interesting aspects of packing behavior of these fibers under compression. It would be of interest to further investigate the packing behavior of these fibers.